PLANAR DYNAMICS AND CONTROL OF SPACE-BASED FLEXIBLE MANIPULATORS WITH SLEWING AND DEPLOYABLE LINKS

MATHIEU CARON

B.Eng., McGill University, Canada, 1994

A THESIS SUBMITTED IN PARTIAL FULFILMENT OF
THE REQUIREMENTS FOR THE DEGREE OF

MASTER OF APPLIED SCIENCE

in

The Faculty of Graduate Studies
Department of Mechanical Engineering

We accept this thesis as conforming
to the required standard

THE UNIVERSITY OF BRITISH COLUMBIA

October 1996

In presenting this thesis in partial fulfilment of the requirements for an advanced degree at the University of British Columbia, I agree that the Library shall make it freely available for reference and study. I further agree that permission for extensive copying of this thesis for scholarly purposes may be granted by the head of my department or by his or her representatives. It is understood that copying or publication of this thesis for financial gain shall not be allowed without my written permission.

Department of MECHANICAL ENGINEERING

The University of British Columbia
Vancouver, Canada

Date 1996/10/28
OCT. 28, 1996

DE-6 (2/88)

ABSTRACT

Space manipulators present several features uncommon to ground-based robots: they are highly flexible, often mobile, and have a degree of redundancy. As space robots become more complex, efficient algorithms are required for their simulation and control. The present study uses an order N algorithm, based on the Lagrangian approach and velocity transformations, to simulate the planar dynamics of an orbiting manipulator with arbitrary number of slewing and deployable flexible links. The relatively general formulation accounts for interactions between orbital, librational, slewing, deployment, and vibrational degrees of freedom, and thus is applicable to a large class of manipulator systems of contemporary interest. Validity of the formulation and computer code is established through verification of energy conservation and comparison with particular cases reported by other investigators. A parametric analysis of the system dynamics is carried out. Several factors are considered: initial disturbances, variation of system parameters, number of manipulator links, and maneuver profiles. The study suggests significant coupling between the rigid body motion and structural vibrations. It was found that the system's flexibility can significantly affect the manipulator's performance. A nonlinear controller based on the Feedback Linearization Technique is developed to regulate the rigid degrees of freedom. A linear quadratic regulator is designed to suppress the manipulator and platform vibrations.

TABLE OF CONTENTS

LIST OF SYMBOLS

$\mathbf{A}, \mathbf{B}$	state-space representation of the flexible subsystem, Eq. (5.21)
C_i^J	equivalent viscous damping coefficient for the ith joint
$C_{u,i}^L, C_{v,i}^L$	equivalent viscous damping coefficients for the longitudinal and transverse modes of vibration for the ith body (link), respectively
$\vec{d}_i$	translation of the frame F_i from the tip of the (i^{th} - 1) body
$\vec{D}_i$	inertial position vector to the frame F_i
dm_i	mass of the infinitesimal element located on the ith body
$\vec{e}_i$	displacement of F_i caused by the elastic deformation of the (i^{th} - 1) body
EA_i	product of the Young's modulus of the ith body with its cross-sectional area
EI_i	flexural rigidity of the ith body
$\vec{f}_i(\vec{r}_i)$	displacement of the mass element located at $\vec{r}_i$ due to body flexibility
$\mathbf{F}$	vector containing the terms associated with the centrifugal, Coriolis, gravitational, elastic, and internal dissipative forces, Eq. (1.1)
F_0	inertial reference frame
F_i	reference frame attached to the ith body
$\mathcal{F}_i$	force provided by the linear actuator responsible for the deployment and retrieval of the ith body
F_r	orbital reference frame
$\vec{g}_i$	position of the ith frame relative to the (i^{th} - 1) frame
h	altitude of the system
$\mathbf{I^n}$	$n \times n$ identity matrix

J_{a_i}	moment of inertia of the actuator located at the ith joint
K_i	torsional stiffness of the ith joint
$\mathbf{K_p}, \mathbf{K_v}$	diagonal control matrices containing the proportional and derivative gains, respectively
l_i	length of the ith body
LH, LV	local horizontal and local vertical, respectively
m_{a_i}	mass of the actuator located at the ith joint
m_i	mass of the ith body
$\mathbf{M}$	coupled system mass matrix
$\tilde{\mathbf{M}}$	decoupled system mass matrix
$\tilde{\mathbf{M}}_\mathbf{i}$	decoupled mass matrix of the ith body
$\mathbf{M_r}, \mathbf{F_r}$	values taken by $\mathbf{M}, \mathbf{F}$ when the bodies are taken to be rigid
n_a	number of system actuators
n_c	number of system constraints
n_p	number of generalized coordinates describing the dynamics of the platform
n_u	number of generalized coordinates describing the dynamics of each unit
N	number of bodies (i.e. platform and manipulator units) in the system
$O(N)$	order N
$\mathbf{P^c}$	matrix assigning the Lagrange multipliers to the constrained equations
$\mathbf{q}$	set of generalized coordinates leading to the coupled mass matrix $\mathbf{M}$
$\tilde{\mathbf{q}}$	set of generalized coordinates leading to the decoupled mass matrix $\tilde{\mathbf{M}}$
$\mathbf{q_c}$	controlled component of $\mathbf{q}$
$\mathbf{q_d}$	desired value of $\mathbf{q_c}$

$\tilde{\mathbf{q}}_\mathbf{i}$	set of generalized coordinates associated with the ith body, leading to the decoupled mass matrix $\tilde{\mathbf{M}}_\mathbf{i}$
$\mathbf{q_s}$	specified component of $\mathbf{q}$
$\mathbf{q_u}$	uncontrolled component of $\mathbf{q}$
$\mathbf{Q}$	vector containing the external nonconservative generalized forces
$\mathbf{Q^d}$	matrix assigning inputs to the actuated variables
$\mathbf{Q_{LQR}}$	LQR state weighting matrix
r, s	number of modes considered for the elastic deformation of the ith body in the longitudinal and transverse directions, respectively
r_o	instantaneous distance of the platform's center of mass from the inertial reference frame F_0
$\vec{r}_i$	position vector of the elemental mass dm_i with respect to F_i
$\vec{R}_{a_i}$	inertial position vector of the actuator located at the ith joint
R_d	Rayleigh dissipation function for the whole system
$\vec{R}_{dm_i}$	inertial position vector to the mass element dm_i located on the ith body
$\mathbf{R}, \mathbf{R^C}, \mathbf{R^V}$	transformation matrices relating $\dot{\tilde{\mathbf{q}}}$ and $\dot{\mathbf{q}}$, Eqs. (2.57) and (2.61)
$\mathbf{R_{LQR}}$	LQR input weighting matrix
t	time
T	total kinetic energy of the system
T_0, T_1	torques provided by control momentum gyros for attitude control and vibration suppression, respectively
$\mathbf{T_i}$	Rotation matrix mapping F_0 onto F_i
T_i	torque provided by the slew-actuator located at the ith joint
$\mathbf{u}$	vector containing the FLT control inputs
$\mathbf{u_L}$	vector containing the LQR control inputs

u_i, v_i	longitudinal and transverse components of $\vec{f_i}$, respectively
V_e	total strain energy of the system
V_g	total gravitational potential energy of the system
x_i, y_i	cartesian components of $\vec{r_i}$
$\mathbf{x_L}$	state vector for the flexible subsystem

Greek Symbols

α_i	rotation of the frame F_i caused by the control action of the actuator located at the ith joint
β_i	rotation of F_i caused by the elastic deformation the ith joint
γ_i	rotation of the ith frame relative to the (i^{th} - 1) frame
δ_i	vector containing the time dependent generalized coordinates describing the elastic deformation of the ith body
$\Delta\tau$	time taken for maneuver
η_i	inertial orientation of the actuator rotor on the ith joint
θ	true anomaly of the system
λ_{ij}	eigenvalue corresponding to the jth vibrational mode of the ith body
Λ	vector containing the Lagrange multipliers
μ	Earth's gravitational parameter
ξ_i	rotation of F_i caused by the elastic deformation the (i^{th} - 1) body
τ	time from start of maneuver
$\Phi_i(x_i, l_i)$	matrix containing spatially varying shape functions for the ith body
ψ	platform's pitch angle
ψ_i	inertial orientation of the frame F_i

A dot above a character refers to differentiation with respect to time.

An arrow above a character indicates a two-dimensional position vector.

A boldface character denotes a vector or matrix quantity.

Subscripts 'p', 's', and 'd' refer to the platform, slewing link and deployable link, respectively.

LIST OF FIGURES

ACKNOWLEDGEMENT

I wish to thank Professor V.J. Modi for his guidance and insight throughout my graduate studies. He brought a philosophical perspective on a number of technical and non-technical issues which was greatly appreciated.

Thanks should also be extended to my colleagues, most notably Mr. Spiros Kalantzis, Dr. Satyabratha Pradhan, Dr. Sandeep Munshi, Mr. Yuan Chen, Mr. Mark Chu, Mr. Gary Lim, and Dr. Mae Seto. They not only facilitated my work through numerous technical discussions and suggestions, but also provided me with a friendly and intellectually challenging environment which made my stay in Vancouver a memorable one.

A note of appreciation is due to Dr. A.K. Misra (McGill University, Canada), who introduced me to space dynamics and inspired me to pursue graduate studies in this field at the University of British Columbia.

This investigation was supported by the Natural Sciences and Engineering Research Council of Canada and by the Canadian Space Agency.

1. INTRODUCTION

1.1 Preliminary Remarks

Robotic systems have been used for space exploration as early as the 1960's [1]. From 1966 to 1968, the unmanned Surveyor spacecrafts landed on the lunar surface and used a rudimentary manipulator arm to dig trenches and collect soil samples. The versatility of space robots was demonstrated during the Surveyor 7 mission, when the manipulator was used to nudge open an instrument which had failed to deploy automatically. In 1970 and 1973, the Soviet Lunakhod rovers surveyed large areas of the moon and used deployable arms to lower instruments to the surface. In 1976, the Viking landers used robotic manipulators in order to collect and process martian soil samples.

Robotic systems have not only been used for planetary exploration, but also to augment the capabilities of astronauts in orbit. For that purpose, the NASA space shuttles are equipped with a Remote Manipulator System (RMS), which is shown in Figure 1-1(a). Over the past 15 years, the RMS has performed a broad range of services. On many occasions, it has served as a platform for astronauts. In addition, it has been used for satellite deployment; retrieval of malfunctioning spacecraft for repair; positioning of experimental modules; and even for knocking a block of ice from a clogged waste-water vent that might have endangered the Shuttle upon reentry [2].

More recently, Canada designed a complex robotic manipulator for the proposed International Space Station: the Mobile Servicing System (MSS), which comprises the Space Station Remote Manipulator System (SSRMS) and the Special Purpose Dextrous Manipulator (SPDM). This robotic system is illustrated in Figure 1-1(b). The MSS will play an important role in the construction, operation, and maintenance of the space station [3 - 5]. Furthermore, the MSS will assist the Space Shuttle during docking maneuvers; handle cargo; assemble, release, and retrieve satellites; and serve

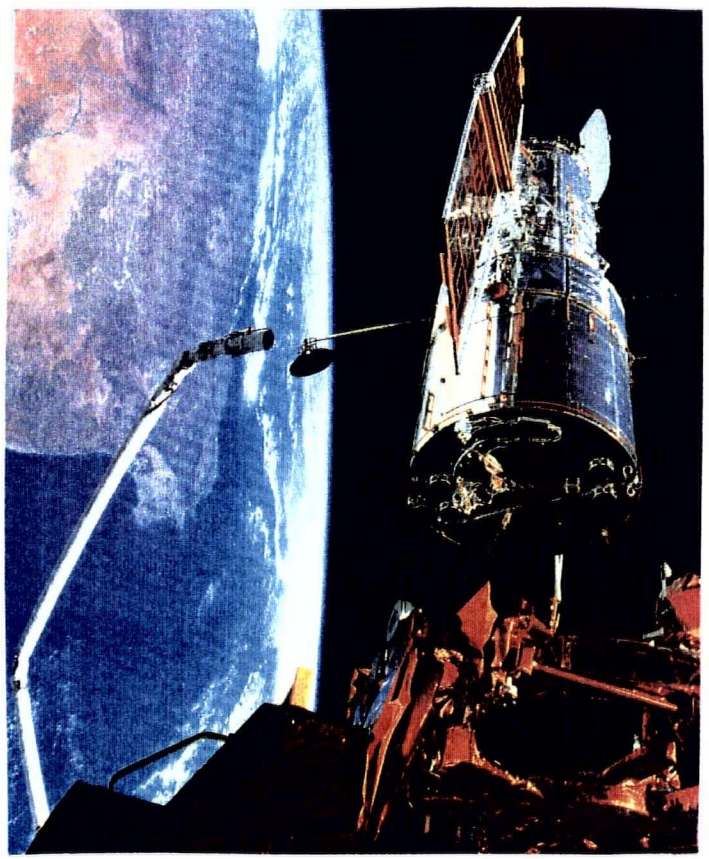

(a)

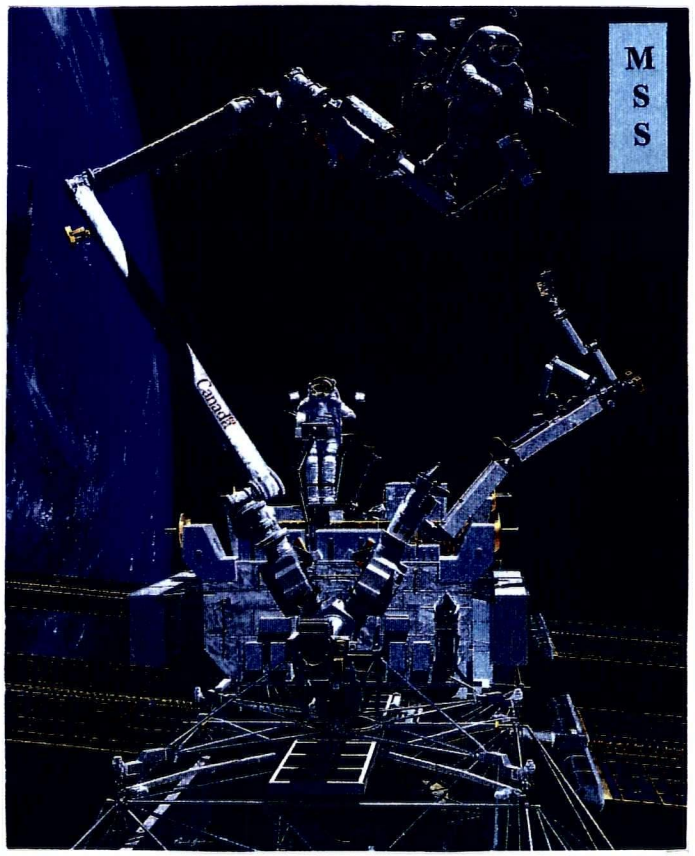

(b)

Figure 1-1 Two examples of space manipulators: (a) the Space Shuttle based Remote Manipulator System releasing the Hubble Space Telescope in April 1990; (b) the proposed Mobile Servicing System (MSS) on the International Space Station.

as a mobile platform for the astronauts during extravehicular activities.

Numerous other space robots have been proposed or are currently being developed. For instance, the American Extravehicular Activity Helper/Retriever (EVAHR) and Ranger Telerobotic Flight Experiment, as well as the Japanese ETS-VII, are examples of free-flying telerobotic systems which will be used for satellite inspection, servicing, and retrieval [6,7].

In brief, past missions have demonstrated the considerable contribution of robotic systems during space activities, and suggest robots will continue to play an important role in future missions. Clearly, robots provide a safer, and comparatively inexpensive, alternative to manned missions, as diverse as space walks and planetary exploration. With this as background, the thesis focuses on the dynamics and control of a rather versatile flexible manipulator based on an orbiting flexible platform.

1.2 A Brief Survey of the Relevant Literature

The literature review begins by summarizing the main characteristics of space manipulators and highlights the differences between robotic manipulators operating in space and those based on the ground. This is followed by a brief review of the literature more directly related to the present study aimed at the dynamics of space robotic systems and their efficient formulation. Finally, strategies proposed for the control of space-based manipulators are briefly touched upon.

1.2.1 Characteristic features of space-based manipulators

Robotic manipulators based on an orbiting platform are significantly different from their ground-based counterparts (Figure 1-2). Firstly, they operate in a microgravity environment, where the environmental torques produced by the gravity gradient, magnetic field, and solar radiation can become important [8]. Furthermore, the large temperature variations experienced in outer space can also have a significant

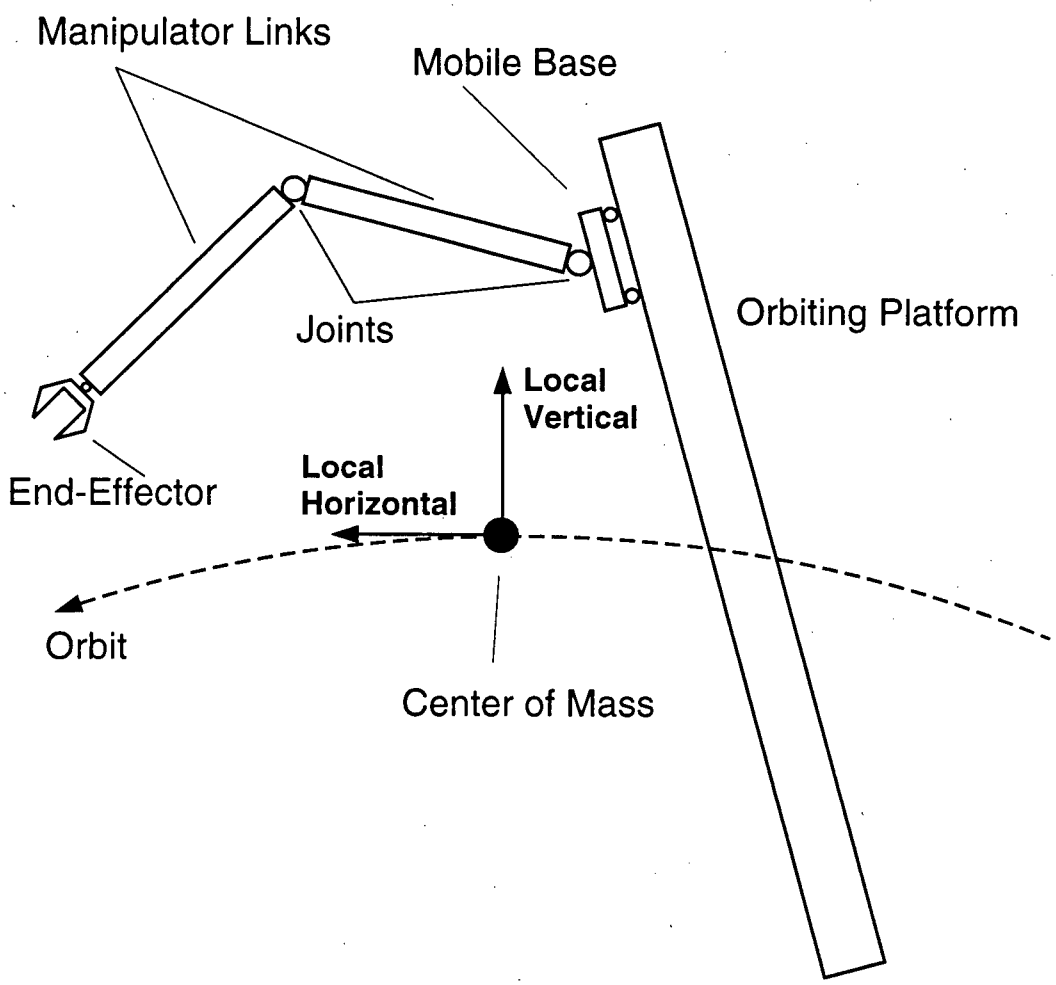

Figure 1-2 Schematic diagram of a space-based robotic manipulator.

impact on the dynamics and control of such systems [9,10].

Secondly, the base (platform) supporting the manipulator negotiates a trajectory in space. In addition, the motion of the manipulator and of its supporting base are coupled [11]. Therefore, manipulator maneuvers can modify the attitude of the base. On the other hand, the libration of the system can also affect the performance of the manipulator.

Thirdly, the links of space manipulators tend to be longer, lighter, and consequently, highly flexible. The manipulator can handle payloads with a mass orders of magnitude greater than its own [12]. Moreover, the supporting base can also be highly flexible, as is the case for the proposed Space Station [13]. The combination of these factors can result in large structural vibrations.

Finally, space robotic systems operate at locations where repair is difficult. Therefore, a level of system redundancy needs to be incorporated in order to cope with possible failure [14]. This implies a greater number of degrees of freedom than required for any given task. The redundancy is also important for obstacle avoidance, as well as for the optimization of given performance indices. Furthermore, the remote location of the system with reference to Earth introduces long transmission delays, which reached around seven seconds during the ROTEX teleoperation experiment [15].

In view of these important differences, the study of space manipulators cannot rely solely on the literature developed for ground-based systems. As robotic manipulators gain more importance in space operations, it is becoming imperative to understand their distinctive dynamics and control characteristics.

1.2.2 Dynamics of space-based manipulators

Space manipulators, as well as large flexible space structures in general, have unveiled a new and challenging field of dynamics and control. Over the years, a large

body of literature has evolved, which has been reviewed quite effectively by a number of authors including Meirovitch and Kwak [16], Roberson [17], Likins [18], as well as Modi *et al.* [19 - 21]. Dubowski and Papadopoulos have discussed the important problems associated with the dynamics and control of space robots and reviewed the advances made in this field [22]. They concluded that a thorough understanding of the fundamental dynamics of these systems would result in effective solutions to their control problems. For this purpose, they introduced the concept of "virtual manipulator" to describe the dynamics of space robots. Other authors have also emphasized the need for realistic dynamic modeling for the precise and accurate control of space robotic systems [23,24]. The need for accurate mathematical models is further justified by the prohibitive cost of conducting dynamic experiments in orbit and the virtual impossibility of simulating the space environment on the ground.

The dynamics of space manipulators have received considerable attention lately. Dynamic simulation codes, such as DISCOS [25] and *treetops* [26], are publicly available for multibody systems consisting of rigid and flexible components. However, the inherent limitations of these software have prompted several researchers to develop their own computer codes.

Pascal developed a simplified model for a flexible space manipulator based on a servicing satellite [27]. She then used this model to study the dynamics and control of the robot while grasping another satellite. Chan investigated the planar dynamics of a two-link revolute manipulator located on a base free to translate on a space platform [28]. While flexibility effects were included in the manipulator links and joints, the platform was assumed to be rigid. Mah derived the equations of motion of a general flexible multibody system in chain topology [29]. He used this model to study the dynamics of a general manipulator based on an orbiting platform, which were both flexible. The studies mentioned so far focused on open-chain configurations. On the other hand, Lilly and Bonaventura developed a generalized formulation for the

simulation of space robots in either open- or closed-chain configuration [30].

Xu and Shum investigated the coupling between the motion of the manipulator and supporting platform [11]. They proposed a coupling factor representing the degree of dynamic interactions between the two. It was suggested that the coupling factor may serve as a performance index for optimizing robot configuration and location to reduce base motion. Papadopoulos focused on large payload manipulation [31]. The effects of satellite capture, berthing, docking, and other types of impacts on the dynamics of the platform/manipulator system have also recently received a considerable amount of attention [32-34].

Several space structures feature deployment capabilities. For instance, a large solar array was deployed from the Space Shuttle cargo bay during the Solar Array Flight Experiment (SAFE), in September 1984. Cherchas [35], as well as Sellappan and Bainum [36] studied the deployment dynamics of extensible booms from spinning spacecraft. Modi and Ibrahim developed the equations of motion for a system with multiple deployable booms, with considerable emphasis on the proposed Waves In Space Plasma (WISP) experiment [37]. More recently, Marom proposed a two-link, deployable manipulator and investigated its planar dynamics and control [38]. Here, the manipulator links were taken to be rigid, however, the joint flexibility was accounted for. Hokamoto *et al.* extended this model by accounting for an arbitrary number of flexible links [39].

In the studies described above, the governing equations assume small bending with the elastic deformations modelled using admissible functions, whose spatial argument contain the time-varying length of the beam. On the other hand, Banerjee and Kane discretize the deploying/retracting boom into a number of rigid links connected by torsional springs [40]. The deployment of a beam is described by an increase in the number of links.

1.2.3 Order N multibody formulations

It is not sufficient for a mathematical model to be accurate in order to control space manipulators. The computation will likely have to be done in real-time, hence its efficiency is a key requirement.

The equations governing the dynamics of the robotic systems described above are highly nonlinear, nonautonomous, coupled, and can be expressed in the general form

$$\mathbf{M}(\mathbf{q},t)\ddot{\mathbf{q}} + \mathbf{F}(\dot{\mathbf{q}},\mathbf{q},t) = \mathbf{Q}(\dot{\mathbf{q}},\mathbf{q},t), \tag{1.1}$$

where: $\mathbf{M}(\mathbf{q},t)$ is the system mass matrix; $\mathbf{q}$, the vector of the generalized coordinates; $\mathbf{F}(\dot{\mathbf{q}},\mathbf{q},t)$ contains the terms associated with the centrifugal, Coriolis, gravitational, elastic, and internal dissipative forces; and $\mathbf{Q}(\dot{\mathbf{q}},\mathbf{q},t)$ represents generalized forces, including the control inputs. Eq. (1.1) describes the inverse dynamics of the system. For simulations, forward dynamics of the system is required, and Eq. (1.1) must be solved for $\ddot{\mathbf{q}}$,

$$\ddot{\mathbf{q}} = \mathbf{M}^{-1}(\mathbf{Q} - \mathbf{F}). \tag{1.2}$$

The solution of these equations of motion generally requires $O(N^3)$ arithmetic operations, where N represents the number of bodies considered in a study. In other words, the number of computations required by an $O(N^3)$ algorithm will vary with the cube of the number of bodies. Clearly, the computational cost can become prohibitive for a large N. Hence, development of an order N algorithm, $O(N)$, where the number of arithmetic operations increases linearly with the number of bodies in the system, has been the focus of several studies in the field of multibody dynamics [41-50]. Such algorithms reduce the computational time and memory requirements considerably, making real-time applications possible.

The Newton-Euler formulation has been used extensively in the past for ground-based robots [41]. It is inherently of $O(N)$, and the computational efficiency has

made it an attractive choice for dynamical simulation studies and control of robots. Although the traditional Lagrange formulation is of $O(N^4)$, Hollerbach has proposed a recursive $O(N)$ Lagrangian formulation for the inverse dynamics of rigid multibody systems [42]. It is not as efficient as its Newton-Euler counterpart, yet it makes real-time applications possible with the Lagrangian approach. It should be noted that the forward dynamics of the same model are not of $O(N)$. Keat has used a velocity transformation approach to obtain an $O(N)$ algorithm describing the dynamics of flexible multibody systems [43]. Rosenthal has based his $O(N)$ formulation, which considers rigid bodies, on Kane's equations [44]. Suzuki and Kojima applied this approach to analyze the deployment of a spacecraft panel [45]. Banerjee extended Rosenthal's algorithm in order to consider deployment and retrieval of beams with large bending and rotation [46]. Jain and Rodriguez used the filtering and smoothing approach of optimal estimation, and introduced spatial operators to obtain a recursive $O(N)$ formulation for flexible multibody systems [47]. On the other hand, Bae and Haug adopted an approach based on the virtual work to the same end [48].

Most $O(N)$ formulations reported in the literature are recursive: they rely on a series of forward and backward passes along the chain of bodies in order to compute the accelerations and forces in the system. However, Kurdila *et al.* have proposed a nonrecursive formulation, based on the range space method, which has its basis in finite element solution procedures [49]. The main advantage of a nonrecursive formulation is that the computations for each body can be executed independently, making it suitable for parallel processing. Pradhan *et al.* have introduced another nonrecursive formulation procedure for flexible multibody systems, which uses the Lagrangian approach, in conjunction with two velocity transformations [50]. The velocity transforms decompose the system mass matrix into a product of matrices. The inversion of this new form of the mass matrix is computationally far less intensive. As most arithmetic operations in Eq. (1.2) arise from the inversion of the mass matrix,

the resulting algorithm is of $O(N)$ and hence considerably more efficient. Fijany *et al.* have proposed another efficient formulation for the computation of forward dynamics, which is based on two parallel O(log N) algorithms [51].

1.2.4 Control of space-based manipulators

In the recent past, experiments have been carried out in orbit to investigate the dynamics and control of robots, as well as large flexible structures. The goal of the Spacecraft Control Laboratory Experiment (SCOLE) was to control a reflector antenna supported by a beam, located in the Space Shuttle cargo bay, during slewing maneuvers [52]. Although tests were carried out on the ground, the experiment was not flown. The German ROTEX experiment took place during the Spacelab II mission: A robotic manipulator, located on the Shuttle Orbiter, was teleoperated from the ground to conduct various maneuvers, including the capture of floating objects [53].

As stated previously, precise and efficient dynamical models are required for the control of space robotic systems. The attitude of the space platform, the motion of the manipulator links, the location of the manipulator base along the platform, as well as the vibration of the various structural components must all be controlled to an acceptable level for successful completion of a given mission.

Relatively coarse control of the space platform's attitude can be achieved even by use of the environmental forces such as Earth's gravity gradient and magnetic field [8]. For instance, the "long" axis (i.e. the axis of minimum moment of inertia) of the platform may be aligned with the local vertical direction. This stable equilibrium configuration can be used to advantage. However, normally thrusters and Control Momentum Gyros (CMG) are used to regulate the attitude of the system [54,55]. Librational control of the platform by re-orienting the manipulator has been suggested [56]. However, this method is limited to cases where the mass of the manipulator is

significant compared to that of the platform.

As mentioned earlier, the orbiting platform and the manipulator links can be highly flexible. Moreover, the compliance of the actuator shafts and transmission drives may lead to significant flexibility in the joints. Undesirable vibrations can arise and the accuracy of the manipulator can be severely affected. Consequently, control of manipulators with flexible links, flexible joints, or both, have received considerable attention lately [57-59]. Structural damping, as well as other passive dampers can reduce the amount of vibrations experienced. However, active vibration suppression is often desirable. Through adequate path planning of the manipulator joints, excessive elastic deformations, as well as attitude disturbances can be avoided. It has been suggested that the extra degrees of freedom provided by redundant manipulators could be used to advantage in isolating the base from disturbances arising from the manipulator motion [60-62]. In fact, Hanson and Tolson have shown that the base reaction could be decreased by as much as 90% with such schemes [62]. Vibration of the manipulator links and joints can also be reduced by applying compensating torques at the revolute joints [28]. The use of distributed piezoelectric films or lumped piezoelectric elements acting as colocated sensor/actuator systems has also been suggested for vibration control [63].

Several strategies are available for the control of space robotic systems. Often, simple proportional-derivative (PD) feedback control schemes are adequate [64]. The computed torque technique has been widely used for ground-based robots [65]. The Feedback Linearization Technique (FLT) has been proposed for the attitude control of the platform, as well as for the control of the rigid motion of the manipulator [66]. Optimal control has also received considerable attention. Here, position and velocity errors, actuator outputs, structural vibration, as well as various other cost functions are minimized throughout the operation of the system. When all state variables are available, a Linear Quadratic Regulator (LQR) may be used for optimal control

[67,68]. If these quantities are not directly available, but are observable, a Linear Quadratic Gaussian (LQG) controller has been proposed [69,70]. The field is wide open to other control procedures including adaptive, knowledge-based and fuzzy logic strategies, to mention a few.

1.3 Scope of the Investigation

In the present investigation, an efficient mathematical model is developed for studying the inplane dynamics and control of a flexible, space-based manipulator (Figure 1-3). The relatively general nature of the model considers a serial manipulator with an arbitrary number (N) of flexible units. Each unit is free to rotate, i.e. *slew*, relative to the other units, and is capable of changing is length, thus is *deployable*.

The formulation provides for arbitrary variation of geometric, inertia, stiffness, and damping characteristics along the manipulator. In the present study, manipulator units are taken to be interconnected through revolute joints. However, combinations of revolute and prismatic joints can also be considered quite readily. The model also accounts for flexibility and dissipation at the manipulator joints. The manipulator is mounted on a mobile base which is free to translate along an orbiting space platform. The coupling effects between the orbital, librational, slew, deployment, and vibrational degrees of freedom, associated with the platform and manipulator, are also taken into account. An essential feature of the model is the time-varying length of each unit, with prismatic joints providing the deployment degrees of freedom. In other words, each of the manipulator units can be deployed and retrieved independently, thereby changing the librational and vibrational characteristics of the overall system. Note, the model considered here is rather general and is applicable to a large class of mobile flexible manipulators based on an orbiting space platform.

In Chapter 2, the governing equations of motion for this system are derived using the *O(N)* approach proposed by Pradhan *et al.* [50]. The formulation is extended

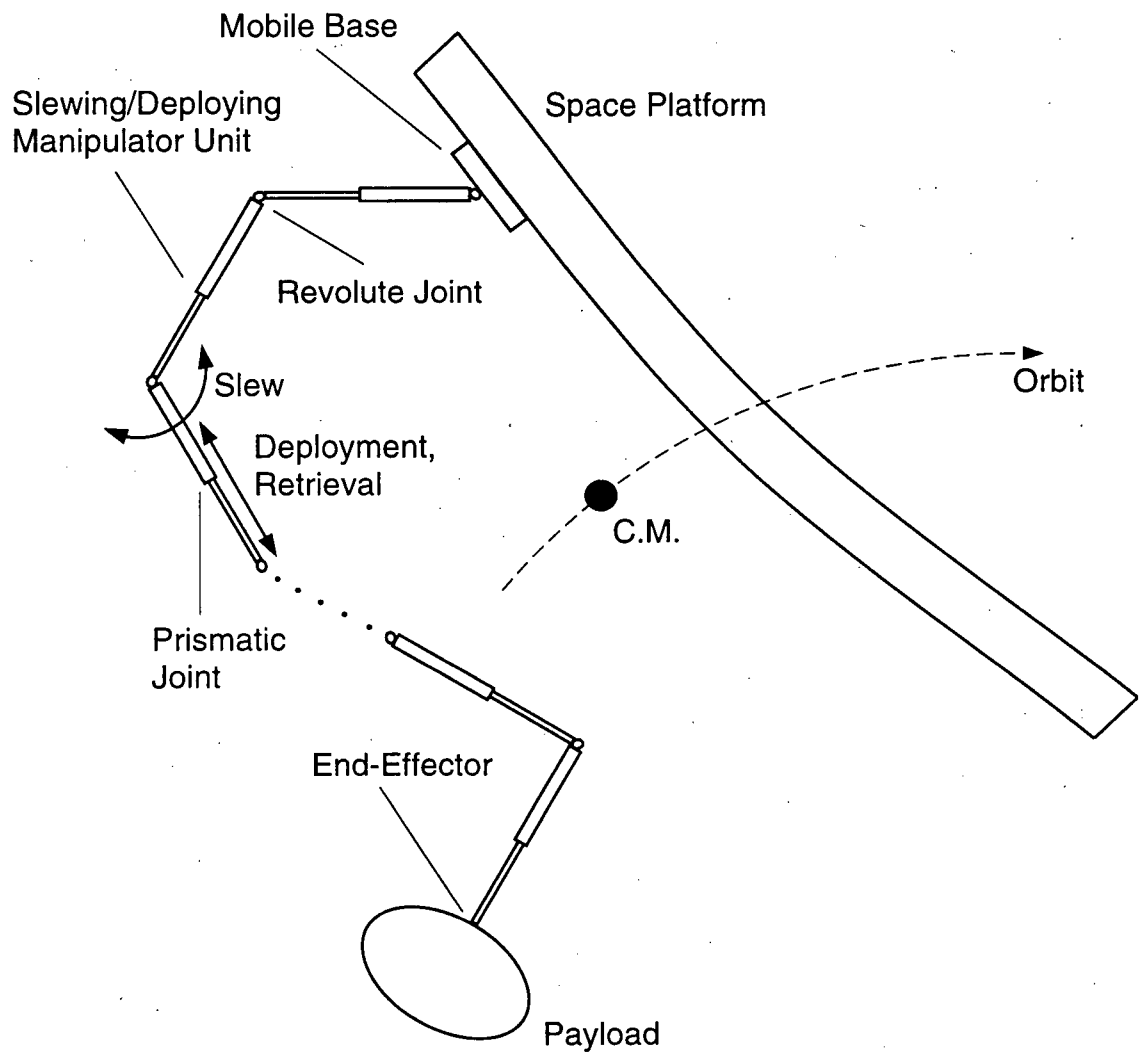

Figure 1-3 A schematic diagram of the mobile flexible deployable manipulator, based on a space platform, considered for study.

to include cases where the length of each body is taken as a generalized coordinate, and to account for flexible joints. The system kinematic equations are first obtained, followed by a discussion on the O(N) approach used. Expressions for the kinetic, gravitational and strain energies, as well as for the Rayleigh dissipation function and generalized forces are then derived, and Lagrange's principle applied to obtain the equations of motion. An explanation on the use of Lagrange multipliers to incorporate the constraint forces into the model concludes the chapter.

Chapter 3 discusses the implementation of the equations of motion into a FORTRAN code. The structure of the program is presented and computational issues are discussed. Validity of the formulation and computer code are checked through the conservation of energy for a few test-cases. When relevant, results are also compared with those reported in the literature for particular cases.

A comprehensive parametric study is presented in Chapter 4. The effects of various sets of initial disturbances, parameter combinations, manipulator maneuvers, and manipulator configurations are assessed. Some combinations of parameters which lead to unacceptable dynamical behavior are identified.

Control strategies are developed in Chapter 5 in order to regulate the dynamical behavior of the system under study. The performance of a nonlinear control strategy, based on the Feedback Linearization Technique (FLT), is assessed in regulating the attitude of the platform, as well as the rigid-body maneuvers of the manipulator. A Linear Quadratic Regulator (LQR) is proposed for active vibration suppression.

Finally, Chapter 6 summarizes the important findings of this thesis, outlines its contributions, and discusses future avenues of investigation.

2. FORMULATION OF THE PROBLEM

2.1 Preliminary Remarks

The present chapter develops the equations of motion for a space-based robotic system, schematically presented in Figure 1-3, using a rather general model described earlier. Essentially, it consists of an orbiting beam-type platform with a translating base supporting a manipulator formed of an arbitrary number of flexible modules (*units*). Each unit comprises two links: One free to slew with a revolute joint at one end, while the other is permitted to deploy (and retrieve) through a prismatic joint at the end of the first link. The second link carries a revolute joint at the other end for connection to the next unit (Figure 1-3). The links and joints are considered flexible.

As can be anticipated, the governing equations of motion turn out to be extremely lengthy, highly nonlinear, nonautonomous, and coupled. Obviously, interactions between orbital mechanics, librational motion, structural flexibility, and manipulator maneuvers would be indeed quite complex. To get better appreciation of the coupling effects, it was purposely decided to focus attention on planar dynamics of the system. Thus all the motions are confined to the orbital plane.

In the following, the kinematic equations of the system are developed first. Issues pertaining to the modeling of body flexibility are examined. The kinetic energy of the system is then derived. Two velocity transformations are introduced in order to arrive at new forms of the kinetic energy. The derivation of expressions for the gravitational and strain potential energies follows. Energy dissipation mechanisms are presented as well, and external generalized forces are discussed. The Lagrangian principle is then used to derive the equations of motion. The final section examines the use of Lagrange multipliers when some of the degrees of freedom are constrained.

2.2 Kinematics of the System

A serial manipulator, supported by a space platform, can essentially be represented as an open chain of flexible bodies as shown in Figure 2-1. The first body (body 1) represents the space platform, while the remaining bodies (bodies 2 to N) symbolize the units of the manipulator. Therefore, the second body represents the first unit, while the body N corresponds the (N^{th} - 1) unit. Note that the length of the bodies 2 through N can vary in time. Furthermore, each body can rotate and translate with respect to its neighbours.

2.2.1 Reference frames

The inertial reference frame F_0 is located at the center of mass of Earth. The x_0, y_0-plane defines the orbital plane and the z_0 axis corresponds to the orbit normal. The position and attitude of each body are described by assigning body-fixed frames to each element of the chain. Thus, the frame F_1 is located at the center of mass of the platform. For each of the remaining bodies, the associated body-fixed frame is attached to the joint at the base of the unit. In other words, the reference frame F_i is attached to the base of the ith body. Since the platform and manipulator units are beam-type bodies, the x_i axis is along the length of the beam; the y_i axis is perpendicular to the x_i direction, in the orbital plane; while z_i is parallel to the orbit normal. Note, for both the platform and manipulator units, the stiffness, damping, and inertia properties can vary along the x_i direction.

No orbital reference frame was defined at the center of mass of the complete system. For convenience, it was decided to describe explicitly the orbital motion of the center of mass of the first body instead of that of the center of mass of the entire system. Since the first body will usually represent a space platform, it will normally constitute most of the mass of the system. Hence, the center of mass of the entire system will lie close to the platform's center of mass. Nevertheless, it should

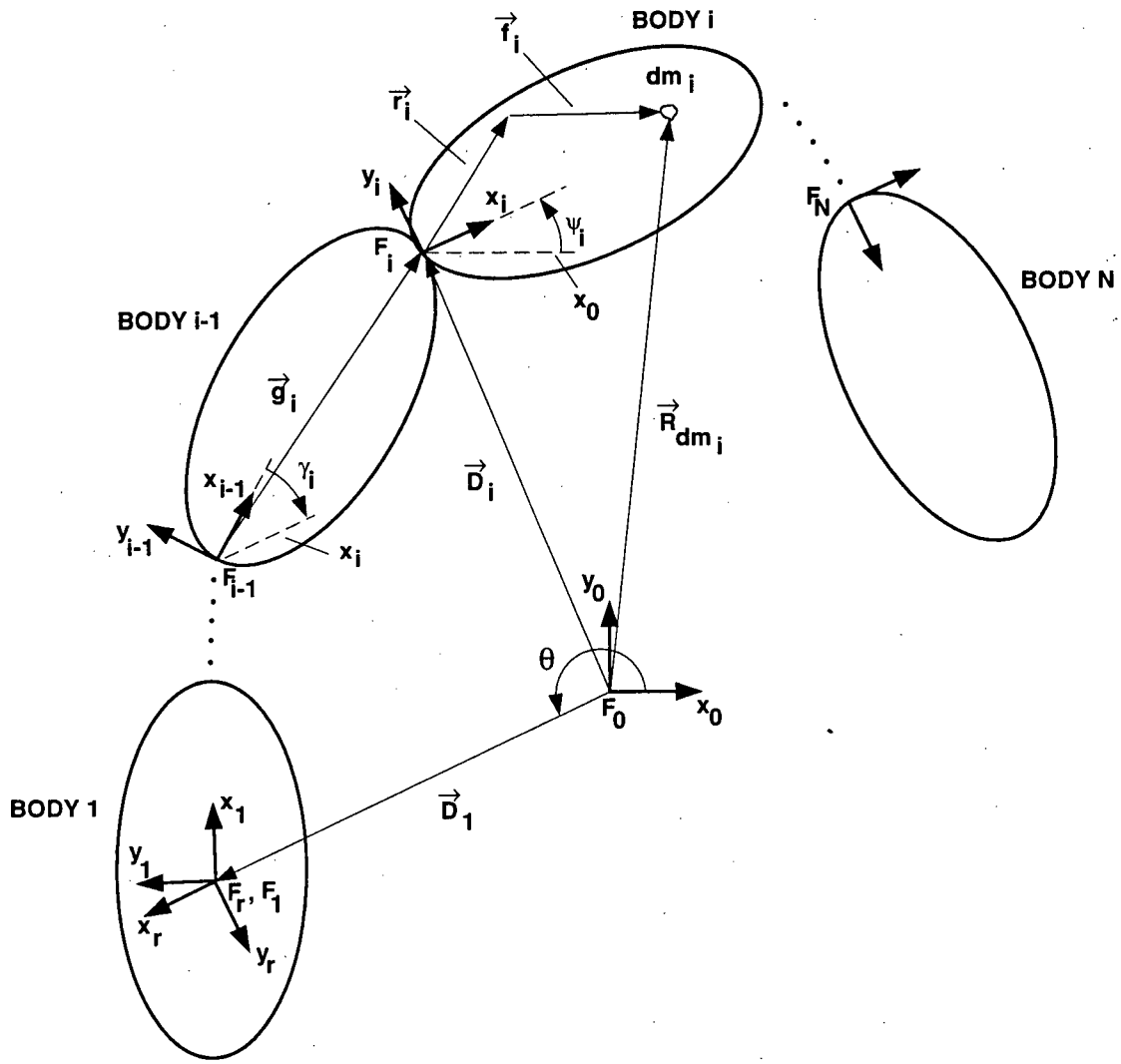

Figure 2-1 Schematic diagram of a multibody system in chain topology with coordinate frames and vectors used to define an elemental mass. Note, each body is composed of two links, one free to slew while the other is deployable.

be emphasized that the effects of the motion of the system's center of mass, due to the rigid and flexible degrees of freedom of all bodies, are accounted for in this formulation.

Finally, an orbital frame F_r is attached to the center of mass of the platform. The x_r direction defines the local vertical; the y_r axis, the local horizontal; and the z_r axis, the orbit normal. This reference frame is useful in describing the attitude of the system.

2.2.2 Position vectors

The position of an infinitesimal mass element dm_i, located on the ith body, can be described with respect to the inertial frame as

$$\vec{R}_{dm_i} = \vec{D}_i + \mathbf{T}_i\{\vec{r}_i + \vec{f}_i(\vec{r}_i)\}. \tag{2.1}$$

Here $\vec{D}_i$ defines the inertial position of the origin of the ith body-fixed frame, with

$$\vec{D}_i = \begin{bmatrix} D_{ix} \\ D_{iy} \end{bmatrix}. \tag{2.2}$$

$\mathbf{T_i}$ corresponds to the rotation matrix which maps the components of $\vec{r}_i$ and $\vec{f}_i(\vec{r}_i)$, expressed in terms of the body-fixed coordinates, onto inertial coordinates. It is defined as

$$\mathbf{T}_i = \begin{bmatrix} \cos\psi_i & -\sin\psi_i \\ \sin\psi_i & \cos\psi_i \end{bmatrix}, \tag{2.3}$$

where ψ_i describes the orientation of the frame F_i and corresponds to the angle formed between the x_i and x_0 axes. $\vec{r}_i$ is the position vector of the elemental mass dm_i with respect to F_i,

$$\vec{r}_i = \begin{bmatrix} x_i \\ y_i \end{bmatrix}. \tag{2.4}$$

Finally, $\vec{f}_i(\vec{r}_i)$ represents the elastic displacement of the mass element located at $\vec{r}_i$ due to the flexibility of the body,

$$\vec{f}_i(\vec{r}_i) = \begin{bmatrix} u_i \\ v_i \end{bmatrix}. \tag{2.5}$$

The following section addresses the question of discretization to describe elastic deformations of the bodies.

2.2.3 Modeling of flexibility

The dynamics of an orbiting robotic system with rigid components can be described by a set of ordinary differential equations. However, the space platform and manipulator units form a highly flexible system. The time dependent elastic deformations of such a system, with distributed parameters, require partial differential equations for their description. Furthermore, such continuous systems possess infinite degrees of freedom. Therefore, it is necessary to approximate the elastic deformation of the structure using ordinary differential equations with a finite number of generalized coordinates.

Finite element methods, or system modes approach, are commonly used for the discretization of the elastic deformation of spacecrafts with fixed or variable geometry [13]. Here, the structure is divided into grids or meshes. The continuous variables are thus represented as a number of discrete ones at the grid level. The accuracy of the approximation is improved by refining the mesh. This method offers the advantage of considering the integrated nature of the system. On the other hand, modeling structures involving slewing and deployment often proves to be difficult with this approach, as the system modes need to be updated.

The approach adopted in the thesis consists in dividing the system into components. The platform, as well as each of the manipulator units, are taken to be separate components. The vibration of each component is expressed in the form of a product of spatially varying shape functions (Φ_i) and time dependent generalized coordinates ($\delta_\mathbf{i}$). Thus, the longitudinal deformation (u_i) of the ith body is described by

$$u_i = \sum_{j=1}^{r} \phi_{ixj}\delta_{ixj}, \tag{2.6}$$

while the expression for the transverse elastic displacement (v_i) is

$$v_i = \sum_{j=1}^{s} \phi_{iyj}\delta_{iyj}. \tag{2.7}$$

In matrix form, the elastic deformation of the ith body can be written as

$$\begin{bmatrix} u_i \\ v_i \end{bmatrix} = \begin{bmatrix} \Phi_{ix} & 0 \\ 0 & \Phi_{iy} \end{bmatrix} \begin{bmatrix} \delta_{ix} \\ \delta_{iy} \end{bmatrix} = \Phi_i \delta_i, \tag{2.8}$$

where: $\Phi_{ix} = [\phi_{ix1}, \phi_{ix2}, \cdots, \phi_{ixr}]$; $\Phi_{iy} = [\phi_{iy1}, \phi_{iy2}, \cdots, \phi_{iys}]$; $\delta_{ix} = [\delta_{ix1}, \delta_{ix2}, \cdots, \delta_{ixr}]^T$; and $\delta_{iy} = [\delta_{iy1}, \delta_{iy2}, \cdots, \delta_{iys}]^T$. Thus, $\Phi_i \in \Re^{2\times(r+s)}$ and $\delta_i \in \Re^{(r+s)}$, where r and s are the number of modes considered in the longitudinal and transverse directions, respectively.

The selection of accurate shape functions often reduces the number of modes required for a given level of accuracy. In general, the shape functions used consist in admissible functions which correspond to the mode shapes of similar, though simpler, problems. This is known as the assumed mode method [71]. For the sake of generality, the formulation accounts for the longitudinal deformation of the bodies. However, this study focuses on the transverse displacements. Therefore, shape functions will not be specified for the longitudinal elastic displacements. However, it should be emphasized that they can be readily included in the formulation.

In the present case, the platform and manipulator units are assumed to behave as Euler-Bernoulli beams. This representation, which is valid for long slender beams, implies that the elastic deformation of the beam remains small and that the effects of rotary inertia, shear deformation, and higher order frequencies are negligible. The equations of motion for an Euler-Bernoulli beam are obtained by applying Newton's law to a differential beam element,

$$\frac{\partial^2}{\partial x^2}\left(EI\frac{\partial^2 v}{\partial x^2}\right) = -\rho\frac{\partial^2 v}{\partial t^2}, \tag{2.9}$$

where EI is the flexural rigidity of the beam and ρ is the mass per unit length. If EI

is taken to be constant and a solution of the form $v = \sum_j \phi_j(x)\delta_j(t)$ is assumed, the mode shapes $\phi_j(x)$ can be written as

$$\phi_j(x) = A_{1j}\sin\left(\frac{\lambda_j x}{l}\right) + A_{2j}\cos\left(\frac{\lambda_j x}{l}\right) + A_{3j}\sinh\left(\frac{\lambda_j x}{l}\right) + A_{4j}\cosh\left(\frac{\lambda_j x}{l}\right), \quad (2.10)$$

where l is the length of the beam; λ_j is the jth eigenvalue which, together with the coefficients A_{1j}, A_{2j}, A_{3j}, and A_{4j}, depends on the boundary conditions.

The boundary conditions model the effects of the other components and their appropriate selection can often be difficult. The standard boundary conditions provided in the literature (i.e. fixed, pinned, free, free with a tip mass, etc.) do not correspond exactly to the conditions encountered in the multibody system studied here. Meirovitch and Kwak proposed the use of quasi-comparison functions in order to alleviate partially this difficulty [72-74]. Each quasi-comparison function, taken alone as a shape function, satisfies neither the geometric nor the natural boundary conditions. However, a complete set of quasi-comparison functions satisfies both the geometric and natural boundary conditions. It has been shown that quasi-comparison functions can speed up convergence significantly compared to admissible functions. On the other hand, the convergence speed relies heavily on the choice of quasi-comparison functions used, and this choice remains somewhat arbitrary. Hence, for the sake of simplicity, only standard admissible functions are used in this thesis. Nonetheless, it should be emphasized that the desired level of accuracy can be achieved simply by increasing the number of modes used to model flexibility, irrespective of the choice of admissible functions.

With this in mind, the platform (i.e. body 1) is assumed to behave as a free-free Euler-Bernoulli beam. Therefore, the boundary conditions at both ends are zero shear and moment:

$$EI_1 \frac{\partial^2 v_1}{\partial x_1^2}\bigg|_{x_1=-\frac{l_1}{2}} = 0; \qquad EI_1 \frac{\partial^3 v_1}{\partial x_1^3}\bigg|_{x_1=-\frac{l_1}{2}} = 0;$$
$$EI_1 \frac{\partial^2 v_1}{\partial x_1^2}\bigg|_{x_1=\frac{l_1}{2}} = 0; \qquad EI_1 \frac{\partial^3 v_1}{\partial x_1^3}\bigg|_{x_1=\frac{l_1}{2}} = 0. \tag{2.11}$$

It should be noted that the mass of the manipulator is assumed not to affect the boundary conditions of the platform. The jth mode shape in the transverse direction (y) for the platform is then written as

$$\begin{aligned}\phi_{1yj}(x_1) =& \cos\lambda_{1j}\left(\frac{1}{2}+\frac{x_1}{l_1}\right) + \cosh\lambda_{1j}\left(\frac{1}{2}+\frac{x_1}{l_1}\right) \\ &- \frac{\cosh\lambda_{1j}-\cos\lambda_{1j}}{\sinh\lambda_{1j}-\sin\lambda_{1j}}\left\{\sin\lambda_{1j}\left(\frac{1}{2}+\frac{x_1}{l_1}\right) + \sinh\lambda_{1j}\left(\frac{1}{2}+\frac{x_1}{l_1}\right)\right\},\end{aligned} \tag{2.12}$$

where the eigenvalue λ_{1j} can be obtained from the transcendental equation

$$\cos\lambda_{1j}\cosh\lambda_{1j} = 1. \tag{2.13}$$

The first four modes of transverse vibration for a free-free Euler-Bernoulli beam are shown in Figure 2-2(a).

The units of the manipulator (bodies 2 to N) are modelled as cantilever beams with tip masses. Although each unit is made of two links, a single shape function is used for the unit, since its actual vibration profile is expected to be continuous in reality. The tip masses model the inertia of the payload, as well as that of the manipulator units which are supported by the unit considered. In other words, the jth body supports a point mass, located at its tip, which is equal to the total mass of $(N-j)$ units, plus that of the payload. Note, as the cantilever beam is used to model vibration, there is zero displacement and slope at its base, and zero moment at its tip. However, the shear force applied at the tip is nonzero, and is equal to the inertia force applied by the tip mass. The boundary conditions for this case can be

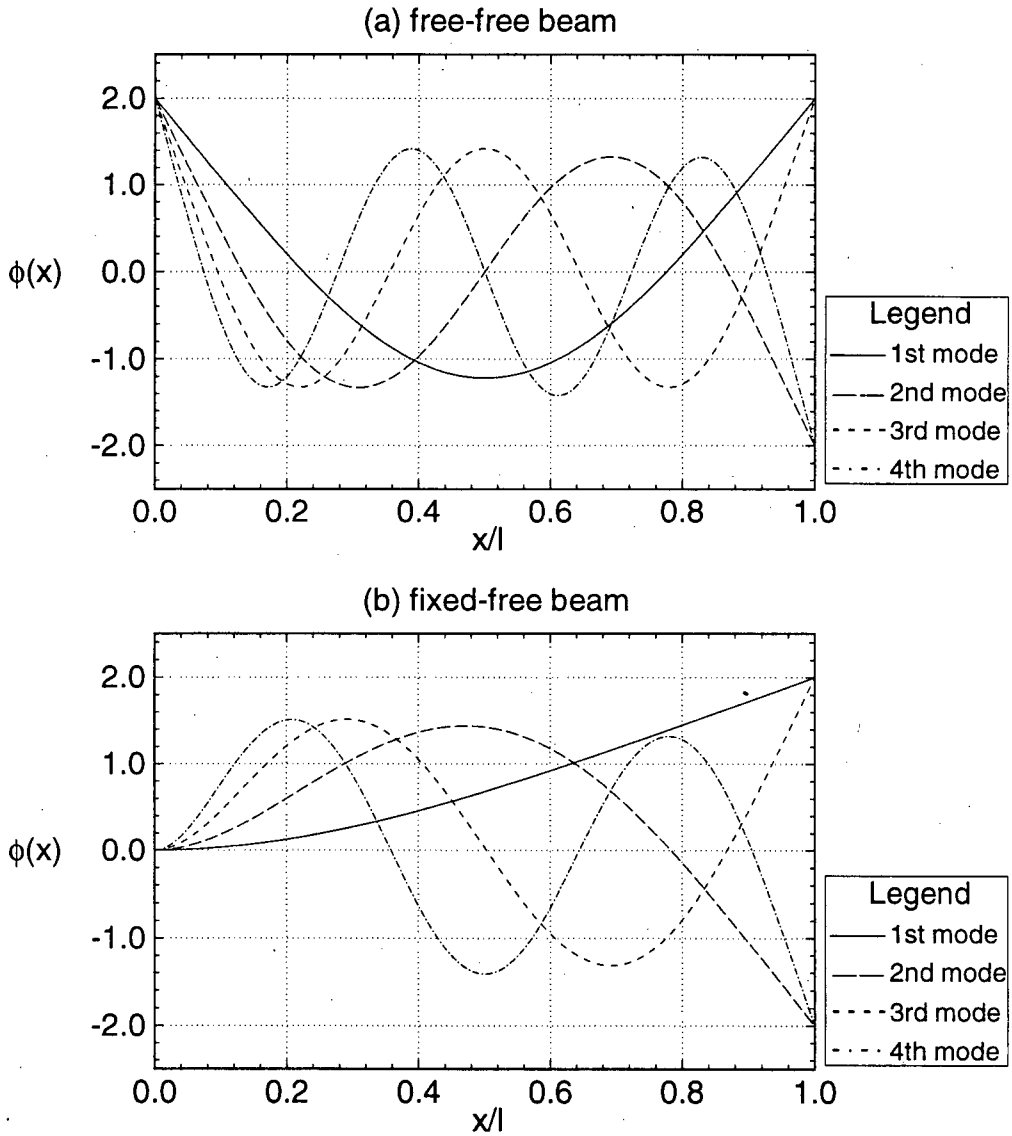

Figure 2-2 The first four mode shapes for: (a) free-free Euler-Bernoulli beam; (b) fixed-free Euler-Bernoulli beam.

summarized as:

$$v|_{x_i=0} = 0; \qquad \left.\frac{\partial v_i}{\partial x_i}\right|_{x_i=0} = 0;$$

$$i = 2, ..., N \tag{2.14}$$

$$EI_i \left.\frac{\partial^2 v_i}{\partial x_i^2}\right|_{x_i=l_i} = 0; \qquad EI_i \left.\frac{\partial^3 v_i}{\partial x_i^3}\right|_{x_i=l_i} = m_{ti}\frac{\partial^2 v_i}{\partial t^2};$$

where m_{ti} is the tip mass.

The jth mode shape in the y direction for the ith body is then written as

$$\begin{aligned}\phi_{iyj}(x_i, l_i) =& \sin\lambda_{ij}\left(\frac{x_i}{l_i}\right) - \sinh\lambda_{ij}\left(\frac{x_i}{l_i}\right) \\ &- \frac{\sin\lambda_{ij} + \sinh\lambda_{ij}}{\cos\lambda_{ij} + \cosh\lambda_{ij}}\left\{\cos\lambda_{ij}\left(\frac{x_i}{l_i}\right) - \cosh\lambda_{ij}\left(\frac{x_i}{l_i}\right)\right\},\end{aligned} \tag{2.15}$$

for $i = 2, ..., N$. The eigenvalue λ_{ij} can be obtained from the following transcendental equation,

$$\cos\lambda_{ij}\cosh\lambda_{ij} + 1 = \frac{m_{ti}}{\rho_i}\lambda_{ij}\{\sin\lambda_{ij}\cosh\lambda_{ij} - \cos\lambda_{ij}\sinh\lambda_{ij}\}, \tag{2.16}$$

where ρ_i is the linear mass density of the beam. The first four modes of transverse vibration for a fixed-free, i.e. with no tip mass, Euler-Bernoulli beam are shown in Figure 2-2(b). It should be pointed out that, because the length (l_i) of the manipulator units can vary with time, the shape functions described by Eq. (2.15) will also be time-dependent. Although the concept of discretization through application of admissible functions is approximate, it can be applied recognizing its limitations. Strictly speaking, modes are undefined for time-varying systems, as is the case during deployment and retrieval. However, over the years, researchers have successfully used modes for discretization in a variety of situations including deployment [35-37].

The eigenvalues λ_{ij} obtained from Eq. (2.13) and Eq. (2.16) are given in Appendix I. The first four modes in transverse vibration for a cantilever beam supporting several sizes of tip masses are also described in Appendix I. It is found that a tip mass has a negligible effect on the fundamental mode. For higher modes however, the ef-

fect becomes noticeable. Nonetheless, as mentioned earlier, the choice of mode shapes only influences the number of them required to model adequately the response.

2.2.4 Velocity vectors

Using the approach described in Section 2.2.3 to replace $\vec{f}_i(\vec{r}_i)$, Eq. (2.1) can now be rewritten as

$$\vec{R}_{dm_i} = \vec{D}_i + \mathbf{T}_i\{\vec{r}_i + \Phi_i\delta_i\}. \tag{2.17}$$

The inertial velocity of a mass element dm_i is obtained by taking the time derivative of Eq. (2.17) giving

$$\dot{\vec{R}}_{dm_i} = \dot{\vec{D}}_i + \mathbf{P}\mathbf{T}_i\dot{\psi}_i\{\vec{r}_i + \Phi_i\delta_i\} + \mathbf{T}_i\{\dot{\vec{r}}_i + \dot{\Phi}_i\delta_i + \Phi_i\dot{\delta}_i\}, \tag{2.18}$$

where $\mathbf{P} = \begin{bmatrix} 0 & -1 \\ 1 & 0 \end{bmatrix}$. Note, $\dot{\vec{r}}_i$ and $\dot{\Phi}_i$ are both nonzero when the length of a body changes, for instance, during deployment:

$$\dot{\vec{r}}_i = \frac{\partial \vec{r}_i}{\partial x_i}\dot{l}_i; \tag{2.19}$$

and

$$\dot{\Phi}_i = \left\{\frac{\partial \Phi_i}{\partial x_i} + \frac{\partial \Phi_i}{\partial l_i}\right\}\dot{l}_i. \tag{2.20}$$

It must be pointed out that x_i varies as a function of l_i which depends on the deployment profile.

Actuators regulating the slewing of the manipulator units are also modelled. Since they are located at the manipulator joints, their inertial velocity, defined as $\dot{\vec{R}}_{ai}$, is described by

$$\dot{\vec{R}}_{ai} = \dot{\vec{D}}_i, \tag{2.21}$$

while the inertial angular velocity of the rotor of the ith actuator is specified by $\dot{\eta}_i$.

2.2.5 Generalized coordinates

If the position and orientation of the body-fixed frames are known relative to the inertial frame, in addition to the length (l_i) and elastic deformation (δ_i) of each

body, then the kinematic description of the system is complete. In Eq. (2.1), the position of F_i is specified directly relative to the inertial frame by $\vec{D}_i$, and similarly, its orientation by the inertial angle ψ_i (Figure 2-1).

The kinematics of the space platform is described by $n_p = 3+(r+s)$ generalized coordinates: r_o, θ, ψ_1, and δ_1. The coordinates r_o and θ characterize the orbital motion of the center of mass of the platform, r_o being the orbital radius and θ, the true anomaly. The set of generalized coordinates which describe the motion of the platform can be represented as

$$\tilde{\mathbf{q}}_1 = \begin{bmatrix} r_o \\ \theta \\ \psi_1 \\ \delta_1 \end{bmatrix} \in \Re^{n_p}. \tag{2.22}$$

The kinematics of the manipulator units is described by $n_u = 5 + (r + s)$ generalized coordinates: $\vec{D}_i$, η_i, ψ_i, δ_i, and l_i. It should be noted that l_i is included as a generalized coordinate for each manipulator unit to account for deployment. Therefore, the set of generalized coordinates describing the kinematics of each manipulator unit is defined as

$$\tilde{\mathbf{q}}_i = \begin{bmatrix} \vec{D}_i \\ \eta_i \\ \psi_i \\ \delta_i \\ l_i \end{bmatrix} \in \Re^{n_u}, \tag{2.23}$$

with $i = 2, ..., N$.

The set of generalized coordinates required for the complete description of the system kinematics can then be written as

$$\tilde{\mathbf{q}} = \begin{bmatrix} \tilde{\mathbf{q}}_1 \\ \tilde{\mathbf{q}}_2 \\ \tilde{\mathbf{q}}_3 \\ \vdots \\ \tilde{\mathbf{q}}_N \end{bmatrix} \in \Re^{n_s}, \tag{2.24}$$

where $n_s = n_p + (N-1)n_u$.

2.3 Kinetic Energy of the System

The total kinetic energy of the system can be written as

$$T = \sum_{i=1}^{N} \frac{1}{2} \int_{m_i} \dot{\vec{R}}_{dm_i} \cdot \dot{\vec{R}}_{dm_i} dm_i + \sum_{i=2}^{N} \left(m_{ai} \dot{\vec{D}}_i \cdot \dot{\vec{D}}_i + J_{ai} \dot{\eta}_i^2 \right), \tag{2.25}$$

where the first term represents the kinetic energy of the platform and manipulator units, while the second term assesses the contribution from the actuators at the manipulator joints, which have a mass m_{ai} and a rotary inertia J_{ai}. Rewriting Eq. (2.18) in matrix form,

$$\dot{\vec{R}}_{dm_i} = [\, \mathbf{I^2} \quad \mathbf{0} \quad \nu_{\mathbf{i1}} \quad \nu_{\mathbf{i2}} \quad \nu_{\mathbf{i3}} \,] \, \dot{\tilde{\mathbf{q}}}_{\mathbf{i}}, \tag{2.26}$$

where $\mathbf{I^2}$ is a 2×2 identity matrix, and

$$\nu_{\mathbf{i1}} = \mathbf{P}\mathbf{T_i} \left\{ \vec{r}_i + \Phi_i \delta_i \right\}; \tag{2.27, a}$$

$$\nu_{\mathbf{i2}} = \mathbf{T}_i \Phi_i; \tag{2.27, b}$$

$$\nu_{\mathbf{i3}} = \mathbf{T}_i \left\{ \frac{\partial \vec{r}_i}{\partial x_i} + \left(\frac{\partial \Phi_i}{\partial x_i} + \frac{\partial \Phi_i}{\partial l_i} \right) \delta_i \right\}. \tag{2.27, c}$$

Therefore, the total kinetic energy of the system can be expressed as

$$T = \sum_{i=1}^{N} \frac{1}{2} \dot{\tilde{\mathbf{q}}}_{\mathbf{i}}^{\mathbf{T}} \int_{m_i} \left(\begin{bmatrix} \mathbf{I^2} \\ \mathbf{0} \\ \nu_{\mathbf{i1}}^{\mathbf{T}} \\ \nu_{\mathbf{i2}}^{\mathbf{T}} \\ \nu_{\mathbf{i3}}^{\mathbf{T}} \end{bmatrix} [\, \mathbf{I^2} \quad \mathbf{0} \quad \nu_{\mathbf{i1}} \quad \nu_{\mathbf{i2}} \quad \nu_{\mathbf{i3}} \,] \right) dm_i \; \dot{\tilde{\mathbf{q}}}_{\mathbf{i}}$$
$$+ \sum_{i=2}^{N} \frac{1}{2} \dot{\tilde{\mathbf{q}}}_{\mathbf{i}}^{\mathbf{T}} \begin{bmatrix} m_{ai}\mathbf{I^2} & \mathbf{0} & \mathbf{0} \\ \mathbf{0} & J_{ai} & \mathbf{0} \\ \mathbf{0} & \mathbf{0} & \mathbf{0} \end{bmatrix} \dot{\tilde{\mathbf{q}}}_{\mathbf{i}}. \tag{2.28}$$

Rearranging Eq. (2.28) in a more compact form yields

$$T = \sum_{i=1}^{N} \frac{1}{2} \dot{\tilde{\mathbf{q}}}_{\mathbf{i}}^{\mathbf{T}} \tilde{\mathbf{M}}_{\mathbf{i}} \dot{\tilde{\mathbf{q}}}_{\mathbf{i}}. \tag{2.29}$$

A detailed description of the matrices $\tilde{\mathbf{M}}_\mathbf{i}$ is provided in Appendix II. When the summation in Eq. (2.29) is expressed in matrix form, a quadratic expression is obtained for the total kinetic energy of the system,

$$T = \frac{1}{2}\dot{\tilde{\mathbf{q}}}^{\mathbf{T}}\tilde{\mathbf{M}}\dot{\tilde{\mathbf{q}}}, \tag{2.30}$$

where $\tilde{\mathbf{M}}$ is the $n_s \times n_s$ mass matrix of the system,

$$\tilde{\mathbf{M}} = \begin{bmatrix} \tilde{\mathbf{M}}_1 & 0 & 0 & \cdots & 0 \\ 0 & \tilde{\mathbf{M}}_2 & 0 & \cdots & 0 \\ 0 & 0 & \tilde{\mathbf{M}}_3 & \cdots & 0 \\ \vdots & \vdots & \vdots & \ddots & \vdots \\ 0 & 0 & 0 & \cdots & \tilde{\mathbf{M}}_N \end{bmatrix}. \tag{2.31}$$

2.4 Alternate Expressions for the Kinetic Energy

Eq. (2.30) gives the total kinetic energy of the system in terms of the set of generalized coordinates $\tilde{\mathbf{q}}$. With this set, where $\vec{D}_i$ and η_i are taken as generalized coordinates, the dynamics of each body is described independently, without referring to adjacent bodies. This results in an elegant mass matrix, given by Eq. (2.31). As a result, the dynamics of each body is decoupled from that of the other bodies. Clearly, this is not the case in reality as the motion of a given body is affected by that of the others. Therefore, the constraint forces between adjacent bodies must be incorporated into the final equations of motion for this system. This process can be simplified through the use of another set of generalized coordinates, $\mathbf{q}$, which is now developed.

2.4.1 Alternate set of generalized coordinates

As pointed out, it is necessary to define a second set of generalized coordinates to account for constraints imposed by the adjacent bodies. While the second set also takes ψ_i, δ_i, and l_i as generalized coordinates, the position and orientation of the body-fixed frames are specified relative to the previous frame instead of the inertial

frame. With this approach, the frame F_i is related to the frame F_{i-1}. F_i can be obtained by translating F_{i-1} along $\vec{g}_i$ and rotating it about the z_i axis by an angle γ_i, as shown in Figure 2-1. Hence,

$$\vec{D}_i = \vec{D}_{i-1} + \vec{g}_i, \tag{2.32}$$

and

$$\psi_i = \psi_{i-1} + \gamma_i. \tag{2.33}$$

Figure 2-3(a) shows that the vector $\vec{g}_i$ consists of the sum of three vectors: $\vec{l}_{i-1}$, which denotes the length of the ($i^{th} - 1$) body, or $\vec{l}_{i-1} = [\, l_{i-1} \quad 0\,]^T$; $\vec{d}_i$, which represents the translation of F_i from the tip of the (i^{th} - 1) body due to a prismatic joint; and $\vec{e}_i$, which gives the displacement caused by the elastic deformation of the ($i^{th} - 1$) body. Therefore,

$$\vec{g}_i = \mathbf{T_{i-1}}(\vec{l}_{i-1} + \vec{d}_i + \vec{e}_i), \qquad i = 2, ..., N. \tag{2.34}$$

The above expression is pre-multiplied by $\mathbf{T_{i-1}}$ so that the components of $\vec{g}_i$ are in terms of inertial coordinates. Furthermore, note that

$$\vec{e}_i = \bar{\Phi}_{i-1}\delta_{i-1}, \qquad \text{where} \qquad \bar{\Phi}_{i-1} = \Phi_{i-1}(x_{i-1}, l_{i-1})|_{x_{i-1}=d_{ix}+l_{i-1}}, \tag{2.35}$$

for $i = 2, ..., N$.

The rotation γ_i of the frame F_i with respect to the frame F_{i-1} has three contributions (Figure 2-3b): elastic deformation of the (i^{th} - 1) body in the transverse direction (ξ_i); rotation of the actuator rotor (α_i), which corresponds to the controlled rotation of the revolute joint; and elastic deformation of joint i (β_i), which could be due, for instance, to flexible coupling. Hence,

$$\gamma_i = \xi_i + \alpha_i + \beta_i. \tag{2.36}$$

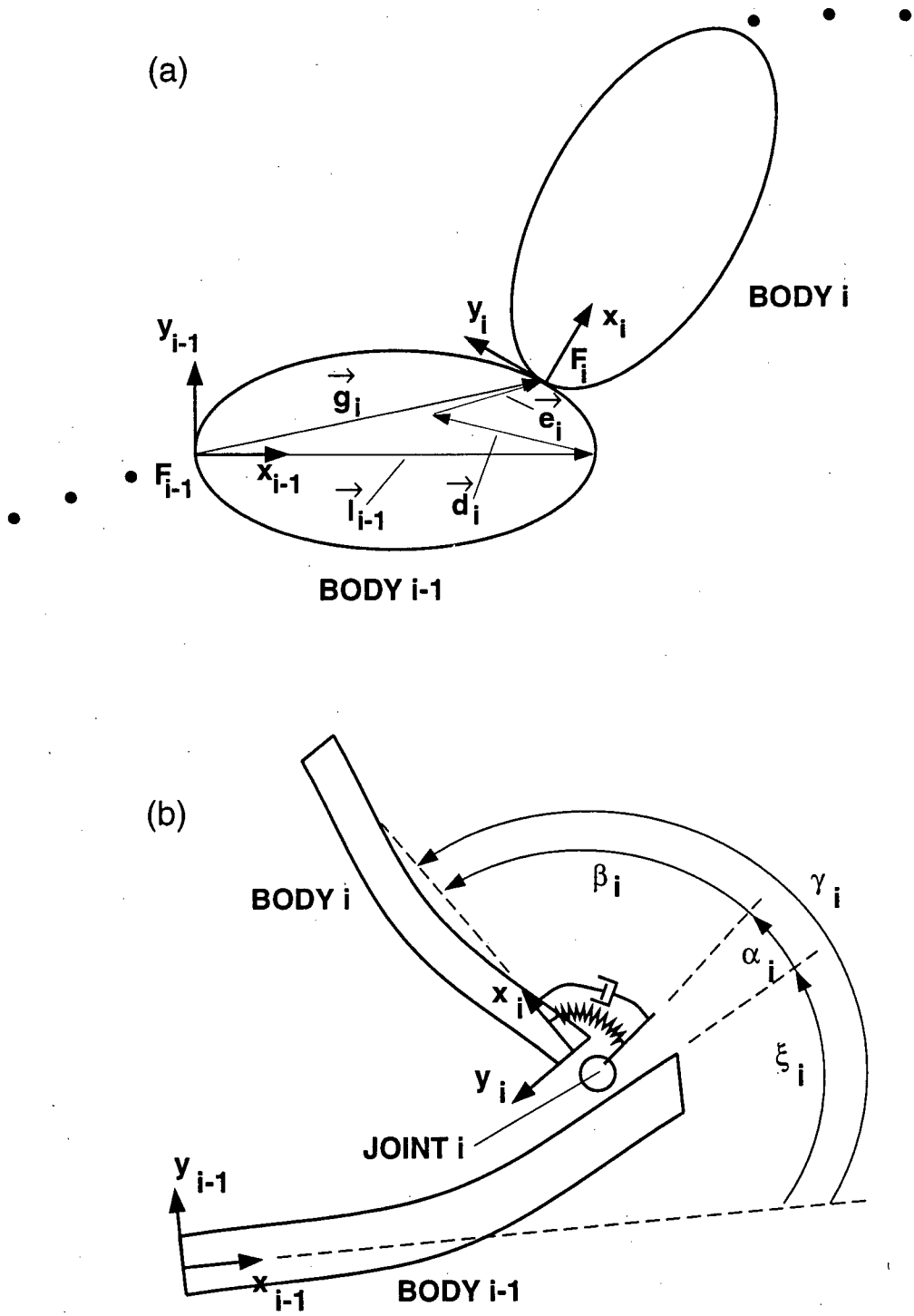

Figure 2-3 Description of a body-fixed frame relative to the preceding frame: (a) position; (b) orientation.

Note,

$$\eta_i = \psi_{i-1} + \xi_i + \alpha_i. \tag{2.37}$$

Furthermore,

$$\xi_i = \bar{\Phi}'_{i-1}\delta_{i-1}, \quad \text{with} \quad \bar{\Phi}'_{i-1} = \Phi'_{i-1}(x_{i-1}, l_{i-1})\big|_{x_{i-1}=d_{ix}+l_{i-1}}, \tag{2.38}$$

for $i = 2, ..., N$ and

$$\Phi'_i = \frac{\partial \Phi_{iy}}{\partial x_i}. \tag{2.39}$$

It must be pointed out that Eq.(2.38) is valid under the assumption that the transverse deformation of each body is small. Special care should be exercised for the case $i = 2$, which describes the location and orientation of the mobile base. Since l_1 is not considered as a generalized coordinate, Eq.(2.34), Eq.(2.35), and Eq.(2.38) must be modified by replacing $\vec{d}_2 + \vec{l}_1$ by $\vec{d}_2$, and similarly, $d_{2x} + l_1$ by d_{2x}.

Thus, the position of the body-fixed frame F_i is expressed in terms of that of F_{i-1}, which itself is related to the location of F_{i-2}. This referencing with respect to the preceding frame continues until the frame F_1 is reached, which is directly described relative to the inertial frame by $\vec{D}_1$ and ψ_1. Thus

$$\vec{D}_i = \vec{d}_1 + \sum_{j=2}^{i} \vec{g}_j, \tag{2.40}$$

where

$$\vec{d}_1 = \vec{D}_1 = \begin{bmatrix} r_o\cos\theta \\ r_o\sin\theta \end{bmatrix}. \tag{2.41}$$

Hence, a second set $\mathbf{q}$ of generalized coordinates is available for the complete description of the motion of the system,

$$\mathbf{q} = \begin{bmatrix} \mathbf{q}_1 \\ \mathbf{q}_2 \\ \mathbf{q}_3 \\ \vdots \\ \mathbf{q}_N \end{bmatrix} \in \Re^{ns}, \tag{2.42}$$

where $\mathbf{q_1} = \tilde{\mathbf{q}}_\mathbf{1}$ and

$$\mathbf{q}_i = \begin{bmatrix} \vec{d}_i \\ \alpha_i \\ \psi_i \\ \delta_i \\ l_i \end{bmatrix} \in \Re^{nu}, \tag{2.43}$$

for $i = 2, ..., N$.

2.4.2 Velocity transformations

The decoupled set of generalized coordinates, $\tilde{\mathbf{q}}$, leads to a simple expression for the system's kinetic energy. On the other hand, the second set, $\mathbf{q}$, simplifies the specification of the constraint forces. For instance, it is simpler to specify that the base of the manipulator unit i is located at the tip of the $(i^{th} - 1)$ unit by stating that $\vec{d}_i = \vec{0}$ rather than by deriving a complex constraint relationship between $\vec{D}_i$ and $\vec{D}_{i-1}$. Therefore, the methodology here consists in deriving the system energy using the decoupled set of coordinates, $\tilde{\mathbf{q}}$, and then converting it to the more convenient coupled set, $\mathbf{q}$. This can be done through the use of the two velocity transformations which are derived now.

As mentioned earlier, both $\dot{\tilde{\mathbf{q}}}_\mathbf{i}$ and $\dot{\mathbf{q}}_\mathbf{i}$ use $\dot{\psi}_i$, $\dot{\delta}_i$, and $\dot{l}_i$, as generalized velocities. Hence, to find a relationship between $\dot{\tilde{\mathbf{q}}}_\mathbf{i}$ and $\dot{\mathbf{q}}_\mathbf{i}$, the task consists in finding expressions for $\dot{\vec{D}}_i$ and $\dot{\eta}_i$ in terms of the second set of generalized coordinates $\mathbf{q}$. For both the velocity transforms, the time derivative of Eq. (2.37) is required,

$$\dot{\eta}_i = \dot{\psi}_{i-1} + \dot{\xi}_i + \dot{\alpha}_i, \tag{2.44}$$

where

$$\dot{\xi}_i = \xi_{i,d}\dot{d}_{ix} + \xi_{i,l}\dot{l}_{i-1} + \bar{\Phi}'_{i-1}\dot{\delta}_{i-1}, \tag{2.45}$$

with

$$\xi_{i,d} = \frac{\partial \xi_i}{\partial d_{ix}}; \quad \text{and} \quad \xi_{i,l} = \frac{\partial \xi_i}{\partial l_{i-1}}. \tag{2.46}$$

In matrix form,

$$\dot{\eta}_i = [\,[0 \quad 0] \quad 0 \quad 1 \quad \bar{\Phi}'_{i-1} \quad \xi_{i,l}\,]\,\dot{\mathbf{q}}_\mathbf{i-1} + [\,[\xi_{i,d} \quad 0] \quad 1 \quad 0 \quad 0 \quad 0\,]\,\dot{\mathbf{q}}_\mathbf{i}, \tag{2.47}$$

which is equivalent to

$$\dot{\eta}_i = [\,[0 \quad 0] \quad 0 \quad 1 \quad \bar{\Phi}'_{i-1} \quad \xi_{i,l}\,]\,\dot{\tilde{\mathbf{q}}}_{\mathbf{i-1}} + [\,[\xi_{i,d} \quad 0] \quad 1 \quad 0 \quad 0 \quad 0\,]\,\dot{\mathbf{q}}_{\mathbf{i}}. \tag{2.48}$$

The case of $\dot{\vec{D}}_i$ is now addressed.

(a) First velocity transformation

For the first velocity transform, the time derivative of Eq. (2.32) is needed,

$$\dot{\vec{D}}_i = \dot{\vec{D}}_{i-1} + \dot{\vec{g}}_i, \tag{2.49}$$

where

$$\dot{\vec{g}}_i = \mathbf{P}\vec{g}_i\dot{\psi}_{i-1} + \mathbf{T_{i-1}}\left(\dot{\vec{d}}_i + \dot{\vec{l}}_{i-1} + \vec{e}_{i,d}\dot{d}_{ix} + \vec{e}_{i,l}\dot{l}_{i-1} + \bar{\Phi}_{i-1}\dot{\delta}_{i-1}\right), \tag{2.50}$$

with

$$\vec{e}_{i,d} = \frac{\partial \vec{e}_i}{\partial d_{ix}}; \quad \text{and} \quad \vec{e}_{i,l} = \frac{\partial \vec{e}_i}{\partial l_{i-1}}. \tag{2.51}$$

Eq. (2.49) can be rewritten as

$$\begin{aligned}\dot{\vec{D}}_i = \left[\mathbf{I^2} \quad 0 \quad \mathbf{P}\dot{\vec{g}}_i \quad \mathbf{T}_{i-1}\bar{\Phi}_{i-1} \quad \mathbf{T}_{i-1}\left(\begin{bmatrix}1\\0\end{bmatrix} + \vec{e}_{i,l}\right)\right]\dot{\tilde{\mathbf{q}}}_{\mathbf{i-1}} \\ + [\,\mathbf{T}_{i-1}\mathbf{S} \quad 0 \quad 0 \quad 0 \quad 0\,]\,\dot{\mathbf{q}}_{\mathbf{i}},\end{aligned} \tag{2.52}$$

where $\mathbf{I^2}$ is a 2×2 identity matrix and $\mathbf{S} = \mathbf{I^2} + \vec{e}_{i,d}[\,1 \quad 0\,]$.

Using Eq. (2.48) and Eq. (2.52), the following matrix relation can be obtained,

$$\dot{\tilde{\mathbf{q}}}_{\mathbf{i}} = \mathbf{R}^{\mathbf{C}}_{\mathbf{i-1}}\dot{\tilde{\mathbf{q}}}_{\mathbf{i-1}} + \mathbf{R_i}\dot{\mathbf{q}}_{\mathbf{i}}. \tag{2.53}$$

The details of the $\mathbf{R}^{\mathbf{C}}_{\mathbf{i}}$ and $\mathbf{R_i}$ matrices can be found in Appendix III. Stacking Eq. (2.53) for $i = 1, ..., N$, a relation between $\tilde{\mathbf{q}}$ and $\mathbf{q}$ is obtained as

$$\dot{\tilde{\mathbf{q}}} = \mathbf{R}^{\mathbf{C}}\dot{\tilde{\mathbf{q}}} + \mathbf{R}\dot{\mathbf{q}}, \tag{2.54}$$

where:

$$\mathbf{R^C} = \begin{bmatrix} 0 & 0 & 0 & 0 & \cdots & 0 \\ \mathbf{R_1^C} & 0 & 0 & 0 & \cdots & 0 \\ 0 & \mathbf{R_2^C} & 0 & 0 & \cdots & 0 \\ 0 & 0 & \mathbf{R_3^C} & 0 & \cdots & 0 \\ \vdots & \vdots & \vdots & \vdots & \ddots & \vdots \\ 0 & 0 & 0 & 0 & \cdots & 0 \end{bmatrix}; \tag{2.55}$$

and

$$\mathbf{R} = \begin{bmatrix} \mathbf{R}_1 & 0 & 0 & \cdots & 0 \\ 0 & \mathbf{R}_2 & 0 & \cdots & 0 \\ 0 & 0 & \mathbf{R}_3 & \cdots & 0 \\ \vdots & \vdots & \vdots & \ddots & \vdots \\ 0 & 0 & 0 & \cdots & \mathbf{R}_N \end{bmatrix}. \tag{2.56}$$

Rewriting Eq. (2.54) yields the first velocity transformation,

$$\dot{\tilde{\mathbf{q}}} = [\mathbf{I}^{n_s} - \mathbf{R^C}]^{-1}\mathbf{R}\dot{\mathbf{q}}, \tag{2.57}$$

where $\mathbf{I^{ns}}$ is a $n_s \times n_s$ identity matrix.

(b) Second velocity transformation

The second velocity transform requires the time derivative of Eq. (2.40),

$$\dot{\vec{D}}_i = \dot{\vec{d}}_1 + \sum_{j=2}^{i} \dot{\vec{g}}_j. \tag{2.58}$$

Rewriting the above equation in matrix form,

$$\dot{\vec{D}}_i = \dot{\vec{d}}_1 + \sum_{j=2}^{i-1} \left[\mathbf{I^2} \quad 0 \quad \mathbf{P}\dot{\vec{g}}_j \quad \mathbf{T}_{j-1}\bar{\Phi}_{j-1} \quad \mathbf{T}_{j-1}\left(\begin{bmatrix}1\\0\end{bmatrix} + \vec{e}_{j,l}\right)\right] \dot{\mathbf{q}}_\mathbf{j} + [\mathbf{T}_{i-1}\mathbf{S} \quad 0 \quad 0 \quad 0 \quad 0]\,\dot{\mathbf{q}}_\mathbf{i}. \tag{2.59}$$

Using Eq. (2.47) and Eq. (2.59) leads to

$$\dot{\tilde{\mathbf{q}}}_\mathbf{i} = \sum_{j=1}^{i-2} \mathbf{R_j^B}\dot{\mathbf{q}}_\mathbf{j} + \mathbf{R_{i-1}^A}\dot{\mathbf{q}}_\mathbf{i-1} + \bar{\mathbf{R}}_\mathbf{i}\dot{\mathbf{q}}_\mathbf{i}, \tag{2.60}$$

The details of the $\bar{\mathbf{R}}_\mathbf{i}$, $\mathbf{R_i^A}$, and $\mathbf{R_i^B}$ matrices are given in Appendix III. Stacking Eq. (2.60) for $i = 1, ..., N$ leads to the second velocity transformation as

$$\dot{\tilde{\mathbf{q}}} = \mathbf{R^V}\dot{\mathbf{q}}, \tag{2.61}$$

where

$$\mathbf{R}^{\mathbf{V}} = \begin{bmatrix} \bar{\mathbf{R}}_1 & 0 & 0 & \cdots & 0 \\ \mathbf{R}_1^{\mathbf{A}} & \bar{\mathbf{R}}_2 & 0 & \cdots & 0 \\ \mathbf{R}_1^{\mathbf{B}} & \mathbf{R}_2^{\mathbf{A}} & \bar{\mathbf{R}}_3 & \cdots & 0 \\ \vdots & \vdots & \vdots & \ddots & \vdots \\ \mathbf{R}_1^{\mathbf{B}} & \mathbf{R}_2^{\mathbf{B}} & \mathbf{R}_3^{\mathbf{B}} & \cdots & \bar{\mathbf{R}}_N \end{bmatrix}. \tag{2.62}$$

2.4.3 Two alternate expressions for the kinetic energy

Using the two velocity transformations derived in the previous section, the kinetic energy can be expressed in terms of $\mathbf{q}$. Therefore, making use of Eq. (2.61), the kinetic energy expression takes the form

$$T = \frac{1}{2}\dot{\mathbf{q}}^{\mathbf{T}} \underbrace{\mathbf{R}^{\mathbf{V}^{\mathbf{T}}} \tilde{\mathbf{M}} \mathbf{R}^{\mathbf{V}}}_{\mathbf{M}} \dot{\mathbf{q}}. \tag{2.63}$$

But, using Eq. (2.57), one has

$$T = \frac{1}{2}\dot{\mathbf{q}}^{\mathbf{T}} \underbrace{\mathbf{R}^{\mathbf{T}}[\mathbf{I}^{ns} - \mathbf{R}^{\mathbf{C}}]^{-\mathbf{T}} \tilde{\mathbf{M}} [\mathbf{I}^{ns} - \mathbf{R}^{\mathbf{C}}]^{-1} \mathbf{R}}_{\mathbf{M}} \dot{\mathbf{q}}, \tag{2.64}$$

where the kinetic energy of the system, as well as the mass matrix $\mathbf{M}$, are both expressed in terms of the coupled set of generalized coordinates. Note that the inverse of the mass matrix, as defined in Eq. (2.64), has the form

$$\mathbf{M}^{-1} = \mathbf{R}^{-1}[\mathbf{I}^{ns} - \mathbf{R}^{\mathbf{C}}]\tilde{\mathbf{M}}^{-1}[\mathbf{I}^{ns} - \mathbf{R}^{\mathbf{C}}]^{\mathbf{T}}\mathbf{R}^{-\mathbf{T}}. \tag{2.65}$$

Now the matrices inverted in Eq. (2.65), i.e. $\mathbf{R}$ and $\tilde{\mathbf{M}}$, are both block diagonal, thus their inversion is an *O(N)* process. Furthermore, the structure of the remaining matrices in Eq. (2.65) allows their multiplication to be also of *O(N)*. Thus, inversion of the system mass matrix, in terms of the coupled set of generalized coordinates, is now an *O(N)* process.

2.5 Potential Energy

2.5.1 Gravitational potential energy

The total gravitational potential energy of the system can be written as

$$V_g = -\sum_{i=1}^{N} \int_{m_i} \frac{\mu dm_i}{R_{dm_i}} = -\sum_{i=1}^{N} \int_{m_i} \frac{\mu dm_i}{\left(\vec{R}_{dm_i} \cdot \vec{R}_{dm_i}\right)^{\frac{1}{2}}}, \tag{2.66}$$

where $\mu = Gm_e$, G being the universal gravitational constant and m_e, the mass of Earth. Using Eq. (2.1) to substitute for $\vec{R}_{dm_i}$, Eq. (2.66) becomes, after some algebra,

$$V_g = -\sum_{i=1}^{N} \frac{\mu}{D_i} \int_{m_i} \left(1 + \frac{(\vec{r}_i^T + \vec{f}_i^T)(\vec{r}_i + \vec{f}_i)}{D_i^2} + \frac{2\vec{D}_i^T \mathbf{T_i}(\vec{r}_i + \vec{f}_i)}{D_i^2}\right)^{-\frac{1}{2}} dm_i, \tag{2.67}$$

where $D_i = |\vec{D}_i|$. Since the geometrical dimensions of the orbiting system are much smaller than the orbital radius, $|\vec{D}_i| \gg |\vec{r}_i + \vec{f}_i|$. Expanding binomially the integrand and ignoring terms of order $1/D_i^4$ and higher gives

$$V_g = \sum_{i=1}^{N} \left\{ -\frac{\mu m_i}{D_i} + \frac{\mu}{2D_i^3} \left(\int_{m_i} (\vec{r}_i^T + \vec{f}_i^T)(\vec{r}_i + \vec{f}_i) dm_i + 2\vec{D}_i^T \mathbf{T_i} \int_{m_i} (\vec{r}_i + \vec{f}_i) dm_i \right) \right.$$
$$\left. - \frac{3\mu}{2D_i^5} \vec{D}_i^T \mathbf{T_i} \int_{m_i} (\vec{r}_i + \vec{f}_i)(\vec{r}_i^T + \vec{f}_i^T) dm_i \mathbf{T_i^T} \vec{D}_i \right\}. \tag{2.68}$$

If the mass of the joint actuators is not negligible, their gravitational potential energy must be added to Eq. (2.68). Treating them as point masses, the gravitational potential energy of the actuators will be

$$V_{ga} = -\sum_{i=2}^{N} \frac{\mu m_{ai}}{D_i}. \tag{2.69}$$

2.5.2 Strain energy

Potential energy is also stored in the form of elastic deformations of the system.

The total elastic potential energy is given by

$$V_e = \sum_{i=2}^{N} \frac{1}{2} K_i \beta_i^2 + \sum_{i=1}^{N} \frac{1}{2} \int_{l_i} EA(x_i) \left(\frac{\partial u_i}{\partial x_i} \right)^2 dx_i + \sum_{i=1}^{N} \frac{1}{2} \int_{l_i} EI(x_i) \left(\frac{\partial^2 v_i}{\partial x_i^2} \right)^2 dx_i, \tag{2.70}$$

where the first term represents the contribution from the deformation of the joints; the second and third terms correspond to the elastic deformations of the platform and manipulator links in the longitudinal and transverse directions, respectively; K_i is the joint stiffness; $\beta_i = \psi_i - \alpha_i - \xi_i - \psi_{i-1}$; and EA, EI are the structural stiffnesses of the bodies (platform and manipulator links) in the longitudinal and transverse directions, respectively. Note, both EA and EI are permitted to vary along the length of a given body.

2.6 Energy Dissipation

Dissipation of energy was included in the model. Accurate mathematical models for damping are an area of research in itself. Here, the objective is to capture the overall effect on the system response. To that end, a Rayleigh dissipation function is used [71]. It is defined as one-half the instantaneous rate of change of mechanical energy occurring in the system,

$$R_d = \sum_{i=2}^{N} \frac{1}{2} C_i^J \dot{\beta}_i^2 + \sum_{i=1}^{N} \frac{1}{2} \int_{l_i} C_{u,i}^L A(x_i) \left(\frac{\partial \dot{u}_i}{\partial x_i} \right)^2 dx_i + \sum_{i=1}^{N} \frac{1}{2} \int_{l_i} C_{v,i}^L I(x_i) \left(\frac{\partial^2 \dot{v}_i}{\partial x_i^2} \right)^2 dx_i, \tag{2.71}$$

where the first term corresponds to the viscous dissipation at the joints, while the second and third terms represent the dissipation due to structural damping in the longitudinal and transverse directions, respectively. Note that C_i^J, $C_{u,i}^L$, and $C_{v,i}^L$ correspond to equivalent viscous damping coefficients for the joints vibration, as well

as longitudinal and transverse modes of vibration of the bodies, respectively.

2.7 Equations of Motion

The equations of motion can be obtained using the Lagrangian procedure

$$\frac{d}{dt}\left(\frac{\partial T}{\partial \dot{\mathbf{q}}}\right) - \frac{\partial T}{\partial \mathbf{q}} + \frac{\partial V}{\partial \mathbf{q}} + \frac{\partial R_d}{\partial \dot{\mathbf{q}}} = \mathbf{Q}, \tag{2.72}$$

where $\mathbf{Q}$ corresponds to the nonconservative generalized forces. They can be written as

$$\ddot{\mathbf{q}} = \mathbf{M}^{-1}\mathbf{Q} - \mathbf{M}^{-1}\underbrace{\left(\dot{\mathbf{M}}\dot{\mathbf{q}} - \frac{1}{2}\frac{\partial(\dot{\mathbf{q}}^{\mathbf{T}}\mathbf{M}\dot{\mathbf{q}})}{\partial \mathbf{q}} + \frac{\partial V_g}{\partial \mathbf{q}} + \frac{\partial V_e}{\partial \mathbf{q}} + \frac{\partial R_d}{\partial \dot{\mathbf{q}}}\right)}_{\mathbf{F}}, \tag{2.73}$$

where V_g, V_e, and R_d are defined in equations (2.68), (2.70), and (2.71), respectively; $\mathbf{M^{-1}}$ is given by Eq. (2.65), and $\mathbf{M}$ is as described in Eq. (2.63). The terms $\dot{\mathbf{M}}$ and $\partial(\dot{\mathbf{q}}^{\mathbf{T}}\mathbf{M}\dot{\mathbf{q}})/\partial\mathbf{q}$ are described in detail in Appendix IV.

2.8 Generalized Forces

The generalized forces $\mathbf{Q}$ can represent nonconservative environmental effects, such as atmospheric drag, solar radiation influence, interaction with Earth's magnetic field, and so on. They can also be used in order to model thermal deformation effects. However, the present study only considers the forces arising from the system's actuators. Therefore, the generalized forces considered here correspond to the torques applied by the control momentum gyros on the platform, revolute joint actuators, as well as forces applied by the linear actuators (at prismatic joints) responsible for link deployment.

The control inputs applied to the space platform are the torques arising from the control momentum gyros which regulate its attitude (T_0) and its vibration (T_1). The actuator located at the ith joint of the manipulator provides the ith body with a torque T_i which results in slewing motion of the unit. Furthermore, each unit is

equipped with a linear actuator responsible for its deployment and retrieval. This actuator provides a force $\mathcal{F}_i$ along the length of the ith unit. Therefore, the set of actuator forces can be written as

$$\mathbf{u} = [T_0, \quad T_1, \quad T_2, \quad \mathcal{F}_2, \quad T_3, \quad \mathcal{F}_3, \quad \cdots, \quad T_N, \quad \mathcal{F}_N]^T, \tag{2.74}$$

where $\mathbf{u} \in \Re^{n_a}$, with $n_a = 2N$.

The components of $\mathbf{Q}$ represent the contributions of all the external forces to the equations of motion corresponding to each generalized coordinate. These contributions can be established through a virtual work approach which leads to the equation

$$Q_i = \sum_{j=1}^{n_a} \vec{F}_{ej} \cdot \frac{\partial \vec{R}_j}{\partial q_i}, \tag{2.75}$$

where Q_i and q_i represent the ith components of $\mathbf{Q}$ and $\mathbf{q}$, respectively; and $\vec{F}_{ej}$ symbolize the jth external force applied at $\vec{R}_j$. Eq. (2.75) is used to derive the relationship between $\mathbf{Q}$ and $\mathbf{u}$,

$$\mathbf{Q} = \mathbf{Q^d u}, \tag{2.76}$$

where:

$$\mathbf{Q^d} = \begin{bmatrix} \mathbf{Q_1^d} & \mathbf{0} & \mathbf{0} & \cdots & \mathbf{0} \\ \mathbf{0} & \mathbf{Q_2^d} & \mathbf{0} & \cdots & \mathbf{0} \\ \mathbf{0} & \mathbf{0} & \mathbf{Q_3^d} & \cdots & \mathbf{0} \\ \vdots & \vdots & \vdots & \ddots & \vdots \\ \mathbf{0} & \mathbf{0} & \mathbf{0} & \cdots & \mathbf{Q_N^d} \end{bmatrix} \in \Re^{n_s \times n_a}; \tag{2.77}$$

with

$$\mathbf{Q_1^d} = \begin{bmatrix} 0 & 0 \\ -1 & 0 \\ 1 & 0 \\ 0 & \bar{\Phi}_{1a} \end{bmatrix} \in \Re^{n_p \times 2}; \quad \text{and} \quad \mathbf{Q_i^d} = \begin{bmatrix} \mathbf{0} & \mathbf{0} \\ 1 & 0 \\ 0 & 0 \\ \mathbf{0} & \mathbf{0} \\ 0 & 1 \end{bmatrix} \in \Re^{n_u \times 2}; \quad \text{for } i = 2, \ldots\ldots, N. \tag{2.78}$$

Note, $\bar{\Phi}_{1a} = \Phi_1$ evaluated at the location of the momentum gyros.

2.9 Specified Coordinates

In this study, the coordinates required to describe the system kinematics are taken to be generalized coordinates in order to make the formulation as general and versatile as possible. However, it is often useful to specify some of these generalized coordinates. For instance, in the particular case of the manipulator studied, $\vec{d_i} = 0$ for $i = 3, ..., N$. In other words, each manipulator unit is attached to the tip of the previous unit in the chain. Furthermore, cases where the length of the units is varied in a specified manner, or where joint rotors are locked in place at a specified angle, require the use of specified coordinates. These coordinates are prescribed through constraint relations which are introduced in the equations of motion through Lagrange multipliers. Therefore, when constrained, Eq. (1.1) takes the form

$$\mathbf{M}\ddot{\mathbf{q}} + \mathbf{F} = \mathbf{Q^d u} + \mathbf{P^c \Lambda}, \tag{2.79}$$

where: $\mathbf{u} \in \Re^{n_a}$ is a vector containing the n_a actuator forces and torques; $\mathbf{Q^d}$ is the matrix assigning the components of $\mathbf{u}$ to the actuated variables ($\mathbf{Q} = \mathbf{Q^d u}$); $\mathbf{\Lambda} \in \Re^{n_c}$ is the vector containing the n_c Lagrange multipliers; and $\mathbf{P^c}$ is the matrix assigning the multipliers to the constrained equations. In order to find the values of the Lagrange multipliers and achieve the desired constraints, the above equation can be rewritten in the form

$$\ddot{\mathbf{q}} + \mathbf{F^g} - \mathbf{F^u u} = \mathbf{F^s \Lambda}, \tag{2.80}$$

where $\mathbf{F^g} = \mathbf{M}^{-1}\mathbf{F}$, $\mathbf{F^u} = \mathbf{M}^{-1}\mathbf{Q^d}$, and $\mathbf{F^s} = \mathbf{M}^{-1}\mathbf{P^c}$. Separating the specified variables ($\mathbf{q_s}$) from the generalized ones ($\mathbf{q_g}$) gives

$$\begin{bmatrix} \ddot{\mathbf{q}}_\mathbf{g} \\ \ddot{\mathbf{q}}_\mathbf{s} \end{bmatrix} + \begin{bmatrix} \mathbf{F^g_g} \\ \mathbf{F^g_s} \end{bmatrix} - \begin{bmatrix} \mathbf{F^u_g} \\ \mathbf{F^u_s} \end{bmatrix} \mathbf{u} = \begin{bmatrix} \mathbf{F^s_g} \\ \mathbf{F^s_s} \end{bmatrix} \mathbf{\Lambda}. \tag{2.81}$$

From the equation associated with the specified coordinates, the Lagrange multipliers can be determined,

$$\ddot{\mathbf{q}}_\mathbf{s} + \mathbf{F^g_s} - \mathbf{F^u_s u} = \mathbf{F^s_s \Lambda}, \tag{2.82}$$

i.e.

$$\mathbf{\Lambda} = \mathbf{F_s^{s-1}} \left(\ddot{\mathbf{q}}_\mathbf{s} + \mathbf{F_s^g} - \mathbf{F_s^u u} \right). \qquad (2.83).$$

It may be pointed out that the equations of motion still retain their *O(N)* character, even in the presence of constraints, as the Lagrange multipliers can be obtained recursively [50]. Thus, in the case where the jth variable is constrained to be constant at its initial value, $\ddot{q}_{s_j} = 0$. In the case of prescribed maneuvers, $\ddot{q}_{s_j}$ is simply defined as the desired acceleration profile. In the present study, a sinusoidal acceleration profile is adopted for prescribed maneuvers. It assures zero velocity and acceleration at the beginning and end of the maneuver, thereby reducing the structural response of the system. The maneuver time history considered is as follows,

$$q_{s_j}(\tau) = \frac{\Delta q_{s_j}}{\Delta \tau} \left\{ \tau - \frac{\Delta \tau}{2\pi} \sin\left(\frac{2\pi}{\Delta \tau} \tau \right) \right\}, \qquad (2.84)$$

where q_{s_j} is the constrained coordinate; Δq_{s_j} is its desired variation; τ is the time; and $\Delta\tau$ is the time required for the maneuver. The time history for q_{s_j}, $\dot{q}_{s_j}$, and $\ddot{q}_{s_j}$ are plotted, for the case $\Delta q_{s_j} = 1$ and $\Delta\tau = 1$, in Figure 2-4.

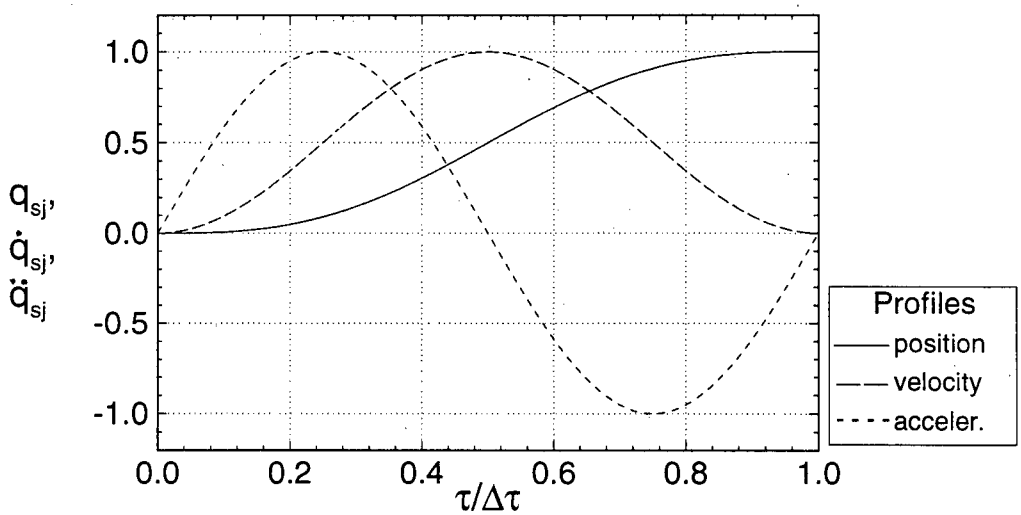

Figure 2-4 Normalized time histories of the sinusoidal maneuvering profile showing displacement, velocity, and acceleration.

3. COMPUTER IMPLEMENTATION

3.1 Preliminary Remarks

The equations governing the inplane dynamics of a general N-body space-based manipulator system were derived in the previous chapter. When these equations are cast in the form given in Eq. (1.1), the mathematical model is said to describe the inverse dynamics of the system. If the desired values of the system's generalized coordinates are specified, in addition to their first two time derivatives, then this model can be used to estimate the generalized forces required from the control actuators. Chapter 5 explains in details how the inverse dynamics model can be incorporated into control strategies. However, Chapters 3 and 4 focus on the simulation of the system's dynamics. In this case, the forward dynamics of the system is required, and Eq. (2.73) must be used. The acceleration vector $\ddot{\mathbf{q}}$ must be integrated twice over time to obtain the time history $\mathbf{q}(t)$ of the various degrees of freedom. Knowledge of $\mathbf{q}(t)$ then leads to a complete description of the system's motion.

The simulation of the system's dynamics requires Eq. (2.73) to be solved. While the solution of Eq. (2.73) is conceptually simple, the integration of $\ddot{\mathbf{q}}$ is not. For simplified models, a closed-form solution can be sought using existing linear and nonlinear analytical approaches. However, the full set of coupled nonlinear differential equations requires a numerical approach. The problem is further complicated by the fact that the equations of motion form a stiff set of differential equations, i.e. the time-scales involved show large differences. For instance, the librational period of the system corresponds roughly to one orbit while the structural vibrations of the various components have frequencies of the order of a few Hz. The numerical algorithm used to solve Eq. (2.73) must take this into account, otherwise excessive numerical error may result.

This chapter discusses the *FORTRAN77* program written for the dynamical

simulation of the manipulator and supporting platform. The aim was to develop an efficient computer code capable of dealing with a wide range of cases. The structure of the computer code is first introduced and the main features of the program are discussed. Then, the procedure followed to validate both the formulation and computer code is presented. Some sample test-cases are provided to illustrate the validation procedure and confirm the accuracy of the numerical model.

3.2 Structure of the Computer Code

As mentioned earlier, the simulation of the system's dynamics requires Eq. (1.2) to be solved, where $\mathbf{F}$ is defined in Eq. (2.73). Therefore, the main task of the program consists essentially in finding $\mathbf{M}^{-1}$, $\mathbf{F}$, $\mathbf{Q}$, and thus $\ddot{\mathbf{q}}$, for each time step. The system dynamics is then cast in first order form,

$$\dot{\mathbf{x}} = \begin{bmatrix} \dot{\mathbf{q}} \\ \ddot{\mathbf{q}} \end{bmatrix} = \begin{bmatrix} \dot{\mathbf{q}} \\ \mathbf{M}^{-1}(\mathbf{Q} - \mathbf{F}) \end{bmatrix}, \tag{3.1}$$

where $\mathbf{x} = [\,\mathbf{q}^{\mathbf{T}} \quad \dot{\mathbf{q}}^{\mathbf{T}}\,]^{\mathbf{T}}$. $\dot{\mathbf{x}}$ is integrated at each desired point in time using Gear's method, which is essentially a backward differentiation formula for stiff equations, employing an implicit linear multistep method of the predictor-corrector type [75].

The architecture of the program performing these tasks is shown in Figure 3-1. The program was designed in a highly modular fashion to facilitate modifications. The number of manipulator units and the number of vibrational modes per body are specified in the file "size.inc". It should be pointed out that every time this file is modified, the entire program must be recompiled in order to adjust the size of the program matrices accordingly.

Initially, the program asks the user if the platform and the manipulator links are rigid or flexible. In the rigid case, the corresponding generalized coordinates are "disabled". This is computationally more efficient than modelling rigid bodies by using extremely large stiffnesses. After the choice for a rigid or flexible platform

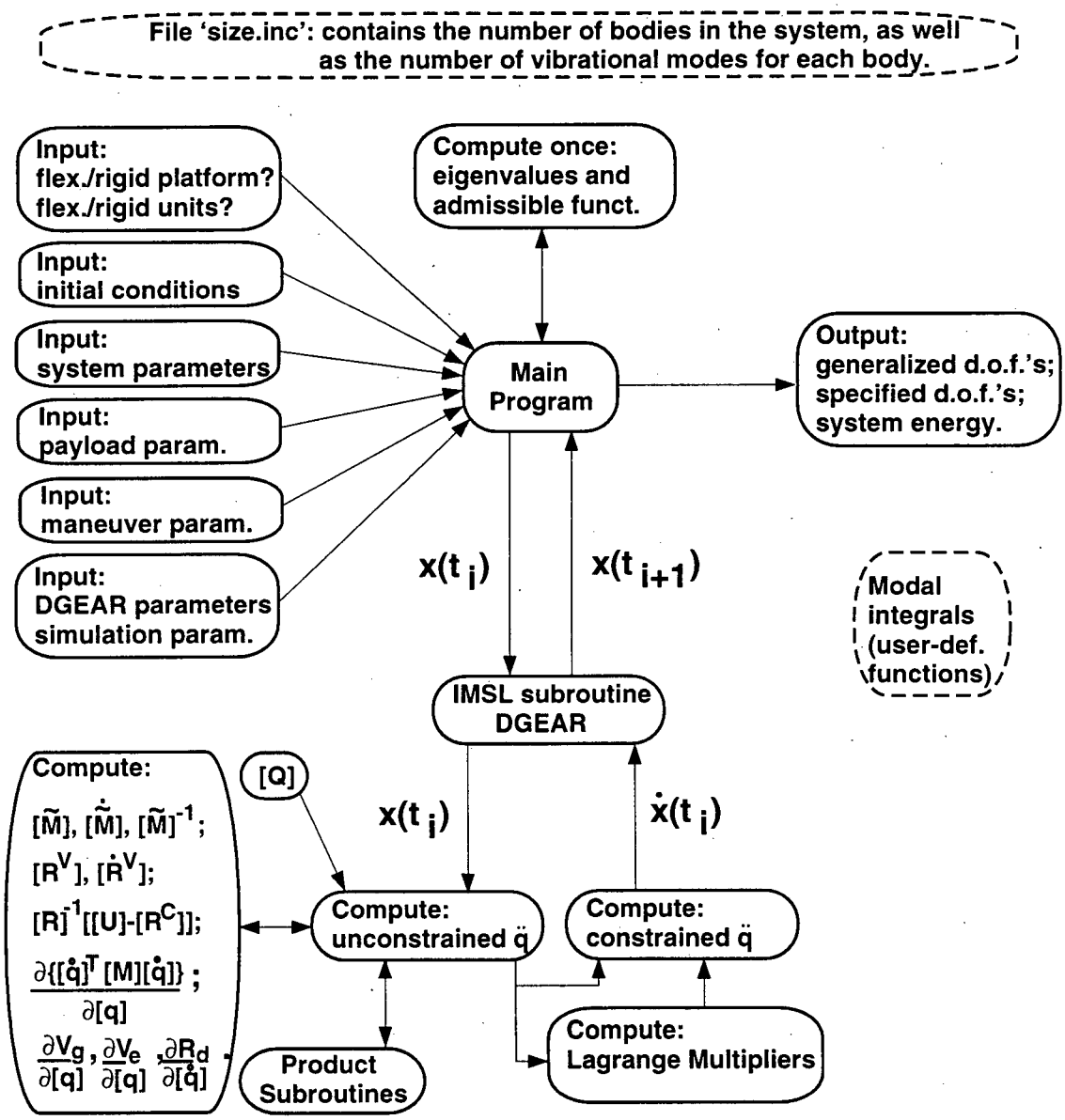

Figure 3-1 Flow diagram showing the modular architecture of the computer code.

has been made, as well as for the manipulator units, the code reads various input parameters from input files:

- initial conditions for all degrees of freedom, i.e. $\mathbf{x}(0) = [\,\mathbf{q}(0)^T \quad \dot{\mathbf{q}}(0)^T\,]^T$;
- system's inertia, stiffness, and damping parameters;
- payload mass and inertia;
- starting time, duration, and amplitude of joint slewing, deployment, and mobile base translation;
- relative error tolerance, initial integration step-size, and number of time-steps for the simulation.

Once the number of bodies and modes have been established, in addition to the mass of the payload, the EIGEN subroutine determines the appropriate frequencies and admissible shape functions for each body. Except for the initial conditions and integration parameters, all input quantities are made available to the other subroutines through common statements. The initial conditions define the state $\mathbf{x}(0)$ and are saved in an output file.

After the input parameters have been specified, the *IMSL* DGEAR subroutine is called in. It features a version of Gear's method where the selection of the integration step-size is automatic, being based on the user-specified relative error-bound. The subroutine reads in the initial state $\mathbf{x}(0)$, the error tolerance, and the initial step-size. It then calls the EQN subroutine, which calculates $\dot{\mathbf{x}}$. The EQN subroutine is called as many times as the number of iterations required by Gear's method to converge to the solution $\mathbf{x}(t_1)$, within the specified error-bounds. The final solution $\mathbf{x}(t_1)$ is recorded in an output file and becomes the new initial state for the following time-step. This procedure is repeated at subsequent time-steps, until the final simulation time-step (t_f). All the solution states ($\mathbf{x}(t_0)$, $\mathbf{x}(t_1)$, $\mathbf{x}(t_2)$, ..., $\mathbf{x}(t_f)$) are recorded in output files. Note, the $\mathbf{x}(t_i)$'s can be modified to more suitable forms using various

output subroutines.

The EQN subroutine constitutes the bulk of the program. For each iteration required by the DGEAR subroutine, it defines the $\tilde{\mathbf{M}}$, $\dot{\tilde{\mathbf{M}}}$, $\tilde{\mathbf{M}}^{-1}$, $\mathbf{R}^{-1}[\mathbf{I} - \mathbf{R}^{\mathbf{C}}]$, $\mathbf{R}^{\mathbf{V}}$, $\dot{\mathbf{R}}^{\mathbf{V}}$, $\partial\{\dot{\mathbf{q}}^{\mathbf{T}}\mathbf{R}^{\mathbf{V}^{\mathbf{T}}}\tilde{\mathbf{M}}\mathbf{R}^{\mathbf{V}}\dot{\mathbf{q}}\}/\partial\mathbf{q}$, $\partial\mathbf{V_g}/\partial\mathbf{q}$, $\partial\mathbf{V_e}/\partial\mathbf{q}$, $\partial\mathbf{R_d}/\partial\dot{\mathbf{q}}$, and $\mathbf{Q}$ matrices. This allows computation of the term $\mathbf{M}^{-1}(\mathbf{Q} - \mathbf{F})$. The EQN subroutine then calls the CONSTRT subroutine, which computes the Lagrange multipliers $\mathbf{\Lambda}$ and the $\mathbf{P^c}$ matrix. The constrained acceleration vector $\ddot{\mathbf{q}}$ is obtained and converted to the first order form $\dot{\mathbf{x}}$. It should be noted that most cases do involve specified coordinates. The specified components of the $\dot{\mathbf{x}}$ vector are not integrated, since their respective time history is already known.

The computations leading to the acceleration vector $\ddot{\mathbf{q}}$ involve a significant number of matrix products and additions. Several of the matrices involved have a number of constituent block submatrices as zero. Efficient subroutines were designed specifically for each matrix product. An effort was made not to multiply the zero elements, thereby reducing considerably the number of computations.

Finally, it should be noted that the shape functions used and their derivatives must be integrated over each body. These integrations can become quite involved for time-varying shape functions. In the past, many researchers have coped with those integrals using numerical integration routines. However, the integrals must be evaluated at each iteration of the ODE solution. Therefore, numerical integration can reduce significantly the speed of the simulation. This emphasized a need for symbolic expressions for the integrals. The symbolic manipulator *MAPLE V* was used in order to evaluate analytically the shape function integrals. It offered the additional advantage of converting the expressions to *FORTRAN* code directly.

3.3 Verification of the Computer Code

The validity of the computer code was established through several checks. The

size of the governing equations of motion, in addition to the number of operations required to derive them (the computer code contains over 10,000 lines!), can easily lead to formulation and programming errors. To some extent, these errors can be avoided through careful and systematic derivation and programming. Furthermore, errors can reveal themselves when the computer code is compiled and its constituting parts are linked, thereby resulting in "compiling" and "linking" errors. However, some errors may be quite elusive and require precise checks.

Ideally, the results obtained with the code should be compared with data collected from an actual spacecraft supporting a flexible manipulator. Unfortunately, few dynamics and control experiments of the type have been carried out in orbit. Furthermore, frequently such information is not made available in open literature. Hence, the lack of relevant data does not permit comparison of the simulation results with those for an actual space-based manipulator. A more convenient avenue is to check the conservation of energy for conservative systems. Similarly, the conservation of angular momentum can also be verified. Another alternative is to match simulation results for particular cases studied by other researchers. In the thesis, the conservation of energy check, as well as comparison of results from other researchers are used to ensure the validity of the computer code and formulation.

3.3.1 Conservation of energy

In the absence of damping and external, nonconservative, generalized forces, the total energy of the system must remain constant. Thus, variation of the total energy for a conservative system would indicate an error in the program or in the derivation of the equations of motion.

A thorough check of the conservation of energy was performed on several cases, involving a variety of system parameters, initial conditions, number of bodies, and manipulator configurations. A check was considered successful if and only if the variation of energy was found to correspond to the numerical noise. It was observed

that even small truncation errors led to significant, and most importantly, smooth variations in the total energy of the system. Hence, even errors which might be considered negligible have a noticeable effect on the conservation of energy. Since the orbital motion of the platform accounts for most of the system's total energy, its effects were removed in several test-cases. In other words, the gravitational parameter μ, as well as the orbital velocity and acceleration, were all set to zero, resulting in a free-floating system. This allowed errors associated with structural vibrations to become more apparent. This phase of the program verification was considered complete when the cases considered led to constant total energy. The following two test-cases serve as examples. They illustrate the methodology adopted and validity of the computer code for widely differing situations.

The first case considers a five-body system. The first body, representing the platform, is a slender rigid beam with a length of 120 m and a mass of 120000 kg. Each of the remaining bodies (manipulator with four links) consists of a 10 m rigid beam with a mass of 400 kg. The bodies are all hinged together and the connecting joints have no torsional stiffness. The chain is initially straight, oriented at an angle of 30° from the local vertical. The system center of mass is initially located at an altitude of 400 km (apogee), and has a velocity of 7.63 km/s in the tangential direction. The orbital eccentricity is 0.01. Figure 3-2 shows the evolution of the system over one orbit. The motion of the system's center of mass is shown, as well as the attitude motion of each individual body. The variation of the total energy is pure noise with no discernible features. Furthermore, its amplitude is of only $10^{-12}\%$. Clearly, the total energy is conserved for this case.

The second case examines the effect of link and joint flexibility on the position of the manipulator's end-effector (Figure 3-3). A five-unit manipulator (i.e. 10 links, five free to slew while the other five deployable), shown in the inset, is located near the tip of the platform with its base held fixed. The individual joints are locked in

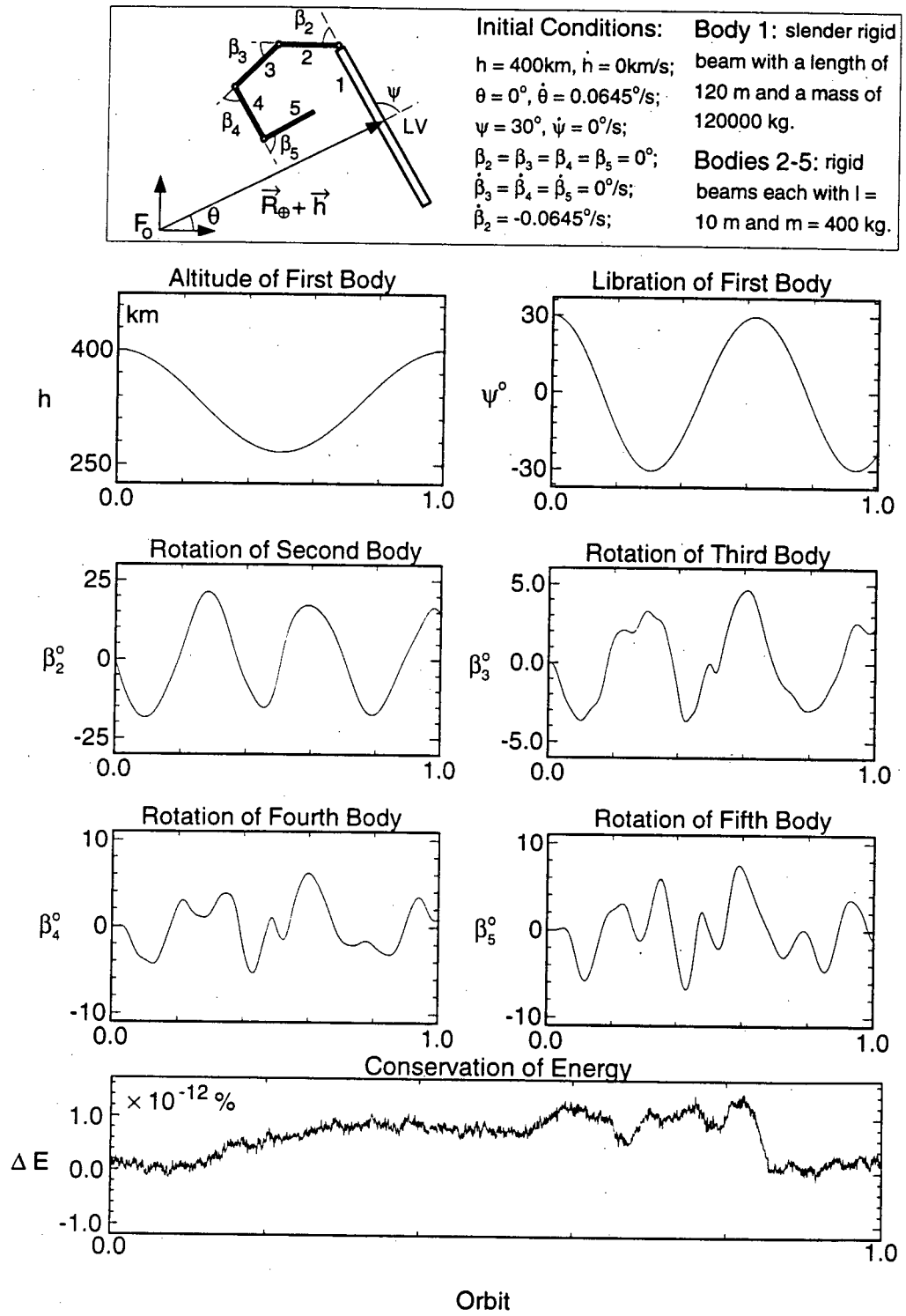

Figure 3-2 Verification of the conservation of energy for a five-body chain system.

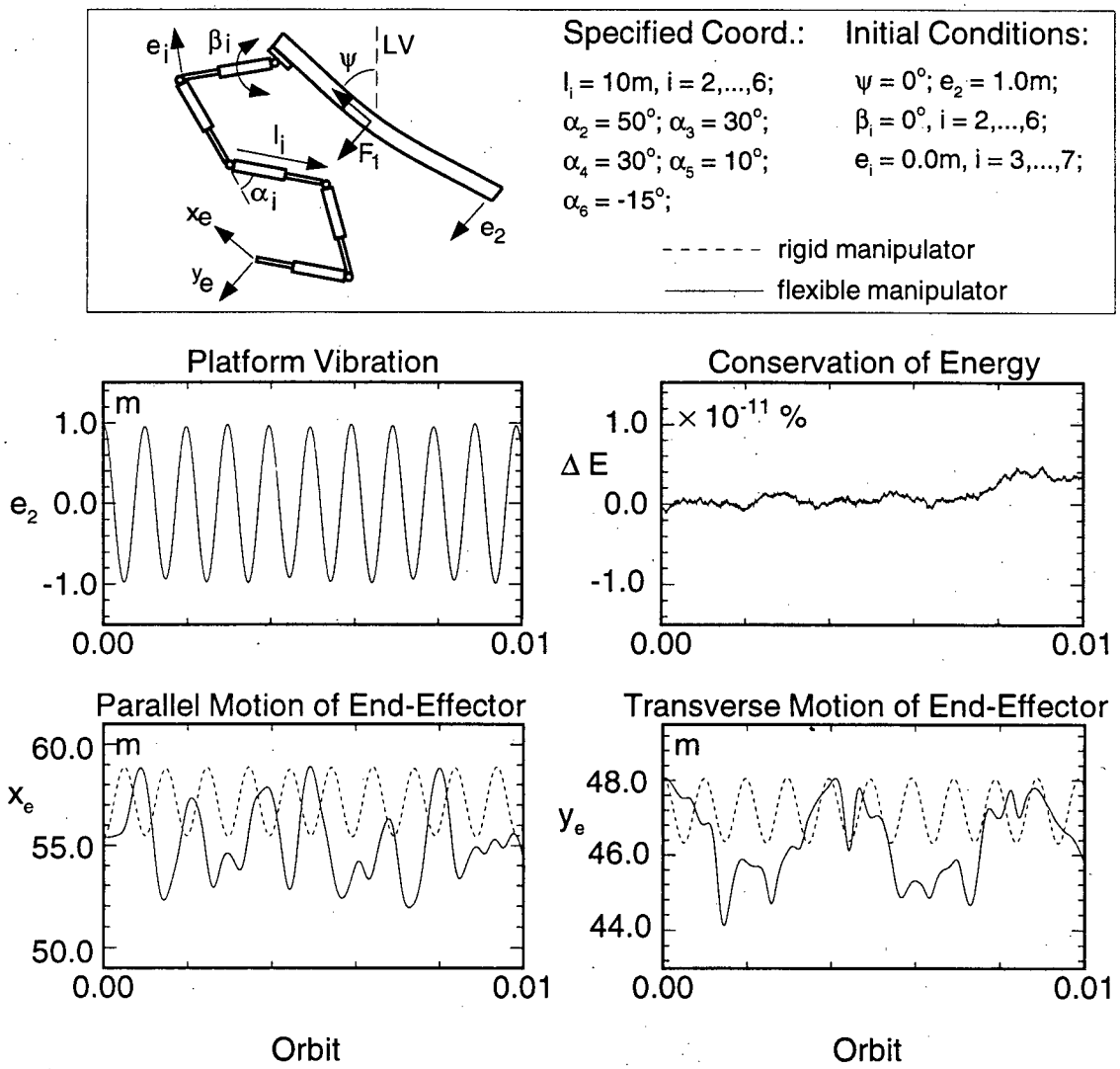

Figure 3-3 Effect of flexibility of the platform and manipulator on the system dynamics with a platform tip displacement of 1 m. The system comprises of a five-unit manipulator supported by an orbiting platform.

position as stated in the legend for the diagram (specified coordinates), and so are the deployable links. The physical characteristics of the system are given in Section 4.2 (page 56). The platform is subjected to an initial tip deflection of 1 m in the first mode. The platform tip oscillations progress undamped. x_e represents the manipulator-tip motion parallel to the undeformed platform, while y_e gives the displacement in the transverse direction, both with respect to the reference coordinate frame F_1. To assess the effects of link and joint flexibility, the response with a rigid manipulator system is also included for comparison. The results clearly show significant influence of the system flexibility on the position of the end-effector. Obviously, this has implication on the path planning. Furthermore, although there is a considerable transfer of energy between various degrees of freedom, the total energy is conserved. The variation in the total energy, of the order of $10^{-12}\%$, is attributed to the computational noise.

3.3.2 Comparison with results from other researchers

The above confirmation does provide considerable confidence in the integrity of the formulation and computer code. However, not all cases investigated in the thesis are conservative. Therefore, it was considered desirable to study particular cases investigated by several other researchers. To that end, some of the cases presented by Chan [28] were selected. In all the cases, the results compared remarkably well.

As an example, consider a rigid platform supporting a flexible, two-link, revolute manipulator. Figure 3-4 shows a schematic diagram of the system, along with its inertia and stiffness parameters. No damping is included. The first manipulator link is positioned at the center of the platform and oriented perpendicular to it, as shown on the figure. The second link undergoes a 180° slewing maneuver in 0.01 orbit. Figure 3-5 compares the results obtained in the present study with those given by Chan. The vibrations of both of the manipulator links, as well as of the two joints are shown. Clearly, the results are in close agreement. The procedure was repeated

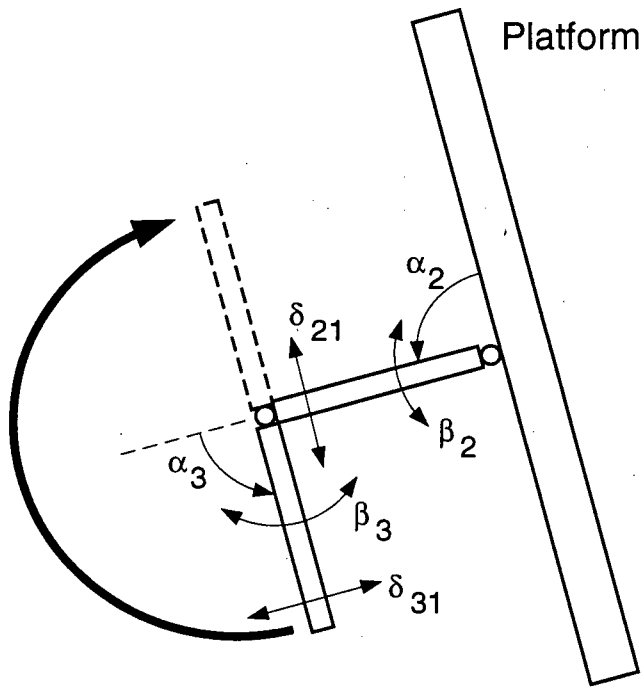

Platform

- orbit: circular at an altitude of 400 km and a period of 92.5 min
- mass: 214 000 kg
- length: 115 m

Links

- mass: 1 600 kg
- length: 7.5 m
- flexural rigidity:
  - Link 1: 3.0×10^6 Nm^2
  - Link 2: 2.0×10^6 Nm^2

Joints

- stiffness: 1.2×10^5 Nm/rad

Figure 3-4 Schematic diagram of a flexible, two-link, revolute manipulator executing a 180° slew at the second joint.

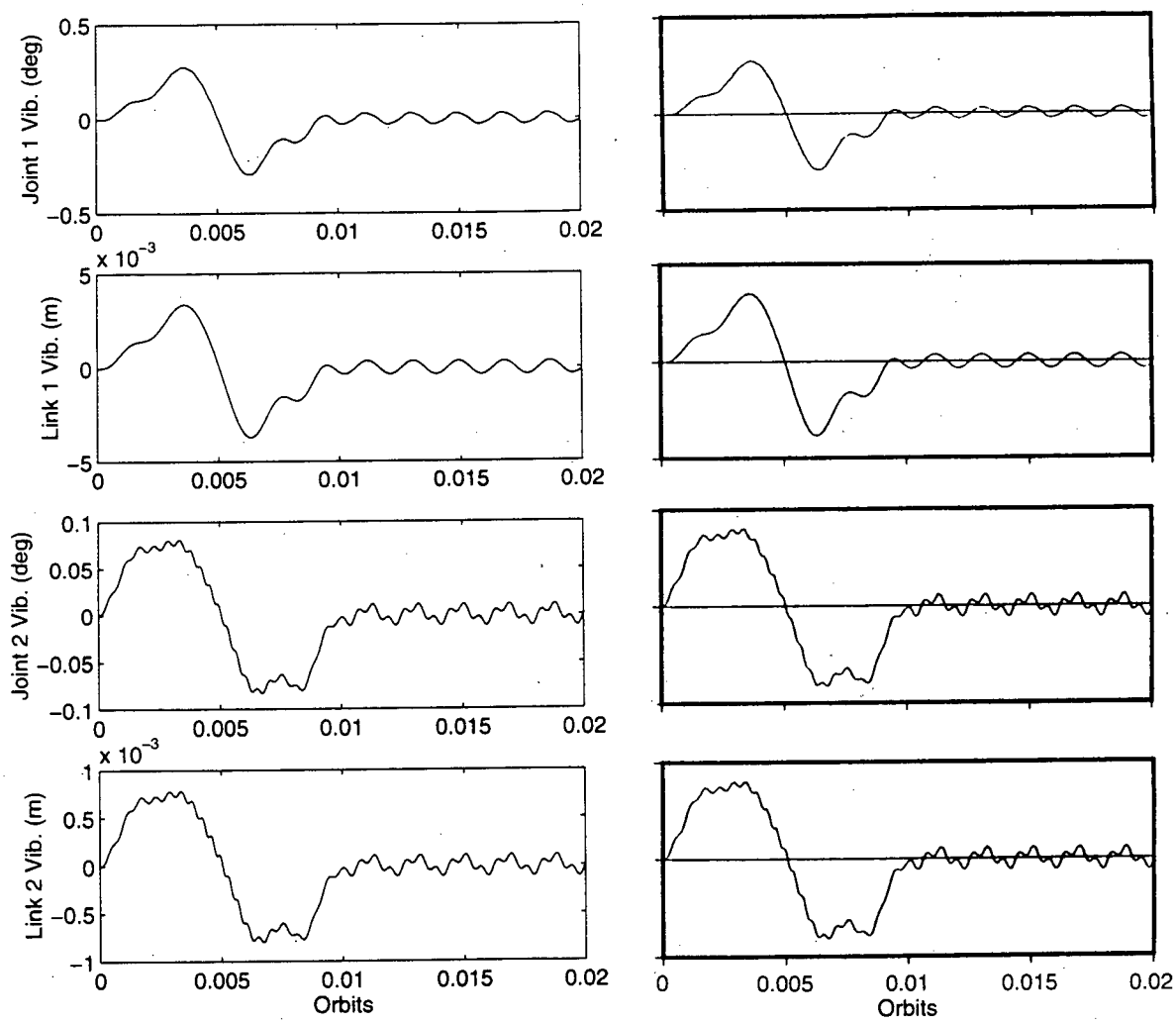

Figure 3-5 Vibrational response of the two-link manipulator due to the slewing maneuver: (a) results from the present multibody code; (b) results obtained by Chan.

with several other cases and the same conclusion was reached.

With this substantiation of the formulation and the numerical code, one can proceed with confidence to explore the system dynamics and control.

4. DYNAMICAL STUDY

4.1 Preliminary Remarks

The previous chapter described the computer model developed to simulate the dynamics of a serial manipulator with an arbitrary number of slewing, deployable units. The next logical step is to gain physical insight into the dynamics of this class of space manipulators through parametric analysis. Several factors are considered: initial disturbances; variation of system parameters; number and type of shape functions used for modeling flexibility; number of manipulator units; and specifications of manipulator maneuvers.

The present chapter reviews the principal findings from a comprehensive investigation. The parametric study generated, literally, a considerable amount of information. For conciseness, only a few representative cases, illustrating typical dynamical behavior, are reported here.

The numerical values used in the simulations are first given. Then, the case of an orbiting platform, supporting a one-unit manipulator, is investigated. This relatively simple system is given considerable attention. It features most of the dynamical characteristics inherent to the more complex systems, and hence helps in the physical understanding of the system behavior. This is followed by the study of more elaborate manipulator systems consisting of two, three, four, and five units connected in series by revolute joints.

4.2 Numerical Data

Unless otherwise specified, the following numerical data were used in simulations:

<u>Orbit</u>

Circular orbit at an altitude of 400 km;

Period = 92.5 min.

Platform

Geometry: cylindrical, with axial to transverse inertia ratio of 0.005;

Mass (m_p)= 120,000 kg;

Length (l_p)= 120 m;

Flexural Rigidity (EI_p) = 5.5 $\times 10^8$ Nm^2.

Manipulator Joints

Type: revolute joints;

Mass (m_j) = 20 kg;

Moment of Inertia (I_{zz}) = 10 kg m^2;

Stiffness (K) = 1×10^4 Nm/rad.

Manipulator Links (Slewing and Deployable)

Geometry: cylindrical, with axial to transverse inertia ratio of 0.005;

Mass (m_s, m_d)= 200 kg;

Length (l_s, l_d) = 7.5 m;

Flexural Rigidity (EI_s, EI_d) = 5.5 $\times 10^5$ Nm^2.

Recall that a manipulator unit consists of two telescopic links: one is free to slew and supports the other, which is deployable.

In the following simulations, longitudinal deformations are neglected, as well as the dynamics of the mobile base. In general, only the first mode of transverse vibration is considered for the deformation of each body. Furthermore, the manipulator supports a point payload at the extremity of the last link. The ratio between the payload mass and the mass of a single unit, referred to as the *payload ratio*, is used to specify the mass of the payload. For most cases, a payload ratio of 1 is considered. Cases involving different values of the payload ratio are clearly identified. It should also be noted that, for most cases, energy dissipation is purposely not included in

order to obtain a conservative estimate of the system response.

In the simulations, the following degrees of freedom are specified:

d_{2x}, d_{2y} offsets of the mobile base from the center of mass of the platform;

d_{ix}, d_{iy} base offsets of the (i^{th}-1) manipulator unit from the tip of the (i^{th}-2) unit;

α_i rigid rotation of the joint i, i.e rigid body rotation of the body i relative to the body (i-1);

l_i length of the (i^{th}-1) manipulator unit.

Here:

$$\begin{aligned} d_{2y} &= 1.5m, \\ d_{ix}, d_{iy} &= 0, \qquad i = 3, ..., N. \end{aligned} \tag{4.1}$$

d_{2x} (from now on referred to as d_2, for convenience), α_i, and l_i are either fixed at their respective initial values or vary as functions of time, as defined by Eq. (2.84). Once the amplitude of motion and its duration are specified for a given variable, Eq. (2.84) can be used to compute the time-history of that variable. Note that, unless mentioned otherwise, the mobile base is taken to be located 30 m from the center of the platform.

At times, it is convenient to describe the response of the system using variables other than the generalized coordinates to get better appreciation of the system dynamics. Hence, the following response variables are used:

ψ 'pitch' angle between the platform's long axis and the local vertical (LV), $\psi = \psi_1 - \theta$;

e_2 elastic displacement of the platform's tip relative to its undeformed position, $e_2 = \Phi_1|_{\frac{l_1}{2}} \delta_1$;

β_i elastic angular deformation of the ith joint, $\beta_i = \psi_i - \alpha_i - \xi_i - \psi_{i-1}$;

e_i tip deflection of the (i^{th}-1) unit relative to its undeformed position, $e_i = \Phi_{i-1}|_{l_{i-1}} \delta_{i-1}$.

Unless other initial conditions are expressly mentioned, the platform is initially oriented along the local vertical, i.e. $\psi(0) = 0$, and:

$$\begin{aligned} \beta_i(0) &= 0, \qquad i = 2, ..., N; \\ e_i(0) &= 0, \qquad i = 2, ..., N. \end{aligned} \tag{4.2}$$

The response variables are illustrated in Figure 4-1.

4.3 One-Unit Manipulator System

The case of the one-unit manipulator system is first investigated. Over the course of the parametric study, the system's initial conditions, physical parameters, and maneuver specifications were systematically varied, and their effects on the system dynamics were assessed. Based on the analysis, several representative cases were selected, which are discussed next.

4.3.1 Response to initial disturbances

The effects of various external disturbances, such as spacecraft docking, satellite capture, or impacts with external bodies, can be incorporated into the model through suitable initial conditions. This section investigates the system response to such external disturbances. The first case examines the response of the one-unit manipulator to the vibration of the supporting platform (Figure 4-2). The manipulator configuration, important parameters, and initial conditions are also indicated in the legend. The slew and deployment joints are both locked in positions ($l_2 = 10$ m, $\alpha_2 = 50^o$). The platform is given an initial tip deflection $e_2 = 1$ m. The figure describes the system response to this disturbance.

Energy is transferred from the platform's vibrations to the other degrees of freedom. Clearly, the joint, link, and platform vibrations, as well as the system pitch librational motion, are coupled. It should be noted that, because of the manipulator's position and orientation, the platform's equilibrium pitch angle changes from $\psi = 0^o$ to $\psi = -0.082^o$. Therefore, the system oscillates about this new equilibrium

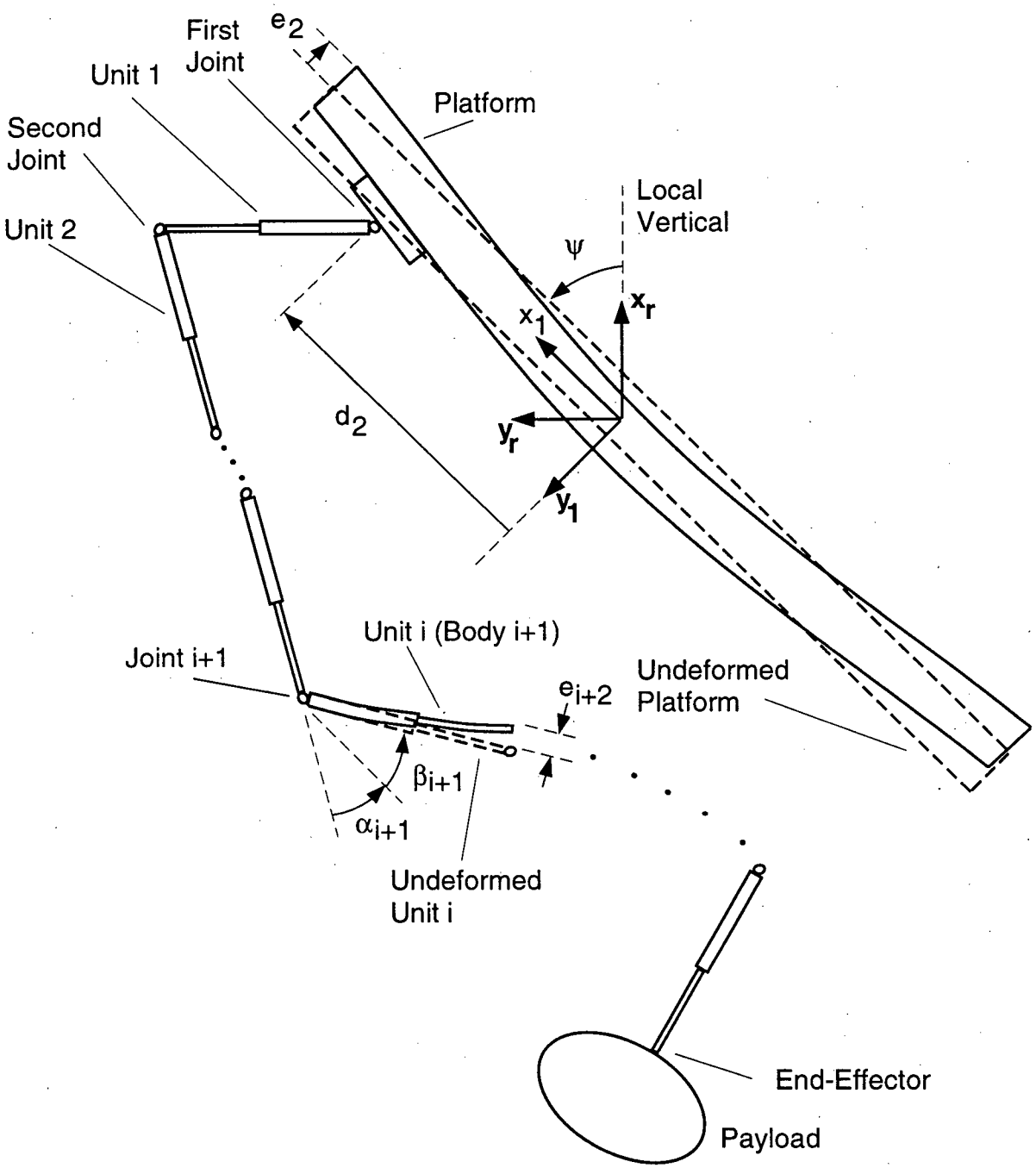

Figure 4-1 Schematic diagram of the manipulator system showing the coordinates considered for the dynamical study.

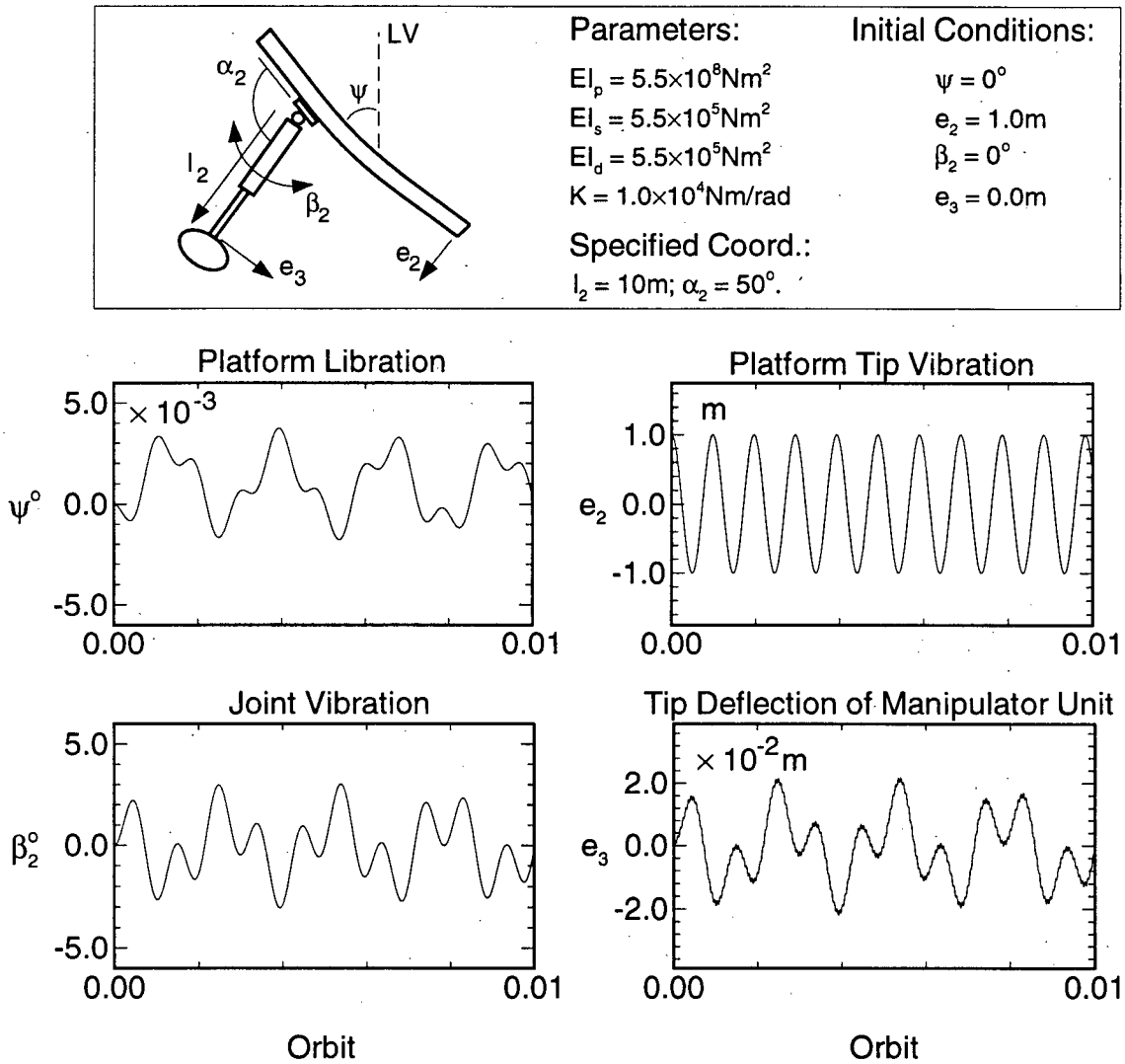

Figure 4-2 Response of the one-unit manipulator to the vibration of the supporting platform.

orientation. Since the librational period is approximately one orbit, this motion is not observable in the figure. Nonetheless, it is apparent that the long period librational response of the platform is modulated at the vibrational frequencies of the platform and manipulator joint.

The vibration of the platform progresses unaffected by the motion of the manipulator. Note that the mass of the platform is 150 times greater than that of the manipulator/payload combination. Therefore, the motion of the manipulator has almost negligible effects on the platform's vibration. On the other hand, it is apparent that the platform dynamics has a significant influence on the manipulator response, which now goes through slewing oscillations with an amplitude of $\beta_2 \approx 3^o$, around the equilibrium position of $\alpha_2 = 50^o$. The joint response clearly shows the presence of its natural frequency (0.07 Hz), as well as that of the platform's vibration (0.18 Hz). Of particular interest are the manipulator tip oscillations, e_3. They clearly show through their modulations the presence of three vibrational frequencies, which correspond to the natural frequencies of the platform, joint and link.

Next, the response of the system to a 0.1 m initial deflection of the manipulator's tip is investigated (Figure 4-3). The manipulator's vibration results in almost imperceptible response of the platform. However, it leads to significant vibration of the joint about its equilibrium position. In turn, the vibration of the joint slightly modulates the link response. Nevertheless, the modulations are small compared to the amplitude of the link vibrations.

It should be noted that the vibrational motion of the platform is also modulated by the joint and link vibrations. The platform's response clearly exhibits all three vibrational frequencies (platform, joint, and manipulator links).

Figure 4-4 considers a case identical to the one which has just been discussed, with the exception that structural damping is included in the manipulator links. A damping ratio corresponding to 0.1% of critical damping is assumed. Figure 4-

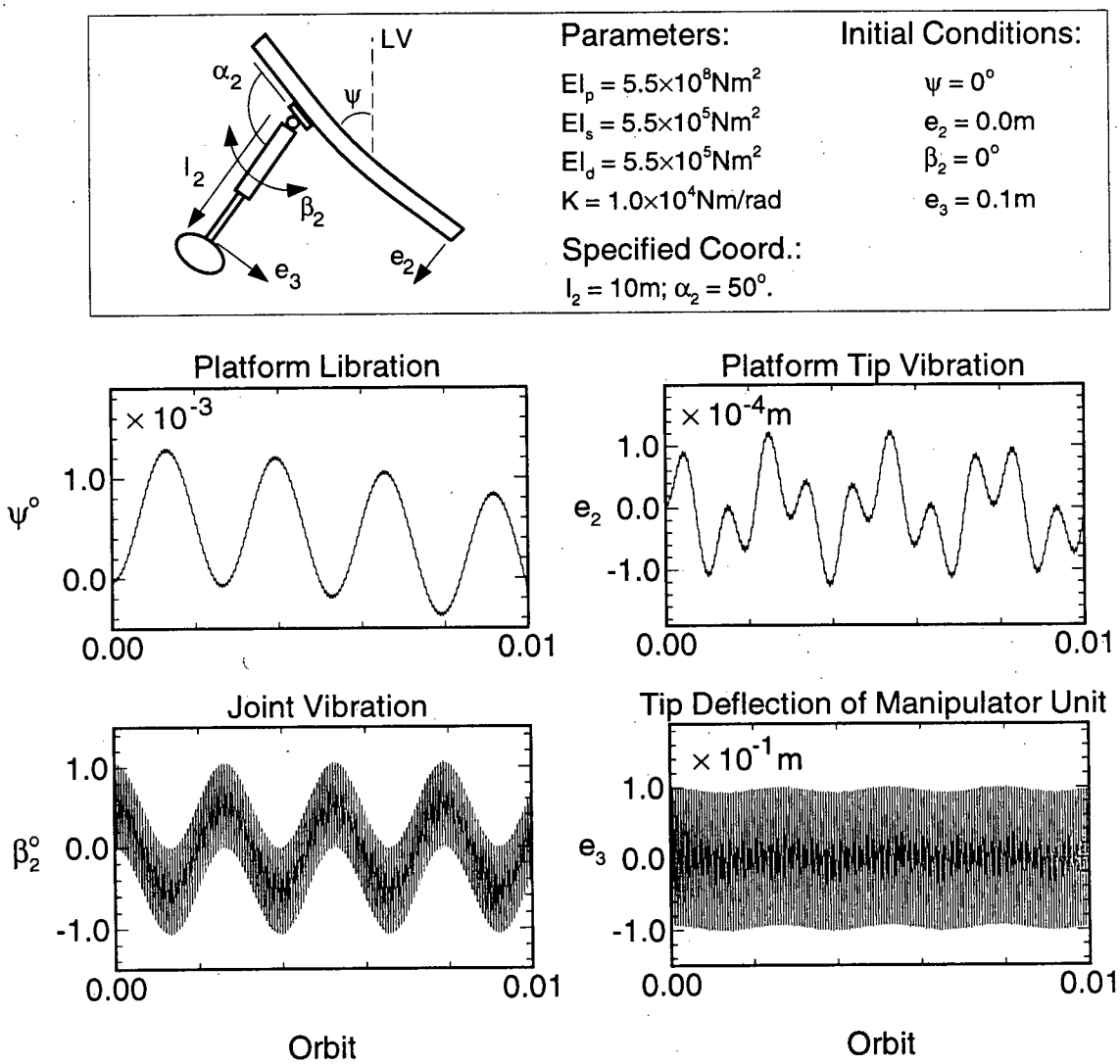

Figure 4-3 Response of the system to a 0.1 m initial deflection of the manipulator tip.

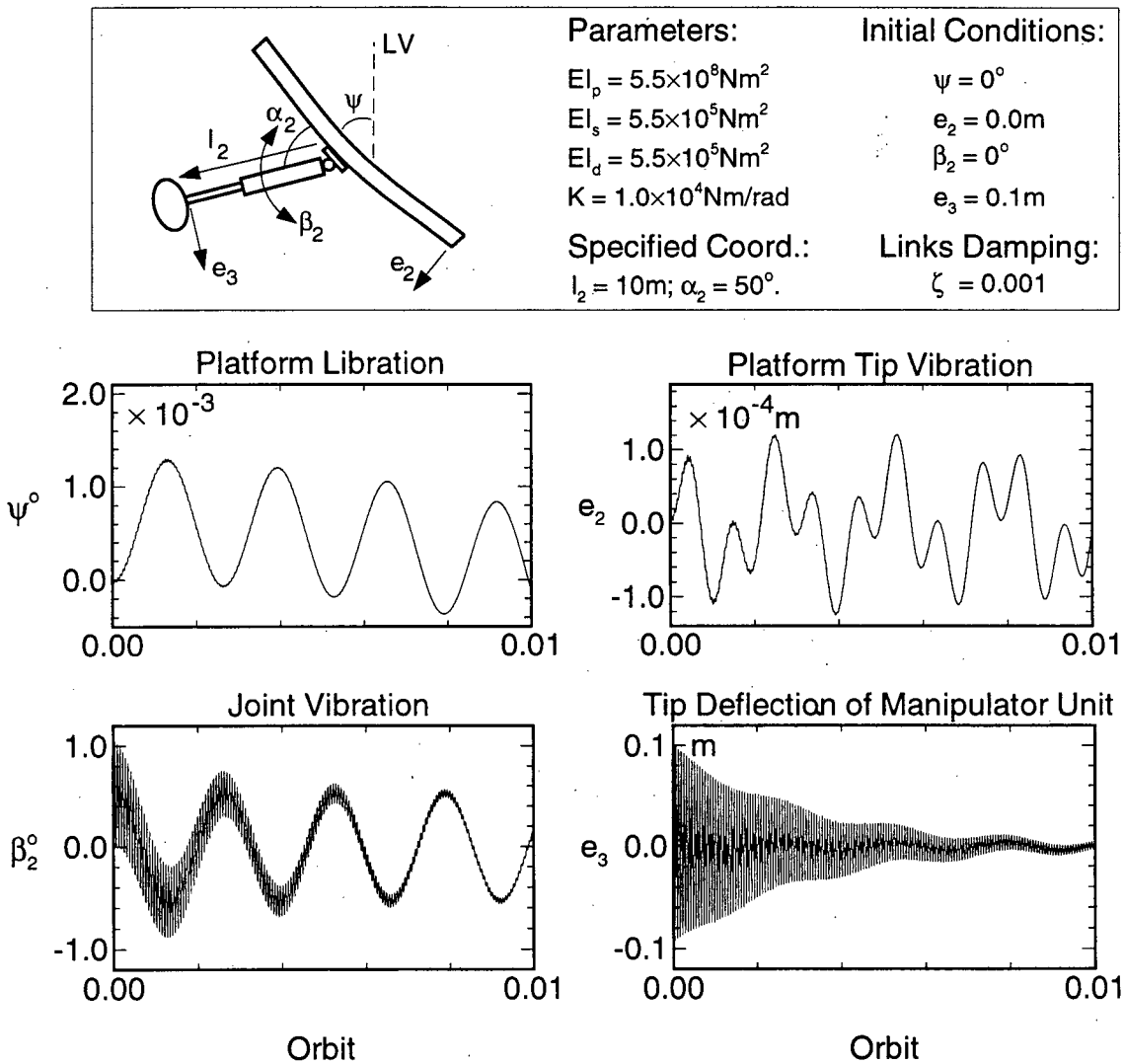

Figure 4-4 Effect of structural damping on the dynamical response of the manipulator to a 0.1 m displacement applied at its tip. A damping ratio corresponding to 0.1% of critical damping is assumed for the manipulator links.

4 shows that even this minute amount of damping has a significant effect on the system response. As expected, the vibration of the manipulator unit decreases in an underdamped fashion. It is interesting to note that the slewing oscillations of the joint also decrease with time; not only the modulation due to the vibration of the links, but also the oscillations at the joint's own natural frequency. This can be attributed to the strong coupling between the joint and link dynamics.

Thus, inclusion of a small amount of structural damping in the manipulator links appears to modify the system response significantly. However, the effect consists mainly in attenuation of the free response. With the exception of the damped oscillations, the qualitative nature of the response remains relatively unchanged. For cases involving maneuvers, damping was observed to have little effect. Therefore, in the remaining cases, the damping is purposely neglected in order to obtain conservative estimates for the system response.

Figure 4-5 describes the response of the system to a 5° elastic deformation of the manipulator joint. Clearly, joint oscillations have an important effect on the overall system dynamics. The amplitudes of the platform's librational and vibrational motions are an order of magnitude larger than those resulting from a 0.1 m initial deflection of the manipulator tip. This is due to the fact that the joint's natural frequency (0.07 Hz) is closer to the platform's fundamental frequency (0.18 Hz), as against the natural frequency of the manipulator links (3.1 Hz). Again, the coupling between the joint and link vibration is evident: The joint oscillations result in vibrations of the manipulator unit with the tip amplitude approaching 8 cm.

In summary, Figures 4-2 through 4-5 show the existence of strong coupling between the joint, link, and platform responses, as well as the librational motion of the system. The natural frequencies considered for the structural components, as well as the natural frequency of the platform's attitude motion, form a widely spaced spectrum. The various natural frequencies of the components can be clearly identified

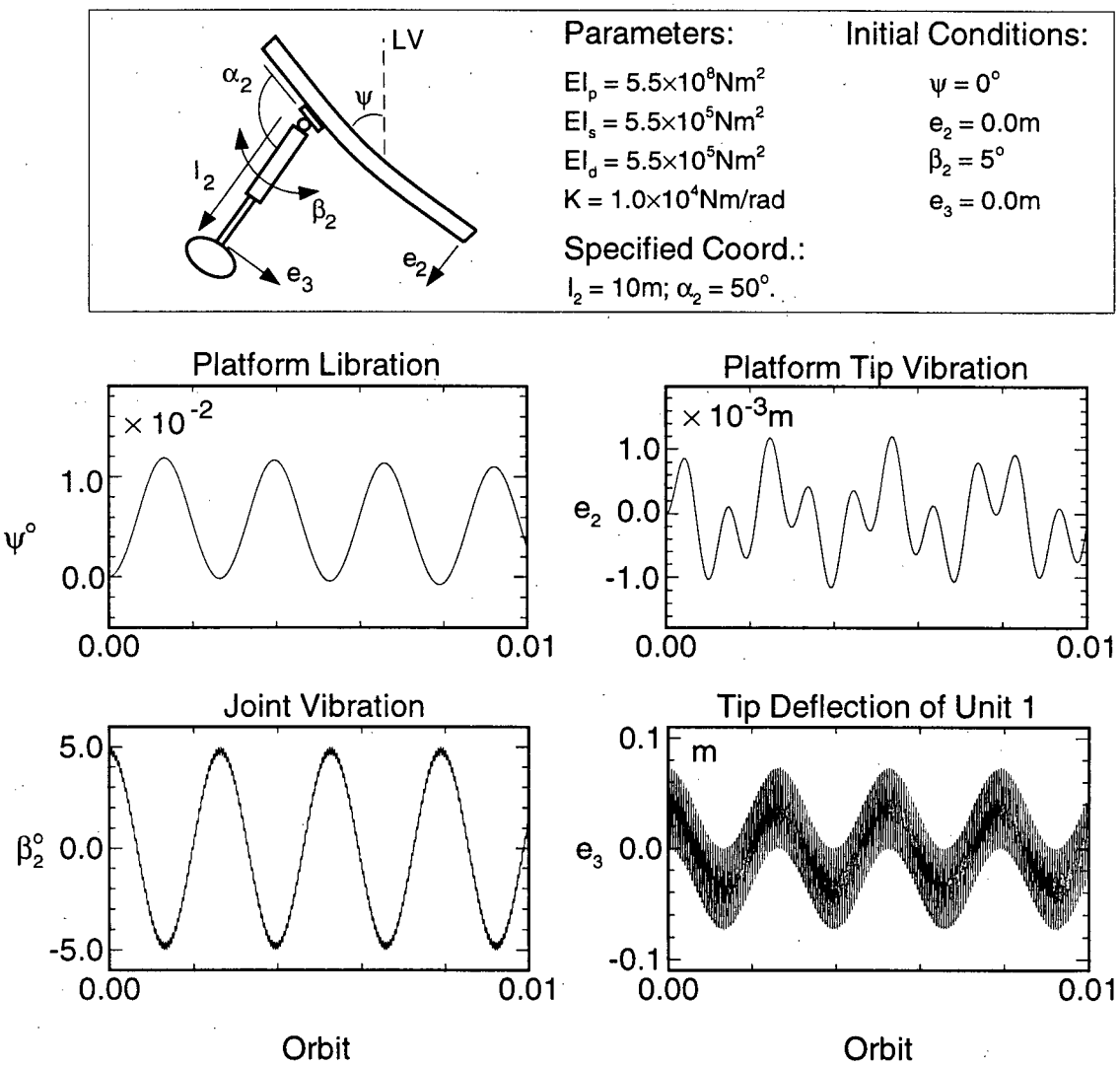

Figure 4-5 System response to a 5° initial deformation of the manipulator joint.

in the modulated time response of the degrees of freedom. Figure 4-6 illustrates a case where two of the system's natural frequencies are brought closer together.

Essentially, the case considered here is the same as the one described in Figure 4-5, with the exception that the manipulator links are taken to be rigid. Figure 4-6(a) shows the response of the joint and the resulting vibrational response of the platform, as given in Figure 4-5. In Figure 4-6(b), the results obtained with the joint stiffness $K = 9.9 \times 10^4$ Nm/rad are presented. This value brings the joint's natural frequency close to that of the platform vibration ($\omega_j = 0.21$ Hz, $\omega_p = 0.18$ Hz). Note, the amplitude of platform vibrations is nearly twenty times greater in the presence of the same initial disturbance. As expected, the platform response exhibits the beat phenomenon. Thus, manipulator maneuvers at critical frequencies can lead to resonance and unacceptable system behavior. This is explored in the following section.

4.3.2 Response to slewing maneuvers

Next, the system response to slewing maneuvers is investigated. Figure 4-7 describes the system's motion with the manipulator executing a 180° slewing maneuver from $\tau = 0$ to $\tau = 0.01$ orbit. The unit is carrying a 400 kg payload. The response is shown for three locations of the mobile base: $d_2 = 0$ (i.e. center of the platform), $d_2 = 30$ m, and $d_2 = 60$ m (i.e. edge of the platform).

The maneuver slightly modifies the system's equilibrium orientation, resulting in rigid-body oscillations of the platform. Librational motion is also induced by the inertia forces of the manipulator transmitted to the platform through the base. It is interesting to note that, during the maneuver, the platform rotates in the direction opposite to the maneuver in order to conserve the angular momentum. Clearly, moving the manipulator base away from the center of the platform increases the system's librational response. The slewing maneuver has a stronger effect on the system's inertia tensor when the mobile base is located farther from the center. When

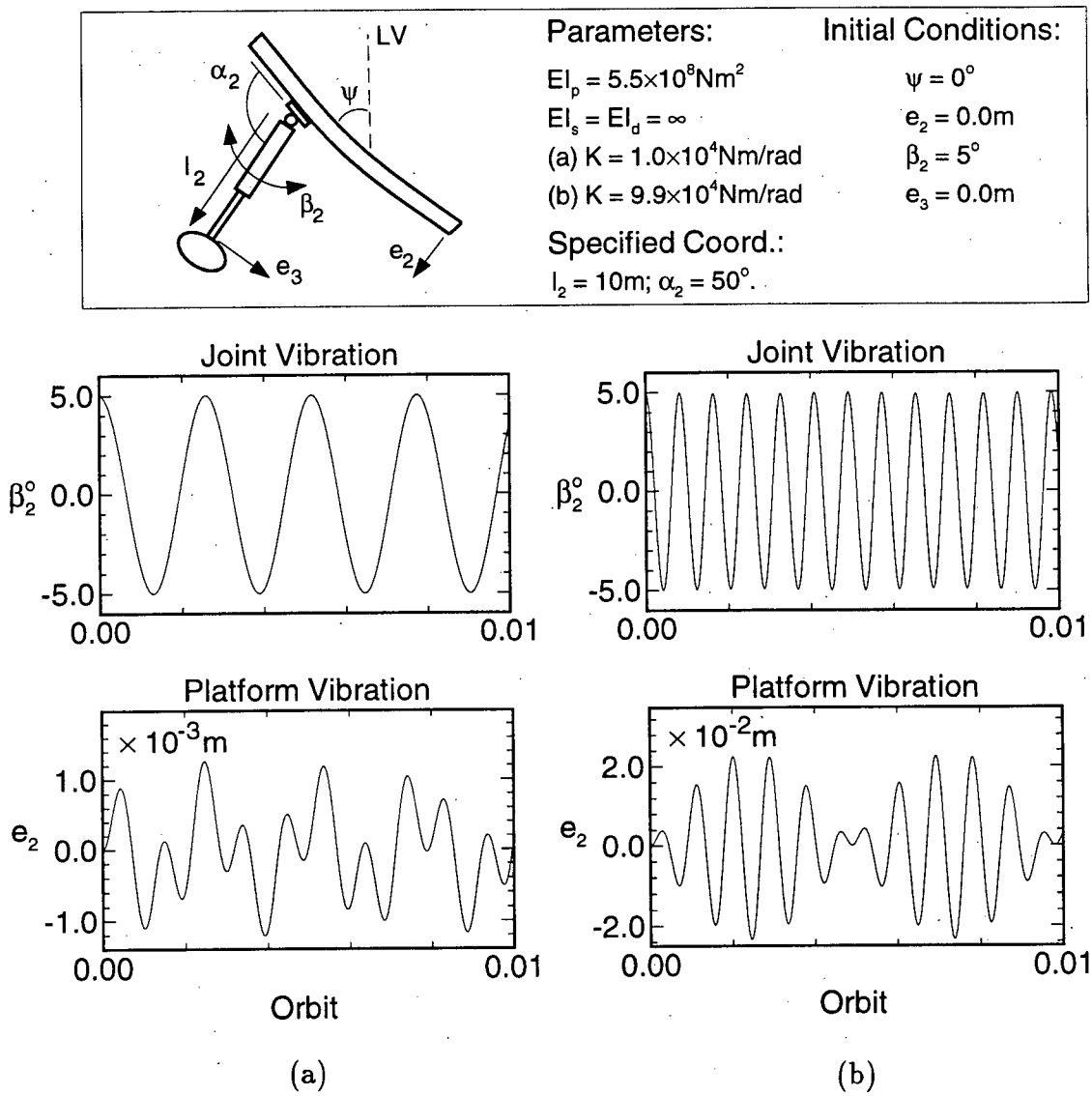

Figure 4-6 Platform and joint vibrational response to a 5° initial elastic deformation of the manipulator joint: (a) $K = 1.0 \times 10^4$ Nm/rad; (b) $K = 9.9 \times 10^4$ Nm/rad. Note, the platform tip deflections in (b) exhibit the beat phenomenon.

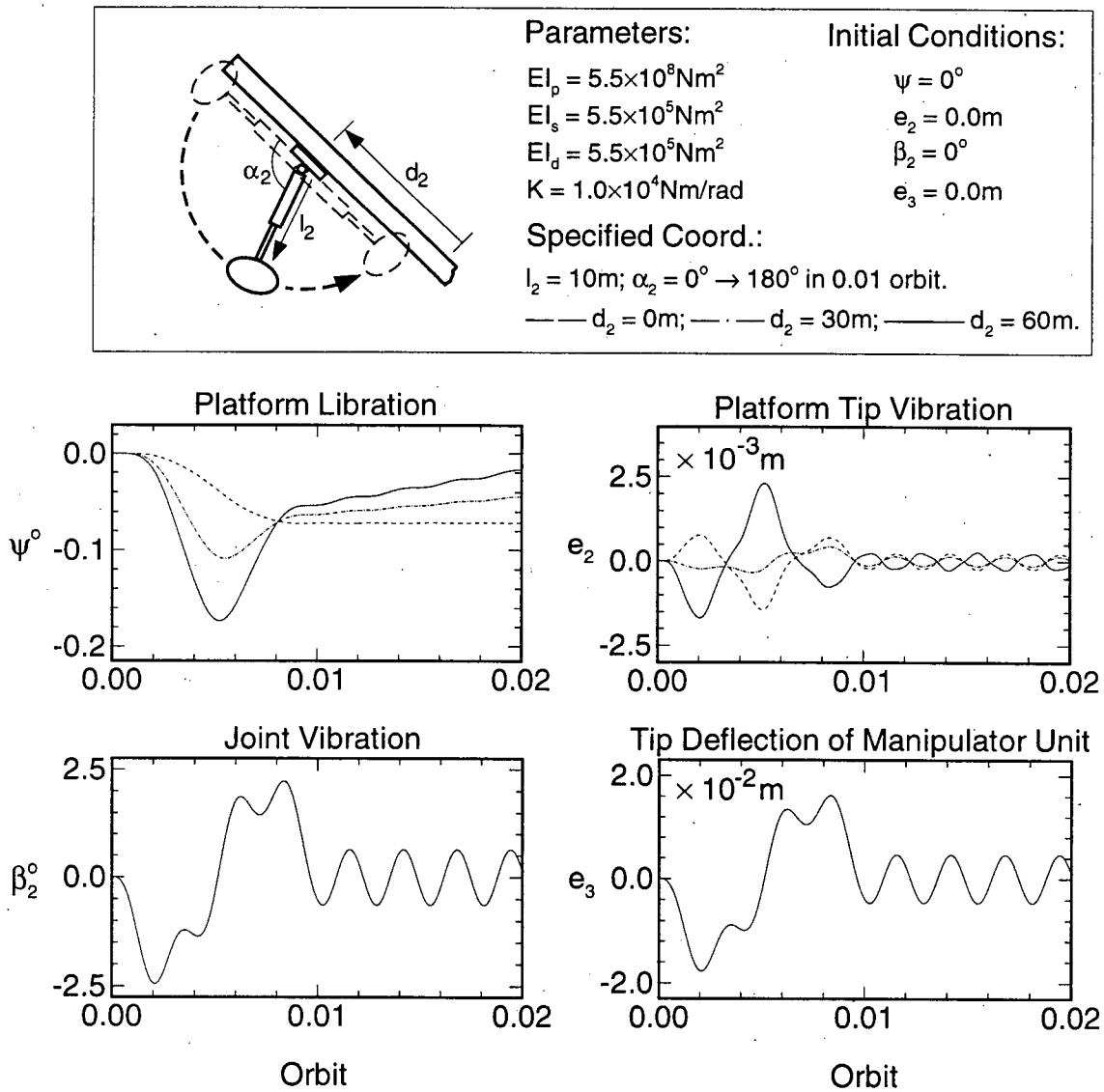

Figure 4-7 System response to a 180° slewing maneuver of the manipulator for various locations of the mobile base.

the base is located near the edge of the platform, the resulting pitch deviation reaches nearly -0.18^o. This is significant as the platform's required pointing accuracy may be as small as 0.1^o.

The slewing maneuver also induces vibration of the platform. The largest elastic deformation is obtained when the base is located near the platform's tip, with tip deflections reaching 2.5 mm during the second half of the maneuver. After the end of the maneuver, some residual vibrations persist in all three cases, but they are of the order of 10^{-4} m. It is interesting to note that the smallest platform vibrations correspond to the case where $d_2 = 30$ m. Here, the mobile base is located close to one of the nodes of the shape function, which is at $x_1 = 33.1$ m. Therefore, it is difficult for the exciting force to deform the platform at this location. One should explore the effect of higher modes in such situations.

It is of interest to recognize that the responses of the manipulator joint and links are quite similar and remain unaffected by the location of the mobile base: All the three cases coincide perfectly. The peak responses are reached during the second half of the maneuver, with a maximum joint deformation of 2.5^o and a peak tip deflection approaching 2.0 cm. After the end of the maneuver (i.e. $\tau > 0.01$ orbit), residual vibrations continue, with amplitudes of 0.7^o for the manipulator joint and 5 mm for its tip deflection.

Figure 4-8 examines the effects of the payload mass on the system response. The mobile base is located at the edge of the platform for maximum effect. The manipulator undergoes a 180° slewing maneuver as before. Payload ratios of 1, 2, and 5 are considered. As before, the maximum amplitudes are reached during the second half of the maneuver, i.e. in the decelerating phase. It is apparent that an increase in the mass of the payload increases the amplitude of the responses. Furthermore, a higher payload also increases the inertia of the system while the system's stiffness parameters remain unchanged. As a result, the vibrational frequencies for the joint

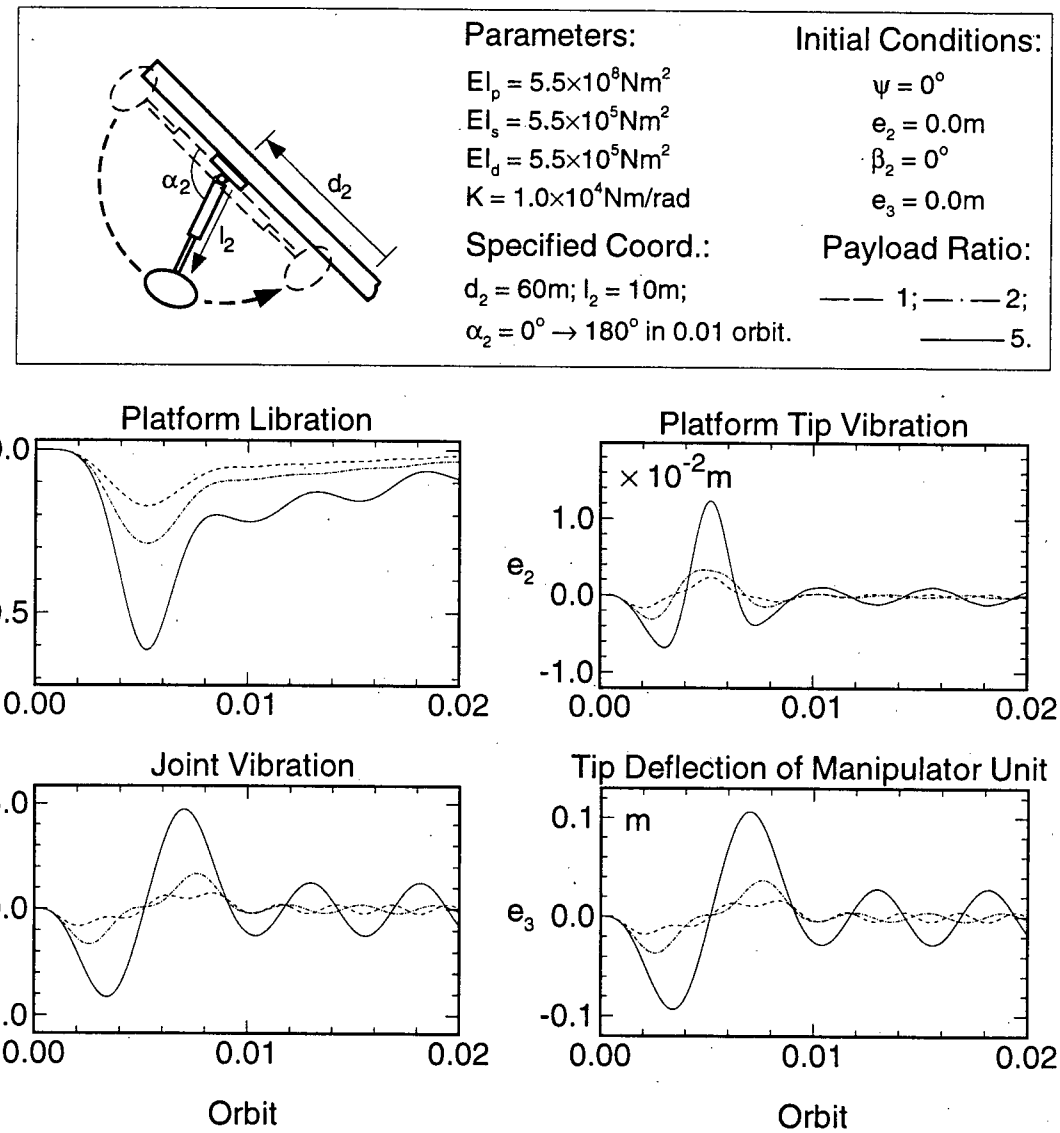

Figure 4-8 Effect of payload mass on the system response to slewing maneuvers.

deformation and manipulator tip deflection become lower. Note that, for the case where the payload ratio is 5, the vibrational amplitudes are of the order of 1 cm for the platform, and reach 15° and 10 cm for the manipulator joint and links, respectively.

Figure 4-9(a) shows the effect of higher order modes on the system response for the case investigated in Figure 4-8 with a payload ratio of 5. Only the time histories of the platform and manipulator tip deflections are shown, as higher modes have no noticeable effects on the platform libration and joint vibration. From the figure, it can be seen that the second mode brings a noticeable correction to the response. Nonetheless, it is clear that the use of only one mode still provides a reasonably accurate result, with a significant saving in computational time. In any case, the third and higher modes have negligible effect on the system response.

Figure 4-9(b) considers the same case, but with $d_2 = 30$ m. As the mobile base gets closer to the node of the first mode ($x_1 = 33.1$ m), it is not sufficient to model the symmetric vibration of the platform and the second mode must be taken into account. Contributions of the third and higher order modes still remain negligible. The first mode continues to be sufficient to describe the vibration of the manipulator unit.

Throughout the investigation of the 180° slew maneuver, which considered values of d_2 ranging from 0 to 60 m, the system's vibrational behavior was found to remain essentially similar to that presented in Figure 4-9(a). Thus it can be concluded that, in general, the fundamental mode is adequate to model the system dynamics. However, a word of caution is appropriate, particularly at higher maneuvering speeds, which may excite higher modes. On the other hand, it is common practise in robotic control to limit the motion frequency to no more than half of the fundamental frequency of the structural components [41]. Thus the use of the fundamental mode appears to be sufficient to describe the system structural response.

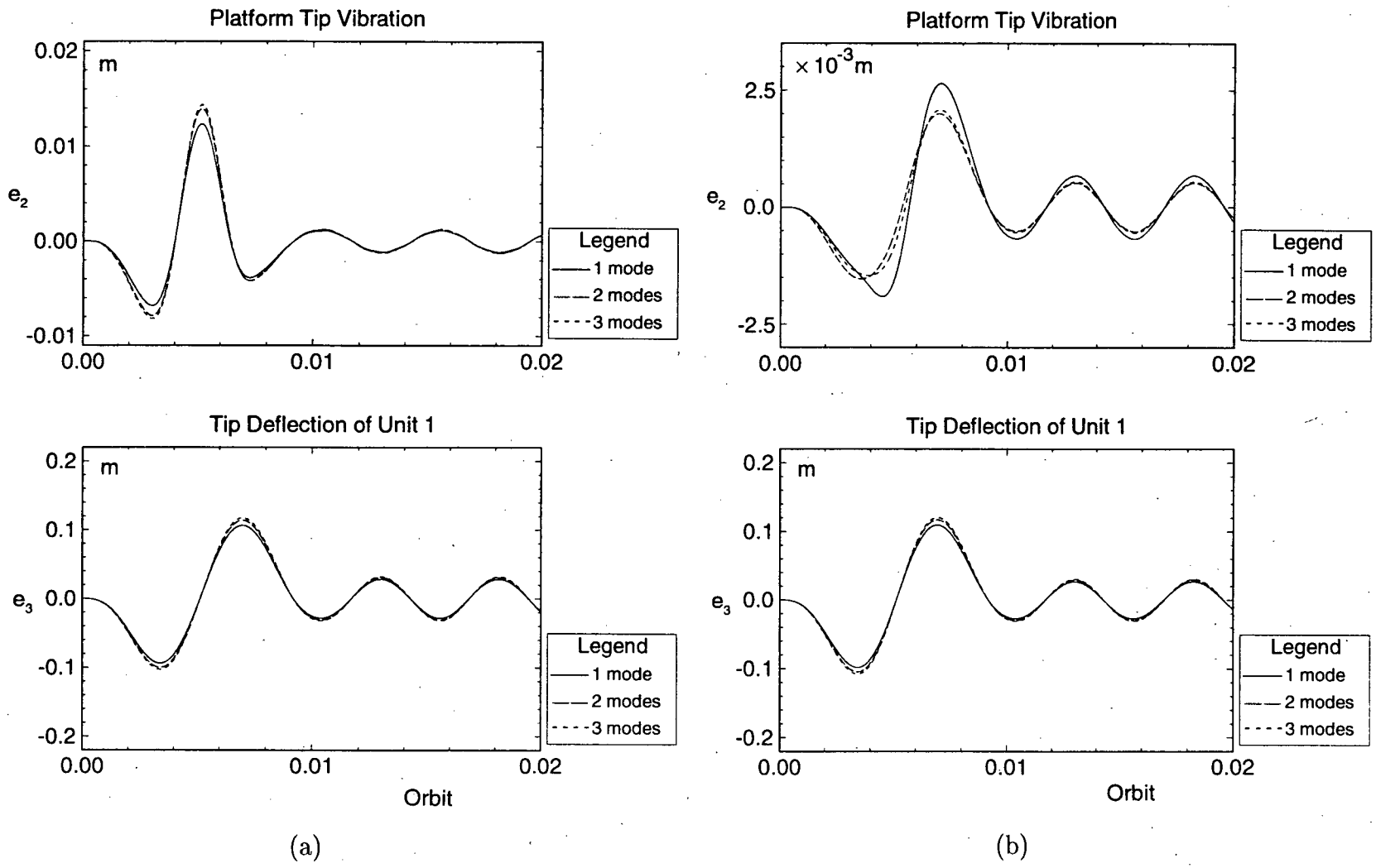

(a) (b)

Figure 4-9 Effect of higher modes on the system's structural vibrations during a 180° slewing maneuver in 0.01 orbit. Note, the manipulator is supporting a 2000 kg payload and is located at: (a) $d_2 = 60$ m; (b) $d_2 = 30$ m.

4.3.3 Response to deployment maneuvers

The effect of manipulator deployment is now assessed. The manipulator is taken to be located near the edge of the platform ($d_2 = 60$ m) and is oriented perpendicular to the platform's long axis ($\alpha_2 = 90^o$). Initially, the manipulator unit is partly deployed to a length of 10 m, and the vibration of the manipulator links is excited with an initial tip deflection of 10 cm. Softer links are considered in this case ($EI_s = EI_d = 5.5 \times 10^4 Nm^2$). From $\tau = 0$ to $\tau = 0.005$ orbit, the manipulator length remains unchanged at $l_2 = 10$ m. From $\tau = 0.005$ to $\tau = 0.01$ orbit, the manipulator is extended to its maximum length of 15 m. It remains fully deployed between $\tau = 0.01$ and $\tau = 0.015$ orbit, then retracts to a length of 10 m from $\tau = 0.015$ to $\tau = 0.02$ orbit, and remains at that length until the end of the simulation.

The system response is shown in Figure 4-10. The initial tip deflection results in vibrations of the manipulator joint and links, as well as in platform vibrations. The deployment of the manipulator unit changes the inertia tensor of the system and modifies its attitude, as shown on the figure. The maximum platform tip deflections are experienced during the deployment and retrieval of the unit. It should be noted that deployment makes the unit structurally softer and lowers its structural natural frequency. Retrieval has the opposite effect and results in a higher natural frequency. This becomes obvious when the time history of the manipulator's tip deflection is considered: When the unit is fully extended, the vibrational amplitude of the links is larger and its frequency is lower than when the unit is partly retracted, prior to and after the maneuver. This strongly affects the joint vibration as well through coupling.

4.3.4 Response to complex maneuvers

Next, the effects of various maneuvers involving slew and deployment of the manipulator unit, as well as translation of the mobile base, are studied. Figure 4-11 gives the system response to a simultaneous 90° joint rotation and 5 m deployment of

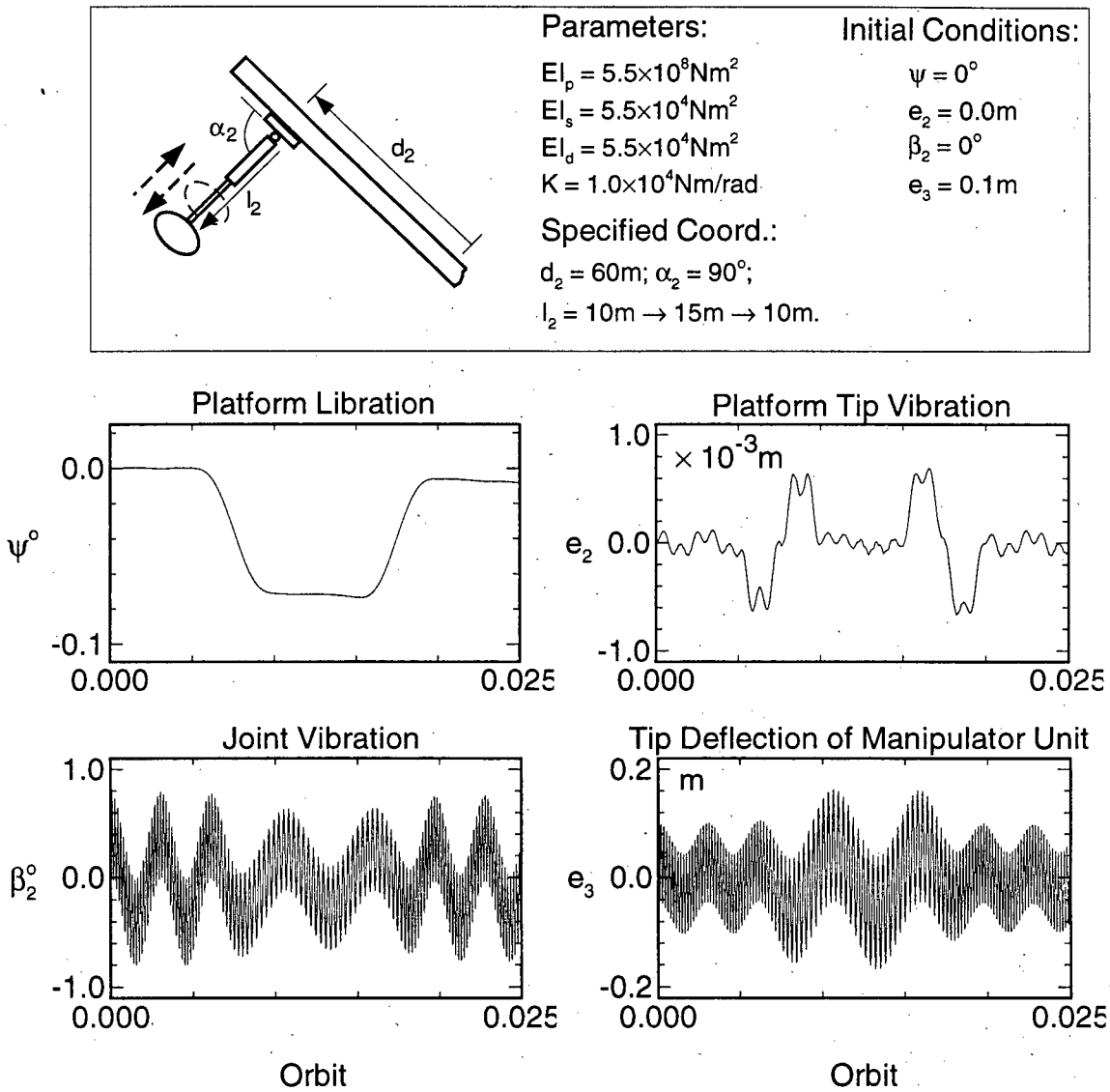

Figure 4-10 Effect of the manipulator's deployment and retrieval maneuver on the system response in the presence of a 0.1 m disturbance of the manipulator tip.

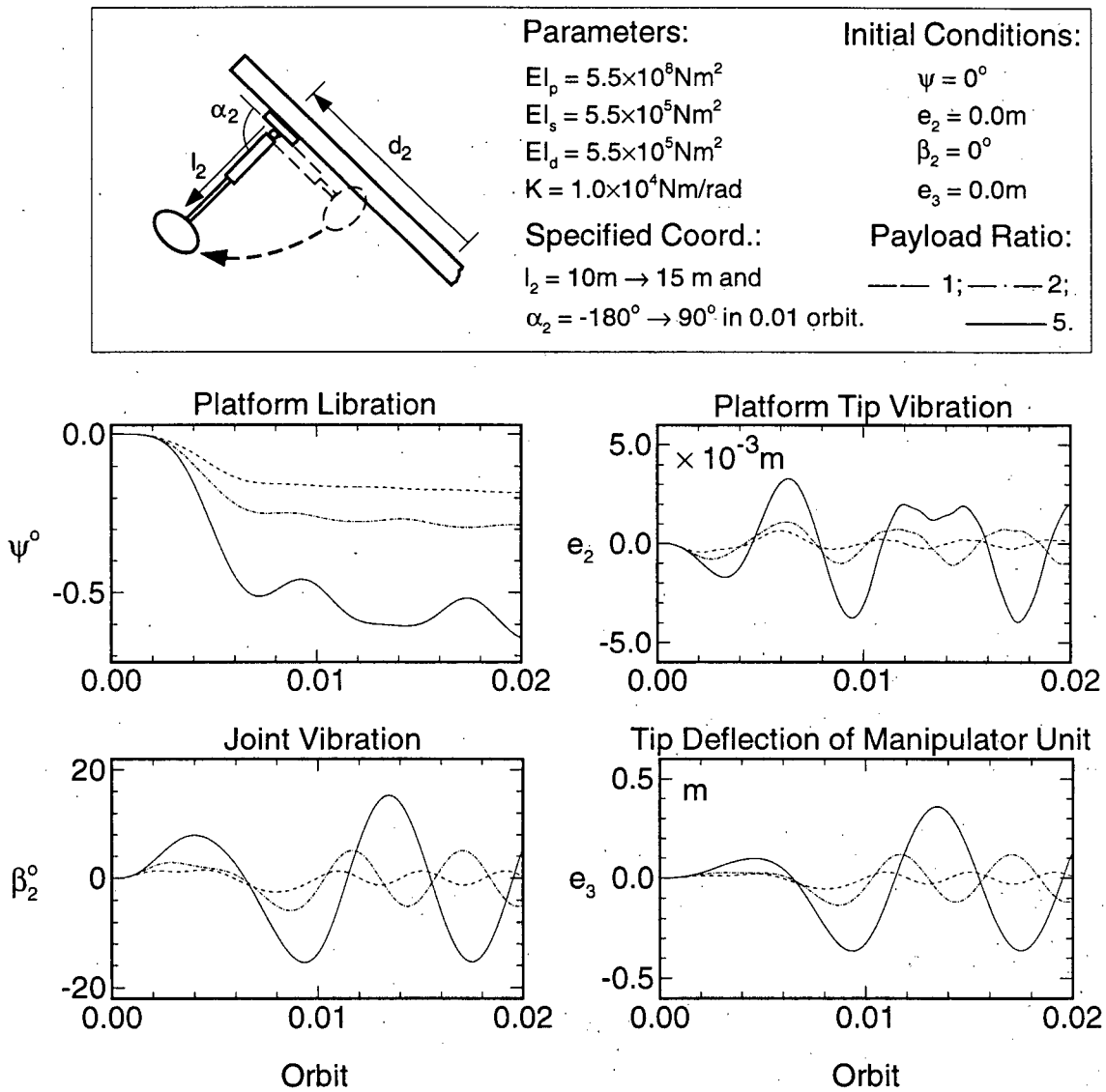

Figure 4-11 System response to a simultaneous 90° joint rotation and 5 m deployment of the manipulator unit.

the manipulator unit. Throughout the simulation, the mobile base remains at the tip of the platform. Initially, the unit is parallel to the platform's long axis ($\alpha_2 = 180^o$) and partially retracted, with $l_2 = 10$ m. At the end of the maneuver (i.e. $\tau = 0.01$ orbit), the unit is perpendicular to the platform ($\alpha_2 = 90^o$) and extended to its maximum length 15 m. Three payload ratios (1, 2, and 5) are considered. As before, larger payloads result in greater vibrational amplitudes and lower vibrational frequencies. The behavior of the joint and link generalized degrees of freedom are quite similar, once again emphasizing the strong coupling between the two.

The maneuver, with a payload ratio of 5, induces a significant response in all degrees of freedom. The platform's pitch angle is modified by as much as 0.7^o and significant platform vibrations arise, with a maximum tip deflection of 3.5 mm. The joint deflection approaching 20° and the manipulator tip deflection of the order of 40 cm severely compromize the positioning accuracy of the manipulator.

The effects of higher modes for this particular case (i.e. payload ratio of 5) are assessed in Figure 4-12(a). As it was the case during the simple slew maneuver (Figure 4-9), higher modes have no noticeable influence on the platform pitch libration and joint oscillations. Despite the presence of deployment, which introduces Coriolis and other inertia forces, second and higher modes have no apparent effect on the structural vibration of the manipulator links. Even for a platform extending to 120 m, the effect of the second mode only amounts to a fraction of a millimeter! Thus, the use of only the fundamental mode provides a reasonable approximation, even during this severe maneuver.

Figure 4-12(b) considers the same case with the exception that the mobile base is located at $d_2 = 30$ m. As for the slewing case, the second mode becomes relatively more important due to the proximity of the base to the node of the first free-free mode.

The next case involves a complex maneuver of the one-unit manipulator, which

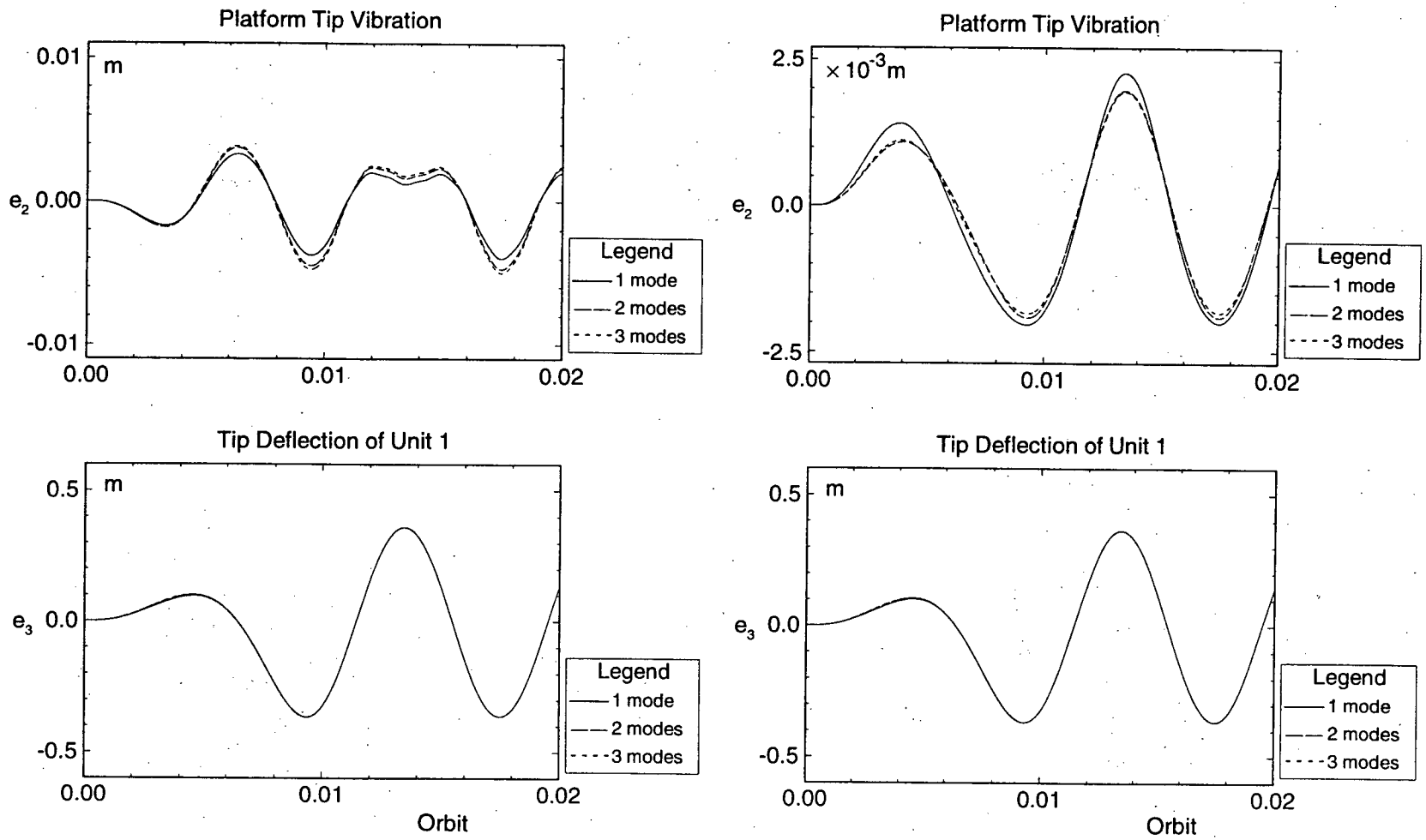

(a) (b)

Figure 4-12 Effect of higher order modes on the system's structural vibration during a simultaneous 90° slew and 5 m deployment in 0.01 orbit. Note, the manipulator is supporting a 2000 kg payload and is located at: (a) $d_2 = 60$ m; (b) $d_2 = 30$ m.

is illustrated in Figure 4-13. The maneuver consists of a simultaneous rotation and deployment of the manipulator unit, along with a translation of the mobile base. The base is initially located at $d_2 = 10$ m, and the manipulator's end-effector is positioned precisely on the center of the platform's surface. The aim of the maneuver is to position the end-effector on the surface of the platform, 50 m from the center. Therefore, the maneuver involves a 30 m translation of the mobile base and a 180° joint rotation in 0.01 orbit. In addition, the manipulator unit is deployed from $l_2 =$ 10 m to $l_2 = 15$ m during the first half of the maneuver, and retracted to its original length during the second half. Therefore, halfway through the maneuver, at $\tau = 0.005$ orbit, the unit is fully extended, perpendicular to the platform, and the end-effector has reached its maximum velocity relative to the platform. The values for the initial conditions, joint rotations, and deployment lengths are indicated on the figure. The maneuver results in significant vibrations of the slew-joint and links, which persist after the end of the maneuver as the system damping is purposely taken to be zero. The maneuver also excites, slightly, the platform vibrational and librational degrees of freedom.

The next case investigates the ability of the one-unit manipulator to track a straight line trajectory with its end-effector. The trajectory in question is a 5 m straight line, going from ($x_1 = 5.00$ m, $y_1 = 10.16$ m) to ($x_1 = 8.54$ m, $y_1 = 6.62$ m), relative to the platform's reference frame F_1. Hence, the time history of the end-effector's position is described by Eq. (2.84) with $\Delta\tau = 0.01$ orbit and $\Delta S = 5$ m, i.e.

$$\begin{aligned} x_1(\tau) &= \frac{\Delta S}{\sqrt{2}\Delta\tau}\left\{\tau - \frac{\Delta\tau}{2\pi}\sin\left(\frac{2\pi}{\Delta\tau}\tau\right)\right\} + 5.00 \\ y_1(\tau) &= \frac{-\Delta S}{\sqrt{2}\Delta\tau}\left\{\tau - \frac{\Delta\tau}{2\pi}\sin\left(\frac{2\pi}{\Delta\tau}\tau\right)\right\} + 10.16. \end{aligned} \tag{4.3}$$

In the present case, the mobile base is locked in place ($d_2 = 0$). Two degrees of freedom are then available for tracking: the rotation of the joint and the deployment

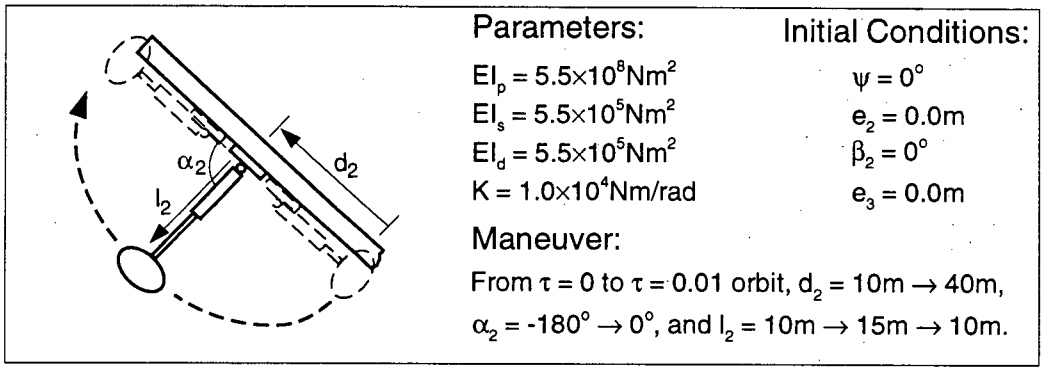

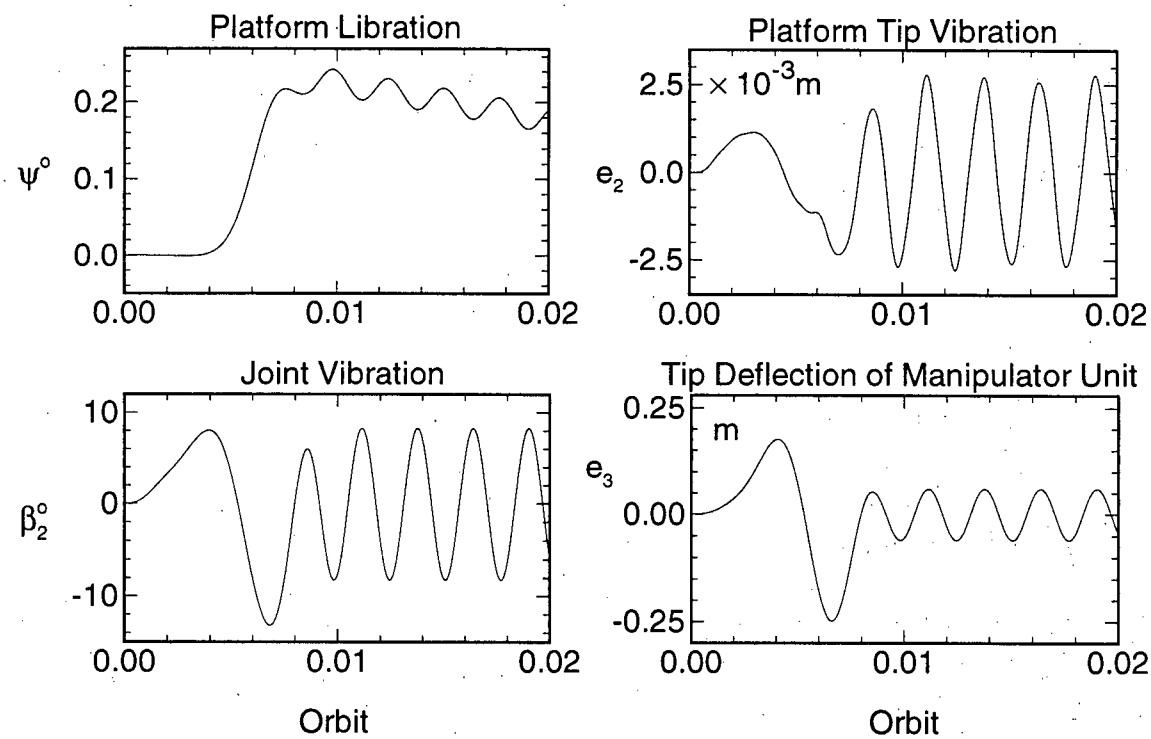

Figure 4-13 System response during a complex maneuver of the one-unit manipulator. The maneuver involves slew, deployment, translation, and retrieval.

of the unit. The time-history for each degree of freedom can be obtained through simple inverse kinematics. From:

$$\begin{aligned} x_1 &= d_{2x} + l_2 \cos\alpha_2; \\ y_1 &= d_{2y} + l_2 \sin\alpha_2; \end{aligned} \tag{4.4}$$

one gets

$$\begin{aligned} l_2 &= \sqrt{(x_1 - d_{2x})^2 + (y_1 - d_{2y})^2}; \\ \alpha_2 &= \tan^{-1}\left(\frac{y_1 - d_{2y}}{x_1 - d_{2x}}\right). \end{aligned} \tag{4.5}$$

It should be noted that Eq. (4.5) is only valid for $-90^o < \alpha_2 < 90^o$, which includes the trajectory considered here. For $\alpha_2 > 90^o$ or $\alpha_2 < -90^o$, alternate expressions should be derived. Furthermore, the situation where $\alpha_2 = \pm 90^o$ represents a singularity and should be avoided. Finally, it must be noted that Eq. (4.5) does not account for the system's flexible character when computing the inverse kinematics.

Figure 4-14(a) shows the joint rotation (α_2) and deployment (l_2) time-histories. The trajectory of the end-effector is also illustrated. The desired trajectory is presented as a reference. Clearly, the end-effector deviates slightly from the desired trajectory. This is a consequence of the flexible nature of the system. Figure 4-14(b) indicates that the maneuver does excite the flexible degrees of freedom. Although the platform's pitch libration and structural vibrations remain quite small, the manipulator's tip deflection, and especially the joint oscillations, cannot be considered negligible. They reduce the positioning accuracy of the end-effector.

4.4 Two-Unit Manipulator System

The present section focuses on the dynamics of a two-unit manipulator supported by an orbiting platform. When the length of the units remains constant, this model can be used to study the dynamics of manipulators with two revolute joints such as the Space Shuttle based RMS and the Space Station's MSS.

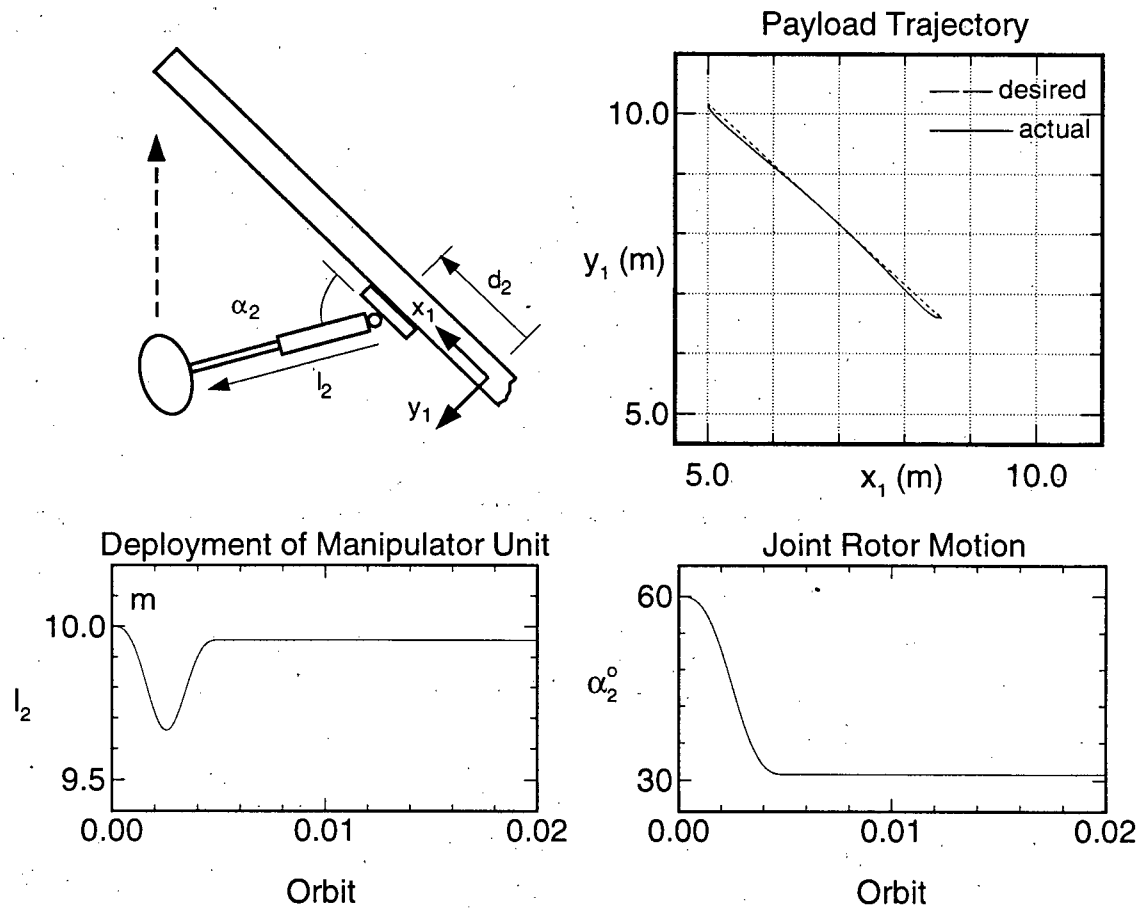

(a)

Figure 4-14 Tracking of a straight line trajectory using the slew and deployment degrees of freedom: (a) time histories of the joints and position of the end-effector.

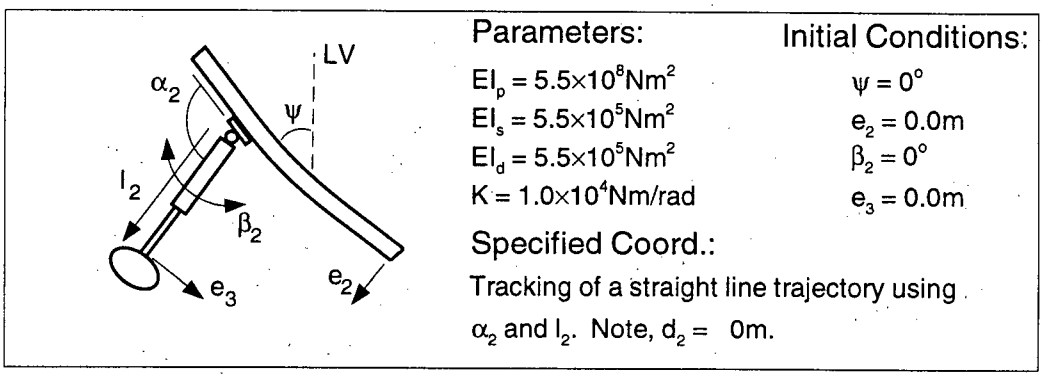

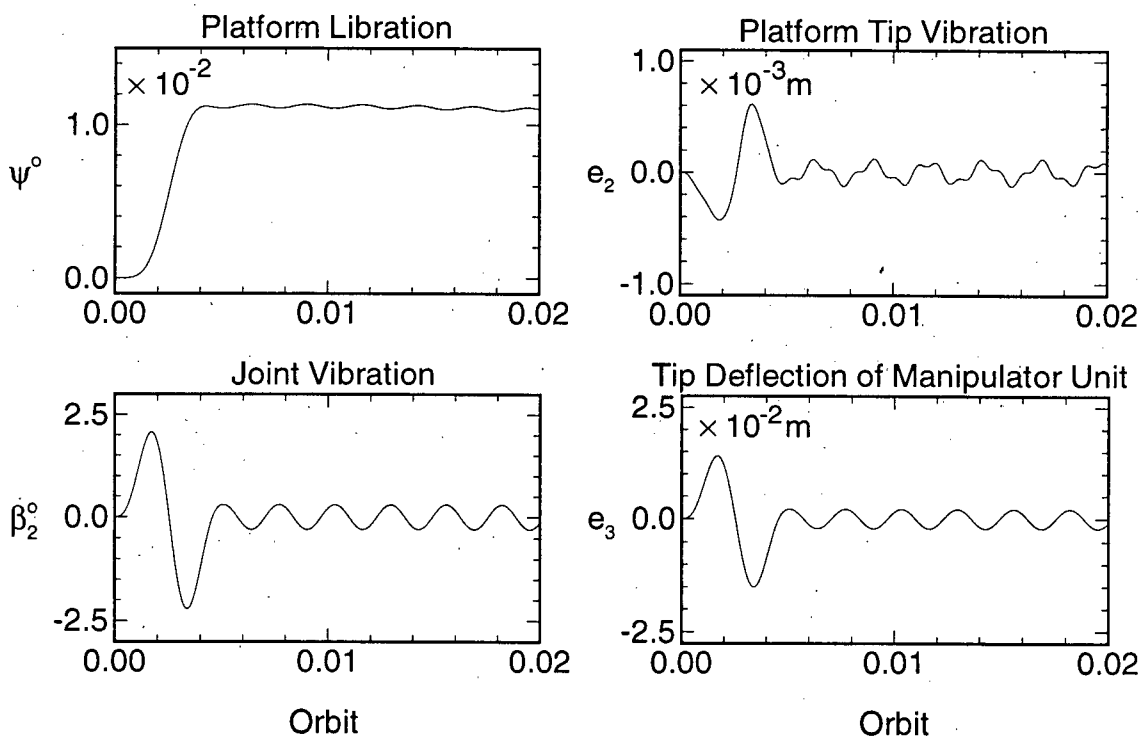

(b)

Figure 4-14 Tracking of a straight line trajectory using the slew and deployment degrees of freedom: (b) system response during the maneuver.

4.4.1 Response to initial disturbances

The first case investigates the system response to an initial 1.0 m deflection of the platform's tip (Figure 4-15). The manipulator's configuration is described in the inset of Figure 4-15. The base of the manipulator is located near the edge of the platform, where the platform vibrations reach their maximum values. This results in a significant excitation of the manipulator's degrees of freedom. It is interesting to note that the tip deflections of the second unit are considerably larger than those for the first unit. The same can be said for the vibration of the second joint compared to the first one. In fact, the joint vibrations are so large, with amplitudes approaching 20° and 40° for the first and second joint, respectively, that they slightly modulate the platform's vibration. Note, the motion of the manipulator also induces small librational motion. Of interest are the high frequency modulations at the first unit's natural frequency in its response (e_3).

At this point, it should be reiterated that the shape functions used for the manipulator units correspond to the mode shapes of a cantilever beam with tip masses. For the second unit, a point tip mass of 400 kg, which corresponds to the mass of the payload, is considered. For the first unit, a tip mass of 800 kg is taken, which represents the combined mass of the payload and second unit. Figure 4-16 compares the results obtained using the above modes (Figure 4-15) with the system response to the same initial disturbance but employing the free cantilever modes (i.e. without payload). Only the tip deflections of the manipulator units are shown, as the platform and joint vibrational motion, as well as the system's librational response, were not affected by the choice of the shape functions. The solid line represents the response with shape functions incorporating the effects of tip masses. The dash line shows the dynamics with free cantilever modes. Figure 4-16 leads to the conclusion that, except for minor local differences, the effect of mode shapes does not seem to be dominant. Incorporation of higher modes would further reduce its importance.

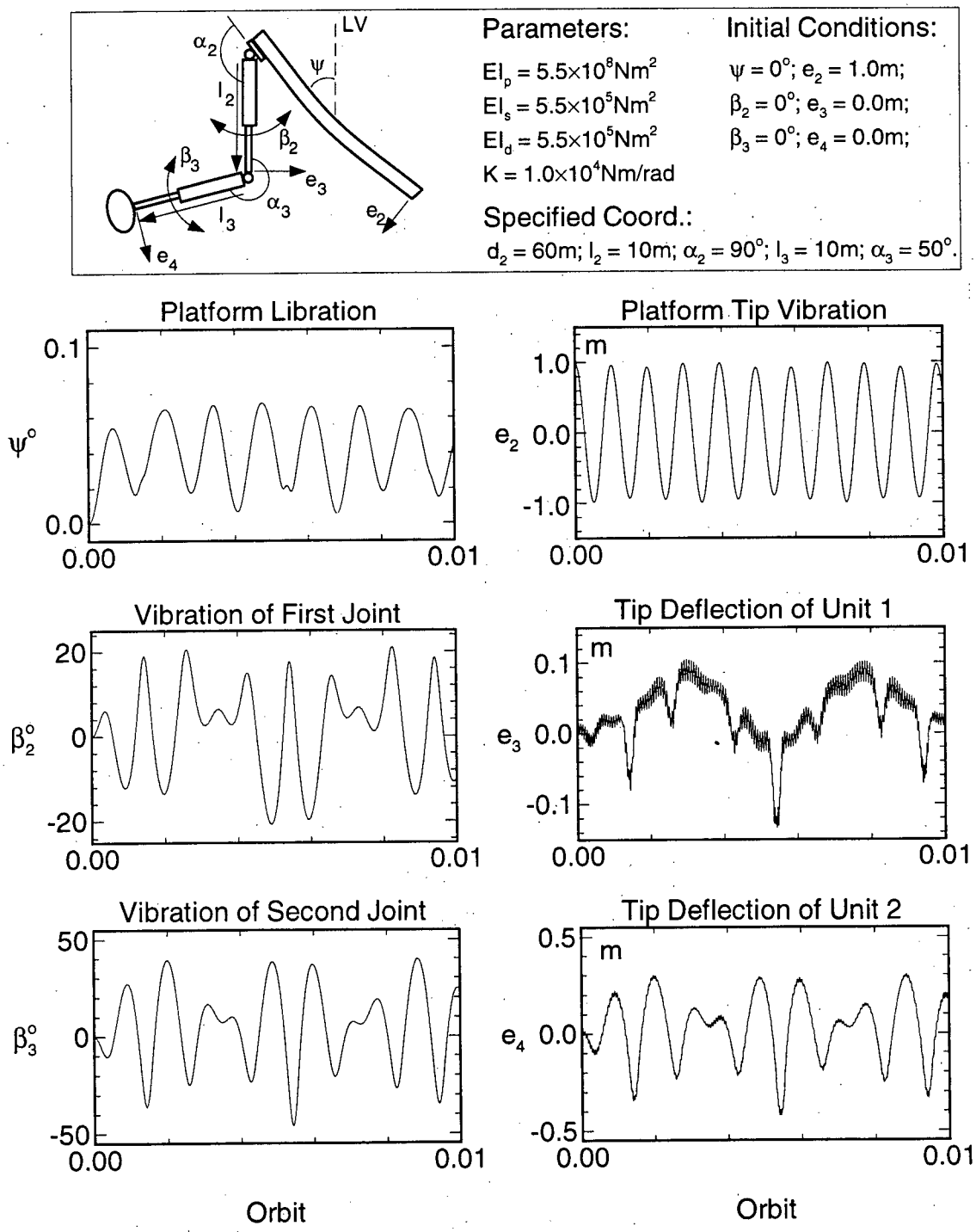

Figure 4-15 Response of the two-unit manipulator to a 1.0 m initial disturbance of the platform tip.

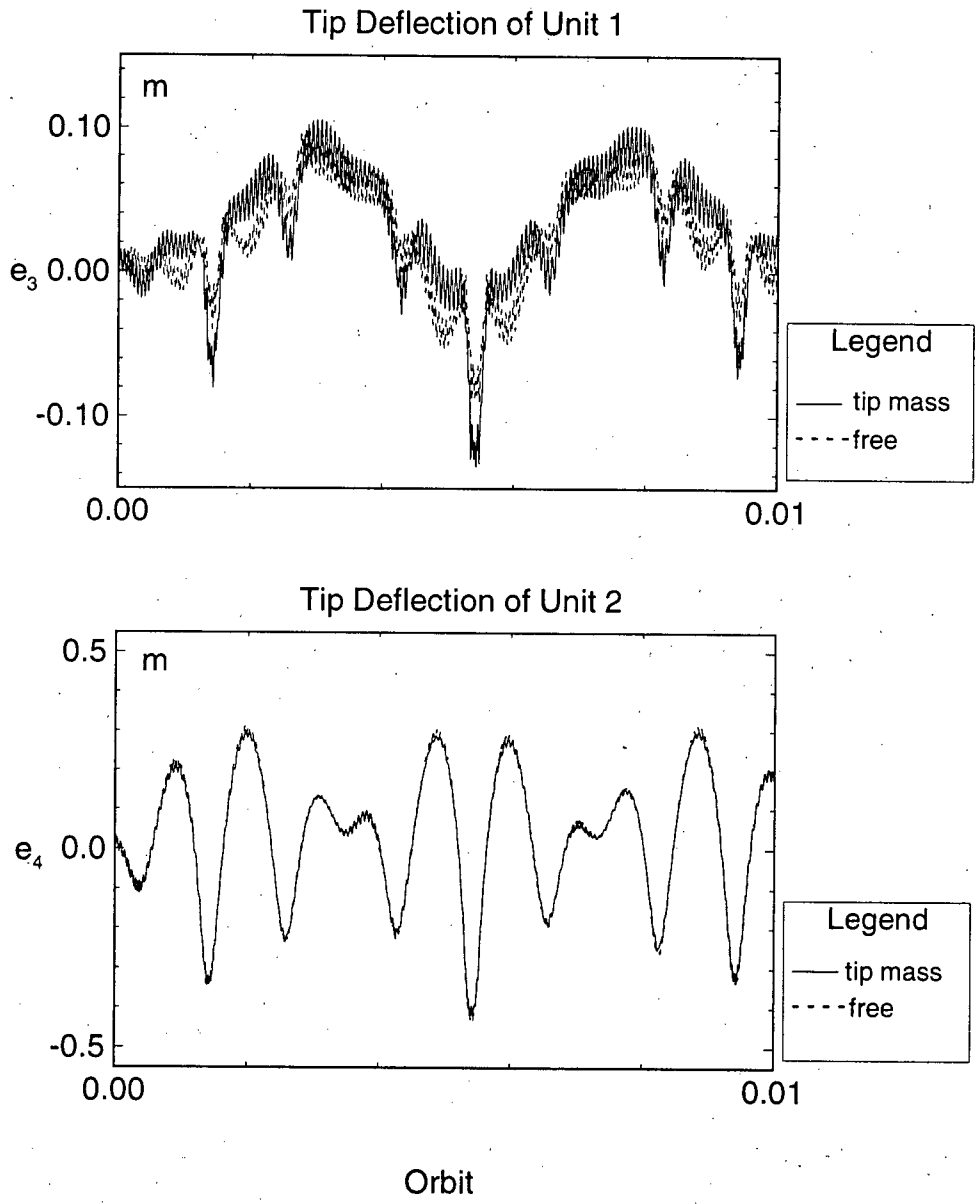

Figure 4-16 Comparison of the manipulator tip dynamics as affected by the choice of the component modes.

4.4.2 Response to maneuvers

The next case studies the response of the system when it is subjected to slewing maneuvers from both units (Figure 4-17a). The manipulator is initially "folded over" ($\alpha_2 = 180^o, \alpha_3 = -180^o$), with both units parallel to the platform, and its base and tip are located exactly at the center of the platform. From $\tau = 0.00$ to $\tau = 0.01$ orbit, the joints rotate until the links are aligned along the direction perpendicular to the platform. Throughout the maneuver, the length of each unit remains constant ($l_2 = l_3 = 10$ m). Figure 4-17(a) shows the vibrational response of the manipulator units and joints, as well as the platform's flexible motion. The system's librational response is also presented. The maneuver is illustrated in the inset. The slewing maneuvers result in tip deflections of the order of a few cm for both units, as well as deformations of approximately 2° for the joints. The maneuver also excites a vibrational response of the platform resulting in a tip deflection of around 3 mm. Note, the coupling between the various degrees of freedom is evident through modulations.

Figure 4-17(b) shows the trajectory traced by the tip of the manipulator during the maneuver. The dash line shows the trajectory followed by the payload if the manipulator joints and links, as well as the platform, are assumed to be rigid. The platform radius being 1.5 m, the terminal position of the manipulator tip is 21.5 m from the platform based reference frame F_1. The solid line shows the actual trajectory followed by the payload when the system flexibility is accounted for. Large differences between the two trajectories are apparent, especially towards the end of the maneuver and after. Despite the small individual contributions of the elastic deformations, their integrated effect is significant, resulting in residual oscillations of 60 cm about the desired final tip position. Clearly, the tip dynamics will have to be regulated. This can be achieved through the introduction of passive damping, selection of higher stiffness for the components, or active vibration control, as described in the next chapter.

Figure 4-18(a) describes the system response to a maneuver similar to the pre-

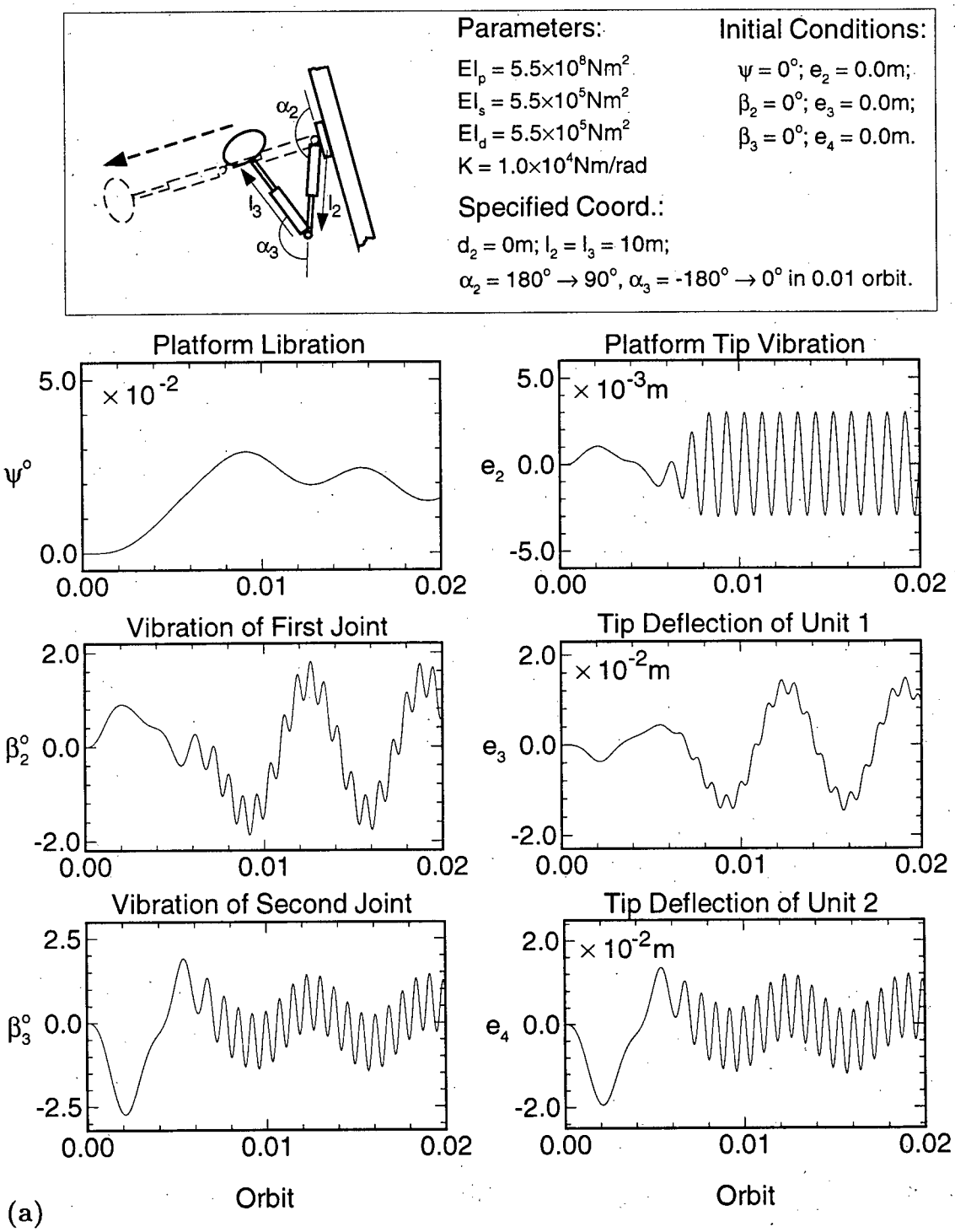

Figure 4-17 Simultaneous slew maneuvers involving both the manipulator units: (a) system dynamics.

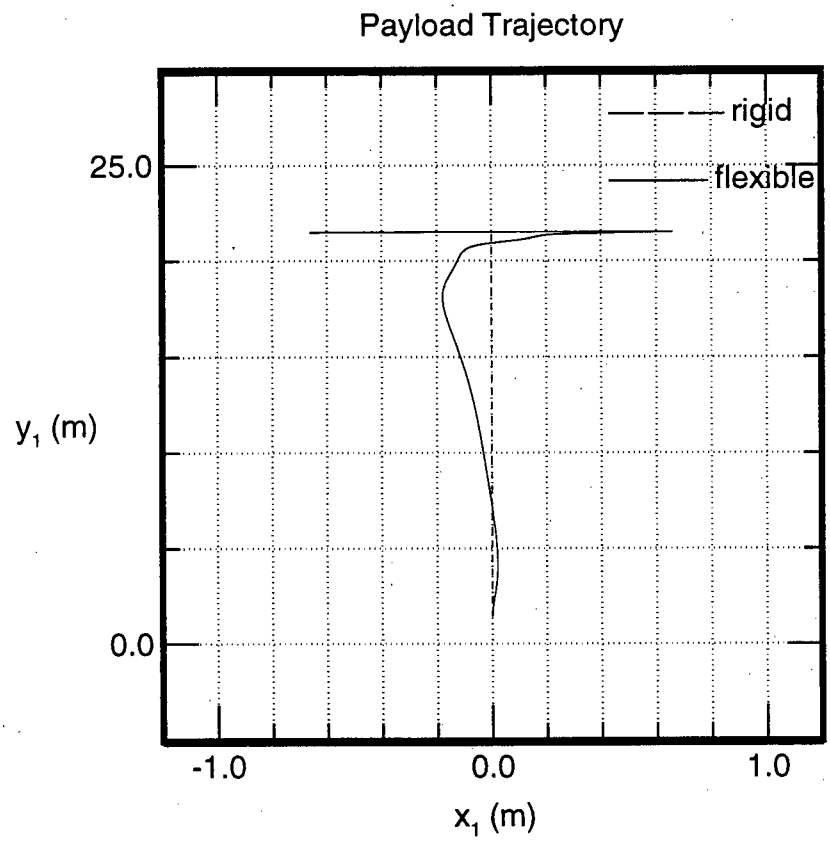

(b)

Figure 4-17 Simultaneous slew maneuvers involving both the manipulator units: (b) effect of system flexibility on the end-effector trajectory.

vious case, with the addition of a 5 m deployment from each unit. As a result, the vertical distance travelled by the end-effector is 50% greater (30 m, as opposed to 20 m). The responses to the maneuver, both with and without deployment are quite similar. However, the deployment of the units increases the inertia of the manipulator and lowers its stiffness. These result in larger vibrational amplitudes for the manipulator links and joints. The deployment also reduces the natural frequencies of the manipulator's components. The attitude motion of the platform is larger as well.

Figure 4-18(b) shows the trajectory followed by the payload throughout the maneuver and after. The dash line shows the trajectory where flexibility effects are neglected while the solid line illustrates the fully flexible case. The trajectories are similar to those observed for the nondeploying case.

Next, a maneuver involving slewing from both units, as well as translation from the mobile base, is investigated. Initially the base is located 10 m from the platform's center. From $\tau = 0$ to $\tau = 0.01$ orbit, the manipulator joints undergo simultaneous rotations while the mobile base translates 30 m away from the center of the platform. The maneuver takes the end-effector from its initial position, at the center of the platform, to a point located 50 m away from the center. The manipulator specifications, initial conditions, and important parameters are given in Figure 4-19(a).

Figure 4-19(a) gives the response of the system's degrees of freedom while Figure 4-19(b) traces the trajectory followed by the payload if the system is rigid (dash line) or fully flexible (solid line). The translation of the manipulator system generates substantial librational motion of the platform, reaching 0.3^o. Similarly, the maneuver excites significant structural vibrations in the platform, with tip deflections approaching 5 mm. Larger responses are observed with the manipulator's degrees of freedom. Note, the joint and link vibrations are larger for the first unit than those for the second unit, despite the fact that the first joint rotates by 84°, while the second joint

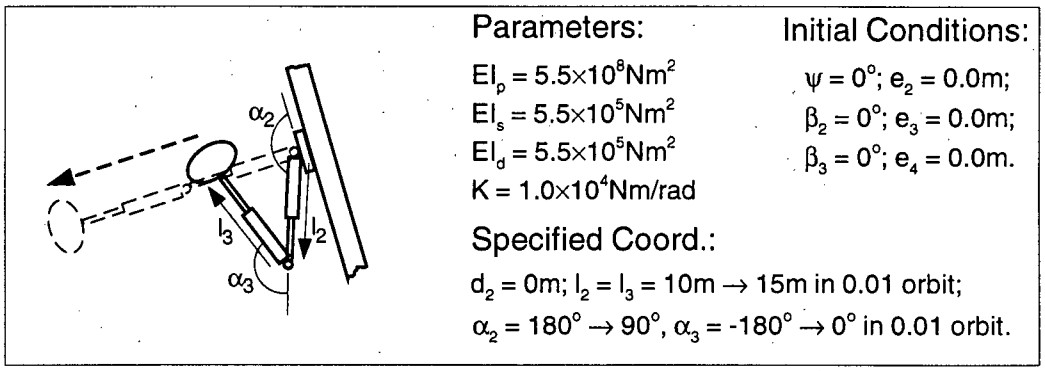

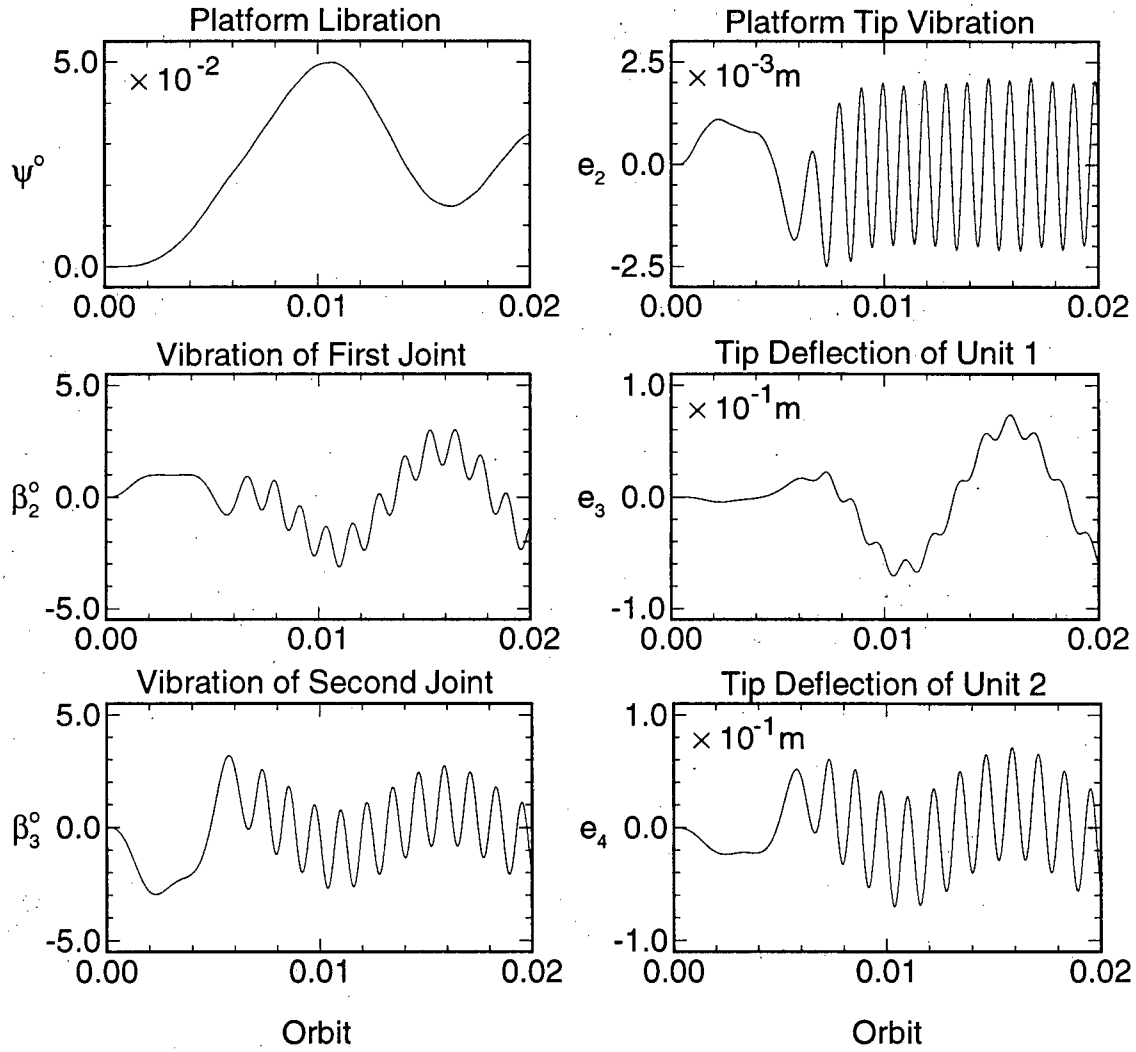

(a)

Figure 4-18 Simultaneous slew and deployment maneuvers involving both the manipulator units: (a) system dynamics.

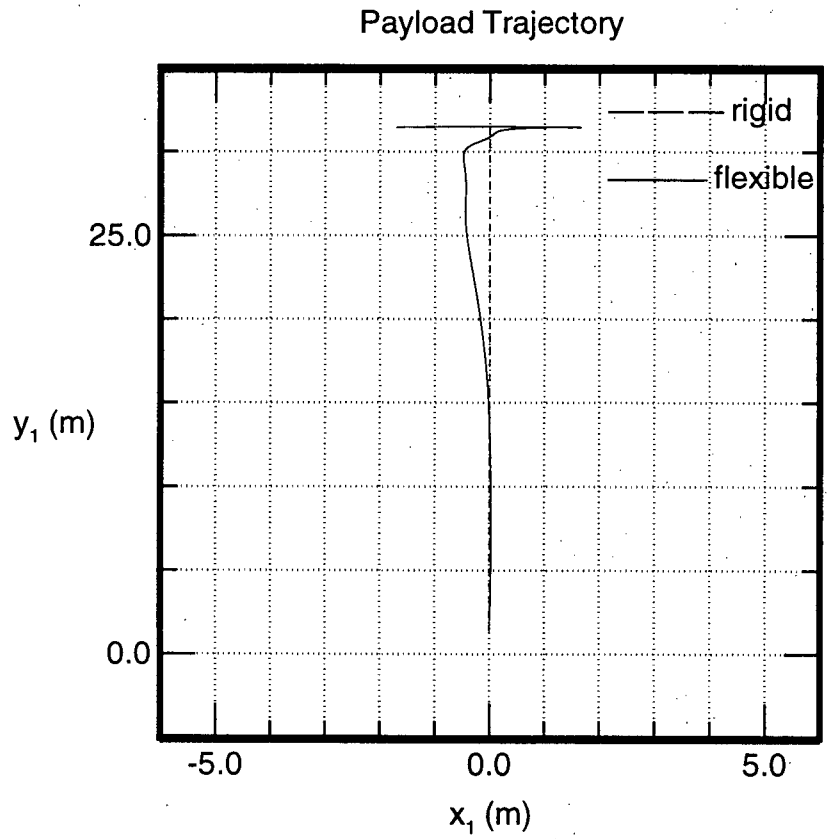

(b)

Figure 4-18 Simultaneous slew and deployment maneuvers involving both the manipulator units: (b) effect of system flexibility on the end-effector trajectory.

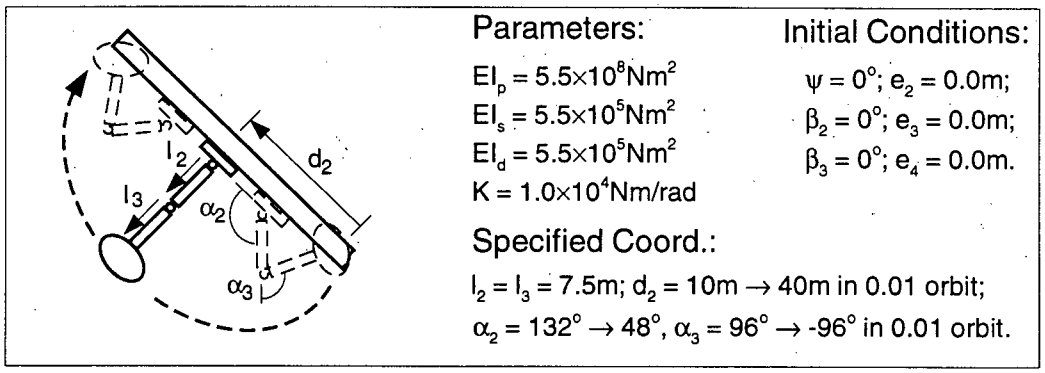

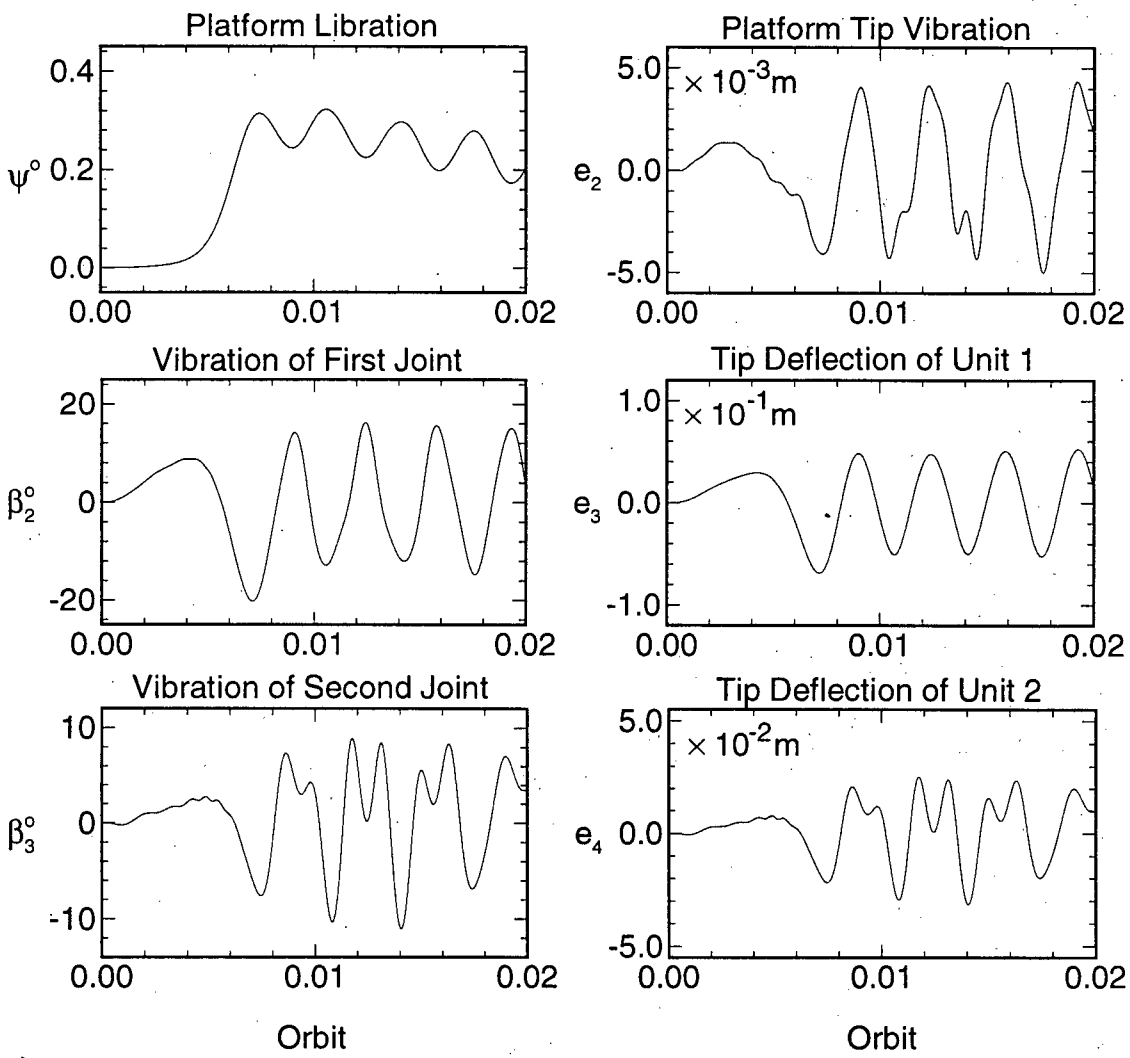

(a)

Figure 4-19 Maneuver involving simultaneous slew and translation of the mobile base: (a) system dynamics.

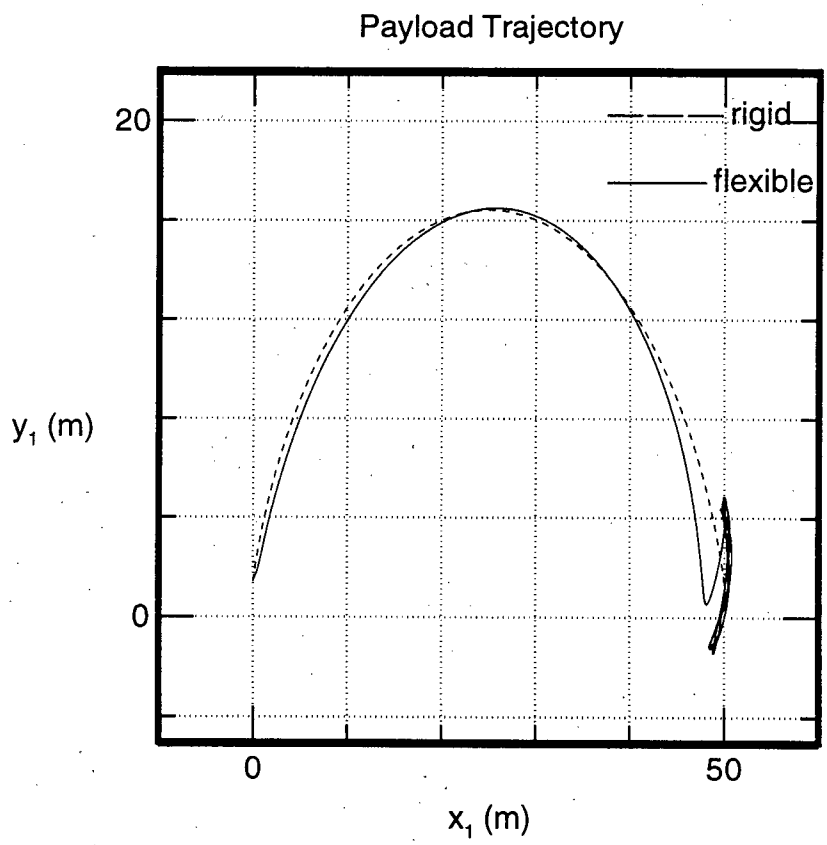

(b)

Figure 4-19 Maneuver involving simultaneous slew and translation of the mobile base: (b) effect of system flexibility on the end-effector trajectory.

through 192°: This clearly shows the importance of the coupling between the two units of the manipulator. The vibrations of the system's flexible degrees of freedom, which continue after the end of the maneuver, result in significant motion of the end-effector after it has reached its desired target position.

The ability of the manipulator to track a straight line trajectory is assessed next. The trajectory in question was described in the Cartesian space by Eq. (4.3), and was illustrated in Figure 4-14(a). For this particular case, the length of units remains fixed at 7.5 m and the base is located at $d_2 = 0$. The required joint angles can be obtained, in radians, through simple inverse kinematics:

$$\begin{aligned} \alpha_2 &= \tan^{-1}\left(\frac{y_1}{x_1}\right) + \frac{1}{2}\cos^{-1}\left(\frac{l_2^2+l_3^2-(x_1^2+y_1^2)}{2l_2l_3}\right) - \frac{\pi}{2}; \\ \alpha_3 &= \pi - \cos^{-1}\left(\frac{l_2^2+l_3^2-(x_1^2+y_1^2)}{2l_2l_3}\right). \end{aligned} \tag{4.6}$$

The maneuver takes place from $\tau = 0.000$ to $\tau = 0.005$ orbit and Eq. (4.6) does not encounter any singularity along the particular trajectory considered here.

Figure 4-20(a) shows both the desired and actual trajectories followed by the end-effector, along with the time-histories for the joint angles. The inverse kinematics does not take into account the flexibility of the system. The oscillations of the end-effector about the final desired position suggests a considerable deterioration of positioning accuracy due to the flexibility of the components. Again, this leads to the conclusion that higher stiffness, damping, or active vibration control are required for acceptable performance. Figure 4-20(b) shows the response of the individual degrees of freedom to the tracking maneuvers. The platform's librational and vibrational motions are rather small. However, the vibrations of the manipulator components are significant. This explains the poor accuracy of the manipulator once the maneuver is completed. The maximum vibrational amplitudes are reached at the end of the maneuver and progress undamped thereafter.

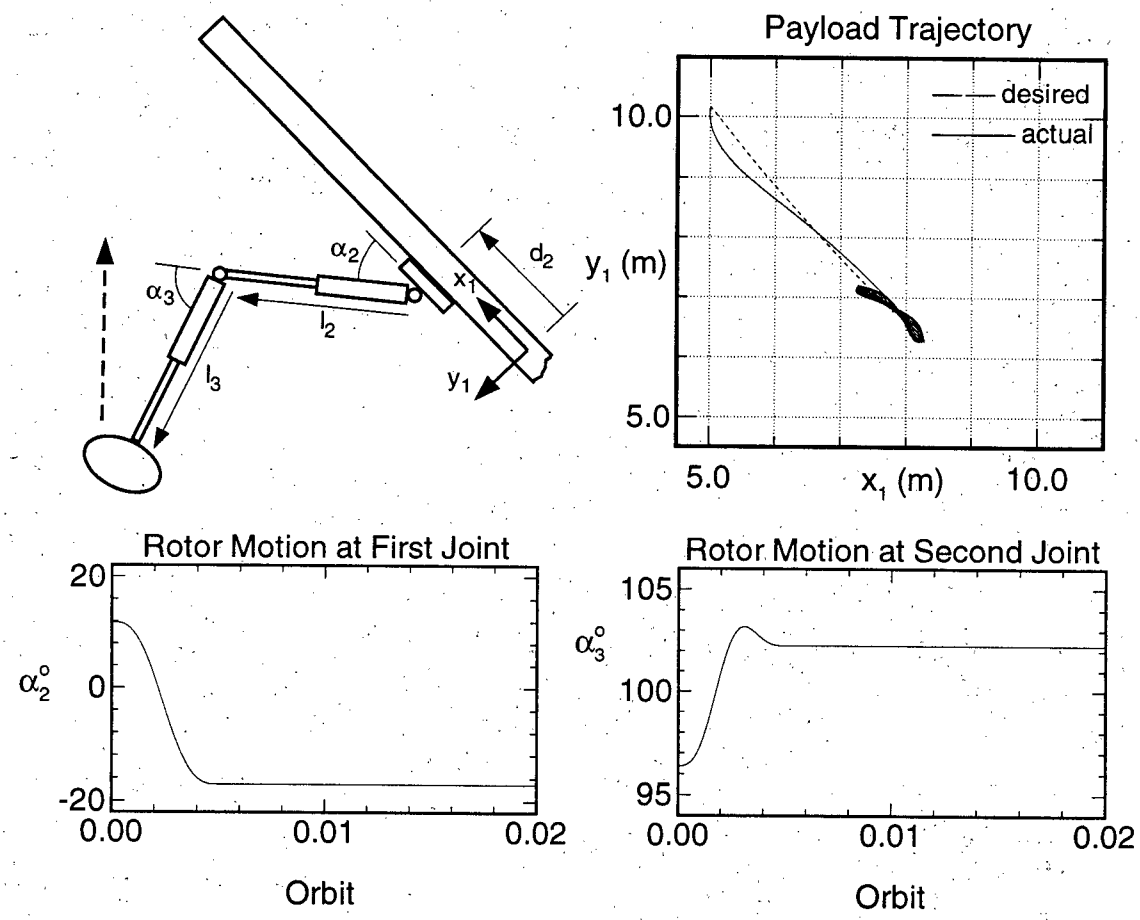

(a)

Figure 4-20 Tracking of a straight line trajectory using the two slew degrees of freedom: (a) time histories of the joints and position of the end-effector.

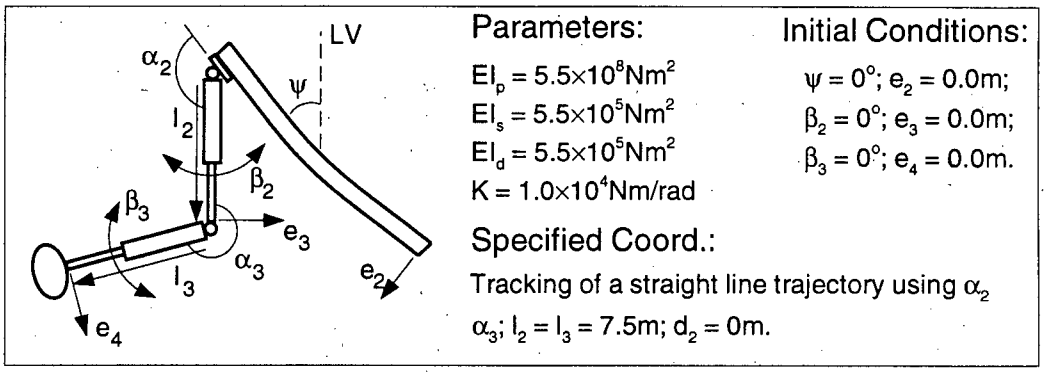

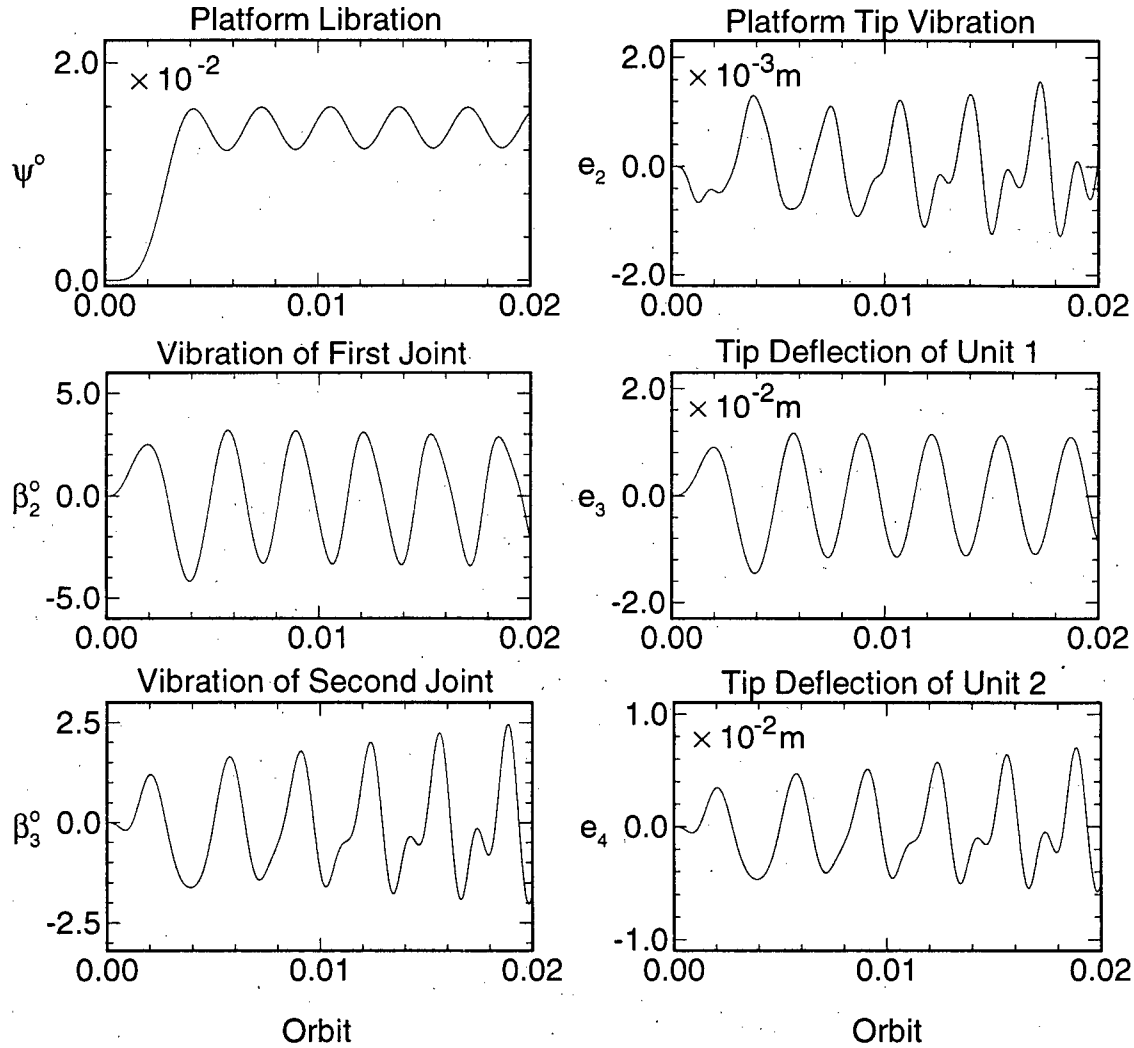

(b)

Figure 4-20 Tracking of a straight line trajectory using the two slew degrees of freedom: (b) system response to maneuver.

4.5 Multi-Unit Manipulator Systems

In the present section, the manipulator systems consist of a greater number, ranging from 3 to 5, of smaller units. The manipulator units and joints have the following specifications:

Manipulator Joints

Type: revolute joints;

Mass (m_j) = 5.0 kg;

Moment of Inertia (I_{zz}) = 2.5 kg m^2;

Stiffness (K) = 1×10^3 Nm/rad.

Manipulator Links (Slewing and Deployable)

Geometry: cylindrical, with axial to transverse inertia ratio of 0.005;

Mass (m_s, m_d)= 50 kg;

Length (l_s, l_d) = 2.5 m;

Flexural Rigidity (EI_s, EI_d) = 1.0 $\times 10^4$ Nm^2.

Thus, each unit has a maximum length of 5.0 m. All other parameters remain unchanged.

4.5.1 Three-unit manipulator system

Figure 4-21(a) presents the response of a three-unit manipulator to a simultaneous rotation of its three revolute joints and deployment of the three units. The manipulator base is located at the extremity of the platform and the manipulator is initially in a folded configuration ($\alpha_2 = -\alpha_3 = \alpha_4 = 180^o$), with all three manipulator units parallel to the platform (inset). In 0.01 orbit, the joints rotate in order to align all units in the direction perpendicular to the platform's long axis. At the same time, each unit deploys from a length of 3.5 m to a length of 5.0 m. Hence, the maneuver takes the tip of the manipulator from its initial location on the surface of the platform, 3.5 m from the platform's tip, to a point located 15 m from the surface

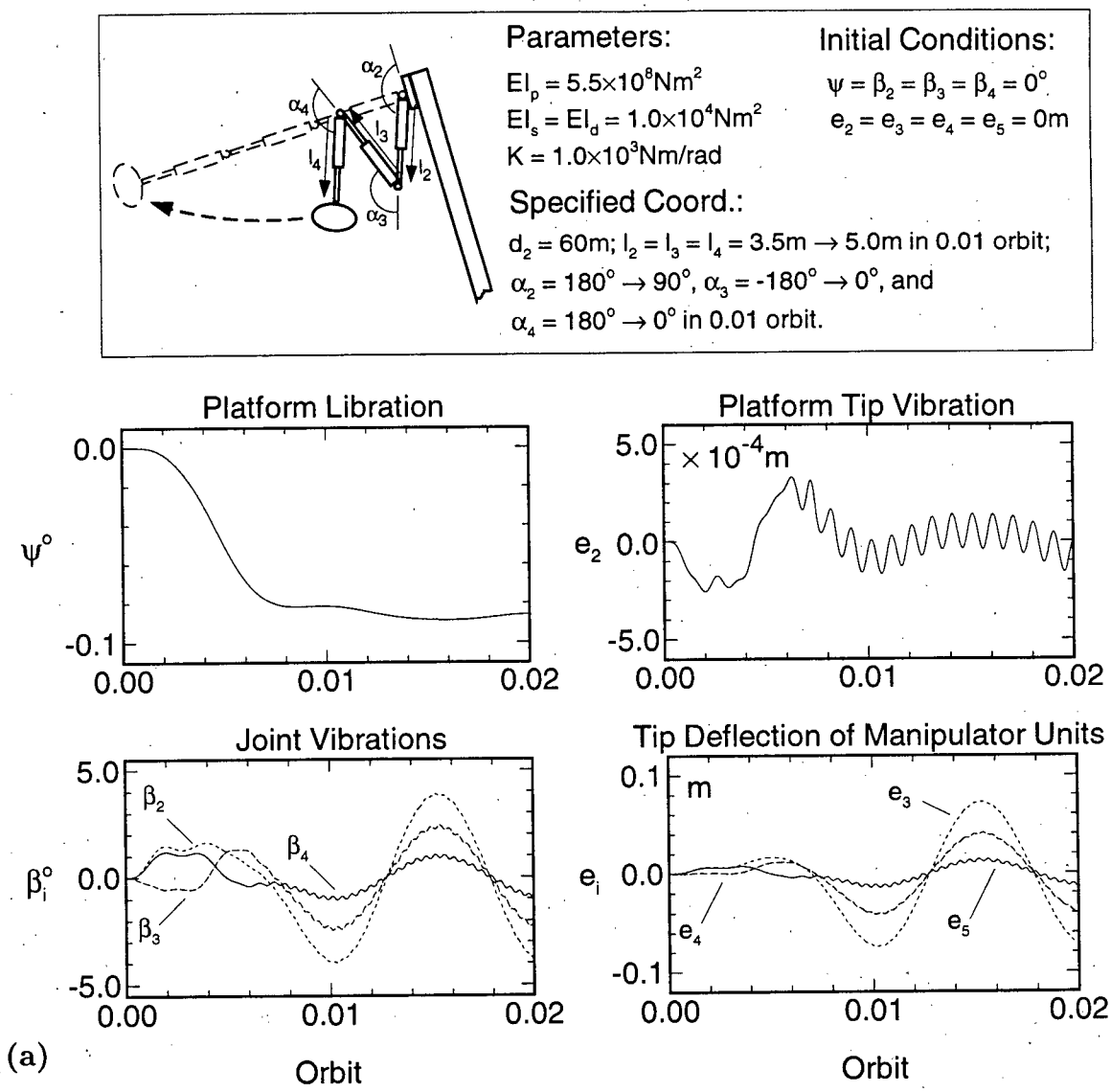

Figure 4-21 Simultaneous slew and deployment maneuvers of a three-unit manipulator: (a) system response.

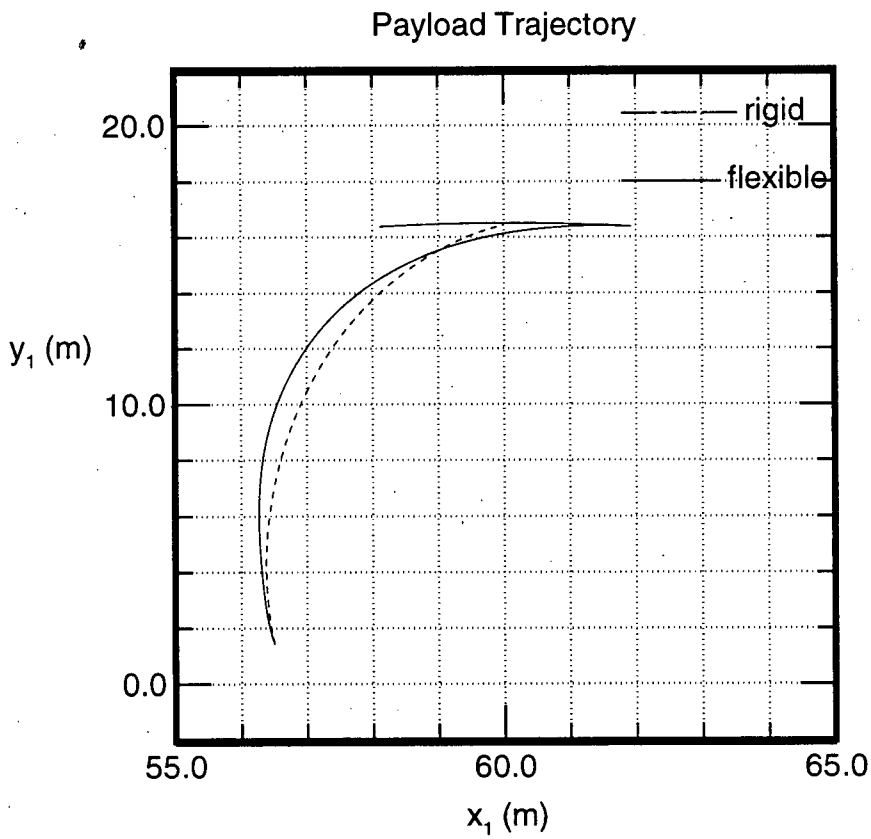

(b)

Figure 4-21 Simultaneous slew and deployment maneuvers of a three-unit manipulator: (b) trajectory followed by the end-effector showing the flexibility effect.

of the platform. The end-effector's trajectory during the maneuver is shown in Figure 4-21(b). Again, the two different paths taken by the end-effector for the cases of rigid and flexible systems are shown and the effect of flexibility on trajectory tracking is observed. It can be seen that there are significant oscillations about the final position of the end-effector.

Figure 4-21(a) gives the response of the individual degrees of freedom. While the vibrational motion induced in the platform remains small, the platform pitch response is relatively large. This can be attributed to the large effect that manipulator maneuvers have on the system's inertia tensor when the base is fixed at that location. The joint and unit vibrations are also shown. One notes that the amplitude of vibration of both joints and links are greater for units close to the platform. Joints and links located near the end of the manipulator exhibit vibrational modulations at the natural frequency of the links. Moreover, after the maneuver, all joint and links deformations seem to pass through zero at the same instant. These trends are also observed for manipulators with a greater number of units and are discussed in the following subsections.

4.5.2 Four-unit manipulator system

The next two cases consider manipulator systems consisting of four units. In the first case, the base of the manipulator is locked at the center of the platform. Each unit is fully deployed to its maximum length of 5.0 m. The first three units are aligned in the direction perpendicular to the platform, while the last unit undergoes a 180° slewing maneuver during 0.01 orbit. Figure 4-22 illustrates the maneuver, as well as the vibrational response of the platform, joints and manipulator units, in addition to the librational dynamics of the system. One notes that the amplitudes of joint and link vibrations are larger for components (i.e. joints, links) which are closer to the platform (i.e. away from the tip). In addition, the vibrational frequencies are higher for components close to the tip of the manipulator. Both observations

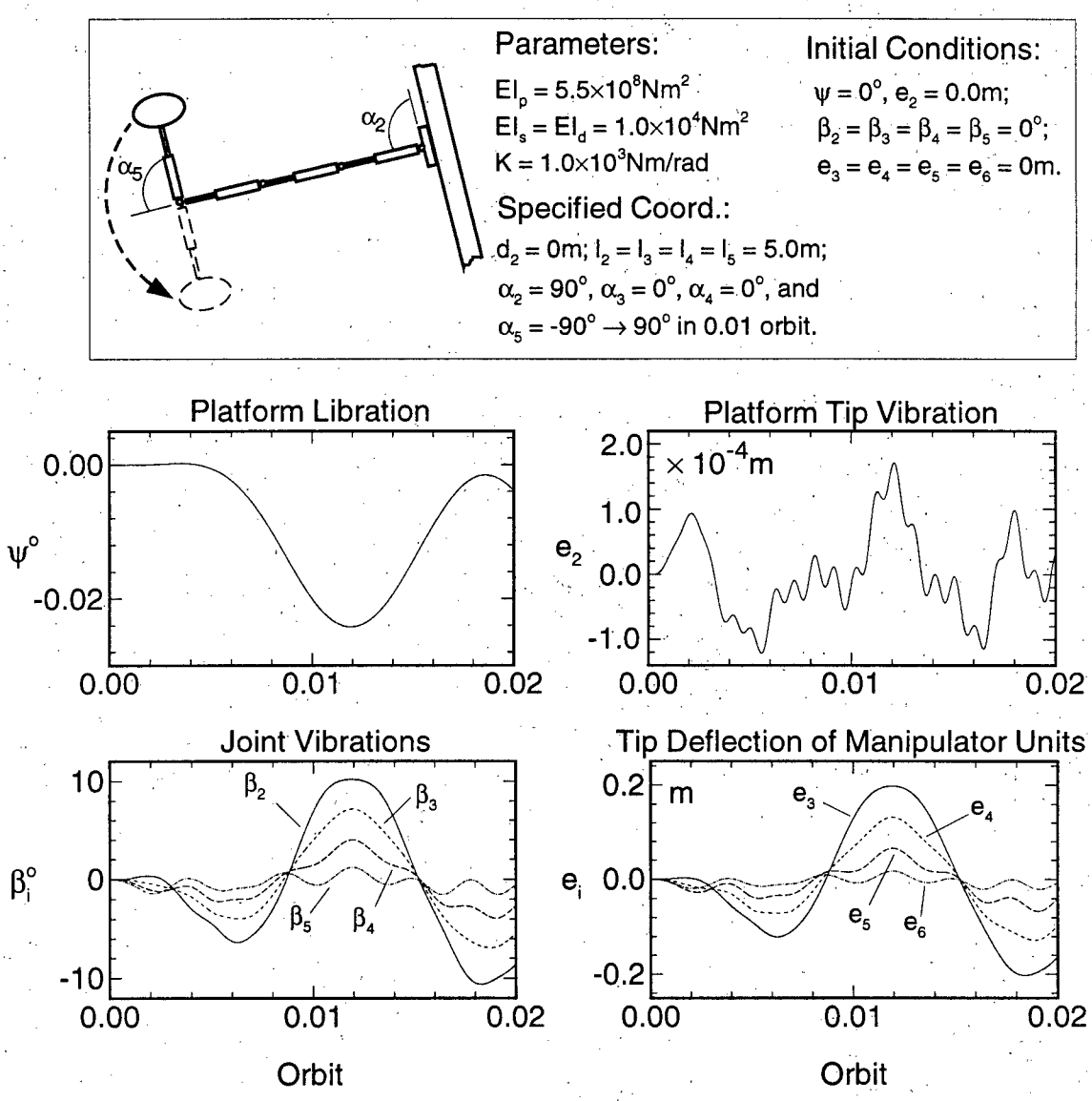

Figure 4-22 System response of a four-unit manipulator to a 180° slewing maneuver from the fourth unit.

seem to indicate that each unit acts as a tip mass for the previous unit and thus effectively reduces its natural frequency. Coupling effects are also apparent from the joint vibrations and tip deflections of the manipulator units. Again, the joint and link deformations pass through zero at the same instant near the end of the maneuver and after it is completed.

In the second case, the manipulator is initially in the configuration shown in Figure 4-23(a), with all units fully retracted to their minimum length of 2.5 m, $\alpha_2 = 45^o$, and $\alpha_3 = -\alpha_4 = \alpha_5 = 120^o$. During the time interval of 0.01 orbit, the units are deployed simultaneously to their maximum length of 5.0 m while the joints remain locked in their initial position. If flexibility effects are neglected, the deployments cause the end-effector to move in the direction perpendicular to the platform, as shown in Figure 4-23(b). However, the system flexibility slightly reduces the positioning accuracy and results in 20 cm amplitude oscillations about the final desired position. Figure 4-23(a) shows the response of the individual degrees of freedom to this maneuver. Note, the vibrational amplitudes are of the same order for all the joints. Same is the case for the tip deflections of the manipulator units. The elastic vibrations are considerably smaller than those observed for the cases involving slewing.

4.5.3 Five-unit manipulator system

The final case studies the system response of a five-unit manipulator to a translation maneuver along the platform. All manipulator units are fully retracted to their minimum length of 2.5 m and are aligned in the direction perpendicular to the platform. Figure 4-24(a) shows the platform and manipulator tip responses as the mobile base translates on the platform through 10 m in 0.01 orbit. x_e represents the motion of the manipulator tip parallel to the undeformed platform, while y_e gives the displacement in the transverse direction, both with respect to the reference coordinate frame F_1. To assess the effects of link and joint flexibility, the response of

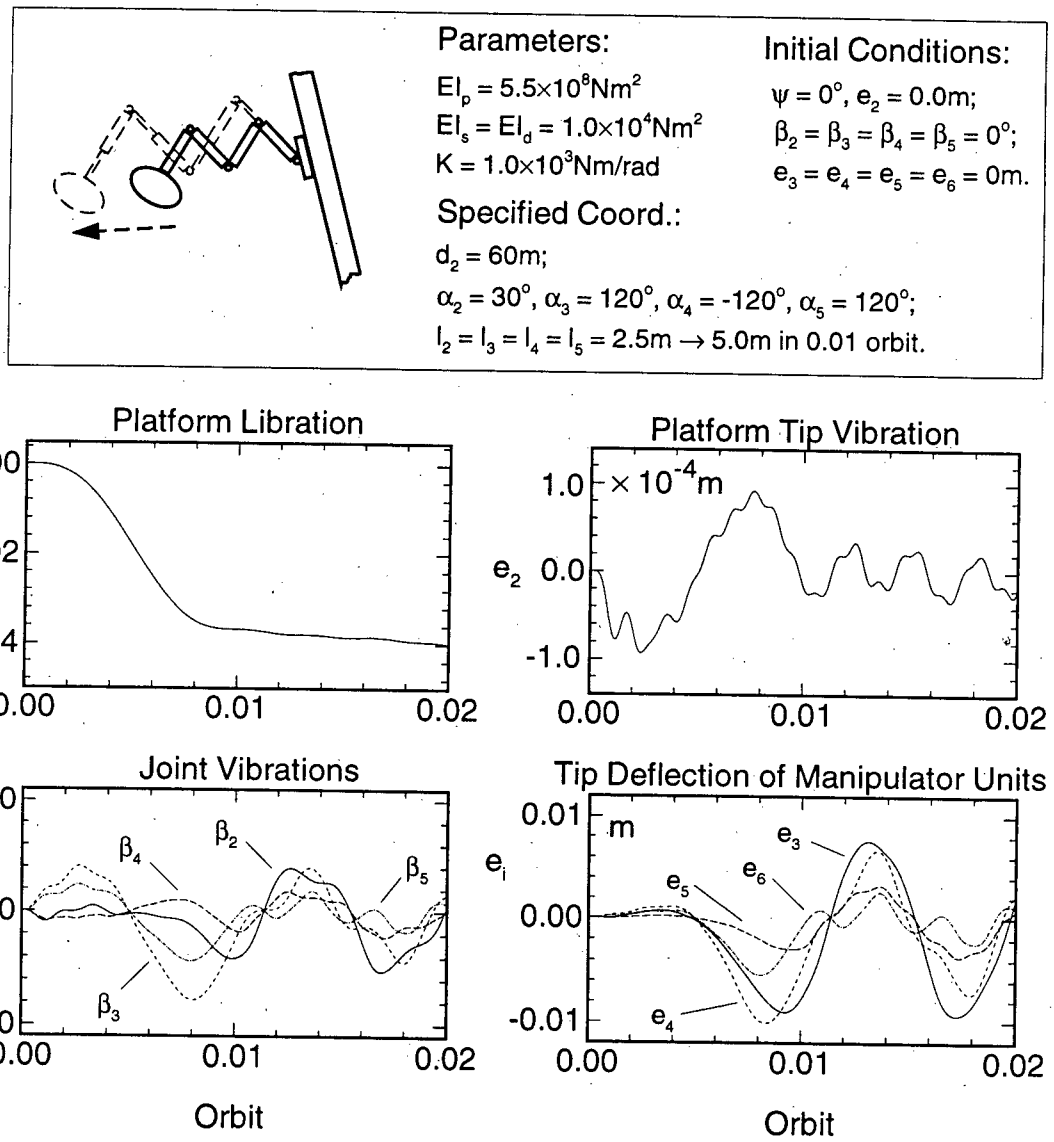

(a)

Figure 4-23 Deployment maneuver of a four-unit manipulator with the base and revolute joints held fixed: (a) system dynamics.

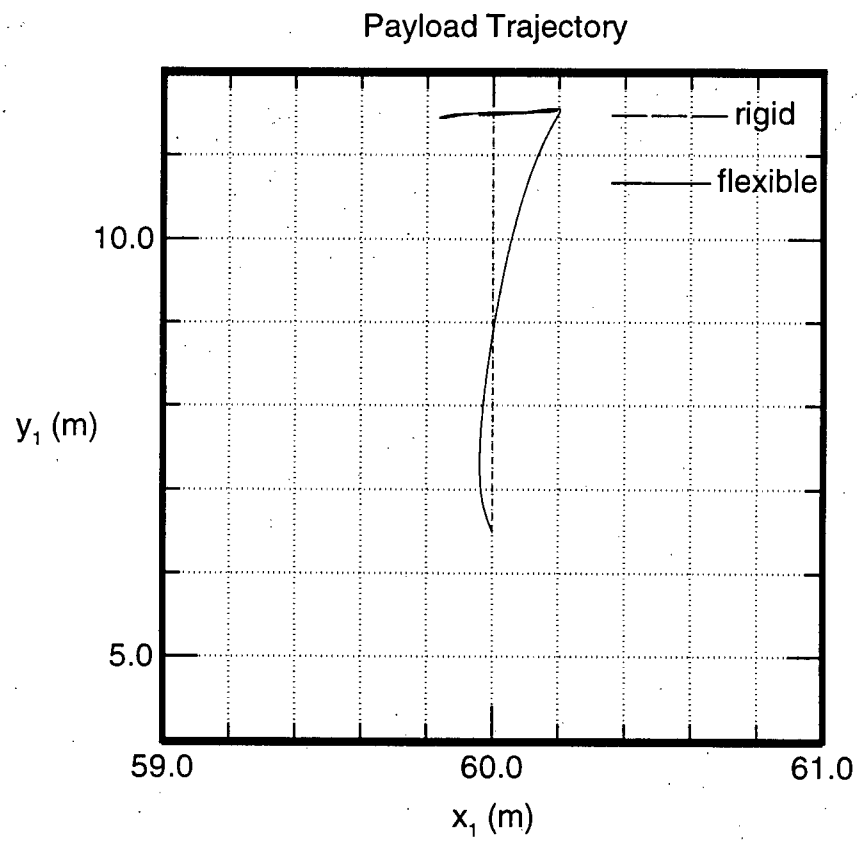

(b)

Figure 4-23 Deployment maneuver of a four-unit manipulator with the base and revolute joints held fixed: (b) effect of the system flexibility on the end-effector's trajectory.

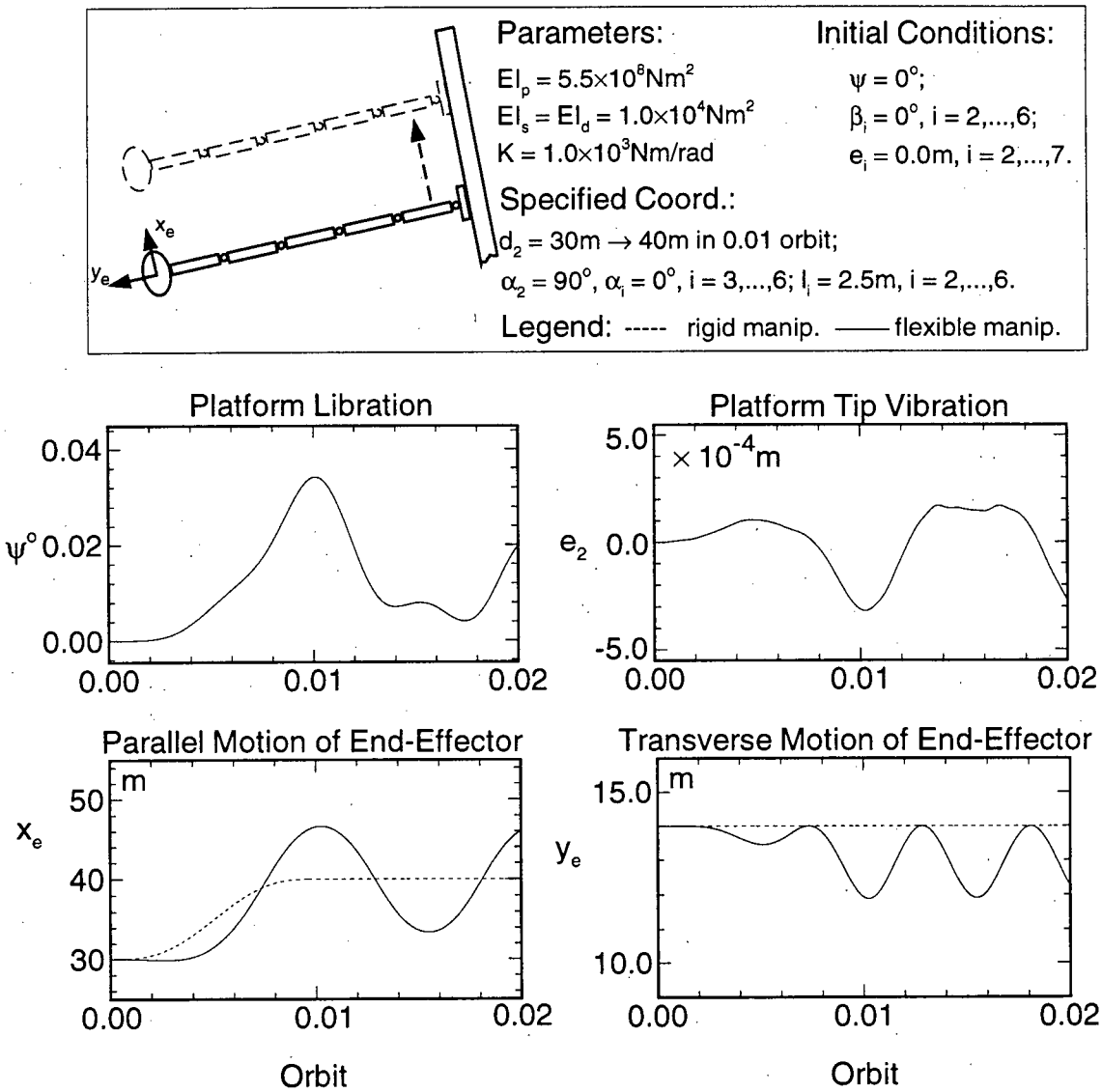

(a)

Figure 4-24 System dynamics during and after a 10 m translational maneuver along the platform: (a) platform response and trajectory of the end-effector.

(b)

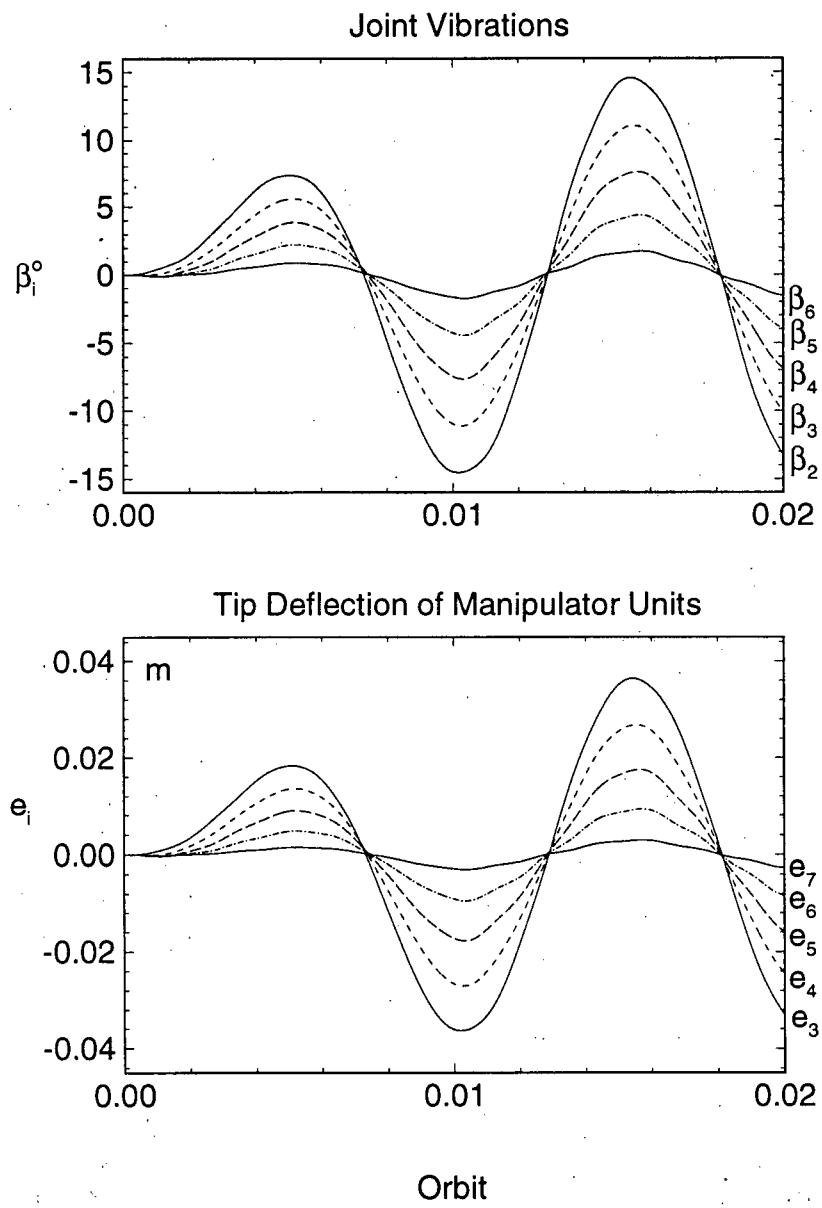

Figure 4-24 System dynamics during and after a 10 m translational maneuver along the platform: (b) joint and manipulator unit response.

a rigid manipulator system is also included for comparison. The results clearly show significant influence of the system flexibility on the position of the end-effector. Obviously, this has considerably implication on the path planning. The joint deformations result in large oscillations, mostly in the x_e direction, about the desired position. The joint and link vibrations are shown in Figure 4-24(b) for all components. As before, the vibrational amplitudes are larger for components located close to the platform because of the inertia effects. Again, the elastic joint deformations and tip deflections of the manipulator units pass through zero at the same instant, i.e. the deformation time-histories are in phase. Thus, all flexible components reach their maximum and minimum elastic potential energy at the same time. Furthermore, these maxima should remain the same once the maneuver is completed as then the total energy of the manipulator system remains constant.

5. CONTROLLED BEHAVIOR

5.1 Preliminary Remarks

In the previous chapter, the specified slewing, deployment, and retrieval of the manipulator links are the result of constraint relations. In reality, however, the maneuvers will take place under the action of forces and moments supplied by actuators. For example, the slewing maneuvers will arise from torques (T_i, $i = 2, ..., N$) provided by actuators located at the revolute joints of the manipulator. A given electromagnetic torque, applied to the rotor of the actuator located at the ith joint, will cause a rotation of the ith body relative to the (i^{th} - 1) one. Similarly, the deployment and retrieval of the units are caused by forces ($\mathcal{F}_i$, $i = 2, ..., N$) provided by actuators located at the prismatic joints of the manipulator. The torques and forces responsible for slewing and deployment maneuvers are illustrated in Figure 5-1.

In addition to joint actuators which regulate the manipulator link dynamics, there are Control Momentum Gyros (CMG's). CMG's are used to control the platform orientation as well as its vibration. A single CMG located at the center of the platform (T_0) controls the rigid body motion of the platform, i.e. its attitude or pitch motion. On the other hand, a pair of CMG's, located symmetrically about the platform's center and providing equal torques ($T_1/2$) in the opposite sense, control its elastic vibration by regulating the local slope.

The present chapter is concerned with the selection of control inputs (T_i, $\mathcal{F}_i$) which will result in the desired motion of the system. From this perspective, the slewing and deployment maneuvers of the previous chapter may be considered to be under perfect control, since the desired motion of the specified degrees of freedom was achieved precisely. In reality however, the system dynamics does not permit the desired motion to be obtained with such accuracy. The adoption of appropriate control strategies is then critical to obtain a response as close as possible to the desired

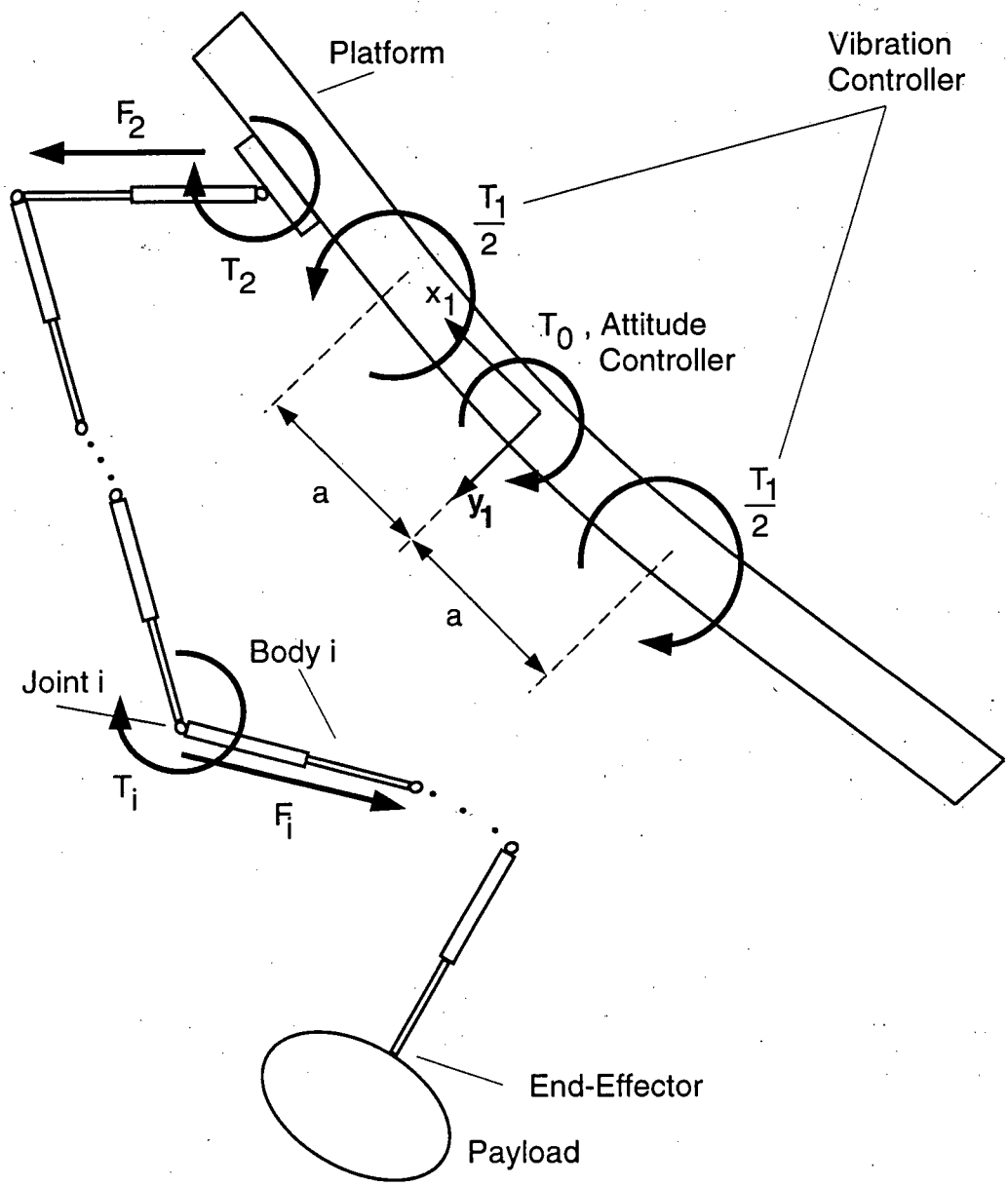

Figure 5-1 Schematic diagram of the manipulator system showing the location of the control actuators. Note, with the two torques $T_1/2$ opposing each other, a resulting generalized force $\mathcal{F}_1 = \bar{\Phi}'_{1a} T_1$ is applied to the platform's vibrational degree of freedom δ_{11}.

behavior.

The present chapter first develops a control strategy based on the Feedback Linearization Technique (FLT), which takes into account the full nonlinear character of the equations of motion, in order to control the rotation of the joints, the deployment of the links, as well as the attitude of the platform. The performance of the controller is then assessed using a few test-cases. A Linear Quadratic Regulator (LQR), based on a linear approximation of the flexible subsystem, is designed for active vibration suppression. The performance of the combined FLT/LQR controller is then evaluated with some illustrative examples.

5.2 Control of Rigid Degrees of Freedom

5.2.1 Feedback Linearization Technique (FLT)

As mentioned before, an FLT controller is now designed to regulate the rotations of the revolute joints ($\alpha_i,\ i = 2, ..., N$), the deployment of the links ($l_i,\ i = 2, ..., N$), and the attitude motion of the system (ψ_1). Essentially, the Feedback Linearization Technique uses a mathematical model in order to decouple and linearize the dynamics of the controlled system [66]. The FLT controller is implemented on a fully flexible multibody system consisting of an orbiting platform supporting a multi-unit manipulator.

The equations of motion of the system as given in Section 2.9 were

$$\mathbf{M}\ddot{\mathbf{q}} + \mathbf{F} = \mathbf{Q^d u} + \mathbf{P^c \Lambda}. \tag{2.79}$$

Note, the position of the mobile base ($\vec{d_2}$) as well as the offset position of the manipulator units ($\vec{d_i},\ i = 3, ..., N$) are constrained to remain fixed and thus require the use of Lagrange multipliers. The controlled degrees of freedom do not require any constraints. The orbital and vibrational motions of the system are also left free.

As pointed out earlier, the FLT controller is based on a mathematical model of the system dynamics. In order to investigate the potential effects of unmodeled dynamics in the controller, the FLT based controller is designed considering a rigid platform and rigid manipulator links. In other words, structural flexibility is neglected in the controller model. However, the effectiveness of the controller is assessed using the original fully flexible system.

If the platform and links are taken to be rigid, but the joint flexibility is accounted for, Eq. (2.79) reduces to

$$\mathbf{M_r}\ddot{\mathbf{q}}_\mathbf{r} + \mathbf{F_r} = \mathbf{Q_r^d u} + \mathbf{P_r^c}\mathbf{\Lambda_r}. \tag{5.1}$$

Here the subscript $\mathbf{r}$ indicates the rigid character of the system (platform and manipulator links). Substituting for $\mathbf{\Lambda_r}$ using Eq. (2.83), Eq. (5.1) takes the form

$$\mathbf{M_r}\ddot{\mathbf{q}}_\mathbf{r} + \mathbf{F'_r} = \mathbf{Q'_{dr}u}, \tag{5.2}$$

where $\mathbf{F'_r} = \mathbf{F_r} - \mathbf{P_r^c}\mathbf{F_{sr}^s}^{-1}\left(\ddot{\mathbf{q}}_\mathbf{s} + \mathbf{F_{sr}^g}\right)$, and $\mathbf{Q'_{dr}} = \mathbf{Q_r^d} - \mathbf{P_r^c}\mathbf{F_{sr}^s}^{-1}\mathbf{F_{sr}^u}$. Solving for $\ddot{\mathbf{q}}_\mathbf{r}$ gives

$$\ddot{\mathbf{q}}_\mathbf{r} = -\bar{\mathbf{F}}'_\mathbf{r} + \bar{\mathbf{Q}}'_\mathbf{dr}\mathbf{u}, \tag{5.3}$$

where $\bar{\mathbf{F}}'_\mathbf{r} = \mathbf{M_r^{-1}F'_r}$ and $\bar{\mathbf{Q}}'_\mathbf{dr} = \mathbf{M_r^{-1}Q'_{dr}}$. The vector $\ddot{\mathbf{q}}_\mathbf{r}$ containing the generalized accelerations can be divided into a controlled component $\ddot{\mathbf{q}}_\mathbf{c}$ and an uncontrolled component $\ddot{\mathbf{q}}_\mathbf{u}$. Note, the uncontrolled component also includes the specified degrees of freedom in $\ddot{\mathbf{q}}_\mathbf{r}$. Thus, Eq. (5.3) can be rewritten as

$$\begin{bmatrix} \ddot{\mathbf{q}}_\mathbf{c} \\ \cdots \\ \ddot{\mathbf{q}}_\mathbf{u} \end{bmatrix} = -\begin{bmatrix} \bar{\mathbf{F}}'_\mathbf{rc} \\ \cdots \\ \bar{\mathbf{F}}'_\mathbf{ru} \end{bmatrix} + \begin{bmatrix} \bar{\mathbf{Q}}'_\mathbf{drc} \\ \cdots \\ \bar{\mathbf{Q}}'_\mathbf{dru} \end{bmatrix}\mathbf{u}. \tag{5.4}$$

Considering only the controlled equation, one has

$$\ddot{\mathbf{q}}_\mathbf{c} = -\bar{\mathbf{F}}'_\mathbf{rc} + \bar{\mathbf{Q}}'_\mathbf{drc}\mathbf{u}. \tag{5.5}$$

In theory, the desired control input can be obtained by solving Eq. (5.5) for $\mathbf{u}$,

$$\mathbf{u} = \left(\bar{\mathbf{Q}}'_{\mathbf{drc}}\right)^{-1}\left(\ddot{\mathbf{q}}_{\mathbf{d}} + \bar{\mathbf{F}}'_{\mathbf{rc}}\right). \tag{5.6}$$

where $\mathbf{q_d}$ represents the desired value of $\mathbf{q_c}$, and the term $\bar{\mathbf{F}}'_{\mathbf{rc}}$ offsets the system's nonlinear effects. However, it can be seen from Eq. (5.4) that the uncontrolled degrees of freedom in the controller model affect and are affected by the control action. Furthermore, the unmodeled dynamics has an unknown effect on the remaining generalized coordinates. Therefore, in order to ensure a robust behavior of the controller, $\ddot{\mathbf{q}}_{\mathbf{c}}$ is taken to have the form

$$\ddot{\mathbf{q}}_{\mathbf{c}} = \ddot{\mathbf{q}}_{\mathbf{d}} + \mathbf{K_v}(\dot{\mathbf{q}}_{\mathbf{d}} - \dot{\mathbf{q}}_{\mathbf{c}}) + \mathbf{K_p}(\mathbf{q_d} - \mathbf{q_c}), \tag{5.7}$$

where $\mathbf{q_c}$ is the controlled generalized coordinates, $\mathbf{q_d}$ is their desired values, and $\mathbf{K_v}$ and $\mathbf{K_p}$ are the derivative and proportional controller gain matrices, respectively:

$$\mathbf{K_v} = \begin{bmatrix} K_{v1} & 0 & 0 & \cdots & 0 \\ 0 & K_{v2} & 0 & \cdots & 0 \\ 0 & 0 & K_{v3} & \cdots & 0 \\ \vdots & \vdots & \vdots & \ddots & \vdots \\ 0 & 0 & 0 & \cdots & K_{vN} \end{bmatrix} \tag{5.8}$$

and

$$\mathbf{K_p} = \begin{bmatrix} K_{p1} & 0 & 0 & \cdots & 0 \\ 0 & K_{p2} & 0 & \cdots & 0 \\ 0 & 0 & K_{p3} & \cdots & 0 \\ \vdots & \vdots & \vdots & \ddots & \vdots \\ 0 & 0 & 0 & \cdots & K_{pN} \end{bmatrix}. \tag{5.9}$$

Here the diagonal elements of both matrices are scalars selected in order to satisfy the prescribed requirements of settling time, maximum permissible overshoot, etc. Equating Eq. (5.5) and (5.7), and solving for the control input $\mathbf{u}$ gives

$$\mathbf{u} = (\bar{\mathbf{Q}}'_{\mathbf{drc}})^{-1}\{\bar{\mathbf{F}}'_{\mathbf{rc}} + \ddot{\mathbf{q}}_{\mathbf{d}} + \mathbf{K_v}(\dot{\mathbf{q}}_{\mathbf{d}} - \dot{\mathbf{q}}_{\mathbf{c}}) + \mathbf{K_p}(\mathbf{q_d} - \mathbf{q_c})\}. \tag{5.10}$$

A block diagram of the FLT controller is shown in Figure 5-2. It should be emphasized that the model used by the controller is incomplete, and the unmodeled dynamics

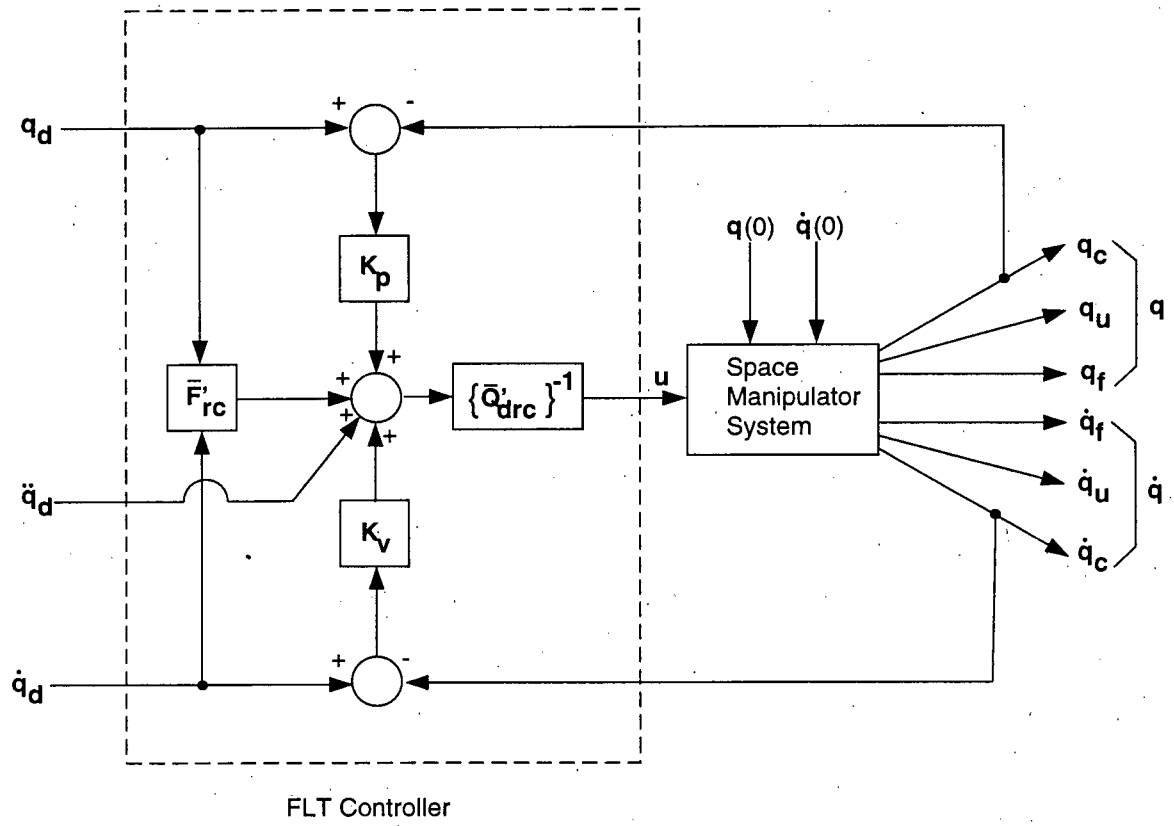

Figure 5-2 Block diagram showing the FLT based controller regulating the system's rigid body motion.

may affect the controller's performance. Fortunately, in a number of situations of practical importance, this effect turns out to be small due to the robust character of the controller.

5.2.2 Response of a one-unit manipulator system with FLT

The performance of the FLT controller is now assessed for a few test-cases involving a platform supporting a one-unit manipulator. The controller gains $\mathbf{K_p}$ and $\mathbf{K_v}$ are selected so as to achieve a critically damped response $\mathbf{q_c}$, as well as reduction of the position error to 2% of its initial value in 40 seconds (0.0072 orbit) for the platform's librational motion, and 20 seconds (0.0036 orbit) for the slew and deployment degrees of freedom. With these:

$$\mathbf{K_p} = \begin{bmatrix} 0.0207 & 0 & 0 \\ 0 & 0.0829 & 0 \\ 0 & 0 & 0.0829 \end{bmatrix}; \quad \text{and} \quad \mathbf{K_v} = \begin{bmatrix} 0.2880 & 0 & 0 \\ 0 & 0.5760 & 0 \\ 0 & 0 & 0.5760 \end{bmatrix}. \tag{5.11}$$

Throughout the control study, the manipulator is taken to carry a payload of negligible mass. Unlike the cases studied in the previous chapter, where the nominal platform orientation was along the local vertical (gravity gradient orientation), the platform's long axis is now taken to be oriented along the local horizontal. This constitutes the new operational attitude for the system.

If the platform's long axis is oriented along the local vertical, the system's librational degree of freedom ψ lies near a stable equilibrium. Any disturbance from this orientation will result in librational oscillations about the equilibrium. Another equilibrium attitude exists for the system, with the platform's long axis oriented along the local horizontal. However, this orientation corresponds to an unstable equilibrium. Thus, any disturbance in pitch will cause the system to oscillate about the other equilibrium orientation, i.e the local vertical. This can potentially lead to catastrophic librational motion. Thus the choice of local horizontal as the operational attitude for the platform represents a demanding control situation.

The controlled response of the system in the presence of pitch disturbances is first investigated. A 1° pitch disturbance is applied to the platform when it is oriented along the local horizontal ($\psi = -90^o$). The objective of the controller is to re-establish the initial equilibrium (unstable) of the platform while maintaining the slew and deployment degrees of freedom at the desired values ($\alpha_2 = 50^o$, $l_2 = 10$ m). The control inputs and controlled response of the system are shown in Figure 5-3. The initial conditions, desired values, and controller gains are indicated in the inset. Clearly, the platform's librational response to the 1° step input is critically damped. The controller is able to achieve the desired orientation in less than 0.01 orbit while maintaining the slew joint and manipulator length within less than 0.3^o and 1 cm from their respective desired values. The joint torque and deployment force time-histories exhibit oscillations corresponding to the vibration of the joint. Since joint flexibility is included in the controller design, it compensates for the forces and torques arising from the joint vibrations.

Next, the controlled response of the system is studied for a step maneuver involving the slew from $\alpha_2 = 50^o$ to $\alpha_2 = 60^o$ with the manipulator being extended from $l_2 = 10$ m to $l_2 = 12$ m. Figure 5-4 shows the effectiveness of the FLT controller under such a demanding situation. The control inputs, as well as the response of the controlled degrees of freedom are presented in Figure 5-4(a). The librational motion appears unaffected by the slew and deployment step-inputs. Clearly, the unmodeled dynamics of the flexible generalized coordinates affect the performance of the controller. The response of l_2 and α_2 (solid lines) is obviously not critically damped. However, the effect of unmodeled dynamics is small and the disturbance is damped out in less than 0.01 orbit. The dash lines show the response of α_2 and l_2 with the system considered rigid (however, with flexible joint). As can be expected, for the rigid case in which there is no unmodeled dynamics, the system behaves exactly according to specifications. Figure 5-4(b) gives the system's vibrational response.

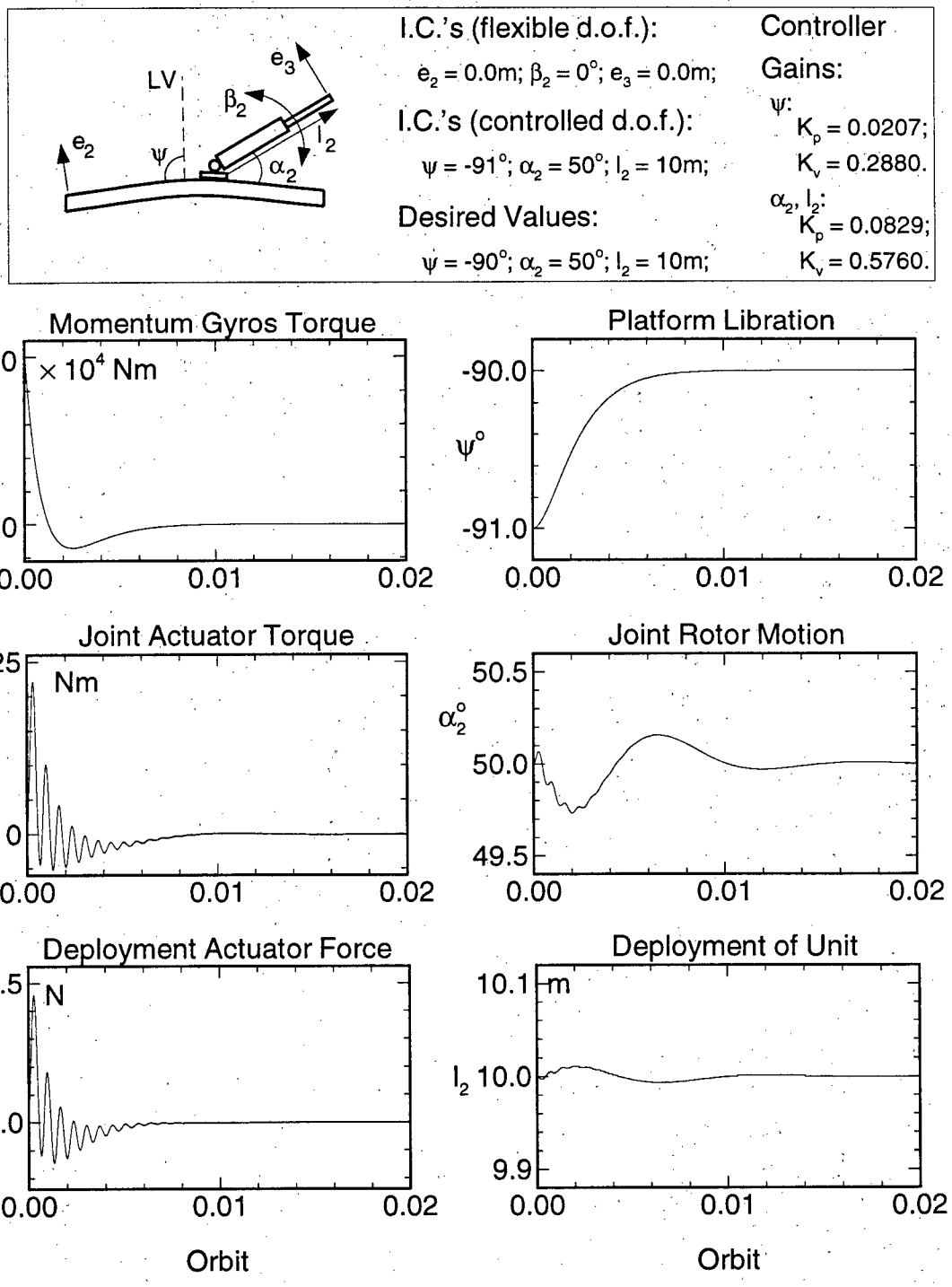

Figure 5-3 Controlled response of the system in the presence of an initial 1° pitch diturbance. It should be emphasized that the system's nominal attitude is inherently unstable.

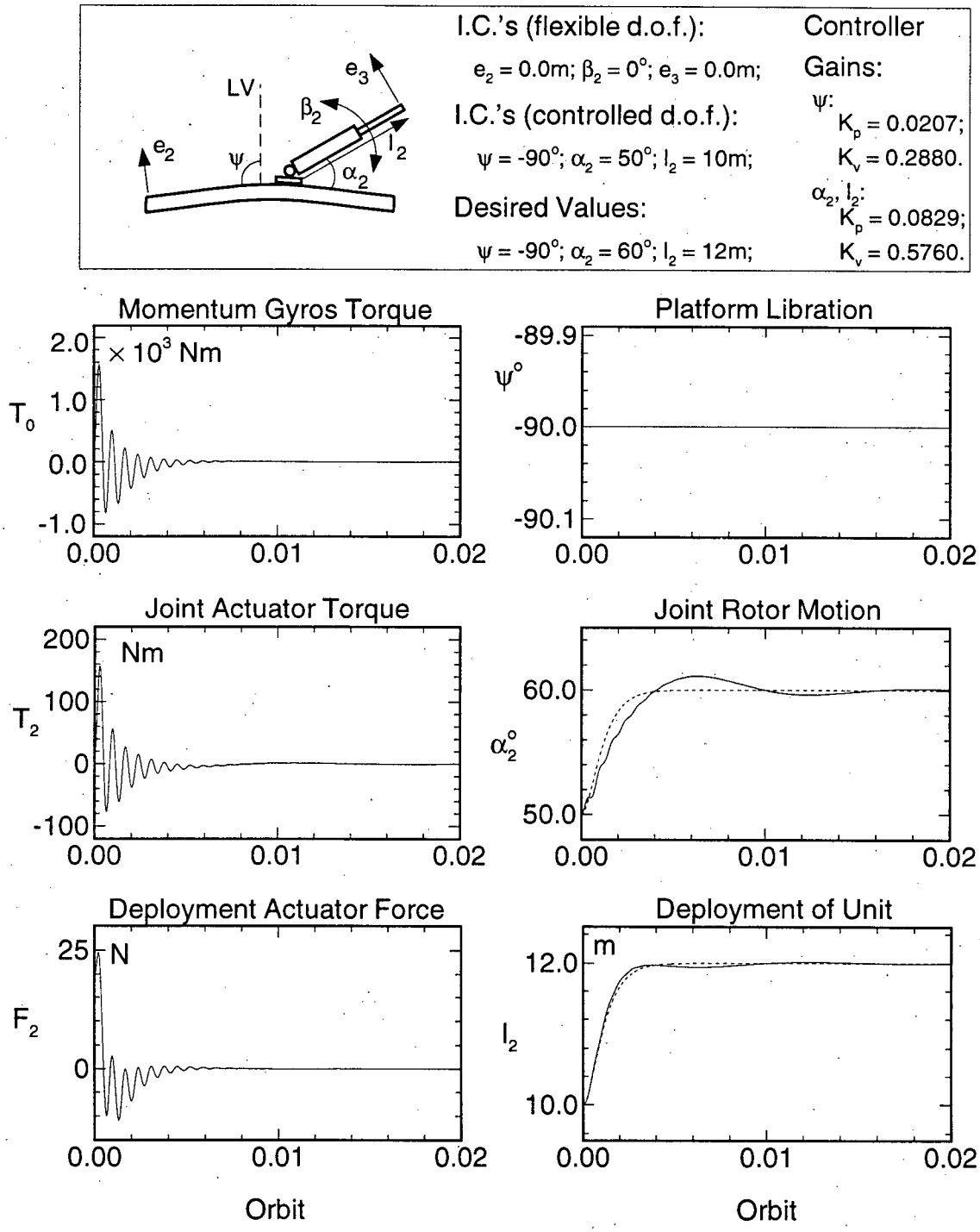

(a)

Figure 5-4 Performance of the FLT controller during a 10° adjustment of the slew angle and a 2 m deployment of the manipulator unit: (a) control inputs and response of controlled degrees of freedom.

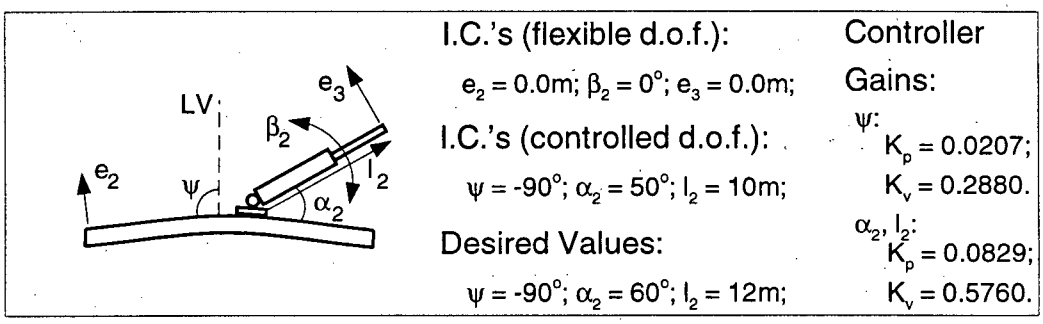

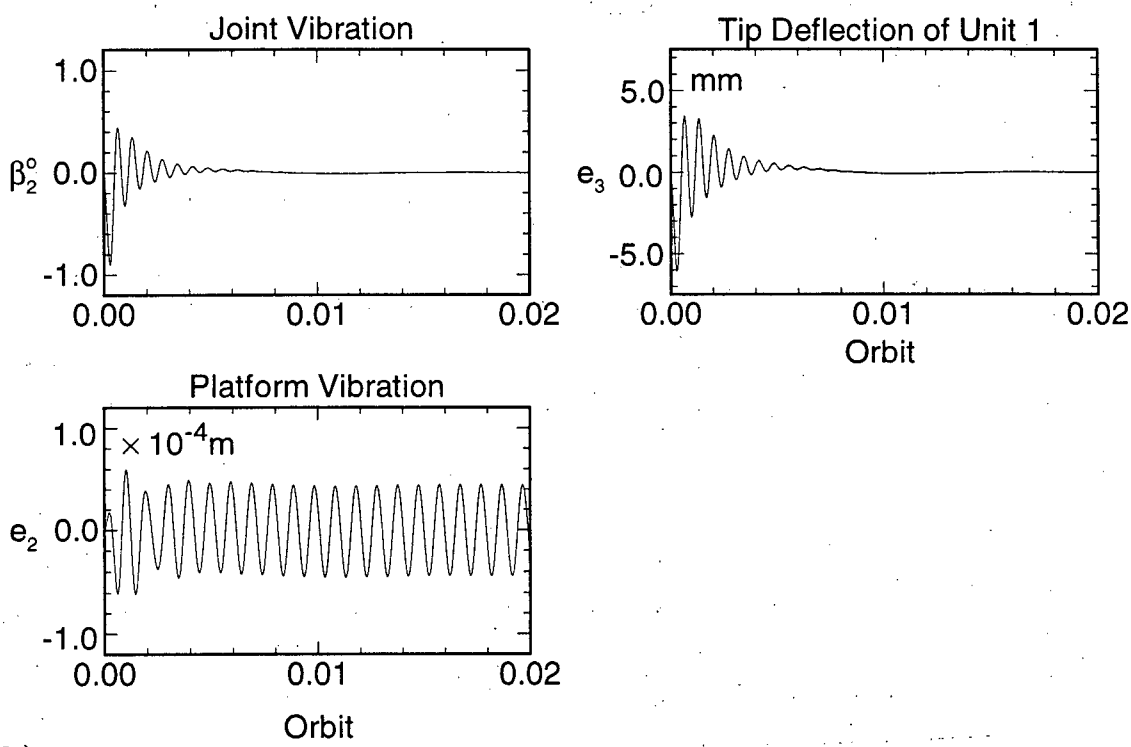

(b)

Figure 5-4 Performance of the FLT controller during a 10° adjustment of the slew angle and a 2 m deployment of the manipulator unit: (b) vibrational response of the system.

It is interesting to note that, because the joint vibration and link deflections are highly coupled with the controlled rotation of the joint, the vibrations arising from the motion of the manipulator are suppressed indirectly by the FLT controller. Even the platform tip vibration, which persists, has an amplitude of less than 0.1 mm. Obviously, the structural damping, which is purposely not accounted for here, can easily tackle this situation quite effectively.

Figure 5-5 illustrates the controlled response of the system during a simultaneous 45° slewing maneuver and a 2 m deployment of the manipulator unit. For large slewing maneuvers, as is the case now, it is not appropriate to use step-input commands, but rather to specify the desired values for α_2, $\dot{\alpha}_2$, $\ddot{\alpha}_2$, l_2, $\dot{l}_2$, and $\ddot{l}_2$ according to the sine-ramp profile defined in Eq. (2.84). Therefore, the controller is now used for continuous regulation rather than point-to-point control. Figure 5-5(a) gives the control inputs time histories as well as the response for all three controlled variables. Again, the dash lines show the controlled response of the rigid system. Throughout the simulation, the controller successfully keeps the platform in its horizontal orientation. As before, the unmodeled dynamics adversely affects the performance of the controller, resulting in small overshoots for both α_2 and l_2. Figure 5-5(b) shows that the maneuver has only small effect on the joint and link vibrations. The effect on the platform tip can be considered negligible.

The final case determines the ability of the FLT controller to track the straight line trajectory defined by Eq. (4.3). The desired values for α_2, $\dot{\alpha}_2$, $\ddot{\alpha}_2$, l_2, $\dot{l}_2$, and $\ddot{l}_2$ are obtained as before through simple inverse kinematics. Figure 5-6(a) shows the control inputs and response of the controlled degrees of freedom. Figure 5-6(b) gives the response of the flexible components in addition to the trajectory followed by the tip of the manipulator. The actual trajectory deviates slightly from the desired one during the maneuver. The path followed by the tip seems to suggest that the controller gains associated with l_2 were too low for this particular case. The manipulator unit does

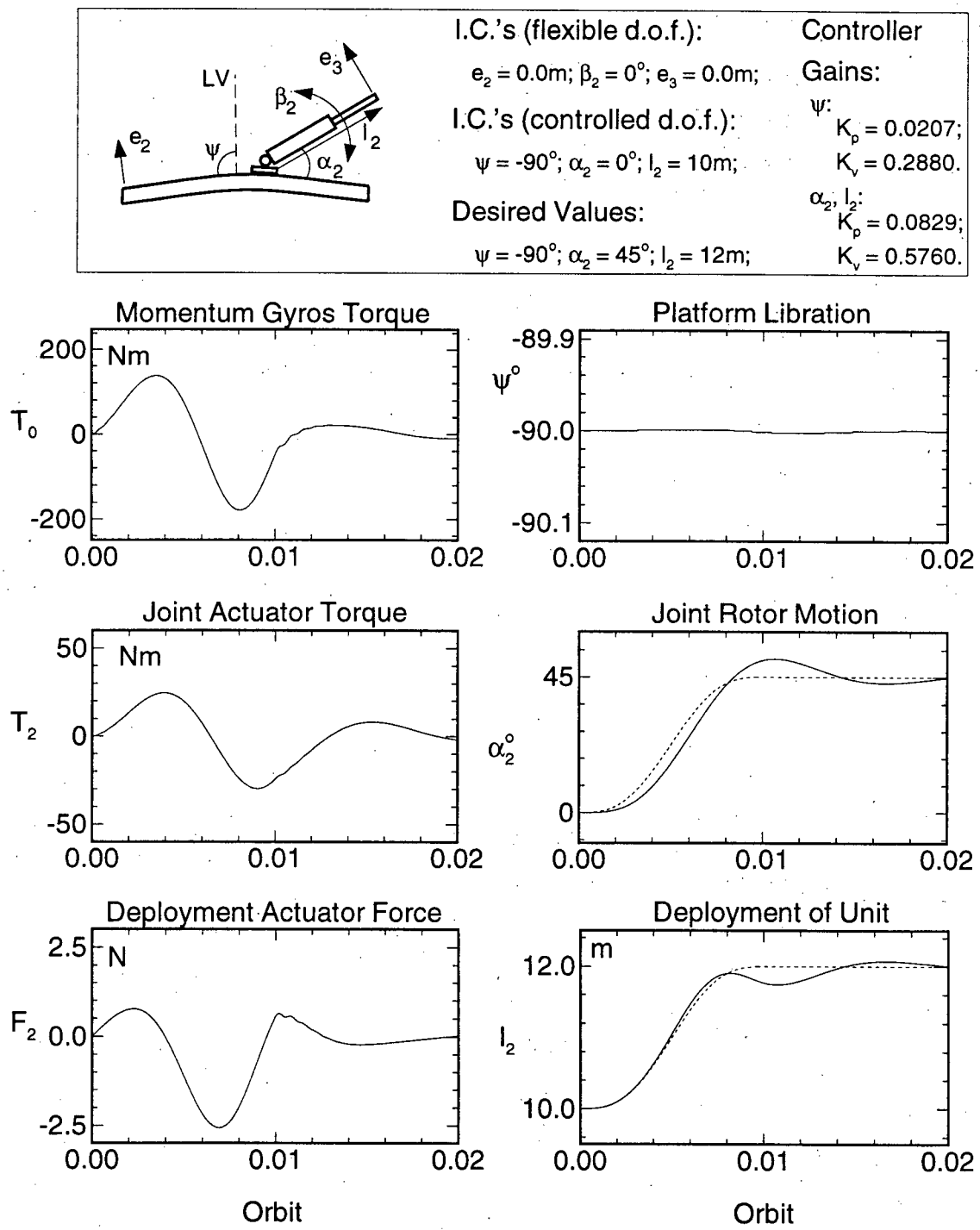

(a)

Figure 5-5 Controlled response of the system during a simultaneous 45° slew and 2 m deployment maneuver of the manipulator unit: (a) control inputs and response of controlled degrees of freedom.

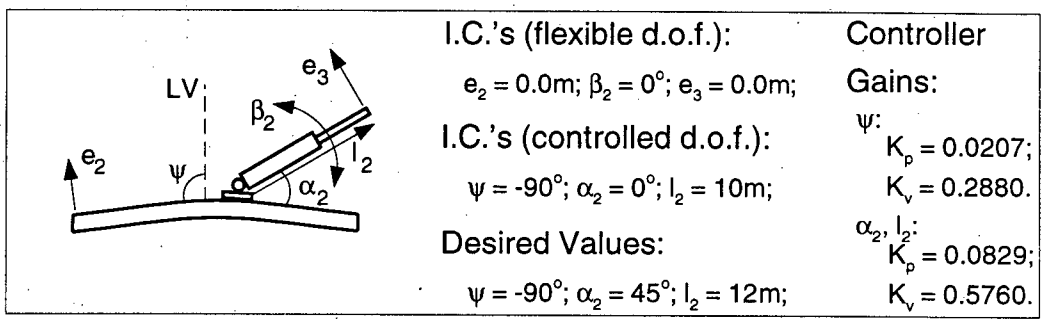

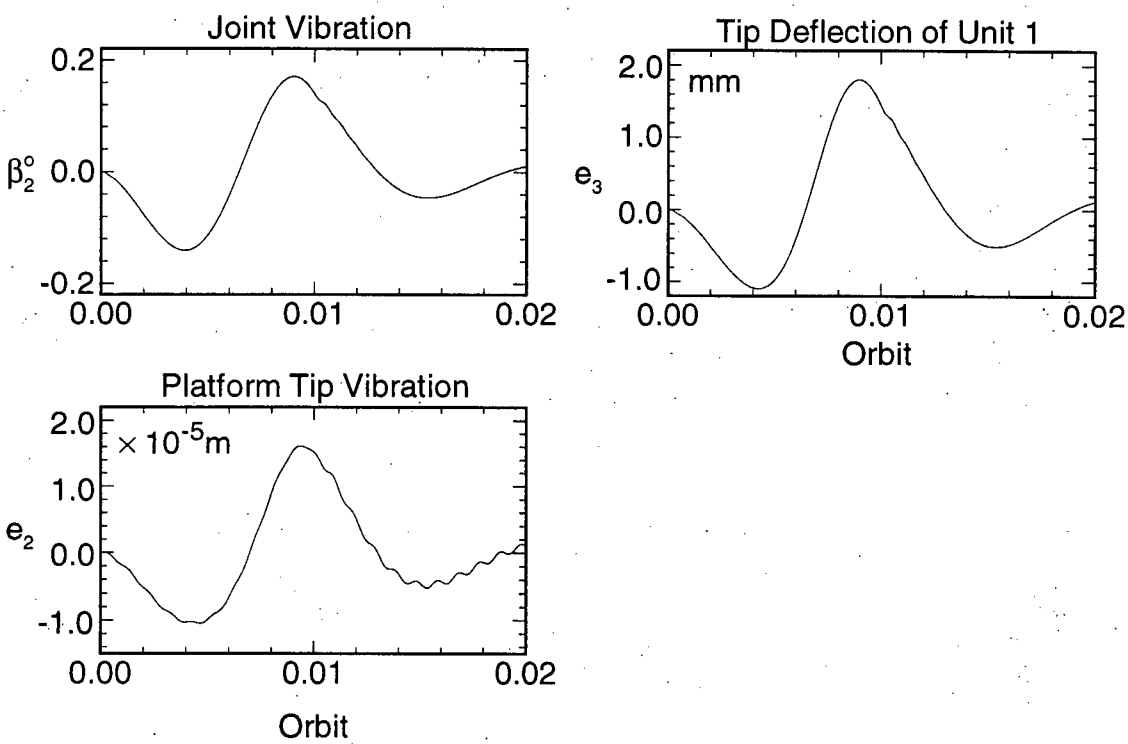

(b)

Figure 5-5 Controlled response of the system during a simultaneous 45° slew and 2 m deployment maneuver of the manipulator unit: (b) vibrational response.

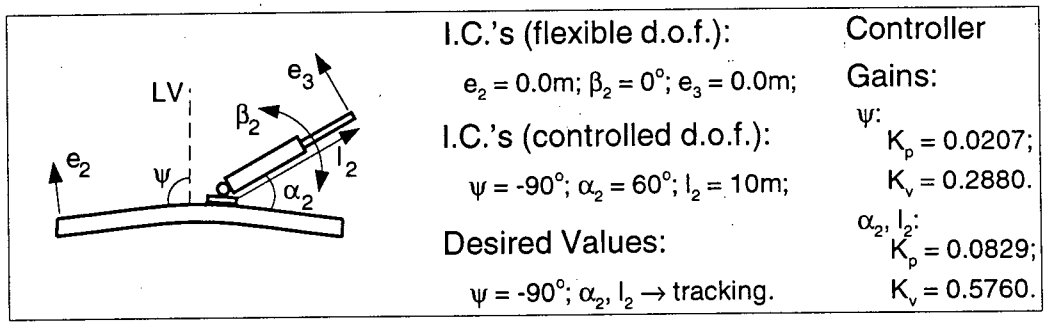

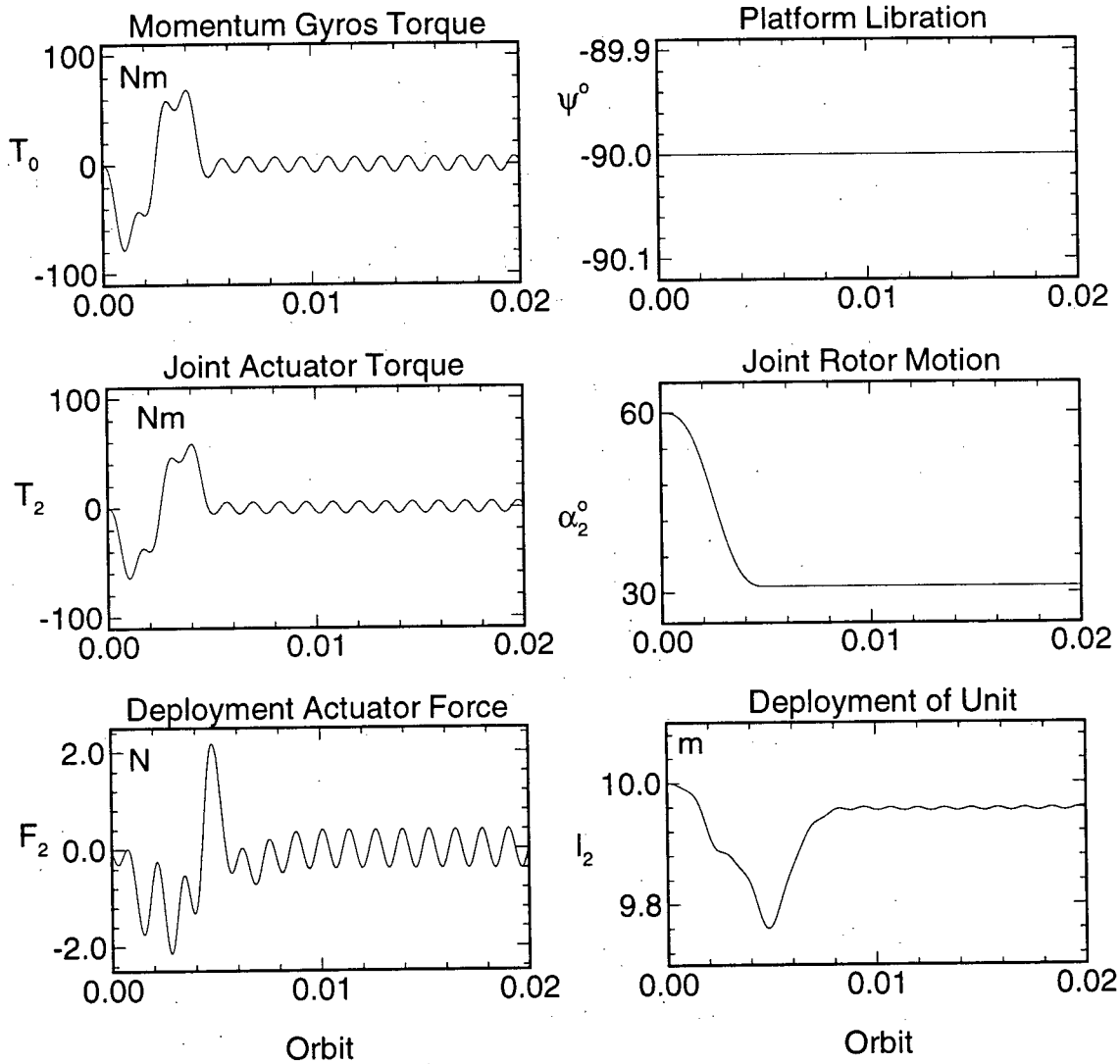

(a)

Figure 5-6 Tracking of a straight line trajectory using the FLT strategy: (a) control inputs and response of controlled degrees of freedom.

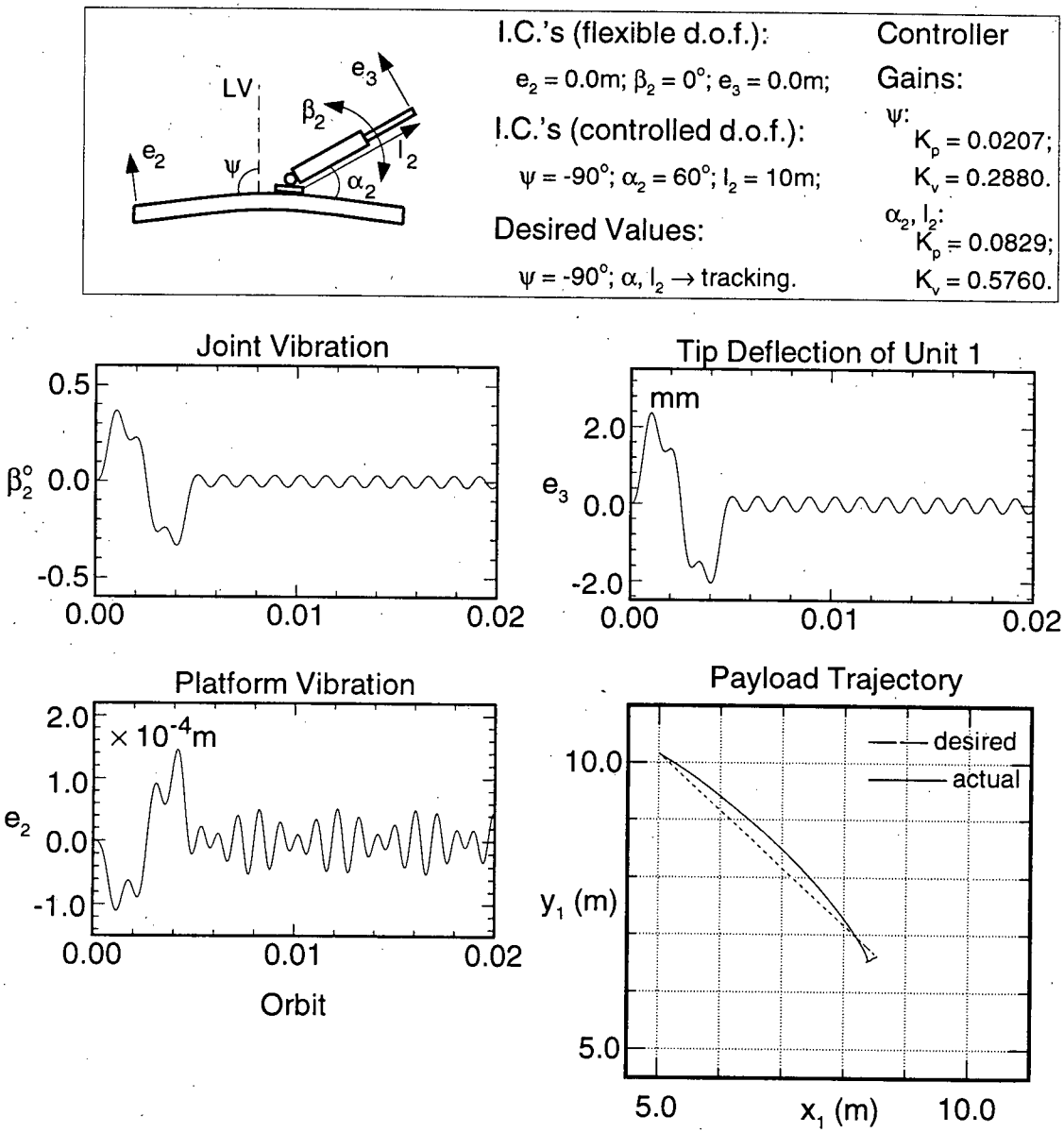

Figure 5-6 Tracking of a straight line trajectory using the FLT strategy: (b) vibrational response and trajectory followed by the end-effector.

not seem to retract sufficiently to precisely follow the desired trajectory during the maneuver. Only when the slewing maneuver is nearly completed does the manipulator extend to reach the final desired position. It is interesting to note that a gross-fine motion scheme seems to arise naturally from this combination of the controller gains.

5.3 Control of Flexible Degrees of Freedom

The dynamical study has demonstrated that maneuvers involving deployment, retrieval, slew, or translation of the manipulator can induce significant vibrations in the system. In turn, the flexible deformation of the components can be detrimental to the manipulator's positioning accuracy. Elastic deformations can be reduced through the use of materials with a higher structural stiffness and damping. However, this option is usually limited by mass restrictions and materials available. It is proposed to use the CMG's and joint actuators for active suppression of the platform, link, and joint vibrations. As mentioned before, the CMG's can modify the platform's slope, and thus its deflection. Controlled oscillations of the joint actuator can be used to suppress joint as well as link vibrations through coupling.

Since the system's flexible degrees of freedom have been found to be highly coupled, the control inputs must be carefully selected so that the control of one does not excite another. To this end, a Linear Quadratic Regulator is designed for vibration control when the manipulator is either in a fixed configuration or during small slewing or deployment maneuvers. The gains of the controller are selected optimally to minimize both the system vibrations and errors in the joint angle.

A combined FLT/LQR approach was applied to the one-unit manipulator system, as shown in Figure 5-7. When the manipulator is in a fixed configuration (no deployment, slew, or translation), the platform attitude (ψ) and manipulator length (l_2) are maintained using the FLT strategy. However, the joint rotation (α_2) and the platform's transverse vibration (δ_{11}) are controlled using the LQR approach. Dur-

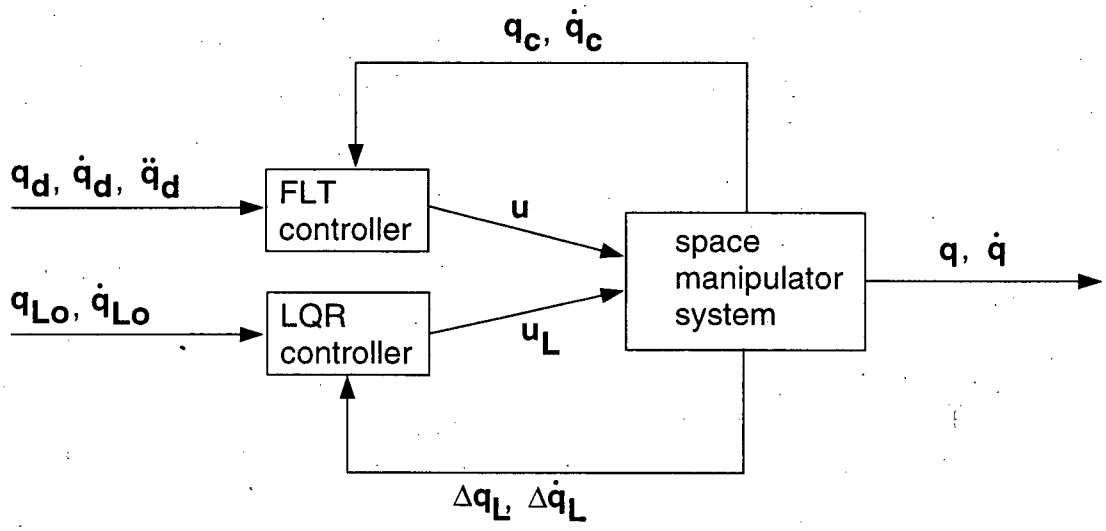

Figure 5-7 Schematic diagram illustrating the combined FLT/LQR approach applied to the manipulator system. The FLT controller regulates the platform attitude (ψ), the length of the unit (l_2), as well as the slew angle (α_2) during large maneuvers. The LQR controller acts on the flexible subsystem ($\delta_{11}, \alpha_2, \beta_2, \delta_{21}$).

ing large slewing and deployment maneuvers, only three variables (ψ, α_2, and l_2) are regulated by the FLT controller until the manipulator reaches the vicinity of its target position. Structural vibrations are left uncontrolled. At the end of the large maneuver, the system's configuration remains nearly constant and nonlinear effects can be neglected. This allows the Linear Quadratic Regulator to take over for α_2, start the CMG vibration suppression action, and actively damp out the vibrations generated during the maneuver.

5.3.1 Linearized subsystem

The optimal controller, based on the LQR design, requires a linear model of the system to be controlled. The equations of motion derived in chapter 2 are highly nonlinear, particularly due to large maneuvers of the manipulator which alter the configuration of the system. However, when the manipulator configuration is fixed or nearly fixed, as is the case near the end of maneuvers, a linear approximation can be sought.

The elastic deformation of the joint (β_2) is only described implicitly in $\mathbf{q}$. The first step in deriving the linear model consists in using β_2 as a generalized coordinate instead of ψ_2. Considering that $\beta_2 = \psi_2 - \alpha_2 - \xi_2 - \psi_1$, a velocity transformation can be developed:

$$\dot{\mathbf{q}} = \mathbf{R^L}\dot{\bar{\mathbf{q}}}, \tag{5.12}$$

where $\bar{\mathbf{q}} = [r_o, \theta, \psi_1, \delta_1^T, \bar{d}_2^T, \alpha_2, \beta_2, \delta_2^T, l_2]^T$ and $\mathbf{R^L}$ is the transformation linking the two velocity vectors. Using Eq. (5.12), a new expression can be obtained for the kinetic energy of the system,

$$T = \frac{1}{2}\dot{\mathbf{q}}^{\mathbf{T}}\mathbf{M}\dot{\mathbf{q}} = \frac{1}{2}\dot{\bar{\mathbf{q}}}^{\mathbf{T}}\underbrace{\mathbf{R^L}^{\mathbf{T}}\mathbf{M}\mathbf{R^L}}_{\bar{\mathbf{M}}}\dot{\bar{\mathbf{q}}}, \tag{5.13}$$

where $\bar{\mathbf{M}}$ is the system mass matrix with β_2 taken as a generalized coordinate. Similarly, the expressions for the potential energy terms can be modified by replacing ψ_2

by $\psi_1 + \xi_2 + \alpha_2 + \beta_2$. Thus,

$$V_g = V_g(\bar{\mathbf{q}}) \quad \text{and} \quad V_e = V_e(\bar{\mathbf{q}}). \tag{5.14}$$

Using the Lagrangian procedure, the equations of motion can be obtained in terms of $\bar{\mathbf{q}}$:

$$\bar{\mathbf{M}}\ddot{\bar{\mathbf{q}}} + \dot{\bar{\mathbf{M}}}\dot{\bar{\mathbf{q}}} - \frac{\partial\{\dot{\bar{\mathbf{q}}}^{\mathbf{T}}\bar{\mathbf{M}}\dot{\bar{\mathbf{q}}}\}}{\partial\bar{\mathbf{q}}} + \frac{\partial V_g}{\partial\bar{\mathbf{q}}} + \frac{\partial V_e}{\partial\bar{\mathbf{q}}} = \bar{\mathbf{Q}}, \tag{5.15}$$

where $\bar{\mathbf{Q}}$ is the generalized force associated with $\bar{\mathbf{q}}$.

The governing equations are linearized about an operation point $\bar{\mathbf{q}}_{\mathbf{o}}$. The following substitutions are made in Eq. (5.15):

$$\bar{\mathbf{q}} = \bar{\mathbf{q}}_{\mathbf{o}} + \boldsymbol{\Delta}\bar{\mathbf{q}};\ \dot{\bar{\mathbf{q}}} = \dot{\bar{\mathbf{q}}}_{\mathbf{o}} + \boldsymbol{\Delta}\dot{\bar{\mathbf{q}}};\ \ddot{\bar{\mathbf{q}}} = \ddot{\bar{\mathbf{q}}}_{\mathbf{o}} + \boldsymbol{\Delta}\ddot{\bar{\mathbf{q}}}. \tag{5.16}$$

The components of $\dot{\bar{\mathbf{q}}}_{\mathbf{o}}$ and $\ddot{\bar{\mathbf{q}}}_{\mathbf{o}}$ are either zero or extremely small for the operating conditions considered. Therefore, their contributions are neglected. Trigonometric functions are expanded in the Taylor series, and the second and higher order terms in $\Delta\bar{q}_i$ and $\Delta\dot{\bar{q}}_i$ are neglected. After some algebra, this leads to

$$\bar{\mathbf{M}}(\bar{\mathbf{q}}_{\mathbf{o}})\boldsymbol{\Delta}\ddot{\bar{\mathbf{q}}} + \bar{\mathbf{K}}(\bar{\mathbf{q}}_{\mathbf{o}})\boldsymbol{\Delta}\bar{\mathbf{q}} = \bar{\mathbf{Q}}, \tag{5.17}$$

where $\bar{\mathbf{K}}$ is the stiffness matrix for the linearized system. Note, both $\bar{\mathbf{M}}$ and $\bar{\mathbf{K}}$ are evaluated at $\bar{\mathbf{q}}_{\mathbf{o}}$ and thus made time-invariant.

Now, in general, the orbital motion has a negligible effect on the vibrational response. Furthermore, the system's librational motion and the deployment length of the manipulator are controlled by the FLT. Therefore, it is convenient to obtain the linear equations governing the vibrational motion of the system considering the orbital, librational, and deployment degrees of freedom as specified. The decoupled vibrational subsystem is now described by

$$\bar{\mathbf{M}}_{\mathbf{L}}\boldsymbol{\Delta}\ddot{\bar{\mathbf{q}}}_{\mathbf{L}} + \bar{\mathbf{K}}_{\mathbf{L}}\boldsymbol{\Delta}\bar{\mathbf{q}}_{\mathbf{L}} = \bar{\mathbf{Q}}^{\mathbf{d}}_{\mathbf{L}}\mathbf{u}_{\mathbf{L}}, \tag{5.18}$$

where: $\mathbf{\Delta\bar{q}_L} = [\delta_1^T, \Delta\alpha_2, \beta_2, \delta_2^T]^T$, with $\Delta\alpha_2$ as the deviation of the slew angle from its desired value; $\mathbf{\bar{M}_L}$, $\mathbf{\bar{K}_L}$, and $\mathbf{\bar{Q}_L^d}$ correspond to $\mathbf{\bar{M}}$, $\mathbf{\bar{K}}$, and $\mathbf{\bar{Q}^d}$, respectively, with the rows and columns corresponding to r_o, θ, ψ_1, d_{2x}, d_{2y}, and l_2 removed; and $\mathbf{u_L}$ is the output of the Linear Quadratic Regulator. Note, the operational point is $\mathbf{\bar{q}_{Lo}} = [\mathbf{0}, \alpha_{20}, 0, \mathbf{0}]^T$.

Since the structural vibrations of the platform and manipulator links are dominated by their respective first modes, only the fundamental mode of transverse vibration is considered here. Hence, $\mathbf{\Delta\bar{q}_L} \in \Re^{4\times1}$; $\mathbf{u_L} \in \Re^{2\times1}$; $\mathbf{\bar{M}_L}$, $\mathbf{\bar{K}_L} \in \Re^{4\times4}$; and $\mathbf{\bar{Q}_L^d} \in \Re^{4\times2}$. Solving for $\mathbf{\Delta\ddot{\bar{q}}_L}$,

$$\mathbf{\Delta\ddot{\bar{q}}_L} = -\mathbf{\bar{M}_L^{-1}\bar{K}_L\Delta\bar{q}_L} + \mathbf{\bar{M}_L^{-1}\bar{Q}_L^d u_L}, \tag{5.19}$$

which can be rewritten in state-space form as

$$\underbrace{\begin{bmatrix} \mathbf{\Delta\dot{\bar{q}}_L} \\ \mathbf{\Delta\ddot{\bar{q}}_L} \end{bmatrix}}_{\mathbf{\dot{x}_L}} = \underbrace{\begin{bmatrix} \mathbf{0} & \mathbf{I}^4 \\ -\mathbf{\bar{M}_L^{-1}\bar{K}_L} & \mathbf{0} \end{bmatrix}}_{\mathbf{A}} \underbrace{\begin{bmatrix} \mathbf{\Delta\bar{q}_L} \\ \mathbf{\Delta\dot{\bar{q}}_L} \end{bmatrix}}_{\mathbf{x_L}} + \underbrace{\begin{bmatrix} \mathbf{0} \\ \mathbf{\bar{M}_L^{-1}\bar{Q}_L^d} \end{bmatrix}}_{\mathbf{B}} \mathbf{u_L}. \tag{5.20}$$

5.3.2 The Linear Quadratic Regulator (LQR)

The state-space equations of the system are

$$\mathbf{\dot{x}_L} = \mathbf{A x_L} + \mathbf{B u_L}, \tag{5.21}$$

where $\mathbf{x_L} \in \Re^{8\times1}$, $\mathbf{A} \in \Re^{8\times8}$, and $\mathbf{B} \in \Re^{8\times2}$. A Linear Quadratic Regulator is now designed to control the vibrational behavior of the one-unit manipulator system. First, the controllability and observability of the system must established. For simplicity, it is assumed that all states are available, thus making the system completely observable. Complete controllability will be ensured if and only if

$$rank\left\{\left[\mathbf{B}, \mathbf{AB}, \mathbf{A^2B}, \cdots, \mathbf{A^7B}\right]\right\} \geq 8 \tag{5.22}$$

for the system configuration considered.

The LQR approach yields a unique set of state feedback gains for a given performance criterion [76]. The control input $\mathbf{u_L}$ can be written as

$$\mathbf{u_L} = -\mathbf{K_{LQR}}\mathbf{x_L}, \tag{5.23}$$

where $\mathbf{K_{LQR}}$ is the optimal gain matrix. It minimizes a quadratic cost function J which considers tracking errors and energy expenditure,

$$J = \int_0^T \left(\mathbf{x_L^T Q_{LQR} x_L} + \mathbf{u_L^T R_{LQR} u_L}\right) dt, \tag{5.24}$$

where $\mathbf{Q_{LQR}}$ and $\mathbf{R_{LQR}}$ are symmetric weighting matrices which assign relative penalties to state errors and control effort, respectively. The matrix $\mathbf{R_{LQR}}$ is required to be positive definite while $\mathbf{Q_{LQR}}$ can be positive semi-definite. The optimal control $\mathbf{u_L}$ is given by

$$\mathbf{u_L} = -\mathbf{K_{LQR}}\mathbf{x_L} = -\mathbf{R_{LQR}^{-1}B^T P_{LQR} x_L}, \tag{5.25}$$

where $\mathbf{P_{LQR}}$ is the solution to the matrix Ricatti equation which, for infinite time, becomes

$$\mathbf{P_{LQR}A} + \mathbf{A^T P_{LQR}} - \mathbf{P_{LQR}BR_{LQR}^{-1}B^T P_{LQR}} + \mathbf{Q_{LQR}} = \mathbf{0}. \tag{5.26}$$

5.3.3 Active vibration suppression for a one-unit system

The ability of the LQR to actively damp out vibrations in the one-unit manipulator system is now evaluated. For all cases studied, the nominal conditions are taken to be $\psi = 0^o$ (platform along the gravity gradient), $d_2 = 30$ m, $\alpha_2 = 50^o$, and $l_2 = 12$ m. For this particular configuration, the rank of the controllability matrix, defined in Eq. (5.22), takes the value of 8. This confirms that the flexible subsystem is completely controllable. Furthermore, the open loop pools are 0, 0, $\pm 1.1522i$, $\pm 19.2546i$, and $\pm 32.0393i$. Note, the subsystem is marginally stable due to the absence of dissipative forces. The two zero poles correspond to the rigid body motion of the joint rotor. The remaining three pairs of poles are closely related

to the free vibrations of the platform, manipulator links, and joint, respectively.

The performance of the optimal controller is determined by the selected state penalty matrix $\mathbf{Q_{LQR}}$ and control penalty matrix $\mathbf{R_{LQR}}$. For the system considered here, $\mathbf{Q_{LQR}} \in \Re^{8\times 8}$ and $\mathbf{R_{LQR}} \in \Re^{2\times 2}$. Since the objective here is to suppress vibrations without any concern for actuator limitations, the matrices are treated as diagonal, with $\mathbf{Q_{LQR}} = diag\{10^9, 10^6, 10^6, 10^6, 10^3, 10^3, 10^3, 10^3\}$ and $\mathbf{R_{LQR}} = \mathbf{I}^2$.

Position errors are given greater importance in order to increase the speed of the controlled response. In particular, the platform's elastic deformation is assigned the greatest weight because of its considerable effect on the other degrees of freedom. With this set of weights, the optimal gain $\mathbf{K_{LQR}}$ can be computed from Eq. (5.25) and Eq. (5.26). With optimal state feedback, the closed loop eigenvalues of the vibrational subsystem become $-0.1556 \pm 0.1726i$, $-0.1139 \pm 1.1578i$, $-0.5479 \pm 19.2695i$, and $-3.0790 \pm 32.0268i$ and are all located in the left half of the s-plane.

Figure 5-8 presents the controller performance in damping the system vibrations caused by an initial 50 cm deflection of the manipulator tip. As mentioned earlier, the Linear Quadratic Regulator acts on α_2 and δ_{11}, while the FLT controller maintains ψ and l_2 at their respective desired values. The figure only shows the control inputs and response variables associated with the vibrational subsystem, as both the platform's attitude and manipulator length remain nearly constant. Despite the fact that it has no direct control action on the large deformation of the manipulator links, the optimal controller succeeds in suppressing the joint and link vibrations, while maintaining the slew angle at the desired orientation of $\alpha_2 = 50^o$. The platform vibrations subsist slightly longer, but they are small and do not affect the other degrees of freedom.

The next case investigates the controlled response of the system to a slew maneuver from $\alpha_2 = 50^o$ to $\alpha_2 = 60^o$. Figure 5-9 shows that the controller achieves the target orientation and suppresses joint and link vibrations in less than 30 seconds (0.0055 orbit). At all times, the joint deformation and tip deflection of the ma-

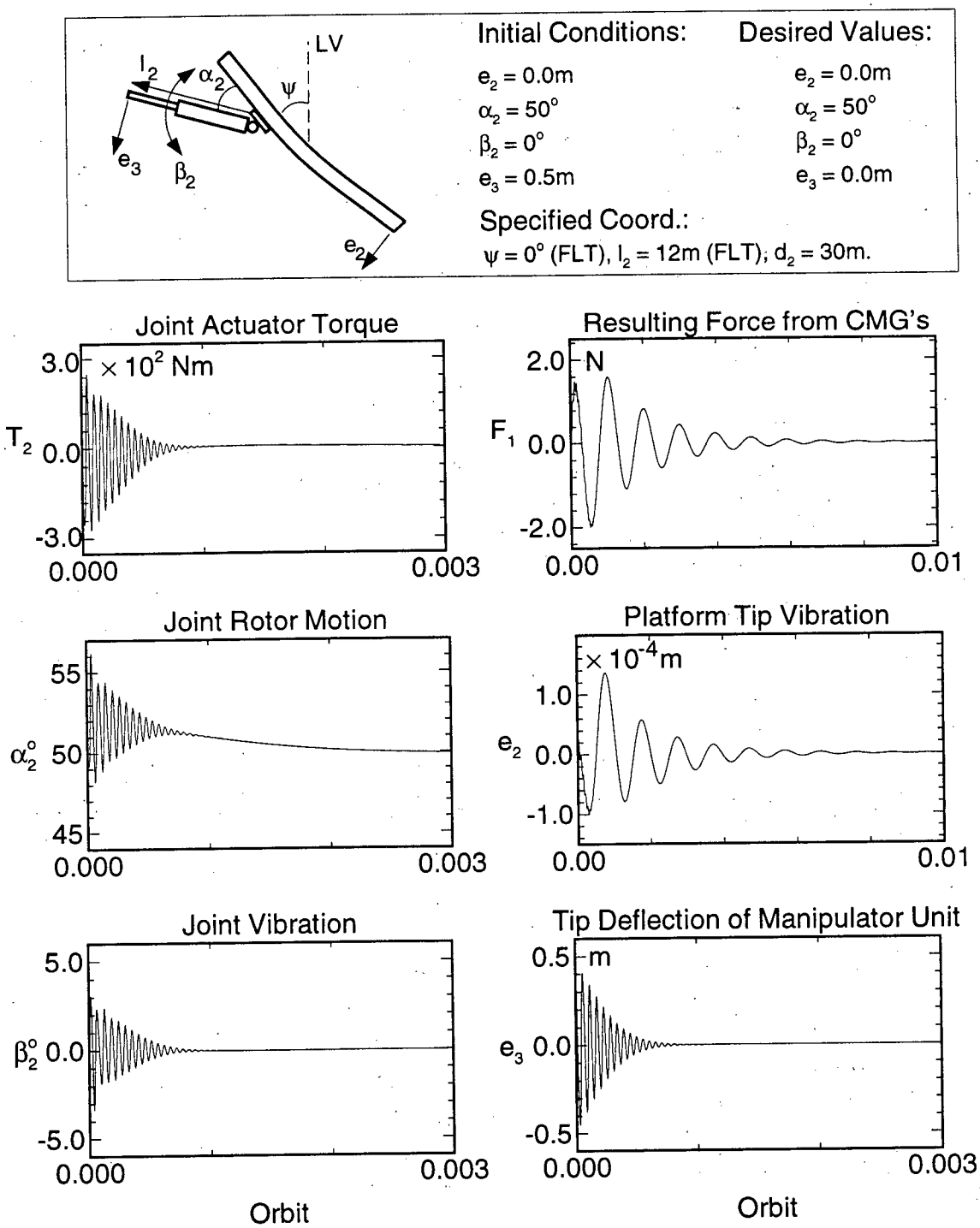

Figure 5-8 Suppression of the vibrations arising from an initial 50 cm deflection of the manipulator tip.

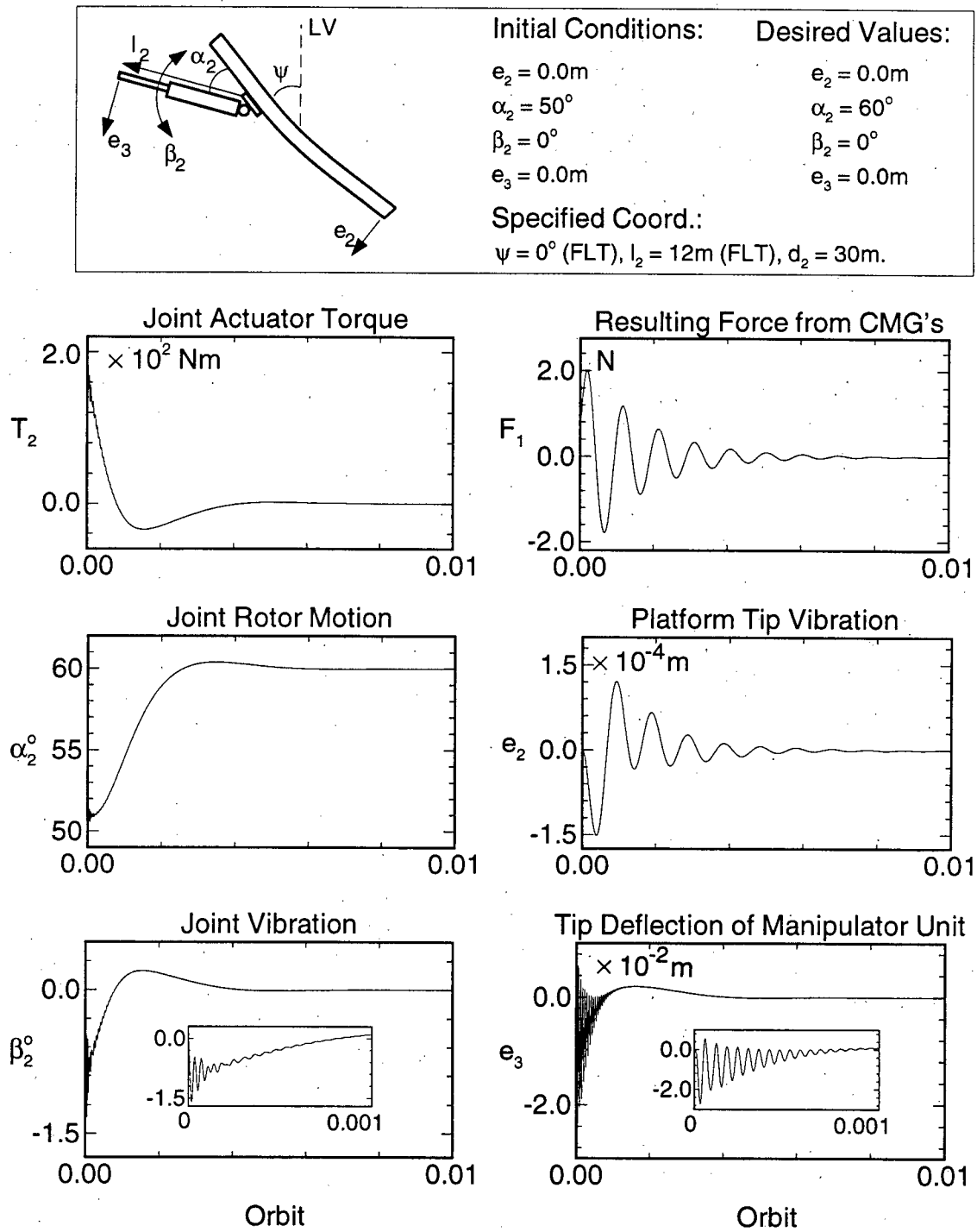

Figure 5-9 Performance of the LQR controller during a 10° slew maneuver with α_2 changing from 50° to 60°.

nipulator remain below 1.6^o and 2.5 cm, respectively. Although the small platform vibrations persist slightly longer, they have negligible effect on the system.

Figure 5-10 considers the case where the FLT controller commands the manipulator to extend from $l_2 = 10$ m to $l_2 = 12$ m in the presence of large platform vibrations, arising from an initial 1.0 m deflection of the platform's tip. Note, the manipulator angle of $\alpha_2 = 50^o$ also acts as a pitch disturbance although it is not commanded to slew. Figure 5-10(a) shows the librational and vibrational response of the system, as well as the time histories for both the slew angle (α_2) and manipulator length. Despite the presence of large unmodelled flexible dynamics, the FLT strategy is quite succesful in bringing the length of the manipulator to its desired value in less than 0.008 orbit and returns the platform to the gravity gradient orientation in less than 0.01 orbit. Due to the action of the Linear Quadratic Regulator, the platform, link, and joint vibrations subside in less than 0.01 orbit. The slew angle α_2 has also returned to its nominal value of 50° by that time.

Figure 5-10(b) presents the control effort required to achieve this succesful performance. As mentioned before, two sets of CMG's are used: one to control the attitude, and the other responsible for vibration suppression. The magnitude of the torque and force required from the CMG's suggest that it might be preferable to damp the vibrations over a longer period, in order to avoid saturation of the actuators. Hence, the control penalty can be assigned higher weights to this effect.

Finally, it should be emphasized that the objective here was to gain some insight into the possibilities offered by active vibration control. This summary study of optimal vibration suppression is only preliminary. The extension of the optimal controller to account for a greater number of manipulator units, the development of a systematic approach for the selection of the weighting matrices $\mathbf{Q_{LQR}}$ and $\mathbf{R_{LQR}}$, as well as the use of gain scheduling during large maneuvers, present challenging avenues to pursue.

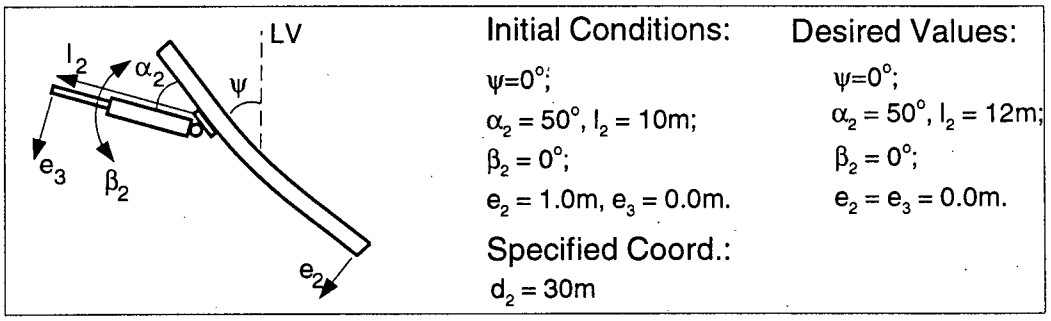

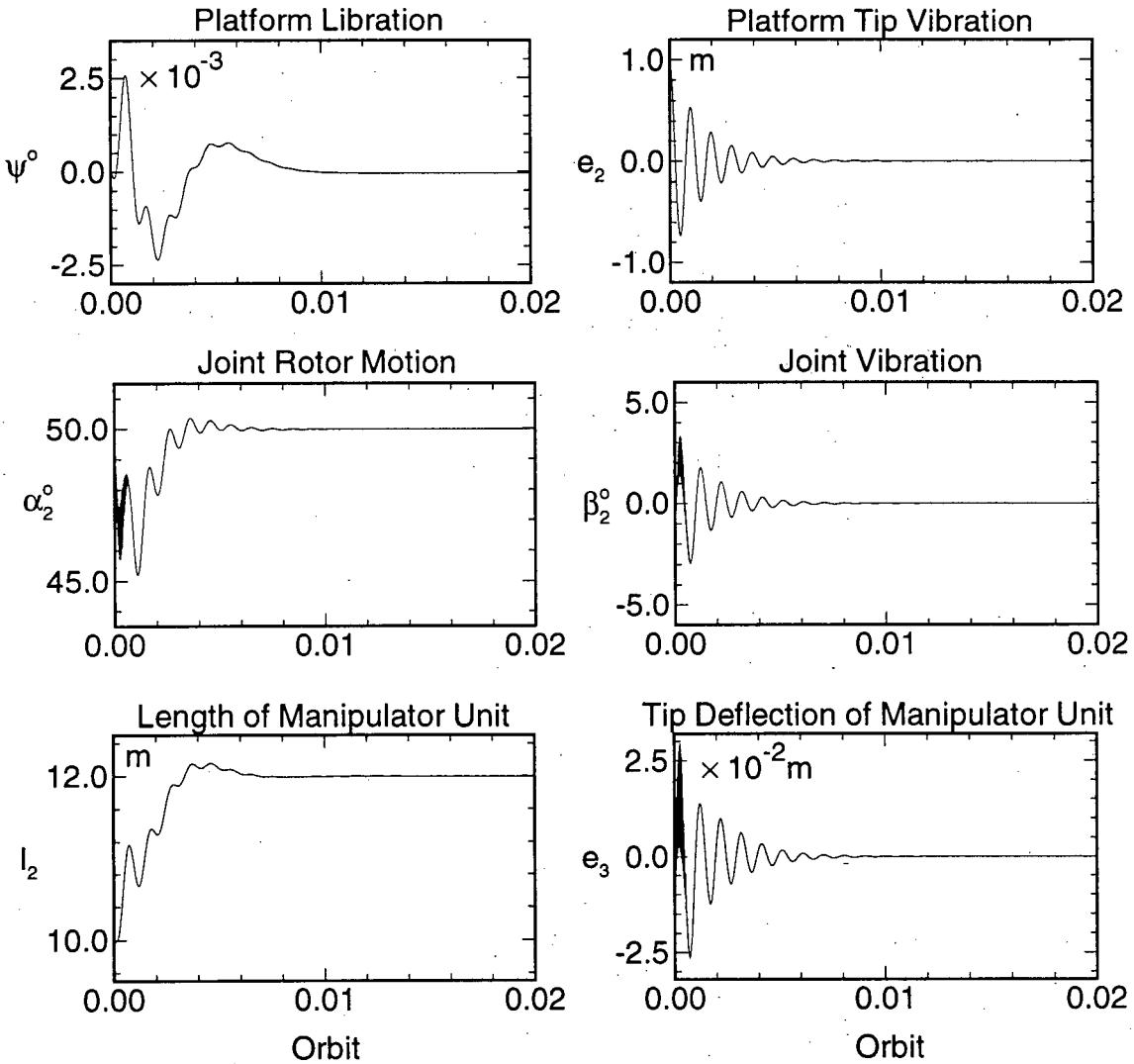

(a)

Figure 5-10 2 m deployment of the manipulator unit in the presence of large platform vibrations: (a) controlled response of the system.

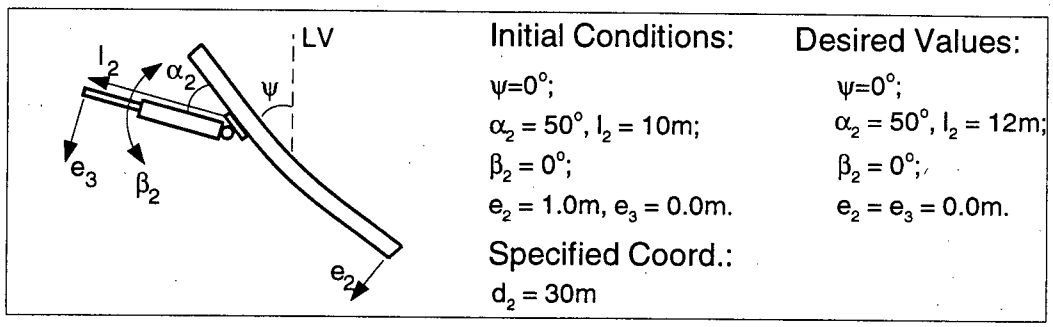

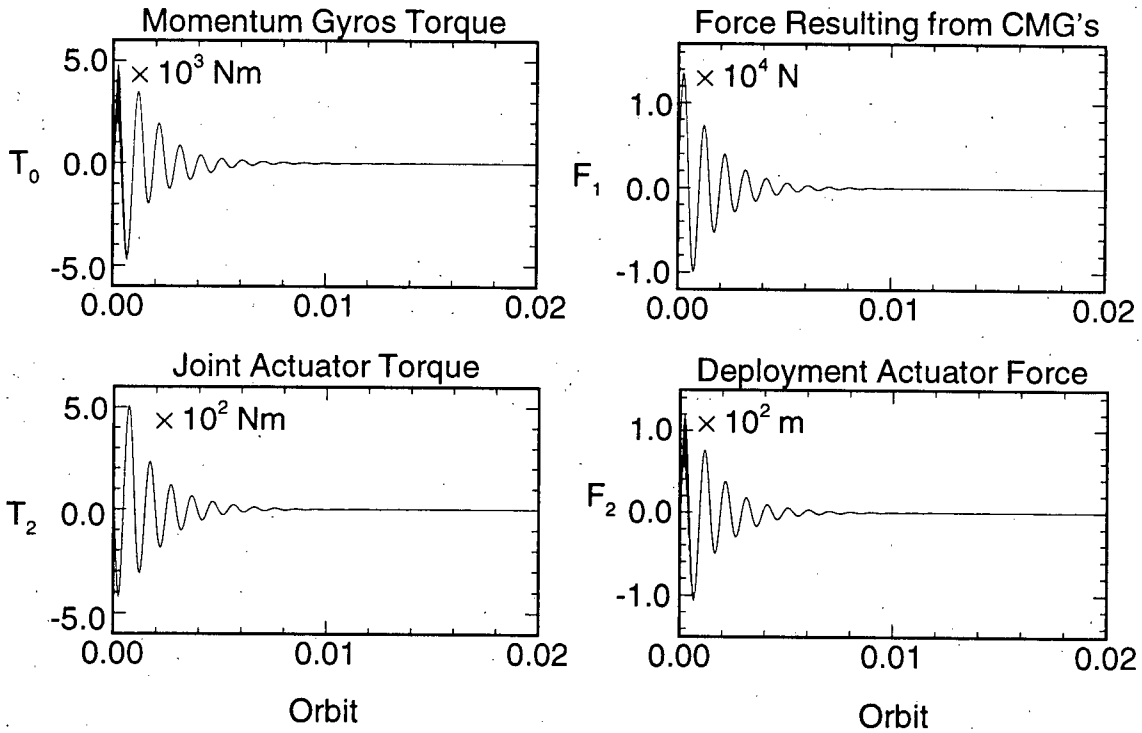

(b)

Figure 5-10 2 m deployment of the manipulator unit in the presence of large platform vibrations: (b) time histories of the control effort.

6. CONCLUDING REMARKS

6.1 Summary of Conclusions

The main contributions of the thesis can be summarized as follows:

(i) A relatively general mathematical model is developed to simulate the two-dimensional dynamics of a multibody chain-type system undergoing orbital, librational, and vibrational motions. The model accounts for flexibility in all bodies and interconnecting joints.

(ii) This versatile tool can be applied to a large class of space systems of contemporary interest: each body can rotate and translate with respect to the others. Furthermore, the length of each body can be time-varying, a feature not common to most multibody formulation.

(iii) The forward dynamics is based on a nonrecursive $O(N)$ Lagrangian formulation which computes efficiently the system's acceleration vector.

(iv) The computer code developed can simulate the dynamics of a flexible manipulator consisting of an arbitrary number of 'units'. Each unit is made up of two links: one free to slew, while the other is deployable. The manipulator is attached to a mobile base capable of translating along an orbiting platform.

(v) A nonlinear controller, based on the Feedback Linearization Technique (FLT), is designed to regulate the slew and deployment degrees of freedom, as well as the attitude of the platform.

(vi) A Linear Quadratic Regulator (LQR) is designed to suppress the vibrations arising in the manipulator links and joints, as well as in the platform.

The emphasis throughout is on the development of a methodology to understand the complex dynamical interactions involved with the particular class of manipulators studied here. It was not intended here to conduct a comprehensive analysis for system

design, although the established methodology can be readily used to that end. The objective was to assess the versatility of the tools developed here through the study of a few representative cases and establish general trends.

Based on the investigation, the following general conclusions can be made:

(a) The manipulator units act as payloads, and lower the natural frequency of those supporting them. The choice of shape functions used to model their flexibility can affect the speed of convergence. In general, the fundamental mode is sufficient to capture important features of the system dynamics.

(b) Significant coupling exists between the platform, link, and joint vibrations, as well as system libration. The most pronounced coupling was observed between the joint and link vibrations. In general, slewing and deployment maneuvers have a significant effect on the flexible degrees of freedom response.

(c) Motion of the manipulator modifies the system's inertia tensor and thus can induce considerable librational motion during the translation of the mobile base. When the manipulator base is located near the platform's extremity, slewing and deployment maneuvers can also result in significant rigid body motion of the platform.

(d) Deployment alters the inertia and stiffness properties of each unit. This feature can be used to advantage to adapt the system's dynamic properties to given specifications.

(e) Excitation of the system's flexible degrees of freedom can deteriorate significantly the accuracy of the manipulator, particularly near the end of maneuvers.

(f) The system exhibits unacceptable response under critical combinations of parameters. The control strategy based on FLT is found to be effective in regulating the rigid-body motion of manipulator links as well as the attitude motion of the platform. The unmodelled flexibility of the platform and manipulator links

slightly decreases the performance of the FLT controller. On the other hand, cases arise where the FLT controller can regulate the manipulator's flexible degrees of freedom through coupling.

(g) Active vibration suppression can be achieved with the platform's momentum gyros and manipulator torque actuators using a LQR strategy.

(h) Such a comprehensive study aimed at a general approach to this class of problems has not been reported before.

6.2 Recommendations for Future Work

Considering the diversity of research areas associated with the field of space robotics, the present thesis should be viewed as an initial step in the analysis and development of this particular class of space manipulators. The general formulation and computer program developed here can serve as useful tools in future studies. However, there are several avenues which remain unexplored or demand more attention. Some of the more interesting and useful aspects include:

(i) extension of the present model to account for the out-of-plane motion, i.e. development of a full three-dimensional model taking into account gyroscopic effects and torsional deformations;

(ii) modelling of system flexibility using various admissible functions, quasi-comparison functions, as well as system modes, and assessment of their effects on accuracy as well as convergence;

(iii) path planning and inverse kinematics with emphasis on obstacle avoidance, as well as minimization of structural vibrations and base reaction; effect of redundancy on system performance; completion of a given mission with one or more joints inoperational;

(iv) dynamics of satellite capture and release with the manipulator;

(v) comparative study of various optimal and adaptive control strategies, such as LQR with gain scheduling, LQG/LTR, H_∞, etc, to regulate the rigid and flexible dynamics of the system;

(vi) two-dimensional ground-based experiments to validate simulation results;

(vii) animation of simulation results for visual appreciation of the physics of the problem.

BIBLIOGRAPHY

[1] Evans, B., "Robots in Space," *Spaceflight,* Vol. 35, No. 12, 1993, pp. 407-409.

[2] Canadian Science and Technology, O'Brien Publishing, Ottawa, Ontario, Fall 1995, p. 11.

[3] Bassett, D.A., Wojcik, Z.A., Hoefer, S., and Wittenborg, J., "Mobile Servicing System Assembly, Checkout and Operations," *46th International Astronautical Congress,* Oslo, Norway, October 1995, Paper No. IAF-95-T.3.04.

[4] Krukewich, K., Sexton, J., Cavin, K., Lee, N.E., and Cox, B., "The Systems Engineering Approach to the Integration of the Space Station Remote Manipulator System on the International Space Station (ISS)," *46th International Astronautical Congress,* Oslo, Norway, October 1995, Paper No. IAF-95-T.2.02.

[5] Kalaycioglu, S., "Robotics Evaluation and Characterization (REACH) of the SSRMS," *46th International Astronautical Congress,* Oslo, Norway, October 1995, Paper No. IAF-95-1.2.03.

[6] Chiun-Hong, C., "Computer Vision System for Extravehicular Activity Helper/Retriever," *Applied Intelligence,* Vol. 5, No. 3, 1995, pp. 251-268.

[7] Lavery, D., "Perspectives on Future Space Robotics," *Aerospace America,* Vol. 32, No. 5, 1994, pp. 32-37.

[8] Brereton, R.C., *A Stability Study of Gravity Oriented Satellites,* Ph.D. Thesis, The University of British Columbia, Vancouver, Canada, September 1967.

[9] Ambrose, R.O., and Askew, R.S., "Experimental Investigation of Actuators for Space Robots," *Proceedings of the 1995 IEEE International Conference on Robotics and Automation,* Nagoya, Japan, 1995, Vol. 3, pp. 2625-2630.

[10] "Too much Sun gives Ulysses the wobbles," *Electronics World and Wireless World,* Vol. 97, March 1991, p. 184.

[11] Xu, Y., and Shum, H.Y., "Dynamic Control and Coupling of a Free-Flying Space Robot System," *Journal of Robotic Systems,* Vol. 11, No. 7, 1994, pp. 573-589.

[12] Kelly, J.H., Glade, R.L., and Depkovitch, T.M., "Addressing the Issue of System Identification for Space Manipulators," *Proceedings of SPIE - The International Society for Optical Engineering,* Vol. 1612, 1992, pp. 36-48.

[13] Modi, V.J., and Suleman, A., "A Dynamical Study of the Proposed Space Station Type Configuration," *Acta Astronautica,* Vol. 19, No. 5, 1989, pp. 377-391.

[14] Kimura, S., Miyazaki, K., and Suzuki, Y., "Application of a Decentralized Autonomous Control Mechanism for Space Robotics," *19th International Symposium on Space Technology and Science,* Yokohama, Japan, May 1994, Paper ISTS 94-c-02.

[15] Hirzinger, G., Landzettel, K., and Fagerer, C., "Telerobotics with Large Time Delays - the ROTEX Experience," *Proceedings of the IEEE/RSJ/GI International Conference on Intelligent Robots and System,* Munich, Germany, 1994,

Published by the IEEE, Piscataway, U.S.A., Vol. 1, pp. 571-578.

[16] Meirovitch, L., and Kwak, M.K., "On the Maneuvering and Control of Space Structures," *Proceedings of the First International Conference on the Dynamics of Flexible Structures in Space,* Cranfield, U.K., May 1990, Editors: C.L. Kirk, and J.L. Junkins, pp. 3-17.

[17] Roberson, R.E., "Two Decades of Spacecraft Attitude Control," *Journal of Guidance and Control,* Vol. 2, No. 1, 1979, pp. 3-8.

[18] Likins, P.W., "Spacecraft Attitude Dynamics and Control - A Personal Perspective on Early Developments," *Journal of Guidance, Control, and Dynamics,* Vol. 9, No. 2, 1986, pp. 129-134.

[19] Modi, V.J., "Attitude Dynamics of Satellites with Flexible Appendages - A Brief Review," *Journal of Spacecraft and Rockets,* Vol. 11, No. 11, 1974, pp. 743-751.

[20] Modi, V.J., and Shrivastava, S.K., "Satellite Attitude Dynamics and Control in the Presence of Environmental Torques - A Brief Survey," *Journal of Guidance, Control, and Dynamics,* Vol. 6, No. 6, 1983, pp. 461-471.

[21] Nagata, T., Modi, V.J., and Matsuo, H., "An Approach to Dynamics and Control of Flexible Systems," *A Collection of Technical Papers, AIAA/AAS Astrodynamics Conference,* Scottsdale, Arizona, U.S.A, August 1994, Paper No. AIAA-94-3756CP, pp. 366-375.

[22] Dubowski, S., and Papadopoulos, E., "The Kinematics, Dynamics, and Control of Free-Flying and Free-Floating Space Robotic Systems," *IEEE Transactions on Robotics and Automation,* Vol. 9, No. 5, 1993, pp. 531-543.

[23] Schebor, F.S. and Turney, J.L., "Realistic and Consistent Telerobotic Simulation," *Proceedings of the IEEE International Conference on Systems, Man, and Cybernetics,* Charlottesville, Virginia, U.S.A., 1991, Vol. 2, pp. 889-894.

[24] Bhatia, I.L., "Modeling of a Nonlinear Space Robotic System for Precision and Control," *Proceedings of the SPIE - The International Society for Optical Engineering,* Vol. 1612, 1992, pp. 98-114.

[25] Bodley, C.S., Devers, A.D., Park, A.C., and Frisch, H.P., "A Digital Computer Program for the Dynamics Interaction Simulation of Controls and Structure (DISCOS)," Vol. I and II, NASA Technical Paper 1219, 1978.

[26] Singh, R.P., Vandervoort, R.J., and Likins, P.W., "Dynamics of Flexible Bodies in Tree-Topology - A Computer Oriented Approach," *AIAA/ASME/ASCE 25th Structures, Structural Dynamics, and Materials Conference,* Palm Springs, California, U.S.A., 1984, Paper No. AIAA-84-1024.

[27] Pascal, M., "Dynamical Analysis of a Flexible Manipulator Arm," *Acta Astronautica,* Vol. 21, No. 3, 1990, pp. 161-169.

[28] Chan, J.K.W., *Dynamics and Control of an Orbiting Space Platform Based Mobile Flexible Manipulator,* M.A.Sc. Thesis, The University of British Columbia, Vancouver, Canada, 1990.

[29] Mah, H., *On the Nonlinear Dynamics of a Space Platform Based Mobile Flexible Manipulator,* Ph.D. Thesis, The University of British Columbia, Vancouver,

Canada, 1992.

[30] Lilly, K.W., and Bonaventura, C.S., "Generalized Formulation for Simulation of Space Robot Constrained Motion," *Proceedings of the IEEE International Conference on Robotics and Automation,* Nagoya, Japan, 1995, Vol. 3, pp. 2835-2840.

[31] Papadopoulos, E.G., "Large Payload Manipulation for Space Robots," *Proceedings of the IEEE/RSJ International Conference on Intelligent Robots and Systems,* Yokohama, Japan, 1993, Published by the IEEE, Piscataway, U.S.A., pp. 2087-2094.

[32] Xavier, C., Jaar, G.J., and Misra, A.K., "Effect of Payload Impact on the Dynamics of a Space Robot," *Proceedings of the 1993 IEEE/RSG International Conference on Intelligent Robots and Systems,* Yokohama, Japan, 1993, Published by the IEEE, Piscataway, U.S.A., pp. 2070-2075.

[33] Yoshida, K., and Sashida, N., "Modeling of Impact Dynamics and Impulse Minimization for Space Robots," *Proceedings of the 1993 IEEE/RSG International Conference on Intelligent Robots and Systems,* Yokohama, Japan, 1993, Published by the IEEE, Piscataway, U.S.A., pp. 2064-2069.

[34] Yoshikawa, S., and Yamada, K., "Impact Estimation of a Space Robot at Capturing a Target," *Proceedings of the IEEE/RSG/GI International Conference on Intelligent Robots and Systems,* Munich, Germany, 1994, Published by the IEEE, Piscataway, U.S.A., Vol. 3, pp. 1570-1577.

[35] Cherchas, D.B., "Dynamics of Spin-Stabilized Satellites During Extension of Long Flexible Booms," *Journal of Spacecraft and Rockets*, Vol. 8, No. 7, 1971, pp. 802-804.

[36] Sellappan, R., and Bainum, P.M., "Dynamics of Spin-Stabilized Spacecraft During Deployment of Telescopic Appendages," *Journal of Spacecraft and Rockets*, Vol. 13, No. 10, pp. 605-610.

[37] Modi, V.J., and Ibrahim, A.M., "Dynamics of the Orbiter-Based WISP Experiment," *Acta Astronautica*, Vol. 26, No. 11, 1992, pp. 749-761.

[38] Marom, I., *A Study of the Flexible Space Platform Based Mobile Deployable Manipulator,* Ph.D. Thesis, The University of British Columbia, Vancouver, Canada, 1993.

[39] Hokamoto, S., Modi, V.J., and A.K. Misra, "Dynamics and Control of Mobile Flexible Manipulators with Slewing and Deployable Links," *Astrodynamics 1995, Advances in the Astronautical Sciences,* Vol. 90, Editors: K.T. Alfriend *et al.*, 1996, Paper No. AAS-95-322, pp. 339-357.

[40] Banerjee, A.K., and Kane, T.R., "Extrusion of a Beam from a Rotating Base," *Journal of Guidance, Control, and Dynamics*, Vol. 12, No. 2, 1989, pp. 140-146.

[41] Fu, K.S., Gonzalez, R.C., and Lee, C.S.G., *Robotics: Control, Sensing, Vision, and Intelligence,* McGraw-Hill Publishing Company, New York, 1987, pp. 82-84, 103-124 .

[42] Hollerbach, J.M., "A Recursive Lagrangian Formulation of Manipulator Dynamics and a Comparative Study of Dynamics Formulation Complexity," *IEEE*

Transactions on Systems, Man, and Cybernetics, Vol. 10, No. 11, 1980, pp. 730-736.

[43] Keat, J.E., "Multibody System Order n Dynamics Formulation Based on Velocity Transform Method," *Journal of Guidance, Control, and Dynamics*, Vol. 13, No. 2, 1990, pp. 207-212.

[44] Rosenthal, D.E., "An Order n Formulation for Robotic Systems," *The Journal of the Astronautical Sciences*, Vol. 38, No. 4, 1990, pp. 511-529.

[45] Suzuki, S., and Kojima, H., "Application of Order-n Formulation to Panel Deployment Problem of a Spacecraft," *Journal of Guidance, Control, and Dynamics*, Vol. 17, No. 3, 1994, pp. 634-636.

[46] Banerjee, A.K., "Order-n Formulation of Extrusion of a Beam with Large Bending and Rotation," *Journal of Guidance, Control, and Dynamics*, Vol. 15, No. 1, 1992, pp. 121-127.

[47] Jain, A., and Rodriguez, G., "Recursive Flexible Multibody System Dynamics Using Spatial Operators," *Journal of Guidance, Control, and Dynamics*, Vol. 15, No. 6, 1992, pp. 1453-1466.

[48] Bae, D.S., and Haug, E.J., "A Recursive Formulation for Constrained Mechanical System Dynamics: Part I. Open Loop Systems," *Mechanics of Structures and Machines,* Vol. 15, No. 3, 1987, pp. 359-382.

[49] Kurdila, A.J., Menon, R.G., and Sunkel, J.W., "Nonrecursive Order N Formulation of Multibody Dynamics," *Journal of Guidance, Control, and Dynamics*, Vol. 16, No. 5, 1993, pp. 838-844.

[50] Pradhan, S., Modi, V.J., and Misra, A.K., "Order N Formulation for Flexible Multibody Systems in Tree Topology - The Lagrangian Approach," *A Collection of Technical Papers, AIAA/AAS Astrodynamics Specialist Conference*, San Diego, California, U.S.A., July 1996, Paper No. 96-3624, pp. 480-490.

[51] Fijany, A., Sharf, I., and D'Eleuterio, G.M.T., "Parallel $O(\log N)$ Algorithms for the Computation of Manipulator Forward Dynamics," *Proceedings of the IEEE Conference on Robotics and Automation,* San Diego, California, U.S.A., May 1994, Vol. 2, pp. 1547-1553.

[52] Bainum, P.M., and Diarra, C.M., "The Dynamics and Control of the Orbiting Spacecraft Control Laboratory Experiment (SCOLE) During Station Keeping," *AIAA/AAS Astrodynamics Conference*, Minneapolis, Minnesota, August 1988, Paper No. 88-4252.

[53] Hirzinger, G., Brunner, B., Dietrich, J., and Heindl, J., "Sensor-Based Space Robotics - ROTEX and its Telerobotic Features," *IEEE Transactions on Robotics and Automation,* Vol. 9, No. 5, 1993, pp. 649-661.

[54] Martin, E., Papadopoulos, E., and Angeles, J., "On the Interaction of Flexible Modes and On-Off Thrusters in Space Robotic Systems", *Proceedings of the 1995 IEEE/RSG International Conference on Intelligent Robots and Systems,* Pittsburgh, Pennsylvania, U.S.A., 1995, Published by the IEEE, Piscataway, U.S.A., Vol. 2, pp. 65-70.

[55] Krishnan, S., and Vadali, S.R., "An Inverse-Free Technique for Attitude Con-

trol of Spacecraft using CMGS," *AAS/AAIA Spaceflight Mechanics Meeting,* Albuquerque, New Mexico, U.S.A., February 1995, Paper No. AAS-95-139.

[56] Parlaktuna, O., Cook, G.E., Strauss, A.M., and Fernandez, K.R., "Fine Attitude Control of Space Vehicles using Space Manipulators," *International Journal of Robotics and Automation,* Vol. 9, No. 1, 1994, pp. 29-35.

[57] De Luca, A., "Dynamic Control of Robots with Joint Elasticity," *Proceedings of the IEEE International Conference on Robotics and Automation,* Philadelphia, U.S.A., 1988, Vol. 1, pp. 152-158.

[58] Bayo, E., "Computed Torque for the Position Control of Open-Chain Flexible Robots," *Proceedings of the IEEE International Conference on Robotics and Automation,* Philadelphia, U.S.A., 1988, Vol. 1, pp. 316-321.

[59] Gebler, B., "Feed-Forward Control Strategy for an Industrial Robot with Elastic Links and Joints," *Proceedings of the IEEE International Conference on Robotics and Automation,* Raleigh, U.S.A., 1987, pp. 923-928.

[60] de Silva, C.W., "Trajectory Design for Robotic Manipulators in Space Applications," *Journal of Guidance, Control, and Dynamics,* Vol. 14, No. 3, 1991, pp. 670-674.

[61] Quinn, R.D., Chen, J.L., and Lawrence, C., "Base Reaction Control for Space-Based Robots Operating in Microgravity Environment," *Journal of Guidance, Control, and Dynamics,* Vol. 17, No. 2, 1994, pp. 263-270.

[62] Hanson, M.L., and Tolson, R.H., "Reducing Flexible Base Vibrations through Local Redundancy Resolution," *Journal of Robotic Systems,* Vol. 12, No. 11, 1995, pp. 767-779.

[63] Bailey, T., and Hubbard, J.E.Jr, "Distributed Piezoelectric-polymer Active Vibration Control of a Cantiliver Beam," *Journal of Guidance, Control, and Dynamics,* Vol. 8, No. 5, 1985, pp. 605-611.

[64] Wang, D., "Comparison of Optimal and Nonoptimal Control Strategies for the Single Flexible Link," *International Journal of Robotics and Automation,* Vol. 9, No. 3, 1994, pp. 130-136.

[65] Craig, J.J., *Introduction to Robotics: Mechanics and Control, 2nd ed.,* Addison-Wesley Publishing Company, Reading, Massachusetts, 1989, pp. 332-359.

[66] Modi, V.J., Karray, F., and Chan J.K., "On the Control of a Class of Flexible Manipulators Using Feedback Linearization Approach," *42nd Congress of the International Astronautical Federation,* Montreal, Canada, October 1991, Paper No. IAF-91-324; also *Acta Astronautica,* Vol. 29, No. 1, 1993, pp. 17-27.

[67] Ericsson, A.J., Bainum, P.M., and Quangqian, X., "The Optimal LQR Digital Control of a Free-Free Orbiting Platform, *41st International Astronautical Congress,* October 1990, Dresden, Germany.

[68] Xu, J., Bainum, P.M., and Li, F., "Vibration Control of a Manipulator Tip on a Flexible Body," *Proceedings of the Eighth VPI & SU Symposium on Dynamics and Control of Large Structures,* May 1991, Blacksburg, Virginia, U.S.A., Editor: L. Meirovitch, pp. 703-714.

[69] Guangqian, X., and Bainum, P.M., "Optimal LQG Digital Control of Orbiting

Large Flexible Beams," *The Journal of the Astronautical Sciences*, Vol. 37, No. 1, 1989, pp. 59-78.

[70] Blelloch, P.A., and Mingori, D.L., "Robust Linear Quadratic Gaussian Control for Flexible Structures," *Journal of Guidance, Control, and Dynamics*, Vol. 13, No. 1, 1990, pp. 66-72.

[71] Meirovitch, L., *Elements of Vibration Analysis, 2nd Ed.,* McGraw-Hill Book Company, New York, U.S.A., 1986, pp. 255-256, 282-290.

[72] Meirovitch, L., and Kwak, M.K., "Convergence of the Classical Rayleigh-Ritz Method and the Finite Element Method," *AIAA Journal*, Vol. 28, No. 8, 1990, pp. 1509-1516.

[73] Meirovitch, L., and Kwak, M.K., "Rayleigh-Ritz Based Substructure Synthesis for Flexible Multibody System," *AIAA Journal*, Vol. 29, No. 10, 1991, pp. 1709-1719.

[74] Meirovitch, L., and Kwak, M.K., "Inclusion Principle for the Rayleigh-Ritz Based Substructure Synthesis," *AIAA Journal*, Vol. 30, No. 5, 1992, pp. 1344-1351.

[75] *IMSL Library Reference Manual,* Vol. 1, IMSL Inc., Houston, Texas, U.S.A., 1980, pp. DGEAR 1 - DGEAR 9.

[76] Bryson, Jr, A.E., and Ho, Y.C., *Applied Optimal Control: Optimization, Estimation, and Control,* Hemisphere Publishing Corporation, Washington, D.C., U.S.A., 1975.

APPENDIX I: MODE SHAPES OF EULER-BERNOULLI BEAMS

In the thesis, the platform supporting the manipulator is assumed to behave as a free-free beam. The jth mode shape for the platform (first body) is then written as

$$\begin{aligned}\phi_{1j}(x_1) =& \cos\lambda_{1j}\left(\frac{1}{2}+\frac{x_1}{l_1}\right)+\cosh\lambda_{1j}\left(\frac{1}{2}+\frac{x_1}{l_1}\right)\\ &-\frac{\cosh\lambda_{1j}-\cos\lambda_{1j}}{\sinh\lambda_{1j}-\sin\lambda_{1j}}\left\{\sin\lambda_{1j}\left(\frac{1}{2}+\frac{x_1}{l_1}\right)+\sinh\lambda_{1j}\left(\frac{1}{2}+\frac{x_1}{l_1}\right)\right\},\end{aligned} \tag{I.1}$$

where the spatial frequency λ_{1j} can be obtained from the following transcendental equation,

$$\cos\lambda_{1j}\cosh\lambda_{1j} = 1. \tag{I.2}$$

The first four eigenvalues for a free-free beam are given below:

$$\begin{aligned}\lambda_{11} &= 4.73;\\ \lambda_{12} &= 7.85;\\ \lambda_{13} &= 11.00;\\ \lambda_{14} &= 14.14.\end{aligned}$$

The units of the manipulator (bodies 2 to N) are modeled as cantilever Euler-Bernoulli beams with tip masses. The jth mode shape for the ith body is then written as

$$\begin{aligned}\phi_{ij}(x_i, l_i) =& \sin\lambda_{ij}\left(\frac{x_i}{l_i}\right)-\sinh\lambda_{ij}\left(\frac{x_i}{l_i}\right)\\ &-\frac{\sin\lambda_{ij}+\sinh\lambda_{ij}}{\cos\lambda_{ij}+\cosh\lambda_{ij}}\left\{\cos\lambda_{ij}\left(\frac{x_i}{l_i}\right)-\cosh\lambda_{ij}\left(\frac{x_i}{l_i}\right)\right\},\end{aligned} \tag{I.3}$$

for $i = 2, ..., N$, where the spatial frequency λ_{ij} can be obtained from the transcendental equation

$$\cos\lambda_{ij}\cosh\lambda_{ij} + 1 = \frac{m_{ti}}{\rho_i}\lambda_{ij}\{\sin\lambda_{ij}\cosh\lambda_{ij} - \cos\lambda_{ij}\sinh\lambda_{ij}\}, \tag{I.4}$$

where ρ_i is the linear mass density of the beam and m_{ti} is the tip mass.

The first four eigenvalues found from Eq. (I.4) are given below for a payload ratio (m_{ti}/ρ_i) ranging from 0 to 5. The associated mode shapes are also plotted in Figure I-1.

Payload ratio = 0	Payload ratio = 2	Payload ratio = 4
$\lambda_{i1} = 1.88$	$\lambda_{i1} = 1.08$	$\lambda_{i1} = 0.92$
$\lambda_{i2} = 4.69$	$\lambda_{i2} = 3.98$	$\lambda_{i2} = 3.96$
$\lambda_{i3} = 7.85$	$\lambda_{i3} = 7.10$	$\lambda_{i3} = 7.09$
$\lambda_{i4} = 11.00$	$\lambda_{i4} = 10.23$	$\lambda_{i4} = 10.22$

Payload ratio = 1	Payload ratio = 3	Payload ratio = 5
$\lambda_{i1} = 1.25$	$\lambda_{i1} = 0.98$	$\lambda_{i1} = 0.87$
$\lambda_{i2} = 4.03$	$\lambda_{i2} = 3.96$	$\lambda_{i2} = 3.95$
$\lambda_{i3} = 7.13$	$\lambda_{i3} = 7.09$	$\lambda_{i3} = 7.08$
$\lambda_{i4} = 10.26$	$\lambda_{i4} = 10.23$	$\lambda_{i4} = 10.22$

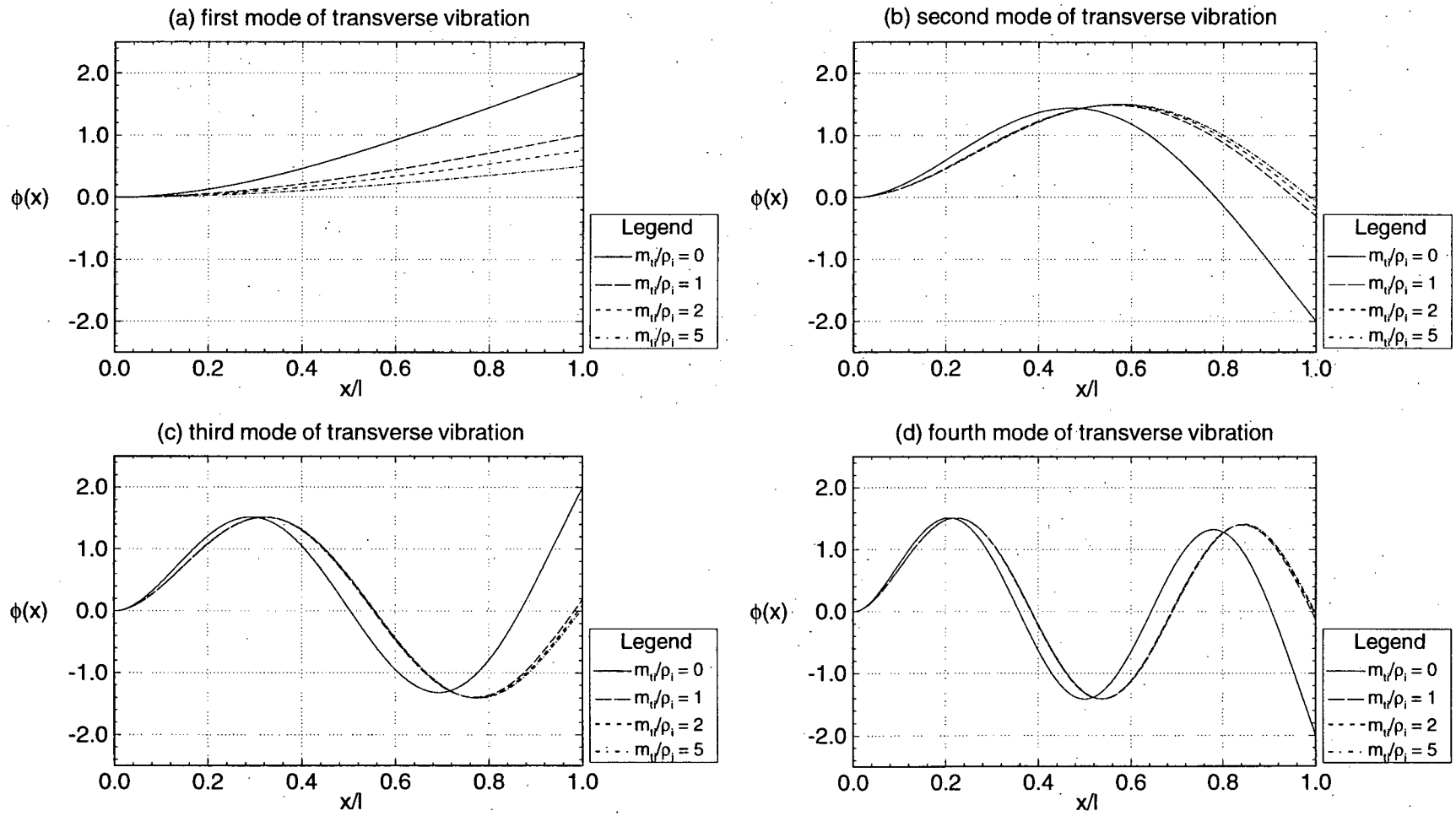

Figure I-1 Effect of tip mass on the eigenfunctions of a cantilever beam: (a) first mode; (b) second mode; (c) third mode; (d) fourth mode.

APPENDIX II: DECOUPLED MASS MATRIX

The decoupled mass matrix of the system was derived in Section 2.3. It can be expressed as

$$\tilde{\mathbf{M}} = \begin{bmatrix} \tilde{\mathbf{M}}_1 & 0 & 0 & \cdots & 0 \\ 0 & \tilde{\mathbf{M}}_2 & 0 & \cdots & 0 \\ 0 & 0 & \tilde{\mathbf{M}}_3 & \cdots & 0 \\ \vdots & \vdots & \vdots & \ddots & \vdots \\ 0 & 0 & 0 & \cdots & \tilde{\mathbf{M}}_N \end{bmatrix}. \tag{II.1}$$

Here, $\tilde{\mathbf{M}}_1$ represents the mass matrix of the platform while $\tilde{\mathbf{M}}_i$, $i = 2, ..., N$, corresponds to the mass matrix of the individual (i^{th} - 1) unit. Therefore,

$$\tilde{\mathbf{M}}_1 = \begin{bmatrix} \int_{m_1} \nu_0^T \nu_0 dm_1 & \int_{m_1} \nu_0^T \nu_1 dm_1 & \int_{m_1} \nu_0^T \nu_2 dm_1 \\ \int_{m_1} \nu_1^T \nu_0 dm_1 & \int_{m_1} \nu_1^T \nu_1 dm_1 & \int_{m_1} \nu_1^T \nu_2 dm_1 \\ \int_{m_1} \nu_2^T \nu_0 dm_1 & \int_{m_1} \nu_2^T \nu_1 dm_i & \int_{m_1} \nu_2^T \nu_2 dm_1 \end{bmatrix}, \tag{II.2}$$

where:

$$\int_{m_1} \nu_0^T \nu_0 dm_1 = \begin{bmatrix} 1 & 0 \\ 0 & r_o^2 \end{bmatrix} m_1;$$

$$\int_{m_1} \nu_0^T \nu_1 dm_1 = \mathbf{\Theta^T P T_1} \{\int_{m_1} \vec{r}_1 dm_1\} + \mathbf{\Theta^T P T_1} \{\int_{m_1} \mathbf{\Phi}_1 dm_1\} \delta_1;$$

$$\int_{m_1} \nu_0^T \nu_2 dm_1 = \mathbf{\Theta^T T_1} \{\int_{m_1} \mathbf{\Phi}_1 dm_1\};$$

$$\int_{m_1} \nu_1^T \nu_1 dm_1 = \{\int_{m_1} \vec{r}_1^T \vec{r}_1 dm_1\} + 2\{\int_{m_1} \vec{r}_1^T \mathbf{\Phi}_1 dm_1\} \delta_1 + \delta_1^T \{\int_{m_1} \mathbf{\Phi}_1^T \mathbf{\Phi}_1 dm_1\} \delta_1;$$

$$\int_{m_1} \nu_1^T \nu_2 dm_1 = \{\int_{m_1} \vec{r}_1^T \mathbf{P}^T \mathbf{\Phi}_1 dm_1\} + \delta_1^T \{\int_{m_1} \mathbf{\Phi}_1^T \mathbf{P}^T \mathbf{\Phi}_1 dm_1\};$$

$$\int_{m_1} \nu_2^T \nu_2 dm_1 = \{\int_{m_1} \mathbf{\Phi}_1^T \mathbf{\Phi}_1 dm_1\};$$

and

$$\mathbf{\Theta} = \begin{bmatrix} \cos\theta & -r_o \sin\theta \\ \sin\theta & r_o \cos\theta \end{bmatrix}; \qquad \mathbf{P} = \begin{bmatrix} 0 & -1 \\ 1 & 0 \end{bmatrix}.$$

Furthermore, for $i = 2, ..., N$,

$$\tilde{\mathbf{M}}_i = \begin{bmatrix} \mathbf{I^2}(m_i + m_{ai}) & \mathbf{0} & \int_{m_i} \nu_1 dm_i & \int_{m_i} \nu_2 dm_i & \int_{m_i} \nu_3 dm_i \\ \mathbf{0} & J_{ai} & 0 & \mathbf{0} & 0 \\ \int_{m_i} \nu_1^T dm_i & \mathbf{0} & \int_{m_i} \nu_1^T \nu_1 dm_i & \int_{m_i} \nu_1^T \nu_2 dm_i & \int_{m_i} \nu_1^T \nu_3 dm_i \\ \int_{m_i} \nu_2^T dm_i & \mathbf{0} & \int_{m_i} \nu_2^T \nu_1 dm_i & \int_{m_i} \nu_2^T \nu_2 dm_i & \int_{m_i} \nu_2^T \nu_3 dm_i \\ \int_{m_i} \nu_3^T dm_i & \mathbf{0} & \int_{m_i} \nu_3^T \nu_1 dm_i & \int_{m_i} \nu_3^T \nu_2 dm_i & \int_{m_i} \nu_3^T \nu_3 dm_i \end{bmatrix}, \quad \text{(II.3)}$$

where:

$$\int_{m_i} \nu_1 dm_i = \mathbf{PT_i}\{\int_{m_i} \vec{r}_i dm_i\} + \mathbf{PT_i}\{\int_{m_i} \mathbf{\Phi}_i dm_i\}\delta_i;$$

$$\int_{m_i} \nu_2 dm_i = \mathbf{T_i}\{\int_{m_i} \mathbf{\Phi}_i dm_i\};$$

$$\int_{m_i} \nu_3 dm_i = \mathbf{T_i}\{\int_{m_i} \vec{r}_i{}' dm_i\} + \mathbf{T_i}\{\int_{m_i} \mathbf{\Phi d}_i dm_i\}\delta_i;$$

$$\int_{m_i} \nu_1^T \nu_1 dm_i = \{\int_{m_i} \vec{r}_i^T \vec{r}_i dm_i\} + 2\{\int_{m_i} \vec{r}_i^T \mathbf{\Phi}_i dm_i\}\delta_i + \delta_i^T\{\int_{m_i} \mathbf{\Phi}_i^T \mathbf{\Phi}_i dm_i\}\delta_i;$$

$$\int_{m_i} \nu_1^T \nu_2 dm_i = \{\int_{m_i} \vec{r}_i^T \mathbf{P}^T \mathbf{\Phi}_i dm_i\} + \delta_i^T\{\int_{m_i} \mathbf{\Phi}_i^T \mathbf{P}^T \mathbf{\Phi}_i dm_i\};$$

$$\int_{m_i} \nu_1^T \nu_3 dm_i = \{\int_{m_i} \vec{r}_i^T \mathbf{P}^T \vec{r}_i{}' dm_i\} + \{\int_{m_i} \vec{r}_i^T \mathbf{P}^T \mathbf{\Phi d}_i dm_i\}\delta_i$$
$$+\delta_i^T\{\int_{m_i} \mathbf{\Phi}_i^T \mathbf{P}^T \vec{r}_i{}' dm_i\} + \delta_i^T\{\int_{m_i} \mathbf{\Phi}_i^T \mathbf{P}^T \mathbf{\Phi d}_i dm_i\}\delta_i;$$

$$\int_{m_i} \nu_2^T \nu_2 dm_i = \{\int_{m_i} \mathbf{\Phi}_i^T \mathbf{\Phi}_i dm_i\};$$

$$\int_{m_i} \nu_2^T \nu_3 dm_i = \{\int_{m_i} \mathbf{\Phi}_i^T \vec{r}_i{}' dm_i\} + \{\int_{m_i} \mathbf{\Phi}_i^T \mathbf{\Phi d}_i dm_i\}\delta_i;$$

$$\int_{m_i} \nu_3^T \nu_3 dm_i = m_{id} + 2\{\int_{m_i} \vec{r}_i{}'^T \mathbf{\Phi d}_i dm_i\}\delta_i + \delta_i^T\{\int_{m_i} \mathbf{\Phi d}_i^T \mathbf{\Phi d}_i dm_i\}\delta_i;$$

and

$$\vec{r}_i{}' = \frac{\partial \vec{r}_i}{\partial x_i}; \qquad \mathbf{\Phi d}_i = \left\{\frac{\partial \mathbf{\Phi}_i}{\partial x_i} + \frac{\partial \mathbf{\Phi}_i}{\partial l_i}\right\}.$$

APPENDIX III: VELOCITY TRANSFORMATION MATRICES

The order N algorithm used in the thesis relies on two velocity transforms which factorize the mass matrix. The details of the transformation matrices involved are given here. It is useful to recall a few definitions:

$$\bar{\Phi}_{i-1} = \Phi_{i-1}(x_{i-1}, l_{i-1})|_{x_{i-1}=d_{ix}+l_{i-1}}; \tag{III.1}$$

$$\bar{\Phi}'_i = \left.\frac{\partial \Phi_{iy}}{\partial x_i}\right|_{x_i=d_{ix}+l_{i-1}}; \tag{III.2}$$

$$\xi_{i,d} = \frac{\partial \xi_i}{\partial d_{ix}}, \quad \xi_{i,l} = \frac{\partial \xi_i}{\partial l_{i-1}}; \tag{III.3}$$

$$e_{i,d} = [0 \;\; 1]\frac{\partial \vec{e}_i}{\partial d_{ix}}, \quad e_{i,l} = [0 \;\; 1]\frac{\partial \vec{e}_i}{\partial l_{i-1}}; \tag{III.4}$$

and

$$\mathbf{P} = \begin{bmatrix} 0 & -1 \\ 1 & 0 \end{bmatrix}, \quad \mathbf{S} = \begin{bmatrix} 1 & 0 \\ e_{i,d} & 1 \end{bmatrix}, \quad \mathbf{\Theta} = \begin{bmatrix} \cos\theta & -r_o\sin\theta \\ \sin\theta & r_o\cos\theta \end{bmatrix}. \tag{III.5}$$

The two velocity transformations were derived in Section 2.4.2. It should be noted that, for clarity, the detailled matrices are given for the case where the longitudinal deformations are negligible. The first velocity transform can be expressed as

$$\dot{\tilde{\mathbf{q}}} = [\mathbf{I}^{n_s} - \mathbf{R}^{\mathbf{C}}]^{-1}\mathbf{R}\dot{\mathbf{q}}, \tag{III.6}$$

where

$$\mathbf{R} = \begin{bmatrix} \mathbf{R}_1 & 0 & 0 & \cdots & 0 \\ 0 & \mathbf{R}_2 & 0 & \cdots & 0 \\ 0 & 0 & \mathbf{R}_3 & \cdots & 0 \\ \vdots & \vdots & \vdots & \ddots & \vdots \\ 0 & 0 & 0 & \cdots & \mathbf{R}_N \end{bmatrix} \in \Re^{n_s \times n_s}; \tag{III.7}$$

and

$$\mathbf{R^C} = \begin{bmatrix} 0 & 0 & 0 & 0 & \cdots & 0 \\ \mathbf{R_1^C} & 0 & 0 & 0 & \cdots & 0 \\ 0 & \mathbf{R_2^C} & 0 & 0 & \cdots & 0 \\ 0 & 0 & \mathbf{R_3^C} & 0 & \cdots & 0 \\ \vdots & \vdots & \vdots & \vdots & \ddots & \vdots \\ 0 & 0 & 0 & 0 & \cdots & 0 \end{bmatrix} \in \Re^{n_s \times n_s}. \tag{III.8}$$

Here:

$$\mathbf{R}_1 = \mathbf{I}^{n_p}; \tag{III.9}$$

$$\mathbf{R}_i = \begin{bmatrix} \mathbf{T_{i-1}S} & 0 & 0 & 0 & 0 \\ \xi_{i,d}[1 \quad 0] & 1 & 0 & 0 & 0 \\ 0 & 0 & 1 & 0 & 0 \\ 0 & 0 & 0 & \mathbf{I}^s & 0 \\ 0 & 0 & 0 & 0 & 1 \end{bmatrix} \in \Re^{n_u \times n_u}, \quad i = 2, ..., N; \tag{III.10}$$

$$\mathbf{R_1^C} = \begin{bmatrix} \mathbf{\Theta} & \mathbf{P}\vec{g}_2 & \mathbf{T_1}\bar{\bar{\mathbf{\Phi}}}_1 \\ 0 & 1 & \bar{\bar{\mathbf{\Phi}}}_1{}' \\ 0 & 0 & 0 \\ 0 & 0 & 0 \\ 0 & 0 & 0 \end{bmatrix} \in \Re^{n_u \times n_p}; \tag{III.11}$$

$$\mathbf{R_i^C} = \begin{bmatrix} \mathbf{I}^2 & 0 & \mathbf{P}\vec{g}_{i+1} & \mathbf{T_i}\bar{\bar{\mathbf{\Phi}}}_i & \mathbf{T_i}\begin{bmatrix} 1 \\ e_{i+1,l} \end{bmatrix} \\ 0 & 0 & 1 & \bar{\bar{\mathbf{\Phi}}}_i' & \xi_{i+1,l} \\ 0 & 0 & 0 & 0 & 0 \\ 0 & 0 & 0 & 0 & 0 \\ 0 & 0 & 0 & 0 & 0 \end{bmatrix} \in \Re^{n_u \times n_u}, \quad i = 2, ..., N. \tag{III.12}$$

The second velocity transform is defined as

$$\dot{\bar{\mathbf{q}}} = \mathbf{R}^{\mathbf{V}}\dot{\mathbf{q}}, \tag{III.13}$$

where:

$$\mathbf{R}^{\mathbf{V}} = \begin{bmatrix} \bar{\mathbf{R}}_1 & 0 & 0 & \cdots & 0 \\ \mathbf{R}_1^{\mathbf{A}} & \bar{\mathbf{R}}_2 & 0 & \cdots & 0 \\ \mathbf{R}_1^{\mathbf{B}} & \mathbf{R}_2^{\mathbf{A}} & \bar{\mathbf{R}}_3 & \cdots & 0 \\ \vdots & \vdots & \vdots & \ddots & \vdots \\ \mathbf{R}_1^{\mathbf{B}} & \mathbf{R}_2^{\mathbf{B}} & \mathbf{R}_3^{\mathbf{B}} & \cdots & \bar{\mathbf{R}}_N \end{bmatrix} \in \Re^{n_s \times n_s}; \tag{III.14}$$

$$\bar{\mathbf{R}}_1 = \mathbf{I}^{np}; \tag{III.15}$$

$$\mathbf{R}_1^{\mathbf{A}} = \begin{bmatrix} \mathbf{\Theta} & \mathbf{P}\vec{g}_2 & \mathbf{T_1}\bar{\mathbf{\Phi}}_1 \\ 0 & 1 & \bar{\mathbf{\Phi}}_1' \\ 0 & 0 & 0 \\ 0 & 0 & 0 \\ 0 & 0 & 0 \end{bmatrix} \in \Re^{nu \times np}; \tag{III.16}$$

$$\mathbf{R}_1^{\mathbf{B}} = \begin{bmatrix} \mathbf{\Theta} & \mathbf{P}\vec{g}_2 & \mathbf{T_1}\bar{\mathbf{\Phi}}_1 \\ 0 & 0 & 0 \\ 0 & 0 & 0 \\ 0 & 0 & 0 \\ 0 & 0 & 0 \end{bmatrix} \in \Re^{nu \times np}; \tag{III.17}$$

and for $i = 2, ..., N$,

$$\bar{\mathbf{R}}_i = \begin{bmatrix} \mathbf{T_{i-1}S} & 0 & 0 & 0 & 0 \\ \xi_{i,d}[1 \quad 0] & 1 & 0 & 0 & 0 \\ 0 & 0 & 1 & 0 & 0 \\ 0 & 0 & 0 & \mathbf{I}^s & 0 \\ 0 & 0 & 0 & 0 & 1 \end{bmatrix} \in \Re^{nu \times nu}; \tag{III.18}$$

$$\mathbf{R}_i^{\mathbf{A}} = \begin{bmatrix} \mathbf{T_{i-1}S} & 0 & \mathbf{P}\vec{g}_{i+1} & \mathbf{T_i}\bar{\mathbf{\Phi}}_i & \mathbf{T_i}\begin{bmatrix} 1 \\ e_{i+1,l} \end{bmatrix} \\ 0 & 0 & 1 & \bar{\mathbf{\Phi}}_i' & \xi_{i+1,l} \\ 0 & 0 & 0 & 0 & 0 \\ 0 & 0 & 0 & 0 & 0 \\ 0 & 0 & 0 & 0 & 0 \end{bmatrix} \in \Re^{nu \times nu}; \tag{III.19}$$

$$\mathbf{R}_i^{\mathbf{B}} = \begin{bmatrix} \mathbf{T_{i-1}S} & 0 & \mathbf{P}\vec{g}_{i+1} & \mathbf{T_i}\bar{\mathbf{\Phi}}_i & \mathbf{T_i}\begin{bmatrix} 1 \\ e_{i+1,l} \end{bmatrix} \\ 0 & 0 & 0 & 0 & 0 \\ 0 & 0 & 0 & 0 & 0 \\ 0 & 0 & 0 & 0 & 0 \\ 0 & 0 & 0 & 0 & 0 \end{bmatrix} \in \Re^{n_u \times n_u}. \tag{III.20}$$

APPENDIX IV: DERIVATIVES OF THE MASS MATRIX

Over the course of the derivation of the equations of motion, it becomes necessary to take the derivative of the coupled mass matrix. The differentiation procedure is now briefly outlined.

When the coupled mass matrix $\mathbf{M}$ is required, the velocity transformation

$$\dot{\tilde{\mathbf{q}}} = \mathbf{R}^{\mathbf{V}}\dot{\mathbf{q}} \tag{IV.1}$$

can be used to obtain

$$\mathbf{M} = \mathbf{R}^{\mathbf{V}^{\mathbf{T}}}\tilde{\mathbf{M}}\mathbf{R}^{\mathbf{V}}. \tag{IV.2}$$

Hence,

$$\dot{\mathbf{M}} = \dot{\mathbf{R}}^{\mathbf{V}^{\mathbf{T}}}\tilde{\mathbf{M}}\mathbf{R}^{\mathbf{V}} + \mathbf{R}^{\mathbf{V}^{\mathbf{T}}}\dot{\tilde{\mathbf{M}}}\mathbf{R}^{\mathbf{V}} + \mathbf{R}^{\mathbf{V}^{\mathbf{T}}}\tilde{\mathbf{M}}\dot{\mathbf{R}}^{\mathbf{V}}, \tag{IV.3}$$

where a dot over a matrix signifies that the time derivative of each component in the matrix must be taken. Furthermore,

$$\frac{\partial\{\dot{\mathbf{q}}^{\mathbf{T}}\mathbf{M}\dot{\mathbf{q}}\}}{\partial\mathbf{q}} = \frac{\partial\{\dot{\mathbf{q}}^{\mathbf{T}}\mathbf{R}^{\mathbf{V}^{\mathbf{T}}}\tilde{\mathbf{M}}\mathbf{R}^{\mathbf{V}}\dot{\mathbf{q}}\}}{\partial\mathbf{q}}. \tag{IV.4}$$

Expanding the expression gives

$$\frac{\partial\{\dot{\mathbf{q}}^{\mathbf{T}}\mathbf{M}\dot{\mathbf{q}}\}}{\partial\mathbf{q}} = \begin{bmatrix} \dot{\mathbf{q}}^{\mathbf{T}}\left\{\frac{\partial\mathbf{R}^{\mathbf{V}^{\mathbf{T}}}}{\partial q_{11}}\tilde{\mathbf{M}}\mathbf{R}^{\mathbf{V}} + \mathbf{R}^{\mathbf{V}^{\mathbf{T}}}\frac{\partial\tilde{\mathbf{M}}}{\partial q_{11}}\mathbf{R}^{\mathbf{V}} + \mathbf{R}^{\mathbf{V}^{\mathbf{T}}}\tilde{\mathbf{M}}\frac{\partial\mathbf{R}^{\mathbf{V}}}{\partial q_{11}}\right\}\dot{\mathbf{q}} \\ \vdots \\ \dot{\mathbf{q}}^{\mathbf{T}}\left\{\frac{\partial\mathbf{R}^{\mathbf{V}^{\mathbf{T}}}}{\partial q_{ij}}\tilde{\mathbf{M}}\mathbf{R}^{\mathbf{V}} + \mathbf{R}^{\mathbf{V}^{\mathbf{T}}}\frac{\partial\tilde{\mathbf{M}}}{\partial q_{ij}}\mathbf{R}^{\mathbf{V}} + \mathbf{R}^{\mathbf{V}^{\mathbf{T}}}\tilde{\mathbf{M}}\frac{\partial\mathbf{R}^{\mathbf{V}}}{\partial q_{ij}}\right\}\dot{\mathbf{q}} \\ \vdots \\ \dot{\mathbf{q}}^{\mathbf{T}}\left\{\frac{\partial\mathbf{R}^{\mathbf{V}^{\mathbf{T}}}}{\partial q_{Nn_u}}\tilde{\mathbf{M}}\mathbf{R}^{\mathbf{V}} + \mathbf{R}^{\mathbf{V}^{\mathbf{T}}}\frac{\partial\tilde{\mathbf{M}}}{\partial q_{Nn_u}}\mathbf{R}^{\mathbf{V}} + \mathbf{R}^{\mathbf{V}^{\mathbf{T}}}\tilde{\mathbf{M}}\frac{\partial\mathbf{R}^{\mathbf{V}}}{\partial q_{Nn_u}}\right\}\dot{\mathbf{q}} \end{bmatrix}, \tag{IV.5}$$

where q_{1j} corresponds to the jth generalized coordinate associated with the platform, while q_{ij}, for $i = 2...N$, corresponds to the jth generalized coordinate associated with

the (i^{th} - 1) unit. Using the fact that each component within the square brackets is a scalar, Eq. (IV.5) can be rewritten in the form

$$\frac{\partial\{\dot{\mathbf{q}}^{\mathbf{T}}\mathbf{M}\dot{\mathbf{q}}\}}{\partial\mathbf{q}} = \begin{bmatrix} \dot{\mathbf{q}}^{\mathbf{T}}\left\{2\frac{\partial\mathbf{R}^{\mathbf{V}^{\mathbf{T}}}}{\partial q_{11}}\tilde{\mathbf{M}}\mathbf{R}^{\mathbf{V}} + \mathbf{R}^{\mathbf{V}^{\mathbf{T}}}\frac{\partial\tilde{\mathbf{M}}}{\partial q_{11}}\mathbf{R}^{\mathbf{V}}\right\}\dot{\mathbf{q}} \\ \vdots \\ \dot{\mathbf{q}}^{\mathbf{T}}\left\{2\frac{\partial\mathbf{R}^{\mathbf{V}^{\mathbf{T}}}}{\partial q_{ij}}\tilde{\mathbf{M}}\mathbf{R}^{\mathbf{V}} + \mathbf{R}^{\mathbf{V}^{\mathbf{T}}}\frac{\partial\tilde{\mathbf{M}}}{\partial q_{ij}}\mathbf{R}^{\mathbf{V}}\right\}\dot{\mathbf{q}} \\ \vdots \\ \dot{\mathbf{q}}^{\mathbf{T}}\left\{2\frac{\partial\mathbf{R}^{\mathbf{V}^{\mathbf{T}}}}{\partial q_{Nn_u}}\tilde{\mathbf{M}}\mathbf{R}^{\mathbf{V}} + \mathbf{R}^{\mathbf{V}^{\mathbf{T}}}\frac{\partial\tilde{\mathbf{M}}}{\partial q_{Nn_u}}\mathbf{R}^{\mathbf{V}}\right\}\dot{\mathbf{q}} \end{bmatrix}. \tag{IV.6}$$

The matrices $\tilde{\mathbf{M}}$ and $\mathbf{R}^{\mathbf{V}}$ were described in details in Appendix II and Appendix III, respectively. The explicit differentiation of the mass matrix is not presented as the result is quite lengthy and does not provide much insight into the equations of motion.